Optimal dispatch & network reconfiguration algorithms for controlling the security of electrical power systems

Department of Electrical and Information Engineering

Electrical and Information Engineering

Ph.D. Program

SSD: IIND-08/B Electrical Power Systems

Final Dissertation

Optimal Dispatch & Network Reconfiguration Algorithms for Controlling the Security of Electrical Power Systems

---

by

Roberto Cometa

Supervisor:

Prof. Massimo LA SCALA

Co-Supervisor:

Prof. Maria DICORATO

Industrial Supervisors:

Dr. Cosimo PISANI
Eng. Tiziano D'AVERSA

Coordinator of Ph.D. Program:
Prof. Mario Carpentieri

XXXVIII Cycle - November 1st, 2022 - January 31st, 2026

Politecnico di Bari

LIBERATORIA PER L'ARCHIVIAZIONE DELLA TESI DI DOTTORATO

Al Magnifico Rettore
del Politecnico di Bari

Il/la sottoscritto/a Roberto Cometa nato/a a Putignano (BA) il 28/01/1996

residente a Monopoli (BA) in via Cosimo Pisonio, 88 e-mail r.cometa1@phd.poliba.it

iscritto al 3° anno di Corso di Dottorato di Ricerca in Ingegneria Elettrica e dell'Informazione ciclo 38

ed essendo stato ammesso a sostenere l'esame finale con la prevista discussione della tesi dal titolo:

"*Optimal Dispatch & Network Reconfiguration Algorithms for Controlling the Security of Electrical Power Systems*"

DICHIARA

1) di essere consapevole che, ai sensi del D.P.R. n. 445 del 28.12.2000, le dichiarazioni mendaci, la falsità negli atti e l'uso di atti falsi sono puniti ai sensi del codice penale e delle Leggi speciali in materia, e che nel caso ricorressero dette ipotesi, decade fin dall'inizio e senza necessità di nessuna formalità dai benefici conseguenti al provvedimento emanato sulla base di tali dichiarazioni;
2) di essere iscritto al Corso di Dottorato di ricerca in Ingegneria Elettrica e dell'Informazione ciclo 38, corso attivato ai sensi del "*Regolamento dei Corsi di Dottorato di ricerca del Politecnico di Bari"*, emanato con D.R. n.286 del 01.07.2013;
3) di essere pienamente a conoscenza delle disposizioni contenute nel predetto Regolamento in merito alla procedura di deposito, pubblicazione e autoarchiviazione della tesi di dottorato nell'Archivio Istituzionale ad accesso aperto alla letteratura scientifica;
4) di essere consapevole che attraverso l'autoarchiviazione delle tesi nell'Archivio Istituzionale ad accesso aperto alla letteratura scientifica del Politecnico di Bari (IRIS-POLIBA), l'Ateneo archivierà e renderà consultabile in rete (nel rispetto della Policy di Ateneo di cui al D.R. 642 del 13.11.2015) il testo completo della tesi di dottorato, fatta salva la possibilità di sottoscrizione di apposite licenze per le relative condizioni di utilizzo (di cui al sito http://www.creativecommons.it/Licenze), e fatte salve, altresì, le eventuali esigenze di "embargo", legate a strette considerazioni sulla tutelabilità e sfruttamento industriale/commerciale dei contenuti della tesi, da rappresentarsi mediante compilazione e sottoscrizione del modulo in calce (Richiesta di embargo);
5) che la tesi da depositare in IRIS-POLIBA, in formato digitale (PDF/A) sarà del tutto identica a quelle **consegnate**/inviate/da inviarsi ai componenti della commissione per l'esame finale e a qualsiasi altra copia depositata presso gli Uffici del Politecnico di Bari in forma cartacea o digitale, ovvero a quella da discutere in sede di esame finale, a quella da depositare, a cura dell'Ateneo, presso le Biblioteche Nazionali Centrali di Roma e Firenze e presso tutti gli Uffici competenti per legge al momento del deposito stesso, e che di conseguenza va esclusa qualsiasi responsabilità del Politecnico di Bari per quanto riguarda eventuali errori, imprecisioni o omissioni nei contenuti della tesi;
6) che il contenuto e l'organizzazione della tesi è opera originale realizzata dal sottoscritto e non compromette in alcun modo i diritti di terzi, ivi compresi quelli relativi alla sicurezza dei dati personali; che pertanto il Politecnico di Bari ed i suoi funzionari sono in ogni caso esenti da responsabilità di qualsivoglia natura: civile, amministrativa e penale e saranno dal sottoscritto tenuti indenni da qualsiasi richiesta o rivendicazione da parte di terzi;
7) che il contenuto della tesi non infrange in alcun modo il diritto d'Autore né gli obblighi connessi alla salvaguardia di diritti morali od economici di altri autori o di altri aventi diritto, sia per testi, immagini, foto, tabelle, o altre parti di cui la tesi è composta.

Luogo e data Bari, 29/04/2026 Firma 

Il/La sottoscritto, con l'autoarchiviazione della propria tesi di dottorato nell'Archivio Istituzionale ad accesso aperto del Politecnico di Bari (POLIBA-IRIS), pur mantenendo su di essa tutti i diritti d'autore, morali ed economici, ai sensi della normativa vigente (Legge 633/1941 e ss.mm.ii.),

CONCEDE

- al Politecnico di Bari il permesso di trasferire l'opera su qualsiasi supporto e di convertirla in qualsiasi formato al fine di una corretta conservazione nel tempo. Il Politecnico di Bari garantisce che non verrà effettuata alcuna modifica al contenuto e alla struttura dell'opera.
- al Politecnico di Bari la possibilità di riprodurre l'opera in più di una copia per fini di sicurezza, back-up e conservazione.

Luogo e data Bari, 29/04/2026 Firma 

"Human rational behavior is shaped by a scissors whose two blades are the structure of task environments and the computational capabilities of the actor."

Herbert A. Simon, *Invariants of Human Behavior*

Contents

List of Figures

List of Tables

Abstract

This doctoral thesis reports the results carried out by the author during the three-year research activities of the XXXVIII cycle of the Ph.D. course in Electrical and Information Engineering at Politecnico di Bari.

The main goal of this work is the development and implementation of advanced algorithms for optimal dispatch and network reconfiguration to ensure operational security and reliability of electrical power systems within the context of the energy transition. The research frames security and flexibility as a multi-layer coordination problem that bridges generation dispatch, service markets, and topology control across both transmission and distribution levels.

At the transmission level, the thesis first introduces a two-stage energy and service market framework that integrates unit commitment and network-based redispatch, enabling Transmission System Operators (TSOs) to handle load and renewable energy sources (RES) forecast errors, and procure reserve services while ensuring system adequacy and security. Moving beyond cost-intensive generation-based solutions, the research investigates topology control as a source of hidden flexibility in power system operation. Switching operations are integrated into Optimal Reactive Power Flow (ORPF) and N-1 Security-Constrained optimization tools to mitigate voltage violations and relieve congestion without incurring additional costs. These methodologies are tested on both standard benchmark systems and realistic transmission grid models, highlighting the practical challenges of their application in real-world control rooms.

The concept of topological flexibility is finally extended to the distribution level, focusing on improving the quality of supply for operational planning purposes. Optimal Network Reconfiguration (ONR) algorithms are specifically designed incorporating the actual Fault Detection, Isolation, and Recovery (FDIR) practices adopted by Italian Distribution System Operators (DSOs). The soundness and generality of the proposed models enable the assessment of adverse weather events impacts, while also supporting automated restoration and black-start procedures.

Acknowledgments

This research work was supported by the Politecnico di Bari and by the strategic partnership with Terna SpA, the Italian Transmission System Operator, which helped identify the key technical challenges that shaped the direction of this doctoral thesis.
My deepest gratitude goes to my supervisor and mentor, Prof. Massimo La Scala. His valuable guidance, constant encouragement, and expertise have been fundamental to my professional growth. I feel very fortunate to have learned from his experience throughout this PhD journey. I will always value his advice, his research insights, the countless hours spent brainstorming and the many meaningful moments shared at the university.
I would also like to thank Prof. Sergio Bruno for his continuous support and professionalism. His teachings have greatly expanded my understanding of power systems. I have very fond memories of his lectures, the conferences we attended together, and the late-night paper submissions, as well as the friendship we have built over time.
I would like to extend my thanks to Prof. Maria Dicorato and Prof. Giuseppe Forte for their valuable insights. This work was also made possible by their encouragement. Thank you for believing in my potential and for your continued support even beyond my graduation.
I would like to express my sincere gratitude to my co-supervisors at Terna SpA, Cosimo Pisani and Tiziano D'Aversa. Working with them has been a truly meaningful experience. Their guidance, together with the practical perspective they brought, has played an important role in shaping this work. A special thanks goes to all the colleagues at *Bari Ovest* for their warmth, kindness, and for making me feel part of a community.
I would also like to acknowledge Prof. Christian Rehtanz and the ie^3 research group at TU Dortmund. I am grateful for the hospitality and the genuine friendship shown

during my time in Germany, which added an international dimension to my studies. To my colleagues at LabZERO and DEEPS-LAB: thank you for the stimulating environment, the many technical discussions, and the collaborative spirit that made working in the lab both productive and enjoyable. Your presence has been essential in creating a positive and supportive working environment. This journey would not have been the same without Cosimo's positive attitude, Angelo's help and support, and the presence of Francesco and Marco. I am also grateful for the kindness of Mohammad and Muzammal. I would like to thank Gioacchino for sharing his passion for research and his programming skills, and for encouraging me to pursue this path. Thanks also to Francesca, who is not only extremely dedicated and professional, but also a dear friend.
Last but not least, my heartfelt thanks go to my parents and friends. Their constant presence, patience, and unwavering confidence in me have been my greatest strength throughout this journey, and I could not have completed it without them.

Roberto Cometa
Bari, April 2026

Author's Publications

Publications resulting from this research work are listed below in chronological order.

International Journal Articles

1. M. R. Nasab, R. Cometa, S. Bruno, G. Giannoccaro, and M. La Scala, "Power Systems Simulation and Analysis: A Review on Current Applications and Future Trends in DRTS of Grid-Connected Technologies," *IEEE Access*, vol. 12, pp. 121 320–121 345, 2024

2. R. Cometa, A. Velini, M. R. Nasab, F. Lorusso, M. La Scala, and S. Bruno, "A MISOCP Formulation for Distribution Optimal Network Reconfiguration Considering Fault Detection Isolation & Recovery Practices," *IEEE Transactions on Industry Applications*, 2026 (under review)

3. A. Velini, R. Cometa, F. Lorusso, M. La Scala, and S. Bruno, "Mitigating the Impact of Adverse Weather Events Via MISOCP-Optimal Network Reconfiguration," *IEEE Transactions on Industry Applications*, 2026 (under review)

4. R. Cometa, G. Tricarico, M. Dicorato, and G. Forte, "A Two-Stage Energy and Service Market Framework Involving Unit Commitment and Network-based Redispatch," *Energies*, 2026 (under review)

International Conference Proceedings

1. M. R. Nasab, P. Ghalebani, S. Bruno, R. Cometa, and M. La Scala, "Adaptive PI Control of PMSM for Electric Vehicle Application Based on Sliding-mode Extremum Seeking Algorithm," in *2023 Asia Meeting on Environment and Electrical Engineering (EEE-AM)*, 2023, pp. 1–6

2. S. Bruno, R. Cometa, M. G. Ippolito, M. La Scala, G. C. Miglionico, R. Musca, and E. R. Sanseverino, "Power Oscillations Damping Control using BESS with Real-Time PHIL Co-Simulation Validation," in *2024 IEEE Power & Energy Society General Meeting (PESGM)*, 2024, pp. 1–5

3. R. Cometa, A. Velini, F. Lorusso, A. Ricca, R. Sbrizzai, and S. Bruno, "An Open-Source Optimal Network Reconfiguration Tool for Improving Distribution Grid Reliability," in *2024 AEIT International Annual Conference (AEIT)*, 2024, pp. 1–6

4. M. R. Nasab, R. Cometa, S. Bruno, and M. La Scala, "Adaptive Scheme for Stability Margin Estimation of Grid-Connected DFIG Based Wind Turbines," in *2024 IEEE International Conference on Environment and Electrical Engineering and 2024 IEEE Industrial and Commercial Power Systems Europe (EEEIC / I&CPS Europe)*, 2024, pp. 1–6

5. R. Cometa, M. R. Nasab, F. Lorusso, A. Velini, M. La Scala, and S. Bruno, "Integration of FDIR Practices in Distribution Optimal Network Reconfiguration Routines," in *2024 IEEE International Conference on Environment and Electrical Engineering and 2024 IEEE Industrial and Commercial Power Systems Europe (EEEIC / I&CPS Europe)*, 2024, pp. 1–6

6. M. R. Nasab, R. Cometa, P. Ghalebani, S. Bruno, and M. La Scala, "Distributed Adaptive Droop Control Method for Flexibility Enhancement of Islanded DC Microgrids Including Electric Springs," in *2024 Energy Conversion Congress & Expo Europe (ECCE Europe)*, 2024, pp. 1–6

7. A. Velini, R. Cometa, F. Lorusso, M. La Scala, and S. Bruno, "Optimal Network Reconfiguration for Mitigating the Impact of Adverse Weather Events on Distribution Networks," in *2024 IEEE International Humanitarian Technologies Conference (IHTC)*, 2024, pp. 1–7

8. R. Cometa, A. Velini, M. R. Nasab, S. Bruno, and M. La Scala, "Optimal Transmission Grid Assets Maneuvering for Improving Voltage Profile in RES Scenarios," in *2024 IEEE International Humanitarian Technologies Conference (IHTC)*, 2024, pp. 1–7

9. M. R. Nasab, R. Cometa, C. Iurlaro, M. M. Islam, S. Bruno, and M. La Scala, "Stand-alone DC Microgrids for Rural Areas: A Decentralized Energy Management and Voltage Regulation Approach," in *2024 IEEE International Humanitarian Technologies Conference (IHTC)*, 2024, pp. 1–7

10. F. Lorusso, A. Velini, R. Cometa, M. Marco, S. Bruno, and M. La Scala, "Primary distribution network re-energization through multiple black start units," in *2025 IEEE International Conference on Environment and Electrical Engineering and 2025 IEEE Industrial and Commercial Power Systems Europe (EEEIC / I&CPS Europe)*, 2025, pp. 1–6

11. M. Menga, R. Cometa, G. Cassettino, C. Iurlaro, S. Bruno, and M. La Scala, "Impact of reactive power dispatch in a recursive two-stage optimal control algorithm for isolated electrical networks," in *2025 IEEE International Conference on Environment and Electrical Engineering and 2025 IEEE Industrial and Commercial Power Systems Europe (EEEIC / I&CPS Europe)*, 2025, pp. 1–6

12. R. Cometa, A. Velini, M. La Scala, R. Musca, M. Minetti, A. Bonfiglio, and S. Bruno, "Employing MISOCP Relaxations to Solve Distribution Optimal Network Reconfiguration," in *2025 IEEE Power & Energy Society General Meeting (PESGM)*, 2025, pp. 1–5

13. A. Bonfiglio, S. Bruno, R. Cometa, M. Minetti, R. Musca, and A. Vasile, "Adaptive feedforward grid-forming controls to preserve inertial capabilities in power systems," in *2025 IEEE PES Innovative Smart Grid Technologies Conference Europe (ISGT Europe)*, 2025, pp. 1–5

14. R. Cometa, F. Lorusso, M. Menga, A. Velini, R. Musca, S. Bruno, and M. La Scala, "Preventive N-1 Security-Constrained Optimal Transmission Network Reconfiguration," in *2026 IEEE Power & Energy Society General Meeting (PESGM)*, 2026 (to be appeared)

Introduction

Background and Motivation

The ongoing transition toward low-carbon energy systems is significantly transforming the operation of modern electric power networks. The increasing penetration of renewable energy sources (RES) introduces unprecedented levels of variability and uncertainty, challenging the conventional paradigms of system operation, market coordination, and network control. Under these conditions, ensuring operational security, flexibility, and economic efficiency has become a central concern for system operators and policymakers alike.

Traditionally, operational security has been mainly ensured by managing the generation side through market coordination, redispatching actions and reserve management. However, such an approach is increasingly inadequate to guarantee secure system operation in the presence of network bottlenecks, market-driven dispatch constraints, and a decreasing share of controllable generation capacity. Ensuring system security now requires a broader perspective, where flexibility is regarded as a system-level attribute that must be coordinated across all network layers — generation, transmission, and distribution — and between market mechanisms and physical infrastructures. This coordinated approach is essential for both Transmission System Operators (TSOs) and Distribution System Operators (DSOs) to maintain reliable and secure operation under evolving grid conditions.

The research activity outlined in this thesis deals with the technological challenges for power system operation, by analyzing two main areas of interest with reference to the management of the grid components controllable by system operators: the influence on the Ancillary Service Market and the analyses of static security. Consequently, optimal grid assets for system's operation can be defined thanks to the use of advanced optimization tools.

Within this context, besides the optimal dispatch of the energy resources, network reconfiguration through topology control emerges as a powerful yet underexplored flexibility resource. By modifying the grid topology through controlled switching actions, system operators can effectively relieve congestion, reduce losses, and enhance voltage stability — often relying solely on existing grid assets and without incurring additional generation costs. Such strategies highlight the importance of treating operational flexibility as a cross-voltage-level system property, requiring coordination across transmission and distribution networks, as well as market and physical layers.

The research activity initially involved the analysis and identification of the main network phenomena that impact on the management of the power system in the context of the change underway. Based on the phenomena that should be countered, it was necessary to model some strategies which allow to appropriately manage the grid, also considering the economic aspects and security constraints.

Furthermore, the identified methodologies have been tested and validated through simulations in static conditions, employing specialized software tools and implementing optimization routines.

Contributions

This doctoral research aims to advance the theoretical foundations and practical implementation of optimization-based and topology-driven flexibility mechanisms for secure and efficient operation of modern power systems.

The main contributions can be summarized as follows:

1. *Integrated view of operational security and flexibility* – The thesis frames security and flexibility as a multi-layer coordination problem involving generation dispatch, energy and service markets sequential interaction, and topology control, highlighting the interdependencies among these elements both in electrical transmission and distribution activities.

2. *Methodologies for mathematical modeling of electrical transmission and distribution systems* – Modeling techniques are proposed to accurately represent the complexity of modern power systems. This involves the topological characterization of transmission and distribution systems, as well as the static modeling of the electrical non-linear components and their integration into automatic

calculation procedures.

3. *Market models & Optimization of redispatch mechanisms* – A mathematical formulation is developed to represent the sequential relationship between the day-ahead and Ancillary Services markets. The latter is modeled as a Unit Commitment and Economic Redispatch problem, considering reserve allocation and network constraints. Benefits and limitations of generation-only preventive actions in renewable-dominated transmission systems are discussed.

4. *Optimization algorithms for topology control* – Innovative methods for optimal network reconfiguration are introduced, addressing both transmission and distribution levels. These algorithms enhance system security through congestion mitigation, voltage regulation, loss reduction and reliability improvement.

5. *Static security analysis approaches* - The work advances power system security assessment by introducing screening techniques and simulation procedures. These approaches allow for a more efficient identification of critical contingencies and the evaluation of the system's static security.

6. *Applications to realistic grid models with the use of specialized software tools* - The theoretical methodologies are tested through simulations on large-scale, realistic test systems. By leveraging advanced software platforms and optimization solvers, the research bridges the gap between abstract optimization models and actual grid operations, discussing possibilities and limits in terms of scalability and practical applicability of the proposed solutions.

Outline of the Thesis

This doctoral thesis addresses the problem of operational security, flexibility, and economic efficiency in both modern transmission and distribution systems, under the increasing penetration of renewable generation and the consequent rise of uncertainty and network issues.

The research develops a coherent framework in which operational, economic, and topological control actions are jointly investigated across different voltage levels, identifying the needs that both TSOs and DSOs have in dealing with issues related to network security.

At the transmission system level, the thesis first focuses on redispatch mechanisms. This analysis naturally leads to the investigation of remunerative grid services, which are required to economically coordinate redispatch actions and ensure incentive compatibility among market participants.

Beyond generation-based solutions, the thesis explores cost-free control actions, such as transmission line switching and network reconfiguration strategies (e.g., substation splitting, transformers' tap settings adjustments) as effective sources of hidden flexibility. These actions allow system operators to relieve congestion, improve voltage profile and enhance security without additional generation costs, thereby complementing traditional redispatch mechanisms.

The concept of topology-based flexibility is subsequently extended to the primary distribution network level, where optimal network reconfiguration is formulated as a means to improve system reliability and accommodate distributed energy resources while respecting radiality and protection coordination constraints.

Chapter 1 - Secure Operation of the Electric Transmission Systems in the Energy & Service Market Framework: discusses the theoretical and regulatory background of secure system operation in liberalized electricity markets. It analyzes the interplay between market-based dispatch and system security constraints, emphasizing the need for coordinated redispatch mechanisms. The chapter concludes with the modeling of the day-ahead/ancillary services market sequential interaction, for the reserve services provision and the compensation of load and renewable forecast errors, ensuring system adequacy and operational security.

Chapter 2 - Optimal Transmission Grid Assets Maneuvering for Improving Voltage Profile: introduces a metaheuristic-based optimization algorithm for coordinated control of transmission assets, including transformer tap changers, shunt devices and switchable lines, to enhance voltage profile during high-RES operating scenarios.

Chapter 3 - N-1 Security-Constrained Optimal Transmission Network Reconfiguration Algorithms for Congestion Management: provides algorithms for topology optimization under N-1 contingency criteria, enabling cost-free congestion management and secure operation under stressed network conditions.

Chapter 4 - Optimal Transmission Network Reconfiguration Algorithms for the Secure Operation of the National Electric Transmission System: thanks to the collaboration with the Italian transmission system operator Terna SpA, this chapter collects case studies relating to the application of the developed optimization methodologies on realistic national transmission grid models. Methodologies are provided to simulate detailed and complex network models according to the actual needs of the system operator, discussing the challenges encountered in the implementation for real world applications (e.g., scalability, time requirements, etc.).

Chapter 5 - Optimal Network Reconfiguration Algorithms for Optimizing the Reliability and Quality of Supply in Primary Distribution Networks: extends the reconfiguration framework to the distribution level, focusing on improving reliability, loss minimization, and the integration of distributed energy resources while maintaining radiality and protection coordination. An Optimal Network Reconfiguration framework is proposed for optimizing the quality of supply in medium voltage radial distribution systems, optimization tool that can be extended to black-start and restoration procedures through intentional islanding procedures.

PhD Program Description

The doctoral research was primarily conducted at the Politecnico di Bari, within the Department of Electrical and Information Engineering (DEI). The research activity is focused on the complex issues related to the economic and secure operation of the electrical power systems, analyzing how grid services provision can be affected by various grid assets.

A six-month industrial research collaboration was carried out at Terna SpA within the SSD-DSC-PIN (Optimal System Programming) unit. This activity focused on the analysis of realistic network models and operating conditions of the Italian National Transmission Grid, aiming at the practical implementation of methodologies developed for Optimal Transmission Network Reconfiguration. This collaboration provided valuable industrial insights and helped align the academic research objectives with the operational needs of the Italian Transmission System Operator.

Subsequently, a six-month research stay was undertaken at the Technische Univer-

sität Dortmund (Germany), within the Institute of Energy Systems, Energy Efficiency and Energy Economics (ie^3), specifically the Power System Stability & Operation (PSSO) group, under the supervision of Prof. Dr.-Ing. Christian Rehtanz. During this period, regular presentations of research progress were held within institute seminars, along with participation in meetings, workshops, and academic activities, including involvement in the examination committee for the Smart Grids course offered by the institute.

This combination of industrial and international experiences provided the candidate with a comprehensive perspective, bridging the gap between theoretical optimization methods and their practical implementation in real transmission system operation.

Parallel to the core research on transmission [1, 2, 10] and distribution [3–5, 7, 8, 15] steady-state optimization, complementary topics regarding power system dynamics and innovative power system simulation techniques. These activities addressed stability challenges [13] in renewable-dominated grids (e.g., inertia preservation [18], oscillation damping [12]) and the control of microgrids [14, 16] and isolated systems [17]. The validation of these strategies through Real-Time and Power Hardware-in-the-Loop (PHIL) simulations provided a comprehensive technical perspective [9], broadening the scope beyond steady-state analysis.

The scientific contributions resulting from the main research line and these complementary activities are detailed in the Author's Publications section.

Chapter 1

Secure Operation of the Electric Transmission Systems in the Energy & Service Market Framework

The secure operation of electric transmission systems is the fundamental cornerstone for ensuring the reliability, stability, and efficiency of modern power grids. Transmission system operators (TSOs) must continuously balance supply and demand, maintaining system frequency and voltage within operational limits, preventing network congestion and cascading failures. In the current global energy transition context, the integration of variable renewable energy sources (RES) introduces unprecedented complexity in the power system operation, challenging TSOs in maintaining the grid in a *normal state*. To achieve these goals, several technical and economic mechanisms can be implemented, ranging from market-based services that incentivize flexible resources, to technical control strategies that enhance system security without direct financial compensation.

This first chapter explores the multi-faceted approach required to ensure system security, ranging from market-based mechanisms to technical control strategies. The discussion is structured as follows:

- Paragraph 1.1 defines the various operating states of the electrical transmission systems and the specific methods employed by TSOs to manage transitions between them.
- Paragraph 1.2 details the technical requirements and services for secure opera-

tion, distinguishing between remunerative services (market-based) and cost-free strategies (topology or control-based).

- Paragraph 1.3 explores the economic aspect of operational security from the TSO's perspective, analyzing the redispatching and balancing mechanisms currently active within the European and Italian electricity markets.

- Paragraph 1.4 introduces an energy and service market framework, proposing an integrated approach involving Unit Commitment and network-based redispatch to procure secondary reserve services in a RES-dominated bulk power system.

1.1 Operating states of the electrical transmission system

The objective of system operational security is the prevention and minimization of the consequences of service interruptions. The TSO pursues the security objective with all available tools and means. Specifically, it fulfills several obligations, including:

- Managing the grid securely by applying the operational criteria and procedures indicated in the Grid Code.

- Binding the operation of the grid to security requirements in all phases of transmission and dispatching activities, including the coordination of unavailability schedules and network development activities.

- Establishing protection criteria and calibration strategies for devices.

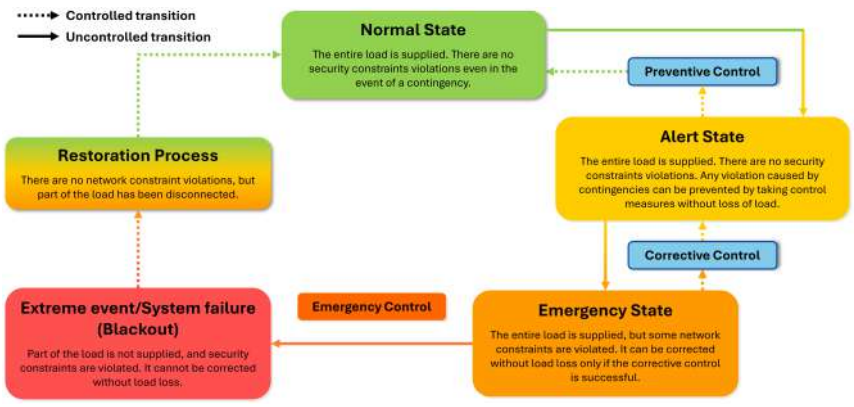

Figure 1.1: Scheme of the transmission system operating states.

To maintain security, the TSO manages its own observable and controllable portion of the grid across various operating states (Fig. 1.1), with the priority objective of countering degradation toward more critical states and returning immediately to the normal state. As can be observed, the flow of the system between states is a balance between uncontrolled transitions (caused by contingencies or disturbances) and controlled transitions (driven by the operator's intervention). To this end, following specific regulations, the TSO implements necessary control actions and maneuvers designed to mitigate risks or recover from failures.

When the system moves from the Normal State to the Alert State, security margins are eroded. While all loads are still supplied and no limits are violated, the system no longer meets the $N-1$ security criterion. This means a single subsequent contingency could lead to immediate violations. In these conditions, the preventive control is the first line of defense to restore security margins. Common measures include redispatching generation units, changing the grid topology (switching operations), or adjusting voltage setpoints to ensure the system can once again withstand a contingency without loss of load.

If a contingency occurs while the system is already in the Alert State, it triggers an uncontrolled transition to the Emergency State. At this point, physical constraints (such as thermal limits of lines or voltage stability limits) are actively violated. In these cases, the corrective control can be implemented immediately after a disturbance occurs in the Emergency State. The aim in this phase is to eliminate the active constraint violations and stabilize the system, ideally returning it to the Alert State.

The last measure that can be adopted is the Emergency Control, acting as a "last resort" when corrective actions are insufficient. When successful, it prevents cascading failure and blackout events often involving under-frequency load shedding actions or system intentional islanding. While these actions result in a loss of load, they preserve the integrity of the remaining grid.

Finally, following a partial or total blackout, the restoration process is implemented. The operators perform black-start procedures, re-energize transmission lines, and gradually reconnect loads in a synchronized manner.

1.1.1 Methods for managing the electrical system in the different operating states

The following subsections detail the management procedures for each operating state and the transitions, as defined in [19].

1.1.1.1 Alert State procedures

In this state, the entire load is supplied, but the system is vulnerable to contingencies. Preventive Control is used to transition back to the Normal State through the following actions:

- *Generation & Dispatching*: dispatching orders are sent to the producers to run generation units at maximum excitation, use of automatic or manual remote tripping, and utilize available dispatching resources for balancing and redispatching.
- *Grid Topology Control*: the network topology can be modified through switching operations to restore security margins.
- *Distribution & Exchange*: the reference voltage set-point for primary substations can vary. Moreover, coordinated increases or decreases in power exchanges with foreign grid operators can be performed.
- *Load Management*: selective load shedding, shedding of pumping units or storage systems, extraordinary slow modulation of injections/withdrawals.

1.1.1.2 Emergency State procedures

Violations of network constraints occur here. Corrective Control aims for a controlled return to the Alert State, while Emergency Control triggers if the system degrades toward a blackout:

- *Defense Systems*: automatic load or generation shedding actions can be executed by the Defense System and the Automatic Load Balancer (EAC).
- *Manual Interventions*: manual shedding of loads and/or pumping plants via the Peripheral Defense and Monitoring Unit (UPDM).

- *Regulatory & Technical Measures*: implementation of agreed countermeasures with neighboring TSOs, application of the Distributed Generation Reduction procedure (RIGEDI), and blocking automatic Under-Load Tap Changers (VSC).

1.1.1.3 Blackout State procedures

This represents a system failure where part of the load is not supplied and security constraints are violated. The focus shifts to:

- Locating the network fault and identifying the perimeter of the de-energized area.
- Performing maneuvers to isolate the area affected by a permanent fault.

1.1.1.4 Restoration State procedures

A controlled transition process to return the system to the Normal State after a failure:

- Initiation of restoration procedures.
- Progressive re-feeding of withdrawal points and auxiliary services.
- Gradual *re-meshing* (reconnecting) of the transmission grid.

1.2 Requirements and services for the secure operation of electric transmission systems

At the European level, the European Network of Transmission System Operators for Electricity (ENTSO-E) ensures the security of the interconnected power system primarily through the System Operation Guideline (SOGL), by defining strict rules for the security of the European bulk power system, which serve as a basis and reference framework for national grid codes such as that of the Italian TSO. This regulation establishes harmonized rules for operational security, which mandates specific limits for voltage, frequency, and short-circuit currents, as well as the implementation of the (N-1) criterion to ensure system resilience against single

contingencies. Furthermore, it details protocols for operational planning and load-frequency control, requiring close coordination between European TSOs to manage cross-border stability. Complementing this, the Emergency and Restoration network code (NCER) sets out the procedures for managing large-scale incidents, ensuring a coordinated defense and recovery strategy across the entire European grid.

The rules for the secure operation of the Italian National Electric Transmission System are reported in the Italian Grid Code [20]. In particular, chapters 3, 4, and 10, collectively establish the operational framework for system security and reliability. Chapter 3 deals with management, operation, and maintenance of the grid, whereas Chapter 4 outlines the dispatching rules (i.e., the procedures for real-time balancing of power supply and demand, power reserves provision). Finally, as seen in the previous paragraph, Chapter 10 (Defense of Security) defines the various operating states of the system—ranging from normal to emergency—and details the defense plans and recovery procedures required to mitigate major disturbances and protect the integrity of the national grid.

To manage the daily operational challenges, TSOs ensure the quality of the dispatching service provided by coordinating two primary categories of operational requirements: remunerative services and cost-free strategies. The first can be procured through the Ancillary Service Market (ASM), whereas the others consist of non-market services.

Table 1.1 outlines the auxiliary resources currently required by the Italian TSO to ensure the secure balancing of the system, even during significant events, classifying them into ancillary services that can be traded on the ASM and non-market services.

Table 1.1: Market-based and non-market-based Ancillary Services

Market-Based (Procured via ASM/Auctions)	**Non-Market-Based (Mandatory/Emergency)**
• Primary Reserve (FCR) — Newly remunerated via auctions	• Primary voltage regulation
• Secondary Reserve (aFRR)	• Secondary voltage regulation
• Fast Tertiary Reserve (mFRR)	• Tertiary voltage regulation
• Spinning & Replacement Reserve (RR)	• Load Shedding — Emergency system defense (Involuntary)
• Congestion Management	• Black Start — Regulated service / Long-term contracts
• Real-time Balancing	• Emergency Frequency Control — Automatic defense plans
• Load Shedding — Capacity auctions	• Topology Control — Corrective remedial actions

1.2.1 Market-based remunerative services

Remunerative services utilize market-based mechanisms to provide economic incentives for resources that contribute to grid stability and security. They involve the participation of various energy generation companies which, together with a multitude of end-users, contribute to the formation of the electricity price in a competitive environment based on market mechanisms. However, as a result of the electricity market, the TSO is required to verify the feasibility of production plans in relation to the operational management of the transmission grid. In order to deal with situations that are unsustainable for the system – linked to the presence of congestion or overloads, forecast errors, and outages – the TSO must implement regulatory actions which, in many cases, involve varying the active power of producers and users, who are then called upon by the TSO through a competitive mechanism to provide adequate levels of ancillary services for the power dispatch.

Recently, the Italian electricity landscape has undergone a massive transformation with the implementation of the Integrated Text on Electricity Dispatching ("Testo Integrato del Dispacciamento Elettrico", TIDE) [21], which reached its full consolidation phase on February 1, 2026. The most recent change concerns the remuneration mechanisms for primary reserve services (Frequency Containment Reserve, FCR), previously listed as mandatory non-market services. In fact, with the displacement of traditional synchronous generators by asynchronous inverter-based resources, system inertia is now managed through market designs like auctions or tenders to maintain frequency stability. In order to comply with the European Electricity Balancing Guideline (EBGL) and to allow new technologies like Battery Energy Storage Systems (BESS) to compete, Italy has transitioned to a competitive, market-based procurement for the FCR. It is now remunerated via pay-as-bid auctions, turning it into a revenue stream for participants.

Beyond the FCR, the Italian ASM serves as the primary arena for procuring automatic Frequency Restoration Reserve (aFRR), manual Frequency Restoration Reserve (mFRR) and Replacement Reserve (RR). These pay-as-bid services are central to the TSO's ability to restore frequency and replacement reserves. Under the TIDE framework, the participation has been broadened to include Virtual Authorized Units (UVAs), allowing distributed energy resources and BESS to provide fast-acting reserves.

Congestion Management (CM) and Real-time Balancing services constitute the

two-stage logic of the ASM. In the *ex-ante* market sessions (operational planning), the TSO fulfills physical network constraints by modifying the injection or withdrawal schedules of power plants. In the real-time Balancing stage, the TSO intervenes to compensate for residual imbalances between supply and demand. Both processes rely on re-dispatching, where the TSO pays for the deviation from the energy market's outcomes.

Concerning Load Shedding, it can be considered as a market-based service if the TSO pays large industrial consumers (through auctions) to be ready to have their power cut when the grid is particularly stressed. In this case, they are compensated for this flexibility. During emergency conditions, instead, the Defense Plan provides for automatic load shedding as an unpaid emergency measure.

1.2.2 Cost-free strategies

While the aforementioned services involve a financial exchange to incentivize flexibility, the TSO also relies on non-market-based corrective actions to ensure grid security without incurring procurement costs. These strategies will be further explored in the subsequent chapters of this thesis. They typically involve automatic or operational measures that do not directly result in monetary compensation for participants. Examples include the activation of voltage control through shunt compensation devices and on-load tap changers, the use of network reconfiguration to manage congestion, and the coordination of protection systems to prevent cascading outages. Such measures are essential for maintaining system stability and ensuring a rapid and coordinated response to disturbances, particularly under stressed operating conditions.

Regarding voltage control, while some European countries are experimenting with reactive power markets [22], in Italy, voltage regulation is a mandatory technical requirement. Unlike frequency reserves, it is not currently traded on a daily/hourly market like the ASM. In particular, voltage regulation is characterized by a three-level hierarchical control structure, where the primary control is a mandatory service for all major production units. It consists in a local and automatic action performed by the Automatic Voltage Regulators (AVRs) of the synchronous generators. It reacts within milliseconds to maintain the generator's terminal voltage set-point. For power electronics interfaced generators, the same task is performed by the converter's voltage control loop. Secondary voltage regulation (SVR), instead, is a regional

control that coordinates groups of generators within specific electric zones defined as *pilot nodes* [23]. The SVR automatically adjusts the reactive power output of all participating generators in a zone keeping the voltage stable. Finally, the tertiary voltage regulation is centrally managed by the TSO involving the optimization of voltage profile across the entire system. The goal is to define the optimal set-points for the *pilot nodes* to minimize grid losses and ensure sufficient security margins against voltage collapse.

Other strategies involve topology control, that unlike re-dispatching flexible resources (which costs money through the ASM), it is a cost-free remedial action that may solve network operational issues without financial compensation to third parties. Topology control allows the TSO to manage congestion and optimize power flows by modifying the grid's physical configuration (e.g., opening/closing circuit breakers, splitting substations, switching-off transmission lines, etc.). However, as will be discussed in the following chapters, such strategies require advanced control architectures and optimization tools in order to determine and implement in real-time the necessary topological changes in response to a given operating event.

1.3 Redispatching and Balancing Mechanisms in the European and Italian Electricity Markets

Network security issues related to renewable energy sources (RES) and load forecast errors are faced by transmission system operators (TSOs) by means of redispatching and balancing services. Balancing resources are exploited to restore system frequency in real-time (RT) operation, whereas redispatch mechanism can be used when energy market outcomes do not fulfil power flow bounds [24], showcasing a high potential for cost optimization to remedy network congestions and to compensate for power fluctuations. Redispatch mechanism is managed by different procurement and remuneration models, depending on national grid rules [25].

In the last years, coupled energy markets were created in order to increase the utilization of generation sources among European market operator members (Nominated Electricity Market Operators, NEMOs), resulting in Single Day-ahead Coupling (SDAC) and Single Intraday Coupling (SIDC) markets [26, 27]. The aim of these markets is to create single pan-European cross zonal energy market to increase the overall trading efficiency among NEMOs. In particular, SDAC couples

wholesale electricity markets from different regions for maximizing social welfare while taking into account price limits of bids and regions cross-border flow constraints. In SIDC, market participants are able to work together across Europe to continuously trade the needed energy through the day, since it has become more challenging for market participants to be in balance (i.e., supplying the correct amount of renewable intermittent production) after the closing of the day-ahead market. Furthermore, the participants can update their bids until one hour before delivery time, reducing the need for reserves and associated costs while allowing enough time for carrying out system operation processes for ensuring system security. This new joint governance structure aims at achieving a better co-operation between NEMOs and TSOs. In fact, the inputs of these markets are the network capacities and constraints provided by the TSOs and the bids and offers provided by the NEMOs. In this structure, the ancillary service provision/delivery is managed in a successive market platform, where a harmonized market among European regions is still in a preliminary stage with some pilot projects, due to the different market frameworks [28]. Further insights on European market context and pilot projects are provided in [29].

Among European countries, Italian TSO has developed a comprehensive expertise in handling generating units and network constraints in market sessions downstream merit-order energy markets, as highlighted in Fig. 1.2 [30]. In particular, the energy markets are the Day-ahead (DAM) and the Intraday (IM) markets, managed by Italian Market Operator, aiming at maximizing the social welfare through a merit-order zonal clearing price mechanism. In this session, the main energy amount is traded defining the preliminary generation and load schedules considering step-wise bids and interzonal power flow constraints. Downstream, the Ancillary Service Market (ASM) sessions take place, managed by the TSO, to provide the required services according to a pay-as-bid auction market. Specifically, the TSO, based on energy market schedules, could redispatch units to procure a certain upward and downward power margin [31], depending on the needed reserve, while complying with branch power flows and unit commitment (UC) constraints along with the RES and load forecasts updates. Finally, Balancing Market (BM) is carried out throughout the whole day, activating the amounts reserved in ASM to mitigate any contingency, such as load and RES mismatches, generation outage, etc., and remunerating only the activated energy.

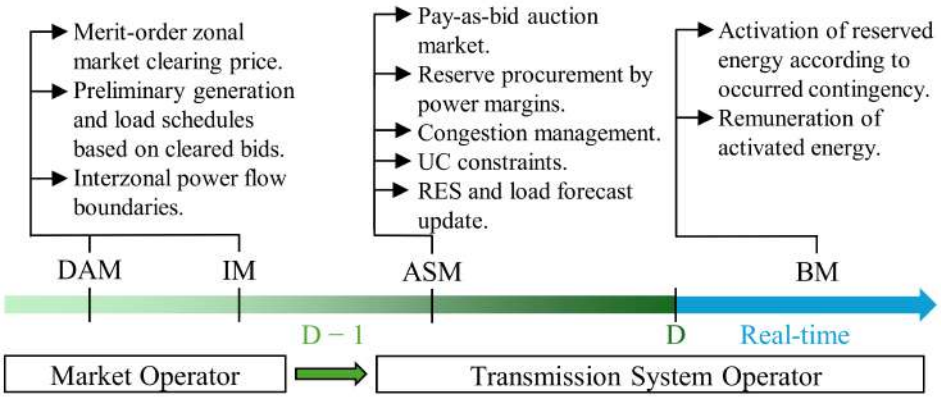

Figure 1.2: Italian market framework and main features.

1.4 A Two-Stage Energy and Service Market Framework Involving Unit Commitment and Network-based Redispatch

The provision of power and grid services requires the co-ordination between Day-Ahead Market (DAM) and Ancillary Service Market (ASM) to attain reserve services and technical feasible operating conditions for market players and for the network. In this context, this work proposes a multi-stage approach to evaluate the dispatched power to balance the forecast updates of renewable energy sources and load from DAM to ASM, taking into account network and Unit Commitment (UC) constraints, according to European approach. The DAM is solved considering a zonal market framework and neglecting the UC constraints. Then, a mechanism to adjust the ASM bids is developed, defining time-varying costs for each regulation. Finally, the ASM is modelled as a network-constrained UC and economic redispatch (NCUCER) optimization problem, aiming at minimizing the overall cost, in order to procure secondary reserve requirement and to adjust the DAM schedules, taking into account network and UC constraints and balancing forecast updates. DC load flow sensitivity factors are exploited to evaluate the influence of redispatch actions and forecast updates on the observed power flow. This procedure is applied to NREL 118-Bus Test System assessing its performances throughout a yearly time horizon.

1.4.1 Literature review

From a methodological point of view, security-constrained unit commitment (SCUC) and economic dispatch (ED) have been largely investigated [32–34], whereas only few works deal with market-based power redispatch to update the production level of generating units depending on power system operating conditions. The amount of redispatched power derives from an optimization problem aiming at solving congestions [35–38], balancing RES and/or load due to uncertainties [36, 37, 39, 40] or outage [41], or procuring reserve requirements [42, 43]. In the most employed formulations, units are allowed to be started-up or shut-down to provide redispatch, adopting integer variables, resulting in a mixed-integer linear programming (MILP) problem. Other formulations are seldom used, such as linear programming [36, 37, 40], mixed-integer non-linear programming [35], non-linear programming [44], or robust optimization [42]. The optimization problem have an economic purpose, mainly aiming at minimizing active power redispatch and start-up costs, and further costs can be due to shut-down [39, 41], reserve provision or deployment [39, 40, 42], RES and/or load curtailment [36, 39–42]. On the other hand, technical objective functions involve congestions mitigation [35, 36] or the minimization of the overload probability risk [37]. Besides power balance and power flow limits, modeled by means of sensitivity factors [35–37] or DC load flow (DCLF) equations [39, 41, 42], constraints could involve generator technical limits [38–41, 44], RES and/or load curtailment limits [40, 41], along with reserve provision, deployment or allocation limits [39, 42]. On the other hand, the work developed in [43] defines three optimization problems to model consecutive markets connecting intraday and reserve markets, in order to find feasible power profiles, provide secondary reserve (SR), and deploy the energy and SR, respectively, defining unit-state constraints for the already committed units.

In literature, the co-ordination between consecutive market sessions has been investigated, especially for energy and real-time (RT) markets in the American framework. In [45], the authors deal with a two-stage day-ahead (DA) clearing model for the energy and RT markets in the presence of high RES penetration considering fast-start generator behaviors as non-spinning reserve providers. In particular, the energy market optimization problem embeds the required amount of energy and reserves. The work proposed in [46] deals with a stochastic model predictive control scheme used to handle the uncertainty related to generation and load profiles combining Chance-Constrained and Machine Learning techniques. This

approach can be applied to participate simultaneously in different energy markets. The authors of [47] analyze the impact of wind farm (WF) power forecast on the co-ordination between energy and RT markets, and particularly focusing on cost implication between DA and RT due to WF uncertainties, handled by the system operator through anticipated RT adjustment bids, aiming to minimize the costs associated with conventional thermal generators and WF generators. In [48] a day-ahead reserve determination method based on two-stage stochastic programming approach is proposed. In the first stage the commitment of thermal units is carried out, whereas in the second stage the operation of the system with and without the failure of key thermal units is evaluated. Further methods, aims, and perspectives on market sessions co-ordination are available in the review paper [49].

Regarding the European framework, the work proposed in [29] presents three models to represent DAM, ASM, and the RT market in a renewable-dominated power system. In particular, they compare the market configuration committing the reserves in DAM, ASM, or in a joined co-optimized market. The problem considers units and network constraints along with reserve provision considering RES and load uncertainties.

1.4.2 Contributions

From the analysis illustrated so far, the need for a clearing procedure accounting for the DAM/ASM interaction along with the technical feasibility of the cleared offers for network and generating units arises. To this purpose, in this chapter, a multi-stage procedure for modeling the electricity market sessions up to ASM schedules is presented [10]. This method is threefold and includes: the merit-order zonal DAM clearance, that provides an initial generation profile coping with forecast load demand and RES generation based on marginal cost bids; the adjustment of ASM bids depending on DAM outcomes and technical operational limits of the dispatchable generators; the nodal ASM solution by redispatching generator schedules through a MILP optimization problem, including UC constraints. The proposed ASM model aims at minimizing redispatching costs, fulfilling power flow and UC constraints, procuring SR and balancing RES and load forecast updates. To this purpose, a Network-Constrainted UC and economic redispatch (NCUCER) optimization problem is proposed.

Particularly, the redispatching actions are referred to the start-up (SU) and

shut-down (SD) constraints of dispatchable thermal (DT) units which could arise downstream of the energy market, along with different technical constraints for DT and dispatchable hydroelectric (DH) units.

The main contributions of this work can be summarized:

- Modeling the sequential interaction between zonal DAM and nodal ASM through a deterministic two-stage optimization framework.
- The formulation of a unified technical-economic optimization problem (NCUCER) to model ASM, entailing the determination of the status and the active power production of DT units in accordance with UC constraints, RES and load forecast variations, branch power flow limits, and secondary reserve requirement (SRR) provision.
- The formulation of novel constraints to handle the service provision, taking into account DT unit operating points derived from DAM clearing process and UC constraints.
- The inclusion of inter-temporal dependencies in terms of availability, minimum up time (MUT) and minimum down time (MDT) of unit clearing process in ASM.
- Application of the methodology to a highly RES-dominated transmission system model featuring hundreds of generation units.

Numerical results demonstrate the practical applicability of the methodology, yielding a complete set of hourly feasible dispatch solutions for an entire year of operation.

1.4.3 Nomenclature

The nomenclature in Table 1.2 refers to the formulation of the zonal DAM and nodal ASM optimization problems described in this chapter.

Table 1.2: Nomenclature for DAM and ASM formulations.

Sets and Indices	
Ω^B	Set of N^B transmission branches (b)
Ω^D	Set of N^D days (d)
Ω^{DT}	Set of N^{DT} dispatchable thermal units (i)
Ω^{DU}	Set of N^{DU} dispatchable units (i)
Ω^G	Set of N^G generators (i)
Ω^H	Set of N^H dispatchable hydro units (i)
Ω^L	Set of N^L interzonal transmission lines (l)
Ω^N	Set of N^N nodes (n)
Ω^{ND}	Set of N^{ND} non-dispatchable thermal units (i)
Ω^R	Set of N^R non-dispatchable RES units (i)
Ω_i^S	Set of N_i^S generators' step-wise bids (s)
Ω^T	Set of N^T time steps within day d (t)
Ω^{TH}	Set of N^{TH} thermal units (i)
Ω^Z	Set of N^Z market zones (z)
Zonal DAM Parameters	
$a_{i,t}$	Hourly availability of DT unit
$c_{i,s}$	Marginal cost for each unit step [$/MWh]
$D_{z,t}^{da}$	Day-ahead zonal load demand forecast [MW]
$e_{i,t}$	Hourly monthly escalator of DT unit
F_l^{ub}, F_l^{lb}	Interzonal lines power flow bounds [MW]
k^H	Bid parameter for DH units
P_i^{max}	Maximum active power [MW]
$P_{i,t}^{H,max}$	Hourly maximum available hydropower [MW]
$\Delta P_{i,s}^{max}$	Maximum bid step width [MW]
$\alpha_{i,z}^G$	Generators-zones incidence matrix
$\alpha_{z,l}^F$	Zones-lines incidence matrix
Nodal ASM Parameters	
C^{rc}	Penalty cost for RES curtailment [$/MWh]
C_i^{su}	Fixed start-up cost of DT unit [$]
C^{voll}	Value of lost load cost [$/MWh]
$c_{i,s,t}^{\downarrow}, c_{i,s,t}^{\uparrow}$	Downward/Upward marginal cost for DT unit step [$/MWh]
$c_{i,t}^{sd}, c_{i,t}^{su}$	Variable shut-down/start-up costs [$/MWh]
$c_{i,t}^{sr\uparrow}, c_{i,t}^{sr\downarrow}$	Secondary Reserve marginal cost [$/MWh]
$D_{n,t}^{rt}$	Real-time load demand [MW]
$E_{i,t}^{av}$	Available energy of hydro unit [MWh]
E_i^{ub}, E_i^{lb}	Energy bounds of hydro unit [MWh]
$F_{b,t}^D$	Active power flow from DCLF [MW]
F_b^{ub}, F_b^{lb}	Power flow bounds [MW]
MU_i, MD_i	Minimum Up/Down Time values [h]

Continued on next page

Table 1.2 – continued from previous page

$P^D_{i,t}$	Cleared active power in DAM [MW]
P^{max}_i, P^{min}_i	Maximum/Minimum active power [MW]
$P^{rt}_{i,t}$	Real-time power output of RES units [MW]
$P^{sd}_{i,t}, P^{su}_{i,t}$	Shut-down/Start-up bids [MW]
P^{sh}_i	Secondary Reserve half-bandwidth [MW]
$S_{n,b}$	Power Transfer Distribution Factor
SRR_t	Secondary Reserve Requirement [MW]
$t^{mu}_{i,t}, t^{md}_{i,t}$	Minimum Up/Down Time durations [h]
$z^{DA}_{i,t}$	ON/OFF status of DT unit downstream DAM
$\Delta D^L_{n,t}$	Change in load absorption [MW]
$\Delta P^R_{i,t}$	Change in RES generation [MW]
$\beta_{i,n}$	Generator-node incidence matrix
$\overline{\Delta P}^{\downarrow}_{i,s,t}, \overline{\Delta P}^{\uparrow}_{i,s,t}$	Max downward/upward energy per step [MW]
Zonal DAM Real Variables	
$F_{l,t}$	Active power flow on interzonal lines [MW]
$P_{i,s,t}$	Cleared step active power [MW]
$P^D_{i,t}$	Cleared active power [MW]
Nodal ASM Real Variables	
$D^{ls}_{n,t}$	Curtailed load shedding at node n [MW]
$E^{ns}_{i,t}$	Non-stored energy of hydro unit [MWh]
$P^{rc}_{i,t}$	RES curtailment [MW]
$P^{sr\downarrow}_{i,t}, P^{sr\uparrow}_{i,t}$	Secondary Reserve accepted [MW]
$\Delta F_{b,t}$	Change in active power flow on a branch [MW]
$\Delta P^A_{i,t}$	Redispatched power of dispatchable unit [MW]
$\Delta P^{\downarrow}_{i,s,t}, \Delta P^{\uparrow}_{i,s,t}$	Downward/Upward redispatched power per step [MW]
Nodal ASM Binary Variables	
$z_{i,t}$	ON/OFF status of DT unit in the ASM
$z^{mu}_{i,t}, z^{md}_{i,t}$	Minimum Up/Down Time status
$z^{ns}_{i,t}$	Hydro unit basin inlet valve status
$z^{sd}_{i,t}, z^{su}_{i,t}$	Shut-down/Start-up status of DT unit
$z^{sr\downarrow}_{i,t}, z^{sr\uparrow}_{i,t}$	Secondary Reserve status of DT unit
$z^{\downarrow}_{i,t}, z^{\uparrow}_{i,t}$	Downward/Upward movement of unit

1.4.4 Methodology

In market-based power systems the ancillary services for the network security can be procured together with energy in a single market session or in a dedicated market downstream the energy procurement [50]. The market process proposed in this work bases its management on the European mechanism involving a multi-stage framework to handle UC and network constraints in the ASM. Particularly, the proposed procedure is composed of four-stages, solved $\forall\, d \in \Omega^D$, as depicted in

Fig. 1.3, each one synthesized in the following:

- *DAM model*: an economic-based merit-order zonal market optimization problem is carried out to define preliminary generation schedules;
- *Unit bids adjustment for ASM*: a bid adjustment mechanism is carried out to participate to the ASM, based on DAM results, unit technologies and technical limits;
- *DCLF and sensitivity factors*: a network feasibility analysis of the DAM outcomes is assessed, and the power transfer distribution factors (PTDFs) for the redispatch actions are determined;
- *ASM optimization problem*: a redispatch procedure that minimizes system costs, with a pay-as-bid mechanism, in the presence of UC and network constraints is employed.

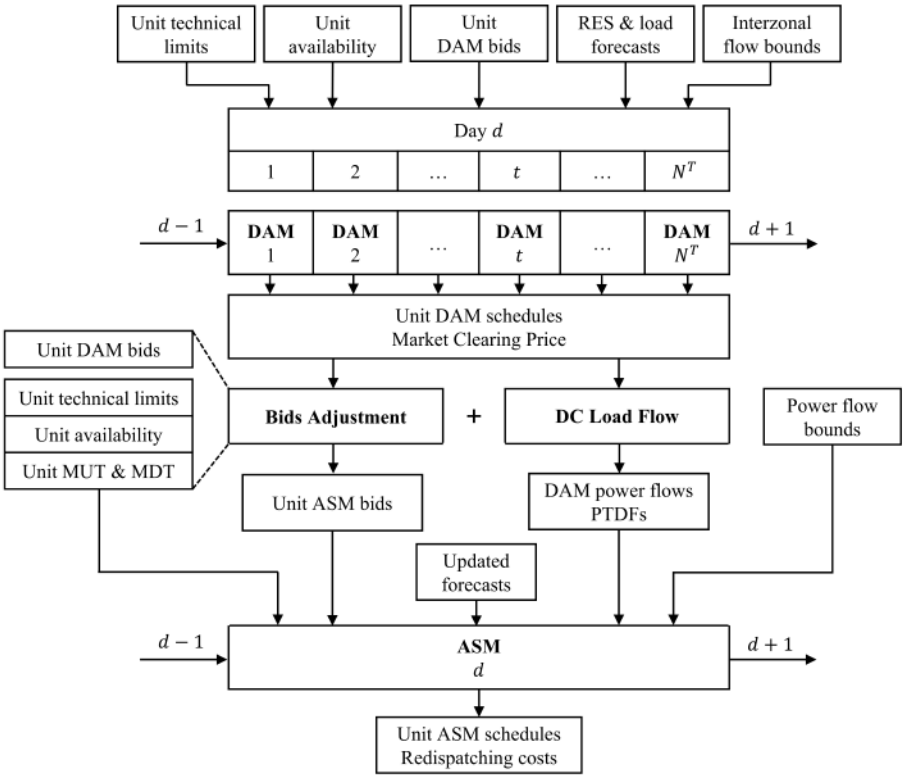

Figure 1.3: Workflow of the proposed procedure to model DAM/ASM sequential interaction.

In the following subsections the formulation and a more detailed description of

the four stages are provided. The notation used for the mathematical formulation of optimization problems is listed in the nomenclature in Table 1.2.

The first stage consists in solving the zonal DAM for each time step t of day d knowing the units' technical limits, availability and DAM bids. All the units are dispatched according to the economic merit-order, taking into account DA RES and load forecasts, as well as the exchange limits between market zones. This yields a preliminary generation schedule and the Market Clearing Price (MCP). The resulting active power flows are then computed through successive DCLF analyses based on the DAM outcomes, while the cleared bids are adjusted starting from the operating condition defined in the DAM, compatibly with the services that will be offered in the ASM. Once the RES and load forecasts are updated, this latter can be solved for day d.

1.4.4.1 DAM Model

The proposed DAM is based on [51] aiming at minimizing step-wise generators bid costs and subject to zonal power flow limits, zonal active power balance, unit maximum bid steps, and generator maximum power in the absence of UC relations. With respect to [51], the thermal unit time-varying maximum power and availability are here considered, along with the DH unit strategy to bid in the DAM. The thermal generator maximum power is determined by means of monthly escalators that consider weather influence on thermal unit rated power and availability due to maintenance, as in (1.1). The DH unit strategy consists in bidding a certain power amount, lower than maximum available level, in the DAM, with a bidding cost equal to 0 \$/MWh, and holding the remaining power amount for the ASM bids, as described in the next section.

$$P_{i,t}^{max} = P_{i}^{max} \cdot e_{i,t} \cdot a_{i,t} \tag{1.1}$$

Assuming that load demand is inelastic with respect to price, the DAM is formulated as a linear programming (LP) optimization problem representative of a zonal market. The goal is minimizing the stepwise generation costs at a single time step $t \in \Omega^T$ over a time window composed of N^T time steps, each with duration τ.

The resulting DAM formulation is stated below:

$$\min_{P_{i,s,t}} \tau \cdot \sum_{i \in \Omega^{DT}} \sum_{s \in \Omega_i^S} c_{i,s} P_{i,s,t} \tag{1.2}$$

subject to:

$$P_{i,t}^D = \sum_{s \in \Omega_i^S} P_{i,s,t}, \forall i \in \Omega^{DT} \tag{1.3}$$

$$0 \leq P_{i,s,t} \leq \Delta P_{i,s,t}^{max}, \forall i \in \Omega^{DT}, \forall s \in \Omega_i^S \tag{1.4}$$

$$0 \leq P_{i,t}^D \leq P_{i,t}^{max}, \forall i \in \Omega^{DT} \tag{1.5}$$

$$0 \leq P_{i,t}^D \leq P_{i,t}^{da}, \forall i \in \Omega^R \tag{1.6}$$

$$0 \leq P_{i,t}^D \leq k^H P_{i,t}^{H,max}, \forall i \in \Omega^H \tag{1.7}$$

$$\sum_{i \in \Omega^G} P_{i,t}^D - \sum_{z \in \Omega^Z} D_{z,t}^{da} = 0 \tag{1.8}$$

$$\sum_{i \in \Omega^G} \alpha_{i,z}^G P_{i,t}^D - \sum_{l \in \Omega^L} \alpha_{z,l}^F F_{l,t} = 0, \forall z \in \Omega^Z \tag{1.9}$$

$$F_l^{lb} \leq F_{l,t} \leq F_l^{ub}, \forall l \in \Omega^L \tag{1.10}$$

The equality constraint (1.3) defines the dispatched power of each thermal generator equal to the sum of the cleared bid steps. Inequality (1.4) limits the power of each bid step within its maximum width. Constraints (1.5) and (1.6) are required to ensure that the thermal units never exceed the maximum power and RES never exceed their hourly forecasted power, respectively. For DH units, (1.7) specifies the maximum power available for each hour according to the dispatch strategy. The total and zonal active power balances of the system are presented in (1.8) and (1.9), respectively, whereas (1.10) expresses the active power exchange boundaries on each interzonal connection. In particular, $\Delta P_{i,s,t}^{max}$ is the maximum bid step width, obtained as below:

$$\Delta P_{i,s,t}^{max} = \Delta P_{i,s}^{max} \cdot e_{i,t} \tag{1.11}$$

1.4.4.2 Unit bids adjustment and DCLF sensitivity factors

In the framework of distinct energy and service market sessions, the market participants could be called to submit ASM bids prior to the determination of energy market schedules [52]. Therefore, the TSO is called to adjust the submitted bids

in order to fit the technical features of the units depending on the closest energy market session results.

On these bases, the proposed bid adjustment process from TSO perspective is aimed at providing different services depending on DAM schedules and generator technical features, and the economic value of each service is weighed by time-varying factors applied to the DAM bid prices. In particular, the DT units are assumed to provide SU, SD, upward redispatch (UR), downward redispatch (DR), and upward (USR) and downward (DSR) SR services, whereas DH units, equipped with a basin, can only bid UR and DR services, thanks to their higher flexibility and the absence of technical minimum, for each time step t. The bid adjustment process for DT units is described by means of the graphical representation shown in Fig. 1.4, where the numbers represent the clearing order of bids.

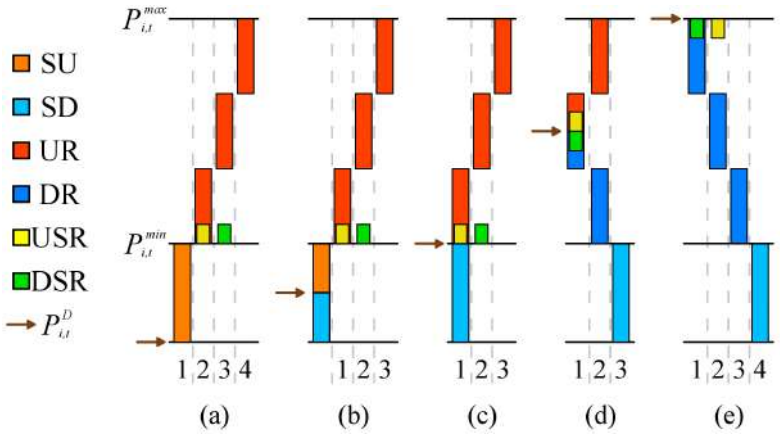

Figure 1.4: Bids' clearance order: not cleared unit (a), unit cleared below the technical minimum (b), unit cleared at the technical minimum (c), unit cleared between the technical limits (d), unit cleared at the rated power (e).

In particular, case (a) represents a DT unit not cleared in DAM, and the first bid that could be cleared in ASM is the SU, followed by the first UR step and the USR bids, whereas the DSR bid can be cleared only if the DT unit is above the technical minimum, and the other UR bid steps can be cleared only after using up the previous bid step. Case (b) is similar to case (a); however, the DT unit is cleared below the technical minimum, and the SU bid, up to the technical minimum, or the SD bid, down to zero, must be cleared to comply with the unit constraint. The SU and SD bids are not numbered because the acceptance of one of the two bids is mandatory. Instead, case (c) shows the condition of a DT unit cleared at technical minimum, pointing out the possibility to be shut down, by clearing the SD bid, or to

provide upward services, as first action. In case (d) the DT unit is dispatched within its minimum and maximum power levels allowing the unit to clear UR or DR bid along with both SR bids. Finally, in case (e) the unit is cleared at its rated power, hence the first bids that can be cleared are the first DR step and DSR, while the following DR step bids can be cleared only after using up the previous one.

In order to evaluate the power flows ($F^D_{b,t}$) deriving from DAM schedules at each time step t of the considered time horizon, the DCLF procedure is carried out [53]. Moreover, PTDFs ($S_{n,b}$) are calculated to quantify how an incremental change in the nodal active power ΔP_n affects the branch power flows [54], and to keep generality, PTDFs are calculated by a distributed slack bus DCLF [55], considering all generation nodes as slack buses.

1.4.4.3 ASM optimization problem

In the nodal ASM optimization problem, assuming TSO viewpoint, the ASM bidding units are redispatched taking into account UC and network constraints to be compliant with SRR procurement and load and RES forecast update. The problem is solved each day ($\forall\, t \in \Omega^T$) over a yearly horizon, composed of N^D days. To this purpose, the objective function f_d aims at minimizing the bid service costs, along with possible load shedding (LS) and RES curtailment (RC) penalties over all time intervals of the day, as follows:

$$f_d = \tau \cdot \sum_{t=1}^{N^T} (C^R_t + C^{UD}_t + C^{SR}_t + C^{LS}_t + C^{RC}_t) \tag{1.12}$$

where each term of the objective function is defined as:

$$C^R_t = \sum_{i \in \Omega^D} \left(\sum_{s=1}^{N^S_i} c^{\uparrow}_{i,s,t} \Delta P^{\uparrow}_{i,s,t} - \sum_{s=1}^{N^S_i} c^{\downarrow}_{i,s,t} \Delta P^{\downarrow}_{i,s,t} \right) \tag{1.13}$$

$$C^{UD}_t = \sum_{i \in \Omega^{DT}} \left(C^{su}_i z^D_{i,t} z^{mu}_{i,t} + c^{su}_{i,t} P^{su}_{i,t} z^{su}_{i,t} - c^{sd}_{i,t} P^{sd}_{i,t} z^{sd}_{i,t} \right) \tag{1.14}$$

$$C^{SR}_t = \sum_{i \in \Omega^{DT}} (c^{sr\uparrow}_{i,t} P^{sr\uparrow}_{i,t} - c^{sr\downarrow}_{i,t} P^{sr\downarrow}_{i,t}) \tag{1.15}$$

$$C^{LS}_t = \sum_{n \in \Omega^N} C^{voll} D^{ls}_{n,t} \tag{1.16}$$

$$C_t^{RC} = \sum_{i \in \Omega^R} C^{rc} P_{i,t}^{rc} \tag{1.17}$$

in which C_t^R is the redispatching cost, C_t^{UD} is the difference between SU and SD costs, C_t^{SR} is the SR provision cost with asymmetric bids. In addition, C_i^{su} is the fixed SU cost, accounted only at first SU time-step through the minimum up time (MUT) binary variable. In particular, $P_{i,t}^{su}$ is the minimum positive value between $P_{i,t}^{min}$ and $P_{i,t}^{min} - P_{i,t}^{D}$, whereas $P_{i,t}^{sd}$ is the minimum positive value between $P_{i,t}^{min}$ and $P_{i,t}^{D}$, obtaining $P_{i,t}^{min}$ as in (1.1) for $P_{i,t}^{max}$.

It has to be noted that from TSO perspective, accepted bids for generation decrease (SD, DR, and SR downward) represent an income for the TSO and are assumed negative in the respective equations, whereas accepted bids for generation increase (SU, UR, and SR upward) are expenses for the TSO, along with LS and RC.

For each $i \in \Omega^{DU}$ the DR and UR constraints limit the accepted quantities up to the relevant ASM power bid amount in each step, as in (1.18) and (1.19), respectively, whereas (1.20) allows either UR or DR action:

$$\Delta P_{i,s,t}^{\downarrow} - \overline{\Delta P}_{i,s,t}^{\downarrow} z_{i,t}^{\downarrow} \leq 0, \quad s = 1, \ldots, N_i^S \tag{1.18}$$

$$\Delta P_{i,s,t}^{\uparrow} - \overline{\Delta P}_{i,s,t}^{\uparrow} z_{i,t}^{\uparrow} \leq 0, \quad s = 1, \ldots, N_i^S \tag{1.19}$$

$$z_{i,t}^{\uparrow} + z_{i,t}^{\downarrow} \leq 1 \tag{1.20}$$

For each $i \in \Omega^{DT}$, the DT unit ASM power redispatch is defined as the algebraic sum of the accepted quantities, except for the SR:

$$\Delta P_{i,t}^{A} = \sum_{s=1}^{N_i^S} \Delta P_{i,s,t}^{\uparrow} - \sum_{s=1}^{N_i^S} \Delta P_{i,s,t}^{\downarrow} + P_{i,t}^{su} z_{i,t}^{su} - P_{i,t}^{sd} z_{i,t}^{sd} \tag{1.21}$$

Since the bid types and their size and order for the ASM depend on the DAM output, the following DT unit-state constraints are defined taking into account the unit-state due to ASM clearing $\forall\, t \in \Omega^T$:

$$z_{i,t} \leq a_{i,t} \tag{1.22}$$

$$P_{i,t}^{sr\downarrow} - \Delta P_{i,t}^{A} \leq P_{i,t}^{D} - P_{i,t}^{min} z_{i,t} \tag{1.23}$$

$$P_{i,t}^{sr\uparrow} + \Delta P_{i,t}^{A} \leq P_{i,t}^{max} z_{i,t} - P_{i,t}^{D} \tag{1.24}$$

$$z_{i,t}^{sr\downarrow} \leq z_{i,t} \quad \wedge \quad z_{i,t}^{sr\uparrow} \leq z_{i,t} \tag{1.25}$$

$$P_{i,t}^{sr\downarrow} - P_i^{sh} z_{i,t}^{sr\downarrow} \leq 0 \quad \wedge \quad P_{i,t}^{sr\uparrow} - P_i^{sh} z_{i,t}^{sr\uparrow} \leq 0 \tag{1.26}$$

$$z_{i,t}^{su} \leq z_{i,t} \quad \wedge \quad z_{i,t} + z_{i,t}^{sd} \leq 1 \tag{1.27}$$

$$\sum_{t'=t}^{t+t_{i,t}^{mu}-1} z_{i,t'} \geq t_{i,t}^{mu} z_{i,t}^{mu} \tag{1.28}$$

$$\sum_{t'=t}^{t+t_{i,t}^{md}-1} (1 - z_{i,t'}) \geq t_{i,t}^{md} z_{i,t}^{md} \tag{1.29}$$

$$z_{i,t}^{\uparrow} \leq z_{i,t}^{su} \quad \text{if } P_{i,t}^{D} < P_{i,t}^{min} \tag{1.30}$$

$$z_{i,t}^{su} + z_{i,t}^{sd} = 1 \quad \text{if } 0 < P_{i,t}^{D} < P_{i,t}^{min} \tag{1.31}$$

$$z_{i,t}^{su} = 0 \quad \text{if } P_{i,t}^{D} \geq P_{i,t}^{min} \tag{1.32}$$

$$z_{i,t}^{sd} = 0 \quad \text{if } P_{i,t}^{D} = 0 \tag{1.33}$$

$$\sum_{s=1}^{N_i^S} \overline{\Delta P}_{i,s,t}^{\downarrow} z_{i,t}^{sd} \leq \sum_{s=1}^{N_i^S} \Delta P_{i,s,t}^{\downarrow} \quad \text{if } P_{i,t}^{D} > P_{i,t}^{min} \tag{1.34}$$

where, in (1.22) the unit state is bound by its availability $a_{i,t}$, considered in DAM as well. The minimum and maximum power constraints are defined in (1.23) and (1.24), respectively where the units can provide the SR only if they have suitable upward or downward margins. With (1.25), upward and downward SR can be bid only by active DT, respectively, whereas (1.26) limit the downward and upward SR provision up to the unit SRH. In (1.27) the unit state is consequent to SU and SD cleared bids, respectively, i.e. if the DT unit is started up in ASM it has to be $z_{i,t} = 1$, whereas if the DT unit is shut down it yields $z_{i,t} = 0$. DT units are subject by MUT and minimum down time (MDT) constraints, which limit how frequently units can be started up or shut down over time. These constraints are respectively modelled in (1.28) and (1.29), where $t_{i,t}^{mu}$ ($t_{i,t}^{md}$) is the minimum between the unit MUT (MDT) and the remaining time steps of the day as defined below:

$$t_{i,t}^{mu} = \min\{MU_i, N^T - t\} \quad ; \quad t_{i,t}^{md} = \min\{MD_i, N^T - t\} \tag{1.35}$$

The activation of constraints (1.30)–(1.33) depend on the DAM schedule $P_{i,t}^{D}$, this is explained by exploiting the cases depicted in Fig. 1.4 as well. If it is below $P_{i,t}^{min}$,

the unit is forced in (1.30) to firstly clear the SU bid before the UR ones, as in the conditions (a) and (b), moreover if it is not null the unit must clear either SU bid or SD bid in (1.31), this condition is depicted in (b) where the SU and SD bids are not numbered because the acceptance of one of the two bids is mandatory. If the DAM schedule is greater than $P_{i,t}^{min}$, in (1.32) the SU bid cannot be cleared - as in the conditions (c)–(e) - whereas if the DAM schedule is null, in (1.33) the SD bid cannot be cleared, as in (a). Instead, in (1.34) the SD bid can be accepted only if all the DR bids are cleared, reaching the minimum power, as in the conditions (d) and (e).

Although the optimization problem is solved on a daily horizon, MUT and MDT constraints introduce inter-temporal dependencies on i-th DT unit. Specifically, if a unit is turned on (off) during the ending hours of day $d-1$, it could still be under MUT (MDT) constraint at the beginning of day d.

To enforce constraint continuity between days, two auxiliary parameters are introduced downstream the ASM solution of the day $d-1$, named $t_{i,d-1}^{on}$ and $t_{i,d-1}^{off}$, representing the number of consecutive time steps with $z_{i,t} = 1$ and $z_{i,t} = 0$, respectively, from the last time-step of the day $d-1$. The conditional constraint provided in Algorithm 1 is defined based on d and t, linking $t_{i,d-1}^{on}$ with MU_i and $t_{i,d-1}^{off}$ with MD_i.

Algorithm 1 MUT & MDT Continuity Algorithm

Set $d \leftarrow \Omega^D$
for $i = 1, ..., N^{DT}$ **do**
  Set $t_{i,d-1}^{on}, t_{i,d-1}^{off}, MU_i, MD_i \leftarrow \Omega^{DT}$
  for $t = 1, ..., N^T$ **do**
    if $t_{i,d-1}^{on} = 0$ **then**
      if $t_{i,d-1}^{off} < MD_i \ \wedge \ t < MD_i - t_{i,d-1}^{off}$ **then**
        $z_{i,t} = z_{i,t}^{mu} = z_{i,t}^{md} = 0$
      else
        $z_{i,t}^{mu} - z_{i,t}^{md} = z_{i,t} - z_{i,t-1}$
      end if
    else if $t_{i,d-1}^{off} = 0$ **then**
      if $t_{i,d-1}^{on} < MU_i \ \wedge \ t < MU_i - t_{i,d-1}^{on}$ **then**
        $z_{i,t} = 1 \ \wedge \ z_{i,t}^{mu} = z_{i,t}^{md} = 0$
      else
        $z_{i,t}^{mu} - z_{i,t}^{md} = z_{i,t} - z_{i,t-1}$
      end if
    end if
  end for
end for

Algorithm 2 MUT & Availability Continuity Algorithm

```
Set d ← Ω^D
for i = 1, ..., N^DT do
    Set a^re_{i,d+1}, MU_i ← Ω^DT
    if a^re_{i,d+1} < MU_i then
        for t = 24, ..., 24 − (MU_i − a^re_{i,d+1} + 1) do
            z^mu_{i,t} = 0
        end for
    end if
end for
```

This ensures that $z^{mu}_{i,t}$, $z^{md}_{i,t}$, and $z_{i,t}$ are either fixed to specific values or related through an additional constraint. For the sake of clarity, consider a unit with $MU_i = 4$ and $t^{on}_{i,d-1} = 2$, hence the unit is operating since the last two hours of the day $d-1$ and it must operate for 2 more hours at d. Therefore, at $t = 1$ and $t = 2$, $z_{i,t} = 1$ and $z^{mu}_{i,t} = z^{md}_{i,t} = 0$, whereas for the rest of the day the unit can keep operating or can be shut down.

An additional inter-temporal dependency involves the programmed availability of the i-th DT unit at day $d+1$ and its MUT constraints at ending hours of the day d.

To ensure constraint consistency between MUT at d and availability at $d+1$ a further auxiliary parameter is introduced upstream the ASM solution named $a^{re}_{i,d+1}$ which counts the $a_{i,t} = 1$ at $d+1$ from the beginning of the day up to the first $a_{i,t} = 0$. The implemented rule, provided in Algorithm 2, relates $a^{re}_{i,d+1}$ and MU_i to fix $z^{mu}_{i,t} = 0$. For example, if the i-th DT unit has a programmed maintenance at $a^{re}_{i,d+1} = 2$ and $MU_i = 4$, the unit can be started up to $t = 23$ of d to make MUT compliant with its availability at $d+1$.

For the DH units, the constraints (1.18)–(1.21) are still valid, whereas (1.21) is modified eliminating SU and SD terms. Specific DH unit constraints are, $\forall\, i \in \Omega^H$ and $\forall\, t \in \Omega^T$:

$$E^{lb}_i \leq E^{av}_{i,t} - \tau \Delta P^A_{i,t} \leq E^{ub}_i \tag{1.36}$$

$$-P^D_{i,t} \leq \Delta P^A_{i,t} \leq \min\{P^{max}_i - P^D_{i,t}, (E^{ub}_i - E^{av}_{i,t})/\tau\} \tag{1.37}$$

$$z^{ns}_{i,t} E^{ub}_i/\tau \leq \sum_{s=1}^{N^S_i} \Delta P^d_{i,s,t} + E^{av}_{i,t-1}/\tau \tag{1.38}$$

in which τ represents the duration, in hours, of each time step. The energy balance is limited in (1.36) within the upper and the lower boundaries of the DH basin, (1.37)

defines the limits of the total DH redispatched power where the maximum power is the minimum between the available energy over the time interval and the upper power margin, whereas the minimum power is the opposite of the DAM schedule. DH units do not have a technical minimum and do not provide a secondary reserve, therefore their ASM contribution involves only UR and DR bids. The DH unit stops storing energy when the sum of the available energy and the DR power reaches the upper bound as in (1.38). At each time step t, $E^{av}_{i,t}$ is updated according to the initial available energy ($E^{av}_{i,0}$), the inlet energy ($E^{M}_{i,t}$) and the DAM schedules up to the actual time step t, and the ASM cleared bids until the time step $t-1$ as follows:

$$E^{av}_{i,t} = E^{av}_{i,0} + \sum_{\hat{t}=1}^{t}(E^{M}_{i,\hat{t}} - \tau P^{D}_{i,\hat{t}}) - \sum_{\hat{t}=1}^{t-1}\tau \Delta P^{A}_{i,\hat{t}} \tag{1.39}$$

The RC and LS are limited to an upper bound defined as:

$$0 \leq P^{rc}_{i,t} \leq P^{rt}_{i,t}, \qquad \forall i \in \Omega^{R} \tag{1.40}$$

$$0 \leq D^{ls}_{n,t} \leq D^{rt}_{n,t}, \quad \forall n \in \Omega^{N} \tag{1.41}$$

Finally, network constraints are:

$$\sum_{i\in\Omega^{D}}[P^{D}_{i,t}+\Delta P^{A}_{i,t}]+\sum_{i\in\Omega^{ND}}P^{D}_{i,t}+\sum_{i\in\Omega^{R}}[P^{rt}_{i,t}-P^{rc}_{i,t}] = \sum_{n\in\Omega^{N}}[D^{rt}_{n,t}-D^{ls}_{n,t}], \quad \forall n \in \Omega^{N} \tag{1.42}$$

$$F^{lb}_{b} \leq F^{D}_{b,t} + \Delta F_{b,t} \leq F^{ub}_{b}, \quad \forall b \in \Omega^{B} \tag{1.43}$$

$$\begin{aligned}\Delta F_{b,t} = \sum_{n\in\Omega^{N}} S_{n,b} \Bigg(\sum_{i\in\Omega^{D}} \beta_{i,n}\Delta P^{A}_{i,t} + \sum_{i\in\Omega^{R}} \beta_{i,n}\Delta P^{R}_{i,t} - \\ -\Delta D^{L}_{n,t} + D^{ls}_{n,t} - \sum_{i\in\Omega^{R}} \beta_{i,n} P^{rc}_{i,t} \Bigg), \quad \forall b \in \Omega^{B}\end{aligned} \tag{1.44}$$

$$\sum_{i\in\Omega^{DT}} P^{sr\downarrow}_{i,t} = SRR_{t} \quad \wedge \quad \sum_{i\in\Omega^{DT}} P^{sr\uparrow}_{i,t} = SRR_{t} \tag{1.45}$$

where (1.42) represents the power balance of the system, (1.43) limits the branches power flow up to the upper or lower bound, (1.44) defines the power flow variation according to the PTDF, the redispatched quantities, the curtailed resources, and the forecast update of load demand and of RES productions, whereas (1.45) defines the UR and DR SR amounts to be procured. Particularly, since the DR SR is

an income for the TSO, the equality constraint is required for the SR to avoid an over-reservation.

1.4.5 Test system features

The proposed methodology is applied to the NREL-118 Bus System which includes datasets of load demand and WF and PV production for a leap year with hourly resolution ($N^T = 8784$), along with costs, availability and escalators of the generation mix, and monthly energy availability of the DH units [56–58]. The generation set consists of 327 units for a total installed capacity of 40.5 GW, composed of 11.0 GW combined cycle (CC), 3.6 GW combustion turbine (CT), 2.5 GW steam turbine (ST), 10.2 GW non dispatchable hydroelectric, 8.5 GW DH, 1.0 GW WF, and 3.4 GW of PV, and the remaining is distributed among internal combustion engine (ICE), biomass (Bio) and geothermal (Geo) technologies.

The rated power of DT and DH units is supposed equal to or greater than 10 MW. Therefore, 89 DT are involved in the ASM, as reported in Table 1.3, where per each technology and fuel–natural gas (NG) and oil–the total number, the P_i^{min}, the P_i^{max} along with the steps costs $c_{i,s}$ and the specific SU fixed cost C_i^{su}/P_i^{max} are reported, and the P_i^{sh} is supposed the 6% of P_i^{max}.

Table 1.3: DT unit parameters

Tech.	**n.**	$\boldsymbol{P_i^{min}}$ **[MW]**	$\boldsymbol{P_i^{max}}$ **[MW]**	$\boldsymbol{c_{i,s}}$ **[$/MW]**	$\boldsymbol{C_i^{su}/P_i^{max}}$ **[$/MW]**	**MUT [h]**	**MDT [h]**
CC NG	28	[4.1, 503.9]	[13.5, 943.5]	[24.5, 61.3]	[83.6, 83.7]	[2, 6]	[2, 8]
CT NG	47	[4.5, 81.0]	[15.0, 180.0]	[27.9, 65.7]	[33.9, 109.2]	[1, 8]	[1, 8]
CT Oil	5	[21.4, 22.4]	[71.2, 74.5]	[192.3, 242.3]	31.8	2	2
Geo	1	11.0	22.0	2.7	0	6	6
ST NG	8	[8.5, 57.0]	[106.3, 712.0]	[43.1, 60.0]	79.5	8	12

Moreover, 15 DH units are individuated, and in Table 1.4, P_i^{max}, the features of DH basin (E_i^{ub} and E_i^{lb}) and the inlet energy are described.

For DH units, the 90% of the daily inlet energy is bid to the DAM, where the hourly quantity of the submitted bids follow five different load behaviours as shown in Fig. 1.5, based on [59], the remaining 10% is held for the ASM. For the elaboration of UR and DR bid prices in Section II, an equivalent DAM price bid is supposed to equal the daily median value of the DAM zonal price of the pertaining market zone.

The time-varying factors of the bid adjustment process are shown in Fig. 1.6a and Fig. 1.6b for the selling and buying bids, respectively. They have been obtained by

Table 1.4: DH unit parameters

		DH basin features		DH inlet energy		
DH	$\mathbf{P_i^{max}}$ **[MW]**	$\mathbf{E_i^{lb}}$ **[MWh]**	$\mathbf{E_i^{ub}}$ **[GWh]**	**daily min [h/d]**	**daily max [h/d]**	**yearly [h/y]**
1-2	75.0	300	12.60	1.44 Nov	7.13 May	1701.1
3-4	77.0	308	12.94	2.53 Nov	10.14 May	2517.2
5	82.0	328	13.78	0.30 Feb	7.09 Jun	842.1
6-10	1225.3	4901	205.85	2.13 Mar	15.08 Jul	2797.2
11-12	810.8	3243	136.21	0.59 Jan	8.84 May	1476.2
13	46.7	187	7.85	2.14 Sep	3.75 May	1139.9
14	110.0	440	18.48	1.51 Nov	12.56 May	2314.3
15	140.0	560	23.52	1.92 Nov	15.98 May	2945.5

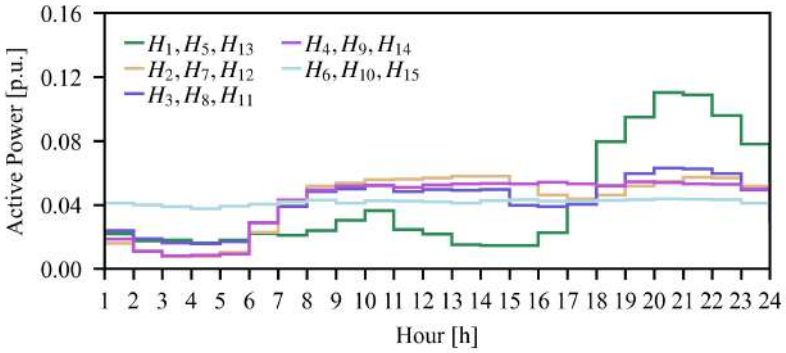

Figure 1.5: DH daily power bid profiles.

processing the hourly Italian market bids, thanks to the similarity of system features in terms of RES impact and the analogous multi-stage market structure by averaging the hourly ratio between the ASM bid prices of each service and the DAM step prices submitted by each market participant. It has to be noticed that, as expectable in a pay-as-bid framework, the selling ASM prices are greater than the selling DAM ones (i.e., time-varying factors for UR, SU and positive SR are greater than 1), in order to make ASM power increase more profitable, whereas the buying ASM prices are mainly lower than the selling DAM ones (i.e., time-varying factors for DR, SD and negative SR are lower than 1), since the buying bids represent an expense for the market participants that should be lower than the marginal production price to ensure a revenue. These average hourly values are therefore assigned to each dispatchable unit considering a gaussian variation with 99.7% confidence interval set at 10% of the value.

In order to allow the activation of RC and LS actions as last resources, the values of C^{rc} and C^{voll} are high enough to represent the most expensive services representing

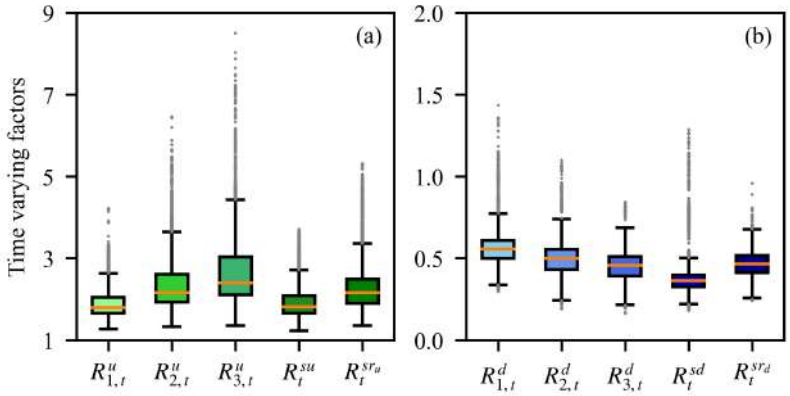

Figure 1.6: Selling (a) and buying (b) bid time-varying factors boxplots.

a cost in the objective function, as follows:

$$C^{rc} = \max\left(c^{\uparrow}_{i,s,t}\right) + 10 \tag{1.46}$$

$$C^{voll} = \max\left(\frac{C^{su}_{i}}{P^{min}_{i}}\right) + 10 \tag{1.47}$$

The load forecast error between DAM and ASM is taken from zonal load [57] and split among nodes through participation factors, whereas RES errors are treated separately for each of the 75 PV units and of the 17 WFs. The maximum, minimum, and average errors of each resource are reported in Table 1.5, noting that load error reaches roughly 10% of peak load, whereas error on PV and WF can reach roughly 40% of installed power. In Table 1.5, the values of the net forecast error (NFE), defined as the difference between total load error and total RES errors, are reported as well.

Table 1.5: Maximum, minimum, and average forecast error values [MW]

	Load	**PV**	**WF**	**NFE**
Max	2987.90	500.82	411.95	3312.48
Min	-3654.28	-1223.80	-391.00	-3667.76
Avg	55.33	-70.01	-15.88	141.21

1.4.6 Result Analyses

The whole framework is implemented in Python-based environment where the DAM and ASM optimizations are developed by means of Pyomo library [60] using Gurobi solver [61] and DIgSILENT PowerFactory is employed for the DCLF and

sensitivity analysis, exploiting the Python API (Application Programming Interface) to automatize the simulation process. Simulations are performed on a computer with 32 GB RAM, 12th Gen Intel® Core™ i9-12900F CPU @ 2.40 GHz, 16 physical cores and 24 logical processors, using up to 24 threads. The daily process is averagely solved within 4 minutes, where the ASM solution represents the highest computational burden with an average elapsed time by roughly 2.5 minutes, in line with the time requirements of SCADA/EMS systems.

1.4.6.1 Elaboration of ASM inputs

The generation schedules yielded by DAM solution, normalized for each technology installed capacity, are reported in Fig. 1.7. It has to be noted that, due to higher availability and lower production costs, CC NG technology is most frequently called to produce, providing 51.48 TWh during the year, followed by DH and CT NG supplying 16.98 TWh and 12.20 TWh, respectively. The total RES contribution amounts to 31.2%, i.e., 30.00 TWh. ST NG and ICE NG turn out to cover the demand peaks, due to higher DAM bid prices. The CT Oil is the most expensive technology, and its bids are not cleared in the DAM. For the remaining technologies, having constant escalators, low price and installed capacity, quite constant power levels are observed. The DAM zonal prices over the year are reported in Table 1.6. Negligible differences among market zones are observed, due to sporadic interzonal congestions (56 occurrences on Zone 1-Zone 2).

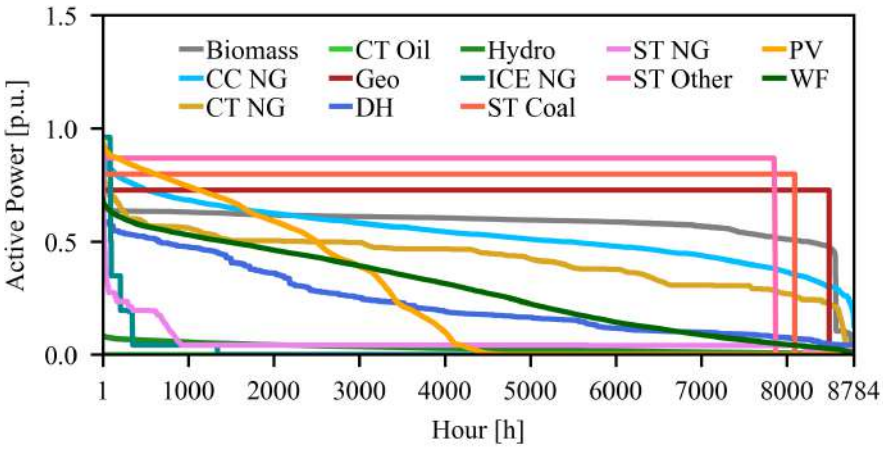

Figure 1.7: DAM dispatched power duration curve.

Table 1.6: DAM zonal prices in $/MWh

Value \ Zone	Zone 1	Zone 2	Zone 3
Maximum	54.72	54.72	54.72
Average	34.75	34.74	34.74
Minimum	27.02	27.02	27.02

The DCLF outcomes show that 11 branches experience DAM overloads, as reported in Fig. 1.8. These are most frequent in branches 31 and 32 since they are close to the most convenient units. Further overloads are detected on contiguous lines 96, 97, and 104.

The SRR values are determined as in [62], and range from 94.4 MW to 302.5 MW according to load demand. The upward (downward) SR margin, USM (DSM), is the sum of the minimum value between the SRH and the upward (downward) margin of each cleared DT unit after DAM solution. During the year, the DSM is sufficient to cover the SRR, whereas for 741 time steps the USM is lower than the SRR, which, in turn, requires SU or DR bid clearances in ASM to fulfil the constraint (1.45).

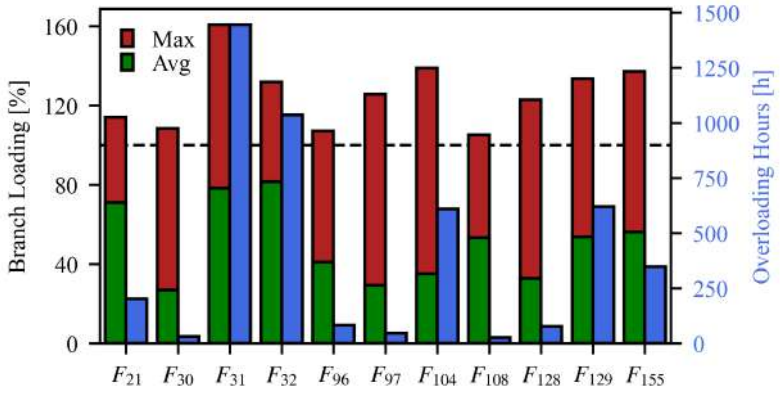

Figure 1.8: Branches overloads after DAM.

1.4.6.2 Yearly ASM results

The NCUCER yearly costs and the redispatched amounts per each service are shown in Fig. 1.9. The yearly TSO disbursement (obtained by summing the objective function (1.12) over the year) is equal to 170.2 M$ due to the higher costs for upward actions with respect to revenues for downward ones. Since the dispatchable units are able to provide the services required by the network, without curtailing any RES production or shedding any load consumption, the system adequacy is proved. It

has to be noted that the most cleared amounts are DR and SU bids, since the former is a revenue for the TSO, whereas the latter is cheaper than UR bids. In fact, UR represents the most expensive term, although the cleared amount is lower than SU.

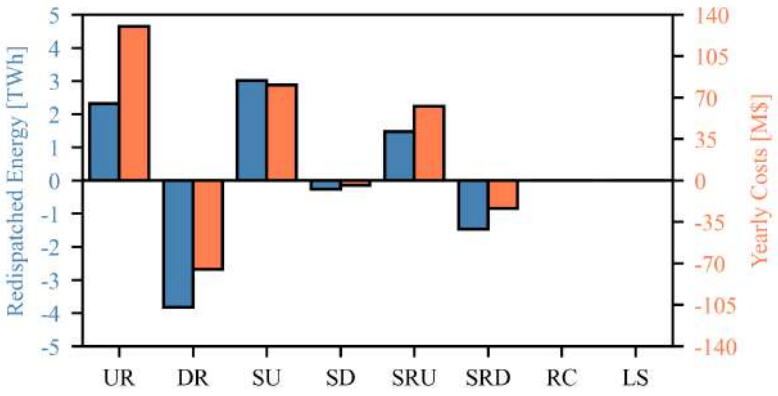

Figure 1.9: Yearly costs and redispatched energy.

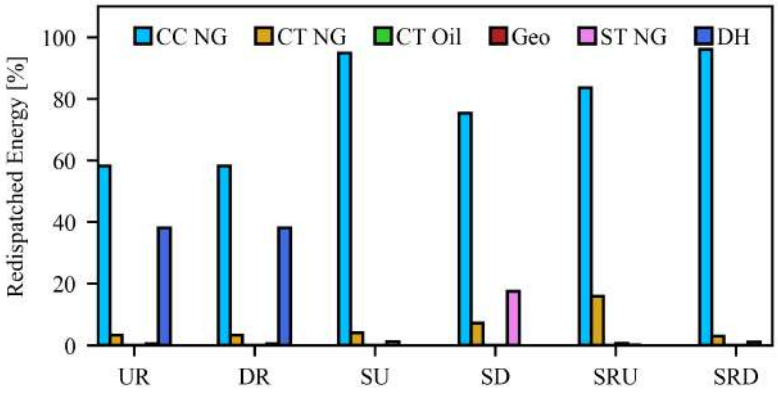

Figure 1.10: Services provided for each technology.

The contributions of each generation technology to service provision are depicted in Fig. 1.10. It can be stated that, CC NG technology is the most exploited thanks to its economic viability, followed by the DH for the UR and DR services. On the other hand, CT NG technology is marginally cleared, mainly providing SRU service due to its higher cost and greater upward and downward availability. Finally, ST NG are mostly cleared for SU and SD due to higher costs.

Regarding the SRR fulfillment, Fig. 1.11a shows the difference between SRR and USM after DAM and ASM, and analogously in Fig. 1.11b for the difference between SRR and DSM. It can be observed that DSM is enough to cover SRR and very slight variation from DAM to ASM is registered. On the contrary, USM in ASM

is increased due to SU and DR clearance, to create a suitable margin to be compliant with SRR constraint–i.e., the illustrated difference is always non-negative.

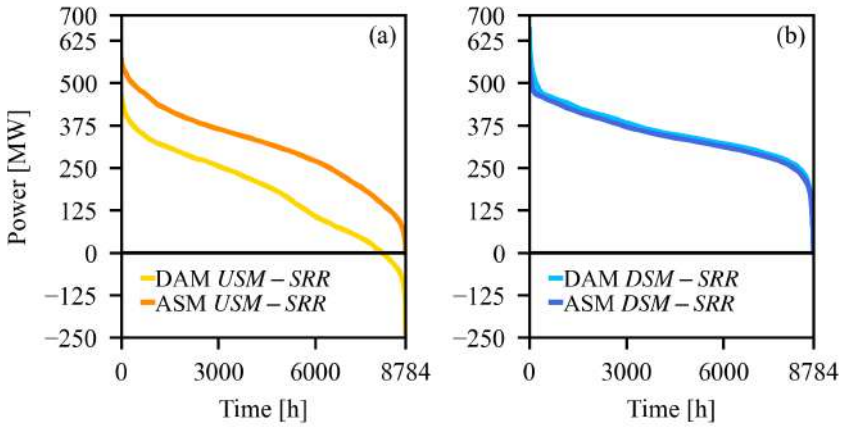

Figure 1.11: SRR and USM difference between DAM and ASM (a) and SRR and DSM difference between DAM and ASM (b).

The number of cleared SU and SD bids in the whole year, for each technology, are reported in Table 1.7.

Table 1.7: Yearly SU, SD occurrences

Tech.	**Total SU #**	**Total SD #**	**Total activation of (1.31) #**	**of which SU #**	**of which SD #**
CC NG	28206	1718	1820	1412	408
CT NG	6176	1200	339	99	240
ST NG	1448	962	64	5	59

It can be noted that the occurrences in which (1.31) is activated represent a quarter of the yearly horizon, and in the majority of cases it is stated for CC NG. This occurs since CC NG represents the most recurrent marginal technology in DAM over year thanks to for its economic viability. As a result, its SU bid is cleared for three quarter of (1.31) activation occurrences. When comparing this condition with the other technologies, the higher SU costs of CT NG and ST NG units imply a greater occurrence of SD with respect to SU.

After ASM, the overloads experienced on the 11 branches are all solved within the maximum loading, as reported in Fig. 1.12. When comparing with Fig. 1.8, the maximum loading after ASM is experienced for less hours with respect to DAM overloads, for all branches, except for F_{31} and F_{129} due to the clearance of cheapest units with a concordant PTDF with the branch flows.

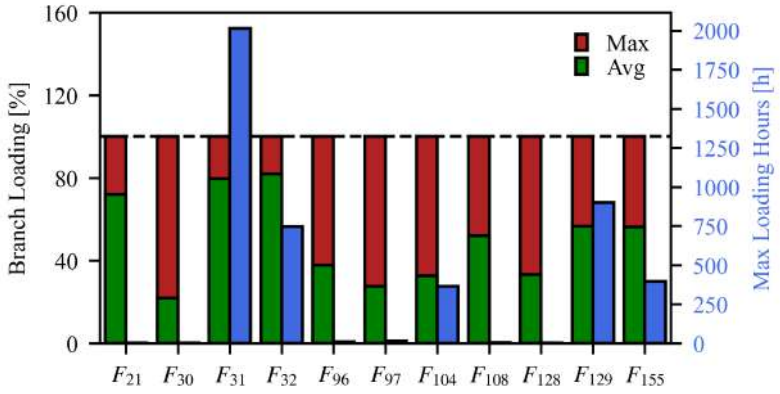

Figure 1.12: Loading after ASM of branches overloaded in DAM

The heat maps depicted in Fig. (1.13a) and Fig. (1.13b) provide the yearly profile of the total upward and downward redispatched energy, respectively, highlighting the hours of the days with highest and lowest movements.

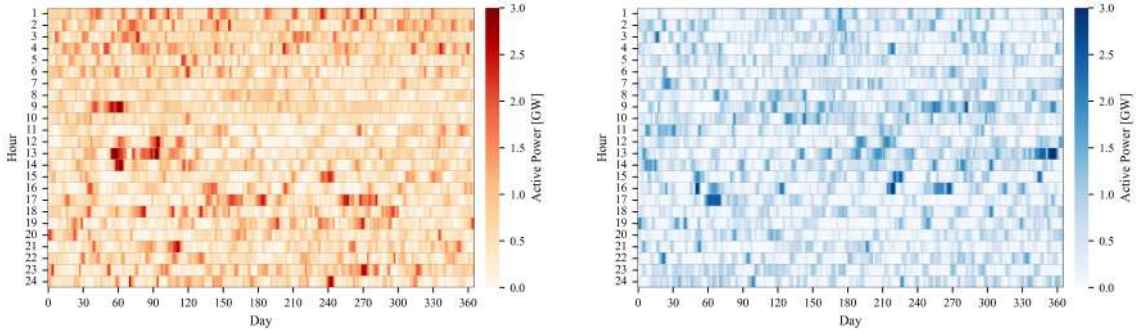

(a) Yearly heatmap of UR + SU cleared amounts.

(b) Yearly heatmap of DR + SD cleared amounts.

Figure 1.13: Yearly heatmaps of upward and downward cleared amounts.

In particular, from Fig. 1.13a can be inferred that in weeks 9 (days 57-63) and 2 (days 8-14) the highest and lowest upward cleared amount are stated, accounting to 98.5 GWh and 55.1 GWh, respectively. Instead, from Fig. 1.13b can be observed that in weeks 43 (days 295-301) and 15 (days 99-105) the highest and lowest downward cleared amount occur, amounting for 98.5 GWh and 55.1 GWh, respectively.

1.4.6.3 Weekly ASM results with the most redispatched energy

In addition to the yearly analysis, the results depicted in Fig. 1.14 show the details of the week 9 with the highest redispatched energy among all services, accounting to 210.2 GWh. In particular, Fig. 1.14a depicts the hourly NFE along with the total cleared amounts of UR, DR, SU, and SD, observing some intervals with total

redispatched amount equal to or greater than the NFE due to the need for mitigation of network or units constraints. Particularly, in Fig. 1.14b and 1.14c the UR and DR and the SU and SD cleared amounts are provided, respectively per technology, remarking the economic driver of the ASM, since the most expensive units, i.e. ST NG followed by CT NG, are mainly redispatched to reduce their production or to be shut down for the higher remuneration. ST NG units are mainly shut down due to the greater MUT and MDT values, CT NG SU bids are cleared only with positive NFE along with the clearance in DAM, whereas CC NG are shut down only with negative NFE lasting for a time window comparable with the MDT value. However, some SU and SD cleared bids depend on the activation of (1.31), as highlighted in 1.14d, observing that only for the CC NG the SU bid is cleared even for negative NFE. This technological feature is mirrored in SRR provision as well, observing in 1.14e, that ST NG provides the downward SR only in the hours with a cleared amount in DAM, while fulfilling the MUT. Finally, Fig. 1.14f and Fig. 1.14g depict the DAM overloaded line number and power, respectively, stating that the hours with the greatest redispatched power require overloads mitigation, whereas the hours with a redispatch slightly higher than the NFE are present to comply with MUT and MDT constraints.

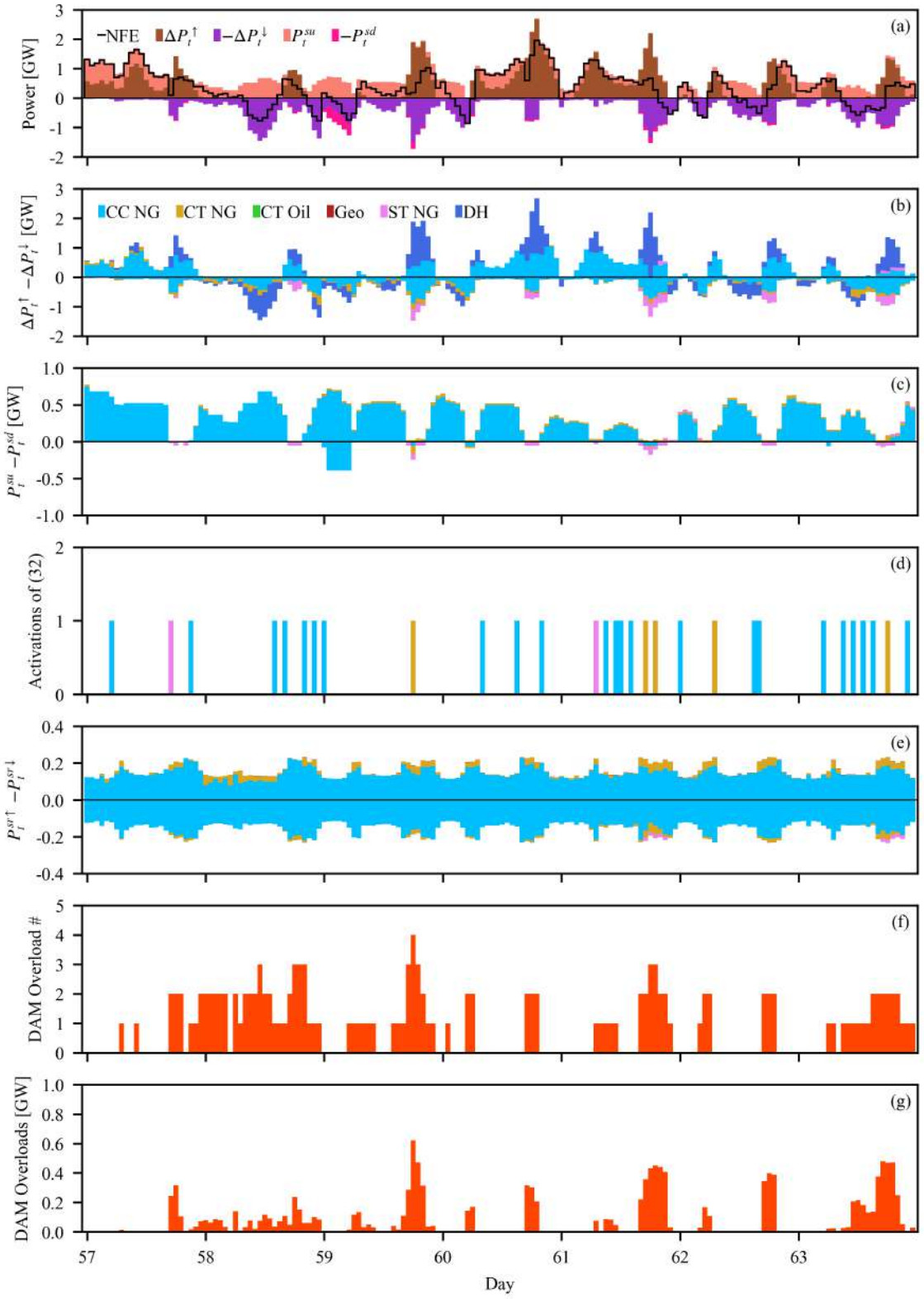

Figure 1.14: Weekly optimal results with greatest redispatched energy.

1.4.7 Remarks and future developments

In this chapter, a NCUCER optimization problem has been employed to efficiently redispatch power from zonal DAM to nodal ASM to meet load and RES forecast updates complying with UC and network constraints, according to European approach. The sequential interaction of the two markets has been managed with a bid adjustment process for ASM, to fit the units' technical limits with respect to the DAM schedules. The proposed procedure has proved to successfully handle RES variability, unit state constraints, and network requirements (e.g., SRR or overloads) with a reasonable computational burden. The developed approach provides a useful tool for evaluating the services needed by the TSOs to comply with the security requirements of the system. The tool could be a promising solution for all ASM participants: the TSO could derive indications about network criticalities and total occurred costs, whereas the generating units could evaluate bidding strategies able to satisfy both network service requirements and operating points. Possible future work could deal with the provision of tertiary reserve services into NCUCER optimization, as well as security-constrained approach. Furthermore, the framework could be extended by adopting stochastic or robust optimization techniques to better hedge against load and RES uncertainties. Finally, the integration of emerging flexibility resources, such as Battery Energy Storage Systems and demand-side management, represents a key step to further enhance the economic efficiency and security of the proposed methodology.

Chapter 2

Optimal Transmission Grid Assets Maneuvering for Improving Voltage Profile

The deep penetration of renewable energy sources (RES) in power systems is increasingly influencing electricity markets and the physical operations of transmission networks. Besides the environmental and climate benefits, RES volatility and aleatory behaviour, combined with the consequent difficulties in control, might lead to voltage issues, which could be particularly critical when the grid lacks reactive power support. In this context, transmission system operators (TSOs) are called upon to make decisions about the use of available grid assets, such as compensating shunt devices and tap-changing transformers. In addition, transmission line switching can be adopted to provide further reactive power control resource. However, it is often difficult to determine which network assets should be enabled within the operation time requirements. Therefore, in this chapter, an Optimal Reactive Power Flow (ORPF) tool for operators is formulated and proposed, including both shunt devices and transmission line switching, as well as the adjustment of transformers' tap settings. The optimization problem is solved by resorting to a genetic algorithm to account for network model nonlinearities. In order to improve inclusiveness and replicability, the whole tool was developed exploiting open-source libraries only. Numerical tests are carried out on a modified IEEE 118-Bus Test System.

2.1 Background

Regulating voltage in electrical transmission systems is essential for the quality of supply and the correct functioning of the loads and all other devices connected to the network, as well as for operational security and system stability. In fact, grid operators are well aware that excessively high voltages values could damage the insulation of the equipment, and encourage the tripping of the generation units. Conversely, too low voltages cause stalling and overheating, voltage instability phenomena and consequent blackouts. Therefore, inadequate reactive power support results in voltage drops and in the worst cases voltage collapse, since generation units would tend to trip due to the protections intervention. For these reasons, transmission system operators (TSOs) provide adequate voltage regulation and reactive power flow management services. In particular, the latter must be correctly dispatched since it involves additional losses respect to the transported active power.

In the past, voltage regulation was mainly provided by conventional power plants (CPPs) because the technology of renewable energy sources (RES) was not well enough established in terms of regulation capability. In recent years, however, as planning activities and connection requests from renewable plant owners have increased, there have been continuous updates in grid codes about the necessary requirements and how RES should provide voltage and reactive power regulation services [63–66]. For instance, modern photovoltaic (PV) plants are equipped with smart inverters enabled with communication capabilities that allow the coordinated operation to offer services such as controlling voltage by appropriately setting the reactive power production [67]. However, the TSO provides a voltage schedule for generators which are expected to adjust reactive power output to keep the voltage close to the setpoint level. Therefore, in a liberalized market context, TSOs do not access such resources to control voltage and reactive power, which are entrusted to the producers, only being able to use their own grid assets performing maneuvers that do not impact operating costs.

Among the TSO-owned network assets to support voltage control, there are mainly synchronous compensators, capacitor banks and shunt inductive reactors, and other Flexible AC Transmission Systems (FACTS) devices. On-Load Tap Changer (OLTC) transformers are also used to regulate the voltage at one side, usually on the higher voltage winding, because for the same transferred power, the currents are

lower reducing wear and the risk of arcing during tap changer commutation.

In addition, TSOs may implement operating maneuvers such as transmission line switching (TLS) as further reactive power control resource. Although this is not a very common practice for stability reasons, removing the capacitive effect of unloaded overhead transmission lines by TLS results in benefits especially under low load conditions (e.g., at night), when the more meshed portions of the network experience voltage rise [68]. This problem becomes particularly critical especially when there is a surplus of RES production and demand is low. During daytime peak hours, instead, the lines are more loaded, longitudinal inductive effects and voltage drops prevail.

Since it is not always easy to effectively control such grid assets within the operation time requirements, TSOs can make use of software tools such as Optimal Reactive Power Flow (ORPF) as support in making decisions. Numerous formulations of the ORPF problem exist in the literature, well known for its difficult resolution due to Mixed-Integer Non Linear Programming (MINLP). The state-of-the-art comprises analytical formulations [69–72] and others based on genetic and metaheuristic algorithms [73–76]. Nevertheless, TLS is not included in any of these formulations and is usually addressed separately as an extension of Optimal Power Flow (OPF) [**?**], or modeled according to DC approximations within the Unit Commitment proving useful in reducing costs [77].

In this work, TLS is incorporated into the formulation of the proposed ORPF problem, which also includes both shunt devices and OLTC transformers as VAR control resources. In a framework in which the European Union intends to reach the 2030 emission reduction targets [78], scenarios with different RES penetration rates were purposely created on a modified IEEE 118-Bus Test System. The optimization routine is solved by resorting to a suitably customized genetic algorithm (GA) to account for network model nonlinearities and address the difficulties derived from the high combinatoriality. The whole methodology was developed exploiting open-source software tools only with the intent of fostering inclusiveness and replicability.

2.2 Integration of Line Switching Actions into an Optimal Reactive Power Flow Formulation

Let us consider the single-phase, balanced equivalent network circuit of a transmission network consisting of the following sets of grid elements: $\mathcal{N}$ denotes the set of the buses, $\mathcal{B}$ the set of branch elements distinguished into transmission lines ($\mathcal{L}$) and transformers ($\mathcal{T}$). The sets $\mathcal{G}$, $\mathcal{D}$, and $\mathcal{S}$ encompass generators, loads and shunt devices, respectively.

The general MINLP formulation for the ORPF problem is stated below:

$$\min_{\boldsymbol{x},\boldsymbol{u}} f(\boldsymbol{x},\boldsymbol{u}) \tag{2.1}$$

subject to:

$$h(\boldsymbol{x},\boldsymbol{u},\boldsymbol{p}) = 0 \tag{2.2}$$

$$g(\boldsymbol{x},\boldsymbol{u},\boldsymbol{p}) \leq 0 \tag{2.3}$$

where the objective function (2.1) is a mathematical expression that may include the dependent variables $\boldsymbol{x}$ and/or the control variables $\boldsymbol{u}$ (both continuous and discrete), while (2.2) and (2.3) represent the equality and inequality constraints respectively, typically nonlinear functions of the optimization variables and problem's parameters $\boldsymbol{p}$.

In the proposed model, $\boldsymbol{u}$ includes only integer variables, such as the shunt devices' connection status $\sigma_s \in \{0,1\}$ and their tap position $\tau_s \in \mathbb{N}$ for voltage regulation, the transformers' OLTC positions $\tau_t \in \mathbb{Z}$, and the transmission lines' connection status $\sigma_l \in \{0,1\}$. The real variables $\boldsymbol{x}$ are the bus voltage magnitude v_i, the reactive power produced by CPPs Q_g, the current flowing through the in service lines I_l and the transformers I_t.

In classical ORPF models, generators' voltage setpoints are considered as additional real control variables, as well as their active power output [69–75]. However, TSOs do not own the generation facilities except for those resources purchased in the balancing market to ensure system stability in critical situations [79]. Hence, these quantities are usually known downstream the operation planning phase, and the operators tend to maneuver proprietary grid equipments without impacting the operating costs. For this reason, in addition to the active and reactive load demand

and RES power production, known parameters $\boldsymbol{p}$ of the proposed formulation include also the generators' active power production and their voltage setpoints with respect to their previously scheduled availability $\gamma_g \in \{0, 1\}$.

The objective function aims to minimize the bus voltage constraint violations, thus it is modeled as the following penalty function:

$$\min_{\sigma_l, \sigma_s, \tau_s, \tau_t} f(v_i) = \sum_{i \in \mathcal{N}} (v_i - \bar{v_i})^2 \tag{2.4}$$

where:

$$\bar{v_i} = \begin{cases} v_i^{max} & \text{if } v_i > v_i^{max} \\ v_i^{min} & \text{if } v_i < v_i^{min} \\ v_i & \text{if } v_i^{min} \leq v_i \leq v_i^{max} \end{cases}$$

subject to:

$$P_i = G_{ii} v_i^2 + \sum_{j \in i, j \neq i} v_i v_j (G_{ij} \cos\theta_{ij} + B_{ij} \sin\theta_{ij}), \quad \forall i \in \mathcal{N} \tag{2.5}$$

$$Q_i = -B_{ii} v_i^2 + \sum_{j \in i, j \neq i} v_i v_j (G_{ij} \sin\theta_{ij} - B_{ij} \cos\theta_{ij}), \quad \forall i \in \mathcal{N} \tag{2.6}$$

$$\sigma_s \leq \tau_s \leq \tau_s^{max} \sigma_s, \quad \forall s \in \mathcal{S} \tag{2.7}$$

$$\tau_t^{min} \leq \tau_t \leq \tau_t^{max}, \quad \forall t \in \mathcal{T} \tag{2.8}$$

$$Q_g^{min} \gamma_g \leq Q_g \leq Q_g^{max} \gamma_g, \quad \forall g \in \mathcal{G} \tag{2.9}$$

$$I_l \leq I_l^{max} \sigma_l, \quad \forall l \in \mathcal{L} \tag{2.10}$$

$$I_t \leq I_t^{max}, \quad \forall t \in \mathcal{T} \tag{2.11}$$

$$\sum_{l \in \mathcal{L}} \sigma_l + |\mathcal{N}^*| + |\mathcal{T}| - |\mathcal{N}| + 1 \geq 0 \tag{2.12}$$

The quadratic function (2.4) allows compliance with operational limits for voltage magnitude to be treated as a hard constraint. In fact, if all the voltages are within their own boundaries (v_i^{min}, v_i^{max}), it converges to its minimum value which is zero. At the same time, infinitesimal values of (2.4) imply negligible constraint violations, therefore the corresponding solutions can be equally considered acceptable.

The equality constraints (2.5) and (2.6) represent the AC Load Flow (ACLF) power balance nonlinear equations, where P_i and Q_i are the net active and reactive

power injections at bus i, G_{ij} and B_{ij} the real and imaginary parts of $(i,j)^{th}$ element of the nodal admittance matrix (dependent on control variables), $\theta_{ij} = \theta_i - \theta_j$ the voltage angles difference between two adjacent buses (i,j).

The constraint (2.7) limits the tap position of each shunt device to the maximum allowed value when it is called to be in service ($\sigma_s = 1$). Note that a shunt device does not provide contribution when $\tau_s = 0$, so the use of the binary variable σ_s could be avoided. Furthermore, (2.8) limits the tap position of each OLTC transformer, (2.9) ensures the respect of the generators' reactive power limits. Constraints (2.10) and (2.11) are considered so that there are no overloads on the branch elements, especially if some TLS maneuvers become necessary.

Finally, since the transmission network is operated with a meshed topology and TLS can lead to unsupplied buses or islanding, (2.12) ensures that the network topology is at the worst radial [80], and consequently the number of open transmission lines is constrained to the number of cycle basis that can be graphed in the network barring any isolated nodes ($\mathcal{N}^*$). Only connected solutions will be considered valid, with the exception of disconnected ones characterized by only unsupplied buses with no generation or load installed.

2.3 Genetic Algorithm Implementation

This section shows the implementation procedure of the GA used to solve the ORPF problem. As depicted in Fig. 2.1, once the initial topology and network scenario are known, any bus voltage violations (VVs) are detected by means of an ACLF that could emulate a state estimator (SE) in a control center. In case this occurs, the ORPF problem is executed to optimally determine which TSO's VAR control resources should be enabled in order to keep the voltage within the allowed limits for secure operation. To address the combinatoriality of the problem, the solution search space is first reduced to select candidate VAR control resources based on which nodes experience VVs. This is reasonable considering that voltage issues are handled locally and each control center is responsible for operating a defined portion of the network.

As in all GAs, the ORPF routine begins with an initial population sampling of N_{pop} individuals, where each individual (Fig. 2.2) is a vector containing the control variables $\boldsymbol{u}$ and represents a possible solution of the problem.

Then, an ACLF calculation is performed for each individual so that the objective function (2.4) can be computed and compliance with constraints verified. In subsequent stages, the population is updated according to the genetic operators' of selection, crossover, and mutation generating new offsprings of individuals in which the best replaces the worst until a stop criterion is met.

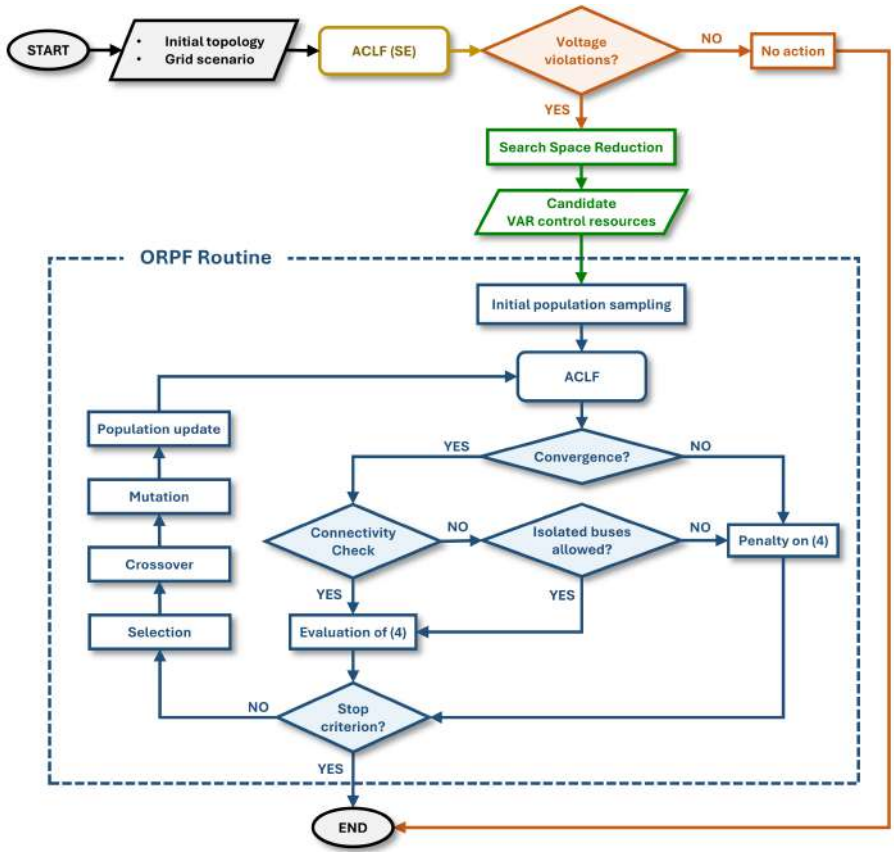

Figure 2.1: ORPF GA solution method [1].

$\sigma_l^{(1)}$	$\sigma_l^{(2)}$	...	$\sigma_l^{(N_L)}$	$\tau_s^{(1)}$	$\tau_s^{(2)}$	...	$\tau_s^{(N_S)}$	$\tau_t^{(1)}$	$\tau_t^{(2)}$	...	$\tau_t^{(N_T)}$

Figure 2.2: Representation of a generic individual from the initial population [1].

2.3.1 Search space reduction (SSR)

Once any VVs are detected by the SE, the involved nodes are included in the set Ω_V. From the graph related to the initial topology of the network, the matrix $\boldsymbol{M}$ of topological distances between buses can be obtained [81, 82], whose elements are natural numbers indicating the shortest distance between a source bus and all other

buses connected to it. The result is a $|\mathcal{N}| \times |\mathcal{N}|$ symmetrical diagonal matrix whose elements on the main diagonal are null. Having fixed a maximum topological distance d^{max}, a submatrix $\boldsymbol{M_V} \subset \boldsymbol{M}$ is considered, where the rows correspond to the nodes of Ω_V. Then, $\forall i \in \Omega_V$, nodes $j \in \Omega_{d^{max}}$ with topological distance $0 \leq d_{ij} \leq d^{max}$ are identified. Lastly, candidate VAR control resources are grouped into three distinct sets: candidate shunt devices are those installed on the buses affected by voltage violation and neighboring nodes within d^{max}, while candidate transmission lines and OLTC transformers are sought among the graph's edges connecting i and j.

2.3.2 Initial population sampling

Usually the initialization of a population of individuals is based on random sampling mechanisms, however, this can lead to solutions that are far from the desired optimum requiring a large number of iterations to reach convergence. For this reason, a simple method is proposed to quickly discard solutions that are worse than the initial operating condition during the GA execution.

Among the N_{pop} individuals, the former corresponds to the values of $\boldsymbol{u}$ relative to the very first ACLF/SE calculation. The remaining $(N_{pop} - 1)$ individuals are generated based on these simple criteria:

1. Concerning TLS maneuvers, only one new opening maneuver is randomly allowed in each individual with respect to any lines already disconnected in the initial topology, only one reclosing maneuver, or no action.

2. Regarding shunt devices, reactors are activated upon violation of v_i^{max} and capacitors upon violation of v_i^{min}. Compensation elements installed on non-violated buses are not activated at this stage.

3. OLTC transformers are adjusted by randomly varying the tap position τ_t by at most one step up or down from the neutral tap position $\bar{\tau}_t$ with respect to (2.8).

2.3.3 ACLF, objective function and constraints evaluation

Having obtained the initial population and known the scenario parameters $\boldsymbol{p}$ (generated active power, generators' voltage setpoints, load demand, active and reactive

RES production), an ACLF routine is run, (2.4) can be calculated for each individual, and compliance with (2.7)-(2.12) is checked.

According to the priority order of control adjustments in [83], the generators reactive power adjustments takes precedence. Therefore, compliance with constraint (8) is facilitated by allowing the downgrading of CPPs from *p*-*v* to *p*-*q* in the ACLF routine. In this way, the generator voltage setpoints can vary from the reference value only if reactive power limits cannot be met, without the need to include them explicitly as decision variables.

It is worth noting that an ACLF calculation may not converge, therefore, combinations among the control variables that prevent convergence are strongly penalized by setting the objective function and constraint relations equal to $w_{nc} \cdot k$, where $w_{nc} \in \mathbb{N}$ is a high weight factor and $k \in \mathbb{N}$ denotes the current offspring in the GA.

Since TLS could result in unsupplied buses or islanding, a network connectivity check is performed downstream the ACLF. Even in such cases, unconnected solutions are still penalized with a weight factor $w^* < w_{nc}$. Only solutions that make unsupplied buses with no generation or load installed can be accepted and not penalized, taking into account that no voltage is applied on an isolated bus and therefore $v_i^{min} = 0, \forall i \in \mathcal{N}^*$.

2.3.4 Selection and survival criteria

In a simple GA, the individuals are often sorted by their fitness function, and survival of the fittest is applied. However, in the transition from one offspring to the next, individuals need to be properly selected to participate in mating. In order to improve the convergence, the binary tournament selection method [84] is implemented: given a subset of individuals in the population, individuals are compared two by two randomly. Based on their fitness, the best individual is selected as the winner of the tournament in order to be counted in the next phase of crossover.

2.3.5 Crossover and mutation

When the parents are selected, the crossover stage can start. This operator combines the genetic information of two parents to create one or more new individuals that could have better fitness than their parents. Among the existing techniques, Simulated Binary Crossover (SBX) [85] was chosen because it is capable of handling discrete

decision variables.

The phase of mutation helps to increase the diversity in the population and it is performed after that new individuals are created through the crossover. In particular, Polynomial Mutation (PM) was adopted as it works well together with the SBX.

Crossover and mutation are operators that work with probability distribution functions p_c and p_m, respectively. These are typically kept constant during the GA such that $p_m < p_c$, i.e. fewer individuals are subject to mutation than to crossover. This is because crossover promotes exploitation of the best current solutions, combining them to generate potentially better offspring, while mutation is useful to avoid getting stuck in local optimum introducing random variations.

In this work, an adaptive annealing strategy was tested varying p_c and p_m dynamically depending on the minimum objective function value f^{min} achieved in each population:

$$p_c(f^{min}) = (p_c^{max} - p^o) \cdot e^{-\alpha f^{min}} + p^o \tag{2.13}$$

$$p_m(f^{min}) = p^o - (p^o - p_m^{min}) \cdot e^{-\alpha f^{min}} \tag{2.14}$$

As long as (2.4) does not decrease, p_c and p_m are equal to the initial probability p^o. Having a high decay factor α, when (2.4) starts to decrease, p_c grows exponentially to a maximum value p_c^{max}, while p_m decreases to a minimum value p_m^{min} preventing the best offspring from being affected by counterproductive mutations.

2.3.6 Stop criterion

The proposed GA can be solved by setting a maximum number of times for the generation of a new population. In this work, a stop criterion was implemented based on tolerance in the space of the fitness, constraints and parameters for which the algorithm stops after a certain number of occurrences of an acceptable solution [86].

2.4 Case study

Simulations in different scenarios are carried on a modified IEEE 118-Bus Test System (Fig. 2.3), making some topological arrangements. Compared with the original test case [87], the modified network model still encompasses 118 buses, 99 loads, and 53 synchronous generators. Nevertheless, 39 are CPPs, 8 PVs, and 6 wind farms. The location of RES generators is drawn from [88].

In the base case scenario, the maximum installed generation capacity is 9161 MW, where up to 2756 MW ($\approx 30.08\%$) can be produced from RES. In addition, 3 reactors (bus 9, 26, 87) and 2 additional shunt capacitors (bus 52, 118) were installed for a total of 19 on/off shunt devices (5 reactors and 14 capacitors with $\tau_s^{max} = 1$).

The number of transformers remained unchanged at 13, all equipped with OLTC installed on the highest voltage winding with $\bar{\tau}_t = 0$ as rated tap position. The OLTC position can vary between $\tau_t^{min} = -8$ and $\tau_t^{max} = +8$ in order to provide a total of 17 tap positions. Finally, 9 new transmission lines were considered for a total of 179.

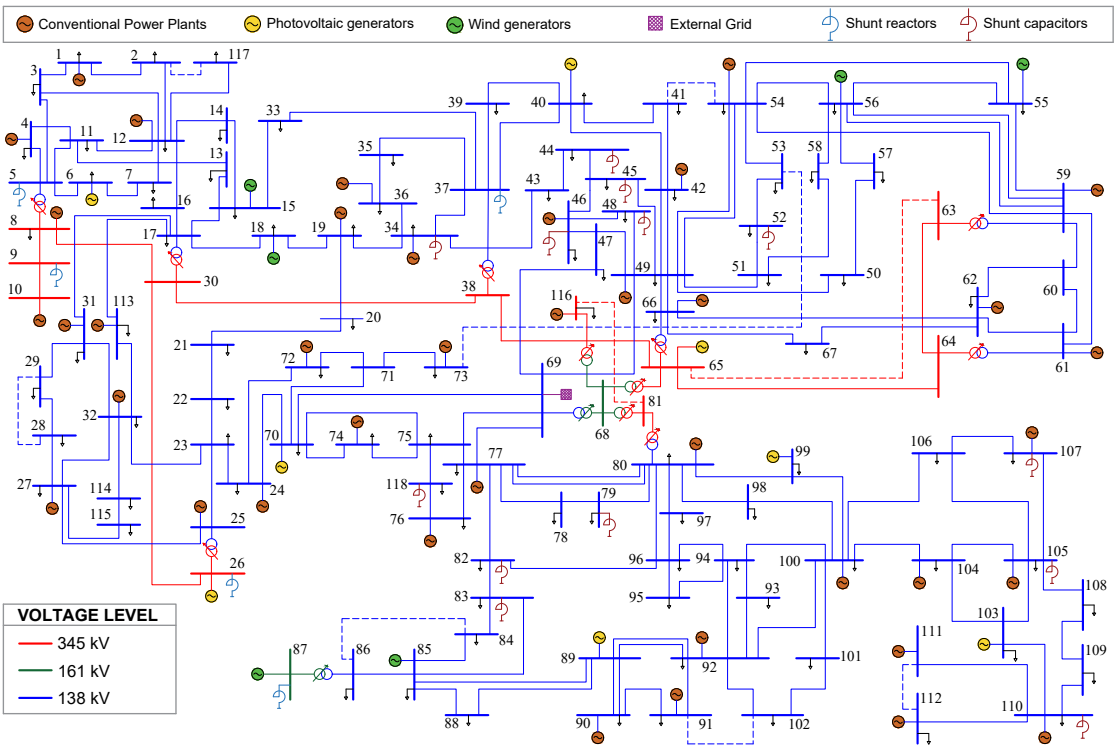

Figure 2.3: Modified IEEE 118-Bus Test System with RES in the base case scenario (the dashed transmission lines are the 9 new links added in the test case) [1].

2.4.1 Data gathering for scenarios creation with voltage violations

In order to simulate the network in different operating conditions, known the bus load participation factors, hourly load profiles for a leap year were obtained assuming that all loads are ohmic-inductive with a power factor of 0.95. Therefore, load shape

curves have been retrieved from the profiles of the test case described in [56] and available in [57]. The same method was used to model the hourly profiles of PV and wind active power generation considering the respective generation participation factors calculated with respect to the maximum capacity.

For each time step, the active power produced by generators is firstly scheduled by means of consecutive OPF routines, as well as the CPPs' voltage setpoints. While RES are dispatched at zero cost, CPPs are required to produce energy according to the quadratic cost curves obtainable by considering the cost coefficients in [87]. The reactive power limits of RES are determined by considering a constant power factor of 0.95 having set the active power.

Therefore, 8784 OPF routines were performed considering that the bus voltage amplitude may vary between ±15% with respect to nominal voltage so that any VVs could be resolved with the proposed ORPF. The rating of all branch elements is derived from [89].

2.4.2 Critical scenarios identification

From the OPF operating conditions, 4 possible development scenarios were created by increasing RES penetration from the base case (a) according to the energy transition goals proposed by the Italian Energy and Climate Plan (PNIEC). In fact, expansions and connection requests of new RES plants are expected in next years, reaching a RES penetration rate of 47.4% in 2025, and up to 63.4% in 2030 [78]. Therefore, in the absence of real data, a development scenario (b) with 40.01% installed RES is achieved by increasing the size of RES plants already installed by 55%. Other two scenarios (c) and (d) are created by further expanding the capacity of these plants and converting some CPPs to renewables.

The following 3 operating conditions are determined for each development scenario considering the load demand unchanged, since they are representative of system operation and challenging for the solution method:

1. Yearly peak load demand;
2. Yearly minimum load demand;
3. Maximum RES production.

This results in 12 different operating conditions to solve listed in Table 2.1, which reports for each case, the demand coverage from RES, the number of buses affected by VVs, the objective function in the initial condition $f(v_i)^o$, the maximum and minimum voltage detected.

Table 2.1: Analyzed Operating Conditions and Initial OPF Solution

#	**Load [MW]**	**RES [%]**	**# VVs**	$f(v_i)^o$ **[p.u.]**	$\max(v_i)$ **[p.u.]**	$\min(v_i)$ **[p.u.]**
1a	6276.90	25.65	8	$3.35 \cdot 10^{-2}$	1.1500	0.9468
2a	2608.05	13.82	10	$3.98 \cdot 10^{-2}$	1.1443	0.9666
3a	4342.88	58.46	8	$3.36 \cdot 10^{-2}$	1.1503	0.9570
1b	6276.90	38.97	8	$1.76 \cdot 10^{-2}$	1.1500	0.9475
2b	2608.05	20.84	10	$4.70 \cdot 10^{-2}$	1.1500	0.9634
3b	4342.88	81.85	2	$3.39 \cdot 10^{-3}$	1.1182	0.9434
1c	6276.90	46.67	15	$1.87 \cdot 10^{-2}$	1.1500	0.8991
2c	2608.05	32.88	10	$5.27 \cdot 10^{-2}$	1.1500	0.9680
3c	4342.88	99.33	7	$2.53 \cdot 10^{-2}$	1.1500	0.8703
1d	6276.90	58.85	25	$4.26 \cdot 10^{-2}$	1.1500	0.9098
2d	2608.05	70.09	10	$5.27 \cdot 10^{-2}$	1.1500	0.9601
3d	4342.88	102.74	3	$1.33 \cdot 10^{-3}$	1.0962	0.9505

The most common VVs are those for which $v_i > v_i^{max}$, particularly pronounced under low load conditions. On the other hand, voltage instability phenomena could occur in cases where the load requirement is met by a high RES rate and more transmission lines are congested at maximum transport capacity (cases 1c and 3c).

In fact, without considering transmission infrastructure expansion plans, a high RES penetration implies greater difficulty in distributing power flows in the grid despite the reduction in operating costs. This is confirmed by the costs obtained from each OPF, shown in Fig. 2.4.

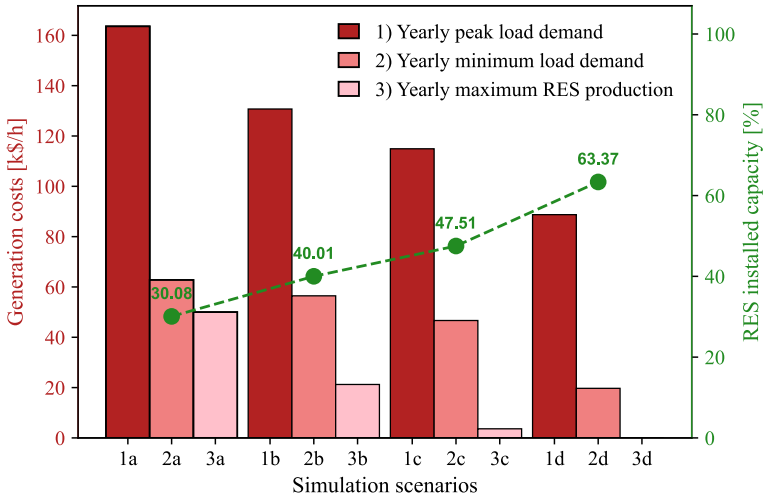

Figure 2.4: Generation costs and RES installed capacity [1].

As can be seen, the scenarios created have gradually decreasing costs as RES production increases, up to the case 3d, in which ideally the entire load is supplied exclusively by RES.

2.4.3 Software tools employed

All numerical simulations were performed on a computer with 16 GB RAM, 11th Gen Intel® Core™ i7-11800H CPU @ 2.30 GHz, 8 physical cores and 16 logical processors.

The ORPF routine is built within *Pymoo* [86], an open-source Python library that offers state-of-the-art global optimization algorithms. Both ACLF and OPF calculations were performed with the appropriate *Pandapower* routines [90] using default settings. Topological search functions, such as $\boldsymbol{M}$ matrix calculation, are also implemented with *Pandapower*, which easily provides access to functions for operations on graphs of the Python library *NetworkX* [91].

In all simulations, the population size is $N_{pop} = 16$, the GA stop criterion tolerances are set at 10^{-9}, while the number of occurrences of a potentially optimal solution can vary from 25 to 50 times.

2.5 Test Results

The proposed ORPF problem was successfully solved in each of the 12 examined operating conditions, considering that the bus voltage amplitude may vary between $\pm 6\%$ with respect to nominal voltage according to [87]. Specifically, in order to evaluate the effectiveness of TLS as a valid remedy against VVs, 3 types of numerical simulations were performed:

- ORPF without TLS;
- ORPF + TLS without SSR and (2.13)-(2.14);
- ORPF + TLS with SSR and (2.13)-(2.14).

While the OLTC transformers regulation is carried out under all the analyzed conditions, the optimal use of shunt devices is summarized in Fig. 2.5 for each kind of simulation. In most cases, shunt reactors are activated to resolve overvoltages. Shunt capacitors, instead, are less used except in cases related to development scenario

(c), which are characterized by higher power flows and lower voltages. Overall, the reactive power reserves provided by these devices proved sufficient in all cases, although their full utilization still results in few residual VVs in cases 1c and 1d.

In addition, TLS maneuvers do not particularly reduce the shunts control effort. These are shown in Table 2.2, in terms of the activation of the binary variable σ_l.

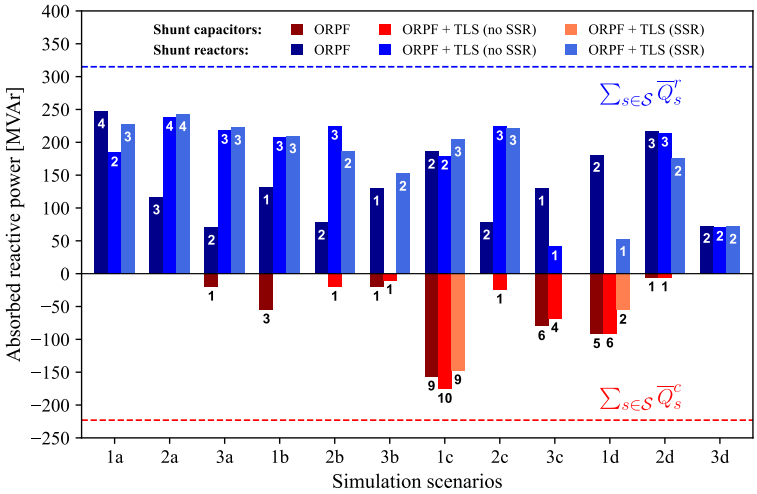

Figure 2.5: Optimal shunt devices utilization (The numbers near the columns indicate the number of shunts in service) [1].

Table 2.2: Optimal Transmission Line Switching Maneuvers

	ORPF + TLS without SSR and (2.13)-(2.14)				**ORPF + TLS with SSR and (2.13)-(2.14)**			
	# σ_l 1/0	# σ_l 0/1	# σ_l 1/1	# σ_l 0/0	# σ_l 1/0	# σ_l 0/1	# σ_l 1/1	# σ_l 0/0
1a	0	1	173	8	4	2	169	7
2a	2	0	171	9	4	0	169	9
3a	2	0	171	9	2	1	171	8
1b	4	0	169	9	1	1	172	8
2b	0	0	173	9	6	0	167	9
3b	2	0	171	9	1	0	172	9
1c	15	5	158	4	12	2	161	7
2c	0	1	173	8	2	0	171	9
3c	22	2	151	7	18	2	155	7
1d	9	1	164	8	6	0	167	9
2d	6	1	167	8	4	0	169	9
3d	1	0	172	9	0	0	173	9

As expected, because TLS maneuvers could weaken the grid, few lines can be disconnected to mitigate VVs except for the development scenario (c), where voltage rises due to the wind generator on the bus 87 are not fully resolved even with the combined action of the shunt reactor and OLTC transformer. In fact, more lines

could be disconnected in an attempt to better redirect the wind power to the loads. However, this makes the number of fully loaded branches increase, and the identified maneuvers may not satisfy the N-1 security criteria, even in cases where the SSR is such that it allows fewer disconnections.

2.5.1 Computational performances

The computational performances comparison of the proposed optimization problem are reported in Table 2.3, where the effects of the SSR when TLS is considered, the crossover and mutation parameters tuning are assessed. The table shows the number of control variables $\boldsymbol{u}$, the optimal values of the objective function (2.4), the number of population generations N_{gen}, and the CPU time for all simulated scenarios and algorithm type performed. The measured CPU times vary depending on the severity of the scenario to be solved and the tuning of the genetic operator parameters. In simulations in which SSR and (2.13), (2.14) are implemented, reductions in CPU time are observed with adherence to the SCADA/EMS systems' time requirements. In addition, the solutions found are of better quality in terms of objective. The presented results, were obtained by setting $p^o = 0.8$, $p_c^{max} = 1$, $p_m^{min} = 0.5$, and $\alpha = \max(1/f^{min}, 128)$. The SSR is performed with $d^{max} = 2$ in all cases except for 3b and 1c, equal to 5 and 7 respectively. Since case 3b is affected by only 2 VVs, too narrow search space leads to worse solutions (as in case 1c).

Table 2.3: Computational Performances Comparison

	ORPF without TLS				**ORPF + TLS without SSR and (2.13)-(2.14)**				**ORPF + TLS with SSR and (2.13)-(2.14)**			
	$\#u$	$f(v_i)$	N_{gen}	CPU time [s]	$\#u$	$f(v_i)$	N_{gen}	CPU time [s]	$\#u$	$f(v_i)$	N_{gen}	CPU time [s]
1a	32	0	32	13.80	214	0	39	29.15	108	0	64	37.21
2a	32	$3.51 \cdot 10^{-5}$	37	17.79	214	0	56	43.25	134	0	64	41.08
3a	32	$5.03 \cdot 10^{-5}$	29	12.97	214	$4.14 \cdot 10^{-4}$	81	64.78	108	0	87	49.12
1b	32	0	78	33.07	214	0	80	60.95	108	0	52	31.60
2b	32	$4.39 \cdot 10^{-5}$	31	14.23	214	0	39	29.20	134	0	54	32.29
3b	32	0	60	26.83	214	$6.63 \cdot 10^{-8}$	46	34.81	121	0	43	28.20
1c	32	$1.29 \cdot 10^{-3}$	137	58.61	214	$1.33 \cdot 10^{-4}$	495	380.59	211	$1.32 \cdot 10^{-3}$	248	195.08
2c	32	$4.10 \cdot 10^{-5}$	31	14.03	214	0	56	44.75	134	0	52	33.11
3c	32	$1.36 \cdot 10^{-4}$	127	61.58	214	$3.08 \cdot 10^{-7}$	359	300.69	122	$1.70 \cdot 10^{-6}$	145	89.21
1d	32	$1.86 \cdot 10^{-2}$	34	15.34	214	$1.60 \cdot 10^{-2}$	195	148.41	174	$1.60 \cdot 10^{-2}$	174	119.27
2d	32	$8.64 \cdot 10^{-4}$	65	28.32	214	$7.39 \cdot 10^{-4}$	119	91.30	144	$7.93 \cdot 10^{-4}$	55	34.67
3d	32	0	26	12.35	214	0	231	195.97	73	0	26	13.35

2.6 Remarks & future research directions

In this chapter, the integration of transmission line switching (TLS) maneuvers into an ORPF MINLP problem formulation for voltage violations mitigation on transmission systems was investigated. By implementing a customized GA, a methodology to determine the optimal network topology involving the disconnection of certain transmission lines is successfully developed. Through comprehensive tests on a medium size test network, the effectiveness of this approach in terms of problem tractability is demonstrated. The obtained results show that the adopted methodology not only can identify the TSO's grid assets optimal activation but is also able to satisfy the operation constraints, ensuring that the network remains connected and within acceptable voltage limits. However, the computational performances in terms of scalability should be addressed. Future developments will include the identification of optimal grid configurations valid for N-1 security assessment, in order to select the final operating maneuvers. These endeavors will continue to advance the understanding of TSOs' strategies for managing the grid, ultimately contributing to the ongoing improvement of transmission grid security and resilience.

Chapter 3

N-1 Security-Constrained Optimal Transmission Network Reconfiguration Algorithms for Congestion Management

The growing complexity of power system operation, driven by increasing load demand and renewable generation variability, challenges Transmission System Operators (TSOs) in maintaining grid security. In case of contingency, TSOs may resort to redispatching generation units, which entails additional operating costs. However, since they typically do not own generation facilities, to comply with network constraints, TSOs tend to leverage their own grid assets relying on cost-free topological reconfiguration actions. These strategies—such as transmission line switching and substation splitting— prove particularly effective, and can therefore be exploited to relieve congestion. Nevertheless, since an inadequate decision could reduce network meshing putting at risk the operational security, identifying the appropriate switching action to resolve a network issue may represent a challenging task for system operators, who will have to implement control measures without compromising the grid stability, N and N-1 security.

In this context, a deterministic preventive N-1 Security-Constrained Optimal Transmission Network Reconfiguration (SCOTNR) problem is formulated and proposed as a congestion management support tool for system operators, so that it can be used to derive N and N-1 secure operative conditions following any single line

contingency. The optimization framework is solved through Mixed-Integer Linear Programming (MILP) techniques, exploring the use of decomposition techniques within algorithms to ensure applicability to larger test cases. Practical implementation approaches are provided, with applications on modified IEEE 14-, 39- and 118-Bus test systems. Additional tests are conducted on an updated version of the Extra-High Voltage (EHV) SimBench grid model, representative of the German transmission network.

3.1 Literature Review

Optimal Transmission Network Reconfiguration (OTNR) is a complex combinatorial Mixed-Integer Nonlinear Programming (MINLP) problem typically used to determine the optimal switching actions for improving grid operation. Most OTNR models in the literature extend the well-known Optimal Power Flow (OPF) [92] and Unit Commitment (UC) problems [77], demonstrating how controlling the grid topology while dispatching generation can positively reduce system costs, still ensuring a secure operation.

The majority of studies only consider transmission line switching [77, 92–95] and model the grid neglecting the substation details, where the electrical components are connected to the busbars by means of circuit breakers (CBs) and disconnectors. Substation reconfiguration (SR) is less addressed, often tackled employing Mixed-Integer Linear Programming (MILP) techniques when implemented for congestion management (CM) [96–98]. These methods formulate deterministic OTNR problem using DC load flow (DCLF) assumptions. Although there are well-established solution methods to integrate N-1 security constraints [96–100], this still poses computational challenges in terms of scalability even under DC approximations, requiring the adoption of decomposition techniques to make the problem treatable. This explains why only a few studies provide analytical AC formulations [101–103]. These works do not model SR strategies and mainly focus on ensuring solution feasibility and on methodologies for dealing with the nonlinearities and non-convexity introduced by the power flow equations. Moreover, the impact of switching operations on N-1 security is not considered. Conversely, [104] and [105] consider SR, but N-1 security is at most verified or addressed through heuristics.

In particular, [97] highlights the importance of formulating a preventive security-

constrained OTNR (SCOTNR) model that derives an optimal grid topology which ensures (N-1) secure operation for any possible contingencies without the need for corrective actions. However, due to its complexity, the preventive SCOTNR problem may yield insecure solutions in small systems or result in an excessive number of switching operations in larger networks, even when both cost-free (switching) and costly (generation dispatch) resources are considered.

To the best of the author's knowledge, no SCOTNR models with only cost-free control actions and SR have been reported in the literature. In addition, most approaches are tested on systems of limited size. Furthermore, other transmission assets such as phase shifting transformers (PSTs) can be controlled by system operators for CM purposes. These have never been included in the formulation of a SCOTNR problem together with N-1 security constraints.

In this work, a deterministic MILP preventive N-1 SCOTNR problem is formulated in a comprehensive framework where cost-free control actions (i.e., line switching, SR, and PSTs operation) are coordinated with non cost-free ones (i.e., generation dispatch and load shedding) taking into account N and N-1 security constraints. The optimization problem considers transmission lines connection status, busbar couplers, and disconnectors in substations, as well as PST tap settings as cost-free integer control variables that can be jointly optimized with remunerative control actions. A Column-and-Constraint Generation (C&CG) iterative solution algorithm is also introduced to address the computational challenges related to the problem size and combinatoriality. The methodology is tested on IEEE 14-, 39- and 118-Bus test cases, modified to include double-bus single breaker substations. The overall problem is tackled through a Python-DIgSILENT PowerFactory co-simulation approach, which is proved to reduce substantially the computational effort.

An other approach based on a multi-cuts Benders decomposition scheme is adopted and tested on a publicly available EHV benchmark grid model [106] for scalability purposes. The algorithm is developed within a Python-DIgSILENT PowerFactory co-simulation framework, demonstrating its feasibility and highlighting its potential to enhance system security without additional operational costs.

3.2 Preventive N-1 SCOTNR Formulation

This paragraph describes the mathematical developments necessary to formalize the preventive SCOTNR problem, which is formulated considering DCLF assumptions. The main challenges to be addressed rely in the modeling of double-bus substations and the inclusion of N-1 security constraints.

The deterministic preventive N-1 SCOTNR problem can be compactly formulated in the following general form:

$$\begin{aligned} \min_{\boldsymbol{x}_0,\ldots,\boldsymbol{x}_c,\boldsymbol{u}_0} \quad & f_0(\boldsymbol{x}_0,\boldsymbol{u}_0) \\ \text{subject to:} \quad & \boldsymbol{g}_c(\boldsymbol{x}_c,\boldsymbol{u}_0)=\boldsymbol{0}, \quad \forall c \geq 0 \\ & \boldsymbol{h}_c(\boldsymbol{x}_c,\boldsymbol{u}_0)\leq \boldsymbol{0}, \quad \forall c \geq 0 \end{aligned} \tag{3.1}$$

where $f_0(\boldsymbol{x}_0,\boldsymbol{u}_0)$ is the objective function, $\boldsymbol{g}_c$ (resp. $\boldsymbol{h}_c$) are the equality (resp. inequality) constraints for the c-th contingency state (with $c=0$ corresponds to the base case), $\boldsymbol{x}$ and $\boldsymbol{u}$ represent the dependent variables and control variables, respectively. The first ($\boldsymbol{x}_c$) are referred to each contingency condition, whereas $\boldsymbol{u}_0$ must be the same $\forall c \geq 0$, such that the grid is secure under both N and N-1 conditions and no corrective actions will be needed in the post-contingency states.

In order to represent typical configurations of transmission busbars, considering that the electrical components in a bulk power system are interconnected by means of switch protection devices (i.e., CBs and disconnectors), a general double-bus single breaker substation model was adopted. The scheme, shown in Fig. 3.1, permits to represent the topological relationships within the optimization framework.

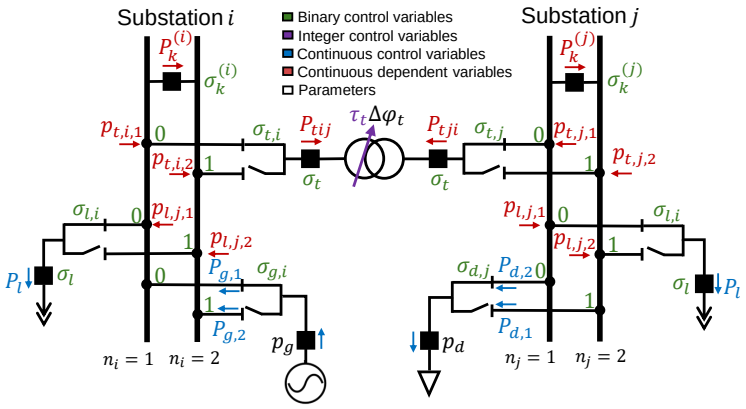

Figure 3.1: General Double-Bus Single Breaker substation model: connection modes of transmission branches, generators and loads [2].

Assuming that each substation $s \in \mathcal{S}$ consists of two busbars $n_s \in \{1, 2\}$ connected by a coupler $k \in \mathcal{K}$, each single-terminal element is connected via a CB and two disconnectors, whereas each two-terminal component has a CB and two disconnectors on each side. This representation avoids the need to define a binary variable to represent the open/closed state of a single switch, which is usually modeled as a zero-impedance line (ZIL). Furthermore, it is equivalent to other standard substation arrangements [105], making it easier to formalize power flow models and the topological relationships between components.

In general, the objective function f_0 aims to minimize system costs, the topological operations (TOs), such as number of switched off lines, splitted substations, and PSTs tap positions from the initial operating condition, and load shedding (LS):

$$\begin{aligned}\min_{\boldsymbol{u}_0} \sum_{g\in\mathcal{G}}\sum_{n=1}^{2} c_g \cdot P_{g,n} + C^{voll} \cdot \sum_{d\in\mathcal{D}}\sum_{n=1}^{2} P_{d,n}^{LS} + \sum_{l\in\mathcal{L}} \frac{w_l}{2} \cdot (1-\sigma_l)^2 + \\ + \sum_{k\in\mathcal{K}} \frac{w_k}{2} \cdot (1-\sigma_k)^2 + \sum_{t\in\mathcal{T}} \frac{w_t}{2} \cdot (\tau_t)^2 \end{aligned} \tag{3.2}$$

where c_g are the generation costs, whereas C^{voll} the penalty cost for Value of Lost Load. This latter is specifically introduced to prioritize TOs and generation dispatch over LS actions. A high penalty value is assigned to C^{voll} in order to limit as much as possible the amount of power not supplied. TOs, instead, are cost-free control actions, so the last three terms in (3.2) were introduced to prevent unnecessary switching operations. The weights coefficients w are chosen sufficiently small so that the control effort due to switching and PSTs operations is always negligible with respect to generation rescheduling or LS.

The following decision variables $\boldsymbol{u}_0$ can be defined:

$$\boldsymbol{u}_0 = [\boldsymbol{P_{g,n}}, \boldsymbol{P_{d,n}^{LS}}, \boldsymbol{\sigma_l}, \boldsymbol{\sigma_k}, \boldsymbol{\sigma_{b,s}}, \boldsymbol{\sigma_{g,s}}, \boldsymbol{\sigma_{d,s}}, \boldsymbol{\tau_t}]^\top \tag{3.3}$$

where $P_{g,n}$ is the active power produced by generator g on bus n, $P_{d,n}^{LS}$ is the load shedding active power. The other are integer variables, with σ related to switching binary decisions and $\tau_t \in \mathbb{Z}$ the PST tap step. In particular, σ_l and σ_k represent the line l and busbar coupler k connection states, respectively, taking the value 1 when in-service (0 otherwise), whereas the other variables represent the connection of an element to busbar 1 or busbar 2 in a substation s. In fact, for a branch $b \in \mathcal{B}$ (line

l or transformer t) connected between two substations i and j, $\sigma_{b,s}$ takes 0 if b is connected to busbar 1 in the substation $s \in \{i, j\}$, 1 if connected to busbar 2. The variables $\sigma_{g,s}$ and $\sigma_{d,s}$ are introduced as for $\sigma_{b,s}$ but refer to generators ($g \in \mathcal{G}$) and loads ($d \in \mathcal{D}$), respectively.

Even if the SR may involve different components and the switching of more than one disconnector, it is considered a single control action by counting only the number of busbar couplers to be opened. The importance of minimizing the control actions is not only related to security reasons, as reducing the meshing of the grid may compromise its stability and increase its vulnerability, but also to the SCADA/EMS time requirements for performing the switching operations.

The aim of the proposed preventive SCOTNR problem is to reconfigure the grid topology while respecting N and N-1 security constraints.

3.2.1 Connection of transmission branches between substations

The following constraints are formulated for each branch $\forall b \in \mathcal{B}$ and for each contingency case $\forall c \geq 0$, where $c = 0$ denotes the pre-contingency state (system in N conditions). For the sake of simplicity, only transmission line contingencies are considered. Therefore, a binary parameter γ_l^c can be defined for each line l and contingency case c, equal to 0 if l is open in the contingency state $c > 0$, 1 otherwise.

In each contingency case, the active power flow P_{bij}^c on a generic branch b is the sum of two contributions, $p_{b,s,1}^c$ and $p_{b,s,2}^c$, depending on whether connected to busbar 1 or busbar 2 on the side s:

$$P_{bij}^c = p_{b,s,1}^c + p_{b,s,2}^c; \quad \forall s \in \{i, j\} \tag{3.4}$$

$$-\bar{P}_b \gamma_b^c (1 - \sigma_{b,s}) \leq p_{b,s,1}^c \leq \bar{P}_b \gamma_b^c (1 - \sigma_{b,s}); \quad \forall s \in \{i, j\} \tag{3.5}$$

$$-\bar{P}_b \gamma_b^c \sigma_{b,s} \leq p_{b,s,2}^c \leq \bar{P}_b \gamma_b^c \sigma_{b,s}; \quad \forall s \in \{i, j\} \tag{3.6}$$

$$P_{bij}^c = -P_{bji}^c \tag{3.7}$$

where $\bar{P}_b$ is the branch rating. Denoting by $\theta_{b,s}^c$ the voltage angles at the ends of a branch (with $s \in \{i, j\}$), and by $\theta_{s,n}^c$ (with $n \in \{1, 2\}$) the voltage angle on busbar n in the substation s, this latter assumes the value of $\theta_{s,1}^c$ or $\theta_{s,2}^c$, depending on which

branch disconnector is closed at each end:

$$-\bar{\theta}\sigma_{b,s} \leq \theta^c_{b,s} - \theta^c_{s,1} \leq \bar{\theta}\sigma_{b,s} \tag{3.8}$$

$$-\bar{\theta}(1-\sigma_{b,s}) \leq \theta^c_{b,s} - \theta^c_{s,2} \leq \bar{\theta}(1-\sigma_{b,s}) \tag{3.9}$$

where $\bar{\theta}$ is the upper bound for voltage angle.

3.2.2 Line Switching Constraints

Assuming that only transmission lines can be switched-off, while transformers can only change connection busbar if a substation should be split, $p^c_{l,s,n}$ and $\sigma_{l,s}$ are linked to σ_l by the following constraints, $\forall l \in \mathcal{L} \wedge c \geq 0$:

$$-\bar{P}_l\gamma^c_l\sigma_l \leq p^c_{l,s,n} \leq \bar{P}_l\gamma^c_l\sigma_l; \quad \forall s \in \{i,j\}, \forall n \in \{1,2\} \tag{3.10}$$

$$\sigma_l - \sigma_{l,s} \geq 0 \quad \forall s \in \{i,j\} \tag{3.11}$$

Moreover, on/off constraints can be formulated choosing a big-M M_l as a real number large enough to make them non-binding when $\sigma_l = 0$:

$$-M_l(2-\sigma_l-\gamma^c_l) \leq b_l(\theta^c_{l,i} - \theta^c_{l,j}) - P^c_{lij} \tag{3.12}$$

$$b_l(\theta^c_{l,i} - \theta^c_{l,j}) - P^c_{lij} \leq M_l(2-\sigma_l-\gamma^c_l) \tag{3.13}$$

$$-M_l(2-\sigma_l-\gamma^c_l) \leq b_l(\theta^c_{l,j} - \theta^c_{l,i}) - P^c_{lji} \tag{3.14}$$

$$b_l(\theta^c_{l,j} - \theta^c_{l,i}) - P^c_{lji} \leq M_l(2-\sigma_l-\gamma^c_l) \tag{3.15}$$

$$-\bar{P}_l\gamma^c_l\sigma_l \leq P^c_{lij} \leq \bar{P}_l\gamma^c_l\sigma_l \tag{3.16}$$

$$-\bar{P}_l\gamma^c_l\sigma_l \leq P^c_{lji} \leq \bar{P}_l\gamma^c_l\sigma_l \tag{3.17}$$

Please note that, for transformers with fixed tap settings, (3.24)-(3.15) are formulated as equality constraints according to DCLF, whereas (3.16) and (3.17) do not require σ_l and γ^c_l. A practical and effective method for computing M_l is provided in [107], where tight values can be efficiently pre-computed by using graph theory and Dijkstra's shortest path algorithms. Further details are provided in the following paragraphs.

3.2.3 Phase Shifter Transformers (PSTs) Constraints

Considering an ideal PST with a limited number of tap positions and a voltage angle step $\Delta\varphi_t$ per tap, the following relations can be written:

$$\underline{\tau}_t \leq \tau_t \leq \overline{\tau}_t; \quad \forall t \in \mathcal{T} \tag{3.18}$$

$$P^c_{tij} = b_t(\theta^c_{t,i} - \theta^c_{t,j} \mp \tau_t \Delta\varphi_t); \quad \forall t \in \mathcal{T}, c \geq 0 \tag{3.19}$$

$$P^c_{tji} = b_t(\theta^c_{t,j} - \theta^c_{t,i} \pm \tau_t \Delta\varphi_t); \quad \forall t \in \mathcal{T}, c \geq 0 \tag{3.20}$$

$$-\bar{P}_t \leq P^c_{tij} \leq \bar{P}_t; \quad \forall t \in \mathcal{T}, c \geq 0 \tag{3.21}$$

$$-\bar{P}_t \leq P^c_{tji} \leq \bar{P}_t; \quad \forall t \in \mathcal{T}, c \geq 0 \tag{3.22}$$

where (3.18) limits the PST tap positions within the bounds. The sign of $\tau_t \Delta\varphi_t$ in (3.19) and (3.20) depends on which side of the transformer the tap changer is located, (3.21) and (3.22) are security constraints.

3.2.4 Substation Splitting Constraints

For each contingency case c, in each substation s, the voltage angles on the busbars must be equal when the coupler k is closed ($\sigma^s_k = 1$), and are otherwise unconstrained according to the chosen big-M M_θ:

$$-M_\theta \cdot (1 - \sigma^s_k) \leq \theta^c_{s,1} - \theta^c_{s,2} \leq M_\theta \cdot (1 - \sigma^s_k); \quad \forall s \in \mathcal{S} \tag{3.23}$$

The active power flow p^c_k through the coupler k follows the Big-M rules, $\forall k \in \mathcal{K}$:

$$-M_k(1 - \sigma^s_k) \leq b_k(\theta^c_{s,1} - \theta^c_{s,2}) - p^c_k \leq M_k(1 - \sigma^s_k) \tag{3.24}$$

$$-M_k\sigma^s_k \leq p^c_k \leq M_k\sigma^s_k \tag{3.25}$$

3.2.5 System Constraints

In order to integrate power flow equations, system constraints include the active power balance at each busbar in both pre-contingency and post-contingency states. Let $\mathcal{G}_n$ and $\mathcal{D}_n$ denote the sets of generators and loads connected to busbar n, respectively, $\mathcal{B}^F_n$ and $\mathcal{B}^T_n$ the sets of branches with from-end and to-end equal to n.

The following constraints must be complied $\forall n \in \mathcal{N}$ and $c \geq 0$:

$$\sum_{g \in \mathcal{G}_n} P^c_{g,n} - \sum_{d \in \mathcal{D}_n} \left(P^c_{d,n} - P^{LS}_{d,n}\right) - \sum_{b \in \mathcal{B}^F_n} p^c_{b,s,n} - \sum_{b \in \mathcal{B}^T_n} p^c_{b,s,n} - (-1)^n \cdot p^c_k = 0 \tag{3.26}$$

3.2.6 Topological Rules

Specific topological constraints between control variables are introduced to avoid ineffective switch combinations, based on the assumption that only one disconnector per side of a component can be closed on a busbar. Irrespective of whether the substation coupler k is open or closed, it is numerically inconsistent to allow both disconnectors to remain closed simultaneously.

3.2.6.1 Search space reduction constraints

The solutions search space is significantly reduced if all elements in a substation s are connected to busbar 1 when the coupler k is closed, free to change busbar otherwise:

$$\sigma^s_k - 1 + \sigma_d \leq 0; \quad \forall s \in \mathcal{S}, d \in s \tag{3.27}$$

$$\sigma^s_k - 1 + \sigma_g \leq 0; \quad \forall s \in \mathcal{S}, g \in s \tag{3.28}$$

$$\sigma^s_k - 1 + \sigma_{b,i} \leq 0; \quad \forall s \in \mathcal{S}, \forall b \in s \tag{3.29}$$

$$\sigma^s_k - 1 + \sigma_{b,j} \leq 0; \quad \forall s \in \mathcal{S}, \forall b \in s \tag{3.30}$$

where (3.27)-(3.28) refer to loads and generators, respectively, whereas (3.29)-(3.30) to the *from*-side (i) or the *to*-side (j) of transmission branches.

3.2.6.2 Loads & generators connection mode

Continuous variables are defined for generators ($P_{g,n}$) and loads ($P_{d,n}$), subject to the following restrictions. If the power injections are assumed to be fixed (non-dispatchable generators/loads), these equalities are valid:

$$P_{d,1} = p_d(1 - \sigma_d) \quad \wedge \quad P_{d,2} = p_d\sigma_d; \quad \forall d \in \mathcal{D} \tag{3.31}$$

$$P_{g,1} = p_g(1 - \sigma_g) \quad \wedge \quad P_{g,2} = p_g\sigma_g; \quad \forall g \in \mathcal{G} \setminus \{g^*\} \tag{3.32}$$

Instead, denoting slack generators by g^*, (3.28) takes the following form, taking into account the technical limits $[\underline{p}_g, \overline{p}_g]$:

$$\underline{p}_g(1-\sigma_g) \leq P_{g,1} \leq \overline{p}_g(1-\sigma_g); \quad \forall g = g^* \tag{3.33}$$

$$\underline{p}_g\sigma_g \leq P_{g,2} \leq \overline{p}_g\sigma_g; \quad \forall g = g^* \tag{3.34}$$

The same inequalities apply when generation is taken as a control variable. Moreover, when load shedding is allowed, the following inequalities constraints are introduced:

$$0 \leq P_{d,1}^{LS} \leq p_d(1-\sigma_d) \ \wedge \ 0 \leq P_{d,2}^{LS} \leq p_d\sigma_d; \forall d \in \mathcal{D} \tag{3.35}$$

3.2.6.3 Reliability Constraints

Finally, these constraints help in ensuring N-1 security when a substation is and avoiding radially connected substations:

$$\sum_{b \in \mathcal{B}_s} \sigma_{b,s} \geq 2(1-\sigma_k^s); \quad \forall s \in \{i,j\} \tag{3.36}$$

$$\sum_{b \in \mathcal{B}_s} [(1-\sigma_{b,s}) - (1-\sigma_b)] \geq 2(1-\sigma_k^s); \quad \forall s \in \{i,j\} \tag{3.37}$$

$$\sum_{l \in \mathcal{L}_s} \sigma_l + |\mathcal{T}_s| \geq 2; \ \forall s \in \mathcal{S} \text{ if } \mathcal{G}_s = \mathcal{D}_s \neq \varnothing \wedge |\mathcal{B}_s| \geq 2 \tag{3.38}$$

In double-bus schemes, the number of connected branches to each busbar must be greater than or equal to 2, so that, if a line is tripped due to a contingency, there will be another path for this busbar to be connected to the grid [98].

The resulting optimization problem (3.2)-(3.38) is a big combinatorial MILP program with a pseudo-parallel structure due to contingency states and N-1 security constraints. This results in a preventive SCOTNR that finds the minimum switching operations required to ensure grid security under N and N-1 conditions.

It should be noted that the MILP formulation is general, since it can be turned into a corrective post-contingency OTNR if run for a specific contingency state c. In this case, each problem is independent and a different set of optimal $\boldsymbol{u}^c$ can be obtained $\forall c > 0$.

3.3 Solution Methodologies

Since solving the preventive SCOTNR for large-scale systems can be particularly costly, decomposition techniques can be adopted to make the problem tractable and solvable in reasonable time.

3.3.1 An iterative Column-and-Constraint Generation algorithm

In a first study, an iterative C&CG algorithm is adopted to efficiently solve the SCOTNR problem. Furthermore, considering the extension of transmission systems, it is essential to perform preliminary screening procedures prior to optimization. Regarding contingencies selection, only transmission line contingencies that do not cause islanding, blackout, or uncontrollable overloads will be considered within the N-1 security constraints. This is because these cases are handled by specific procedures by the TSO, being not manageable only with cost-free reconfiguration actions [19].

The overall MILP problem is decomposed into a smaller MILP master problem (MP) and a set of N_c independent LP slave problems (SPs) solved iteratively. These latter, are a continuous relaxation of the original MILP problem $\forall c > 0$, in which $\boldsymbol{u}_0 \in [0, 1]$. The MP determines an optimal topology in a pre-contingency state ($c = 0$), whereas each SP is a feasibility problem that checks the N-1 security ($\forall c > 0$). Note that the SPs can be solved sequentially or parallelized across multiple CPUs.

3.3.1.1 Master Problem (MP)

The MP minimizes (3.2) subject to (3.4)-(3.26) with $c = 0$ and topological rules (3.27)-(3.38), giving a solution lower bound (LB). No contingency security constraints are included in the first step. The output is a combination of control variables $\hat{\boldsymbol{u}}_0$ to be submitted to the feasibility test carried out by the SPs.

3.3.1.2 Slave Problems (SPs)

Fixing the control variables $\boldsymbol{u}_0 = \hat{\boldsymbol{u}}_0$ derived from the MP, each SP minimizes the busbar power mismatch for each contingency state $c > 0$, where $\delta^{+}_{s,n,c}$ and $\delta^{-}_{s,n,c}$ are surplus and deficit active power mismatches on each busbar n of substation s due to

contingency c, respectively.

$$\min_{\delta^+_{s,n,c},\ \delta^-_{s,n,c}} \Phi_c = \sum_{s\in\mathcal{S}} \sum_{n=1}^{2} (\delta^+_{s,n,c} + \delta^-_{s,n,c}); \quad \forall c > 0 \tag{3.39}$$

subject to (3.4)-(3.25) and the following constraints:

$$\begin{aligned} &\sum_{g\in\mathcal{G}_n} P^c_{g,n} - \sum_{d\in\mathcal{D}_n} \left(P^c_{d,n} - P^{LS}_{d,n}\right) - \sum_{b\in\mathcal{B}^F_n} p^c_{b,s,n} - \sum_{b\in\mathcal{B}^T_n} p^c_{b,s,n} \\ &- (-1)^n \cdot p^c_k + \delta^+_{s,n,c} + \delta^-_{s,n,c} = 0, \quad \forall n \in \mathcal{N}, \forall c > 0 \end{aligned} \tag{3.40}$$

where (3.39) quantifies the violations for each contingency state, (3.40) is the nodal active power balance taking into account slack quantities. From the SPs solution an upper bound (UB) can be derived by identifying the worst case contingency state.

3.3.1.3 Potential Binding Contingencies & Solution Algorithm

The overall solution procedure is stated in Algorithm 3, where ν is the iteration counter and $\Omega_C^{(\nu)}$ the set of binding contingencies to be iteratively added to MP.

Algorithm 3 SCOTNR Iterative C&CG Solution Algorithm

Set $\nu \leftarrow 0$, $\epsilon \leftarrow 10^{-6}$, $\varepsilon \leftarrow 10^{-2}$, $\Omega_C^{(\nu)} \leftarrow \varnothing$
$LB^{(\nu)} \leftarrow -\infty$, $UB^{(\nu)} \leftarrow +\infty$
while $\nu \leq \nu^{max} \wedge (UB^{(\nu)} - LB^{(\nu)})/UB^{(\nu)} \geq \varepsilon$ **do**
    $\hat{\boldsymbol{u}}_0^{(\nu)} \leftarrow$ solve $MP^{(\nu)}$
    $LB^{(\nu)} = f_0(\hat{\boldsymbol{u}}_0^{(\nu)})$
    Fix $\boldsymbol{u}_c^{(\nu)} = \hat{\boldsymbol{u}}_0^{(\nu)}$
    for $c = 1, ..., N_c$ **do**
        $\Phi_c^{(\nu)} \leftarrow$ solve $SP^{(\nu)}$
    end for
    $UB^{(\nu)} = \min\{UB^{(\nu-1)}, f_0(\boldsymbol{u}_0)^{(\nu)} + \max \Phi_c^{(\nu)}\}$
    if $\max \Phi_c^{(\nu)} > \epsilon$ **then**
        update $\Omega_C^{(\nu)} \leftarrow \Omega_C^{(\nu-1)} \cup \arg\max_c(\Phi_c^{(\nu)})$
    end if
    $\nu = \nu + 1$
end while

Based on the conjecture of [108], $\Omega_C^{(\nu)}$ is updated in the iterative process only with the most binding contingencies, leading to a solution that is very close to the SCOTNR solution obtained by keeping them all. This iterative update acts as

contingency filtering. Once convergence is achieved, the set $\Omega_C^{(\nu)}$ will contain only the contingencies strictly necessary to ensure compliance with the imposed N-1 security constraints, making the MP lighter.

It should be noted that the rows 6-9 of Algorithm 3 can be replaced with a static security assessment carried out with N-1 contingency analysis (CA) software tool, resulting in a co-simulation iterative procedure. Infeasibilities under N-1 states can be quickly checked by sorting and identifying the worst branch loading violations. The worst-case will be sent back to the MP as additional contingency case in the successive iterations.

3.3.2 A Benders Decomposition approach

In this section, the Benders Decomposition algorithm used to solved the preventive N-1 SCOTNR problem is explained. Furthermore, two algorithms are provided for practical big-M M_l calculation and the control variable selection. These can be integrated also upstream the previous C&CG decomposition algorithm.

Specifically, in this paragraph, Benders Decomposition is employed to solve the preventive N-1 SCOTNR problem in cases where only cost-free switching operations are allowed. In this regard, the objective function minimizes the number of transmission lines to be switched-off and the number of double-bus substations to be split:

$$\begin{aligned} \min_{\boldsymbol{u}_0} \; f(\sigma_l, \sigma_k) = & \sum_{l \in \mathcal{L}} w_l(1-\sigma_l) + \sum_{k \in \mathcal{K}} w_k(1-\sigma_k) \\ & \text{subject to:} \quad (3.4)\text{-}(3.26), \; \forall c \geq 0; \\ & \text{Topological rules } (3.27)\text{-}(3.38). \end{aligned} \tag{3.41}$$

3.3.2.1 Optimization Framework Initialization

Following DCLF calculations and N-1 contingency analysis (CA), the TSO can monitor which branches would be subject to overloads in both N and N-1 conditions ($\Omega_{overload}$). Based on the identified branches, a solution search space reduction and a proper contingency selection must be performed. In particular, downstream N-1 CA, a fast contingency ranking can be obtained monitoring the maximum % branch loading observed ($\bar{L}_c = \max\{L_b^{max}\}$) for each contingency case. Considering the substations-branches b_l-weighted graph $G(\mathcal{S}, \mathcal{B})$ of the transmission grid, once the set $\Omega_{overload}$ is known, the solutions search space can be reduced by setting binary

control variables for those components outside a designated portion of the network. This results in a subgraph identified using the topological distances matrix $\boldsymbol{D}^{|\mathcal{S}|\times|\mathcal{S}|}$ of $G(\mathcal{S},\mathcal{B})$ within Algorithm 4.

Algorithm 4 Control variables selection

Input: $G(\mathcal{S},\mathcal{B})$; $\Omega_{overload}$; max. topological distance $\bar{r}$
Set candidate substations and branches $\Omega_S \leftarrow \emptyset$, $\Omega_B \leftarrow \emptyset$
Find *bridges* from $G(\mathcal{S},\mathcal{B}) \leftarrow$ non-switchable lines
Compute $\boldsymbol{D}^{|\mathcal{S}|\times|\mathcal{S}|}$ from $G(\mathcal{S},\mathcal{B})$
for $b \in \Omega_{overload}$ **do**
    $(i,j) \leftarrow$substations *from*, *to*
    get substations at a distance $r \leq \bar{r}$ from $i,j \leftarrow \Omega_S$
    get generators and loads installed in s
end for
for $s \in \Omega_S$ **do**
    get branches connected to s $(\mathcal{B}_s) \leftarrow$ update Ω_B
end for
Output: Ω_S, Ω_B

The outputs are the sets Ω_S and Ω_B of the candidate substations and branches. Non-switchable lines are filtered also from Ω_B, allowing disconnectors operations for substation splitting if necessary. The latter can be easily identified by searching for the *bridges* within $G(\mathcal{S},\mathcal{B})$, i.e., those edges whose removal increases the number of connected components in the graph.

Even employing this decomposition technique, only transmission line contingencies that do not cause islanding, blackout, or uncontrollable overloads will be considered within the N-1 security constraints.

Finally, suitable tight values for M_l can be efficiently pre-computed by using graph theory and Dijkstra's shortest path (DSP) algorithms on $G(\mathcal{S},\mathcal{B})$ within the Algorithm 5 [107], as anticipated in 3.2.2.

Although modern commercial solvers are able to handle disjunctive constraints internally (e.g., Special Ordered Sets constraints [61, 109]), the Big-M formulation preserves a MILP structure and also facilitates the calculation of Lagrangian multipliers in decomposition techniques. In fact, by fixing the binary variables, the resulting constraints reduce to an LP.

Algorithm 5 Big-Ms M_l Calculation

Input: Set of lines $\mathcal{L}$, b_l-weighted graph $G(\mathcal{S}, \mathcal{B})$
Set $\Omega_V \leftarrow \emptyset$, $\Omega_E \leftarrow \emptyset$
for $l \in \mathcal{L}$ **do**
    $(i, j) \leftarrow$substations *from*, *to*
    remove edge l from $G(\mathcal{S}, \mathcal{B})$
    vertexes Ω_V, edges $\Omega_E \leftarrow$ get DSP from i to j
    $M_l \leftarrow b_l \cdot \sum_{e \in \Omega_E} |\bar{P}_e / b_e|$
    restore edge l, reset $\Omega_V \leftarrow \emptyset$, reset $\Omega_E \leftarrow \emptyset$
end for
Output: M_l

3.3.2.2 Benders Decomposition Algorithm

The overall MILP problem is decomposed into a smaller MILP master problem (MP) and a LP slave problem (SP) solved iteratively. This latter, is a continuous relaxation of the original MILP problem $\forall c > 0$, in which $\boldsymbol{u} \in [0, 1]$. The MP determines an optimal topology in a pre-contingency state ($c = 0$), whereas the SP is a feasibility problem that checks the N-1 security ($\forall c > 0$). Note that the SP consists of N_c independent subproblems that can be solved sequentially or parallelized across multiple CPUs. If the SP is feasible but violations occur, optimality cuts are added to the MP to exclude the previously obtained integer solutions from the search space in subsequent iterations. Conversely, if the SP is infeasible, feasibility cuts are introduced into the MP. The iterative process continues until a predefined stopping criterion is met, with the MP providing a lower bound (LB) and the SP providing an upper bound (UB) of the overall objective function.

The overall Benders decomposition scheme is stated below (Algorithm 6), where ν indicates the iteration counter and ϵ the optimality tolerance:

Algorithm 6 SCOTNR Benders Decomposition Algorithm

Set $\nu \leftarrow 0$, $\epsilon \leftarrow 10^{-4}$, $LB^{(\nu)} \leftarrow -\infty$, $UB^{(\nu)} \leftarrow +\infty$
while $\nu \leq \nu^{max} \wedge (UB^{(\nu)} - LB^{(\nu)})/UB^{(\nu)} \geq \epsilon$ **do**
    $\hat{\boldsymbol{u}}_{\boldsymbol{0}}^{(\nu)} \leftarrow$ solve $MP^{(\nu)}$
    $LB^{(\nu)} = \max\{LB^{(\nu-1)}, f(\sigma_l, \sigma_k)^{(\nu)} + \sum_{c=1}^{N_c} \varphi_c^{(\nu)}\}$
    $\Phi_c^{(\nu)} \leftarrow$ solve $SP^{(\nu)}$
    $UB^{(\nu)} = \min\{UB^{(\nu-1)}, f(\sigma_l, \sigma_k)^{(\nu)} + \sum_{c=1}^{N_c} \Phi_c^{(\nu)}\}$
    Add Benders Cuts (35), $\forall \nu \leq \nu - 1$
    $\nu = \nu + 1$
end while

3.3.2.3 Master Problem (MP)

The MP minimizes (3.2) and the sum of positive slack variables φ_c representative of the feasibility of switching operations in terms of N-1 security for each contingency case:

$$\begin{aligned} \min_{\boldsymbol{u}} \; & f(\sigma_l, \sigma_k) + \sum_{c=1}^{N_c} \varphi_c \quad ; \quad \varphi_c \geq 0 \\ \text{subject to:} \quad & (3.4)\text{-}(3.26) \text{ with } c = 0; \\ & \text{Topological rules } (3.27)\text{-}(3.38); \\ & < \textit{Benders cuts} > \end{aligned} \tag{3.42}$$

The set of Benders cuts is initially empty in the first iteration. The MP output is a combination of control variables $\hat{\boldsymbol{u}}$ to be submitted to the feasibility test carried out by the SP.

3.3.2.4 Slave Problem (SP)

Fixing the control variables $\boldsymbol{u} = \hat{\boldsymbol{u}}$ derived from the MP, the SP minimizes the busbar power mismatch for each contingency state $c > 0$, where $\delta^+_{s,n,c}$ and $\delta^-_{s,n,c}$ are surplus and deficit active power mismatches on each busbar n of substation s due to contingency c, respectively.

$$\min_{\delta^+_{s,n,c},\ \delta^-_{s,n,c}} \sum_{c=1}^{N_c} \Phi_c(\delta^+_{s,n,c}, \delta^-_{s,n,c}) \tag{3.43}$$

subject to (3.4)-(3.26) and the following constraints, $\forall c > 0$:

$$\Phi_c(\delta^+_{s,n,c}, \delta^-_{s,n,c}) = \sum_{s \in \mathcal{S}} \sum_{n=1}^{2} (\delta^+_{s,n,c} + \delta^-_{s,n,c}); \tag{3.44}$$

$$\sum_{g \in \mathcal{G}_n} P^c_{g,n} - \sum_{d \in \mathcal{D}_n} P^c_{d,n} - \sum_{b \in \mathcal{B}^F_n} p^c_{b,s,n} - \sum_{b \in \mathcal{B}^T_n} p^c_{b,s,n} + \delta^+_{s,n,c} + \delta^-_{s,n,c} = 0; \quad \forall n \in \mathcal{N} \tag{3.45}$$

$$\sigma^c_l = \hat{\sigma}_l \longleftrightarrow \lambda^c_l; \quad \forall l \in \mathcal{L} \tag{3.46}$$

$$\sigma^c_{b,s} = \hat{\sigma}_{b,s} \longleftrightarrow \lambda^c_{b,s}; \quad \forall b \in \mathcal{B}, \forall s \in \{i, j\} \tag{3.47}$$

$$\sigma^c_g = \hat{\sigma}_g \longleftrightarrow \lambda^c_g; \quad \forall g \in \mathcal{G} \tag{3.48}$$

$$\sigma^c_d = \hat{\sigma}_d \longleftrightarrow \lambda^c_d; \quad \forall d \in \mathcal{D} \tag{3.49}$$

where (3.44) quantifies the violations for each contingency state, (3.45) is the nodal active power balance taking into account slack quantities, and (3.46)-(3.49) are introduced to fix the decisions taken from the MP and derive the lagrangian multipliers λ.

3.3.2.5 Optimality cuts & Solution Algorithm

If (3.42) converges to zero, the transmission topology found by the MP is N-1 secure with respect to the N_c considered contingencies. Otherwise the following Benders cuts will be incorporated in the MP for the next iterations, $\forall c > 0$:

$$\varphi_c \geq \Phi_c + \sum_{l \in \mathcal{L}} \lambda_l^c (\sigma_l - \hat{\sigma}_l) + \sum_{b \in \mathcal{B}} \lambda_{b,s}^c (\sigma_{b,s} - \hat{\sigma}_{b,s}) + \sum_{g \in \mathcal{G}} \lambda_g^c (\sigma_g - \hat{\sigma}_g) + \sum_{d \in \mathcal{D}} \lambda_d^c (\sigma_d - \hat{\sigma}_d) \quad (3.50)$$

3.4 Case studies & test results

3.4.1 IEEE benchmark systems

Numerical experiments were carried out on modified IEEE 14-, 39- and 118-Bus test systems (renamed as 14, 39, 118 Double-Bus systems, respectively). Topological arrangements were made to represent double-bus single breaker substations, resulting in three new different benchmark systems for reconfiguration studies. The preventive SCOTNR problem is solved by considering different objective functions, such as economic dispatch (ED), topological operations (TOs)–line switching (LSOs), substation splitting (SSOs), PST operations (PSTOs)–and load shedding (LS).

In the initial operating condition, all the electrical components are connected to busbar 1 within substation. All line loadings must be within 100% and 120% under N and N-1 conditions, respectively.

3.4.1.1 14 Double-Bus System

The first benchmark system has the same features of the network used in [98], involving 13 substations for a total of 26 busbars. A 3-winding transformer is connected to substations #4, #8 and #9. In the initial operating condition, line #4 (2-3) is congested at 102.06%. The SCOTNR results are summarized in Table 3.1.

The same solutions are obtained also with Algorithm 3 with low CPU times considering 16 line contingencies. The same solution described in [98] was obtained

Table 3.1: SCOTNR Results For 14 Double-Bus System

	ED+LS	**ED+TOs**	**TOs+LS**	**ED+TOs+LS**
f_0 **[p.u.]**	2.3116	0.3318	0.5774	0.3318
Gen. costs [$/h]	4957.36	3268.00	4874.40	3268.00
LS costs [$/h]	18159.00		0	0
LSOs [-]		0	0	0
SSOs [-]		0.005	0.005	0.005
PSTOs [-]		0	0.085	0
CPU time [s]	0.12	2.13	4.64	1.43

in the ED+TOs+LS case. When reconfiguration is not considered (ED+LS), 1.82 MW of the load should be curtailed, whereas PSTs help in avoiding LS when only cost free actions are allowed (TOs+LS).

3.4.1.2 39 Double-Bus System

In this test system with 39 substations (70 busbars), line #26 is congested at 101.46%. 34 contingencies are considered within the SCOTNR. As stated in Table 3.2, a N-1 secure configuration cannot be obtained only with TOs+LS. In the ED+LS case, 3.72 MW of load are curtailed and the system costs increase due to generation dispatch. Conversely, switching off line #5 allow to achieve an optimal solution while less generation needs to be redispatched compared to ED+LS case.

Table 3.2: SCOTNR Results For 39 Double-Bus System

	ED+LS	**ED+TOs**	**TOs+LS**	**ED+TOs+LS**
f_0 **[p.u.]**	17.4861	13.6945	infeasible	13.6945
Gen. costs [$/h]	137706.35	136895.45	153683.39	136895.45
LS costs [$/h]	37154.48		infeasible	0
LSOs [-]		0.005	infeasible	0.005
SSOs [-]		0	infeasible	0
PSTOs [-]		0	infeasible	0
CPU time [s]	0.42	47.81	n/a	47.96

3.4.1.3 118 Double-Bus System

In this study case, line #161 is 107.05% overloaded. Results (Table 3.3) are obtained considering 166 line contingencies. Overall, the SCOTNR problem applied to this test case includes 1,268,367 constraints, 336,811 continuous variables, and 837 integer variables (of which 809 are binary).

Additional tests were carried out considering 100% as the maximum line loadings in N-1 conditions. The SCOTNR problem cannot be solved within 1 hour without the use of Algorithm 1 when TO are allowed, except for the case in which only PSTs

with ED are enabled. This case solved with the full MILP formulation took only 23.24 s and the grid can be considered N-1 secure.

Table 3.3: SCOTNR Results For 118 Double-Bus System

	ED+LS	**ED+TOs+LS**	**ED+PSTOs**
f_0 **[p.u.]**	9.8526	9.8206	11.1287
Gen. costs [$/h]	98526.25	98105.61	10893.69
LS costs [$/h]	0	0	0
LSOs [-]		0	0
SSOs [-]		0.01	0
PSTOs [-]		0	0.235

3.4.1.4 Software Tools & Computational Performances

All numerical simulations were performed in a Python environment on a computer with 32 GB RAM, 12th Gen Intel® Core™ i9-12900F CPU @ 2.40 GHz, 16 physical cores and 24 logical processors, using up to 24 threads. DIgSILENT PowerFactory is used to represent the grid and to perform DCLF and N-1 CA calculations. The MILP optimization framework is built within *Pyomo* library using Gurobi 12.0, which uses Branch&Bound and Primal-Dual Simplex algorithms to solve the MILP problem. A CPU time comparison for 118 Double-Bus is shown in Table 3.4, showcasing improvements with the co-simulation approach.

Table 3.4: CPU Times for 118 Double-Bus System [s]

	ED+LS	**ED+TOs**	**ED+TOs+LS**
Full MILP [s]	4.93	> 3600	> 3600
C&CG (MP/SPs) [s]	18.59	51.89	53.85
C&CG (co-simulation) [s]	6.96	6.37	6.52

3.4.2 EHV Simbench grid model

Numerical experiments are carried out on a modified *1-EHV-mixed–0-sw* network model from the publicly available Simbench dataset [106], representative of the 380/220 kV EHV German transmission grid. DIgSILENT PowerFactory software is used to represent the grid and to perform DCLF and N-1 contingency analysis calculations.

Preventive SCOTNR is solved for N_c selected contingencies, reconfiguring the grid so that all branches operate within 100%, tolerating a maximum overload of 120% under N-1 conditions.

Table 3.5 provides a summary of the grid model's components. Conventional power plants (hard coal, brown coal, oil, gas, nuclear and others) are modeled as synchronous machines for a total maximum installed capacity of 87 GW, whereas renewable generation is modeled by means of static generators involving biogas, photovoltaic, wind, hydro run-of-river and others technologies for 13.6 GW.

Although the network model already contained double-bus single breaker substations, additional disconnectors were added within substations to also allow switching operations with generators and loads, thus providing a more realistic and detailed grid model for topological reconfiguration studies.

Table 3.5: Number of components in *1-EHV-mixed–0-sw* grid model

Component type	**Number of components**
Substations	534
Busbars	1101
Transmission Lines	849
2-Windings Transformers	209
Conventional Power Plants	345
Renewable Power Plants	225
Loads	390

The preventive SCOTNR is solved for a day-time winter scenario, in which 40.6% of the total load demand (12.3 GW) is supplied by renewable generation.

In the initial configuration (Fig. 3.2a), where all the transmission assets are supposed to be in-service, and the substation electrical components are connected to busbar 1, two 380 kV overhead transmission lines in the north-west area are congested at 103.3% (line #331) and 103% (line #830), respectively. Congestion is caused by excess wind generation (2276.7 MW) in the substation. Since local loads absorb only 26.6 MW, and substation #523 needs only additional 33 MW to help the SM328 synchronous generator balance the load, the remaining power must necessarily be distributed to the other branches of the grid. Congestion could be also mitigated by shutting down SM328, but this would entail additional costs for the TSO, which would have to remunerate the producer.

Downstream contingency ranking, having already excluded cases that lead to islanding or blackouts, the tripping of line #331 or #830 would cause an overload of approximately 261% on line #272 (not represented for the sake of brevity). For this reason, these contingencies are identified as the worst cases that can be analyzed and not considered in the reconfiguration problem.

A scalability test consisted of solving the preventive SCOTNR considering the first

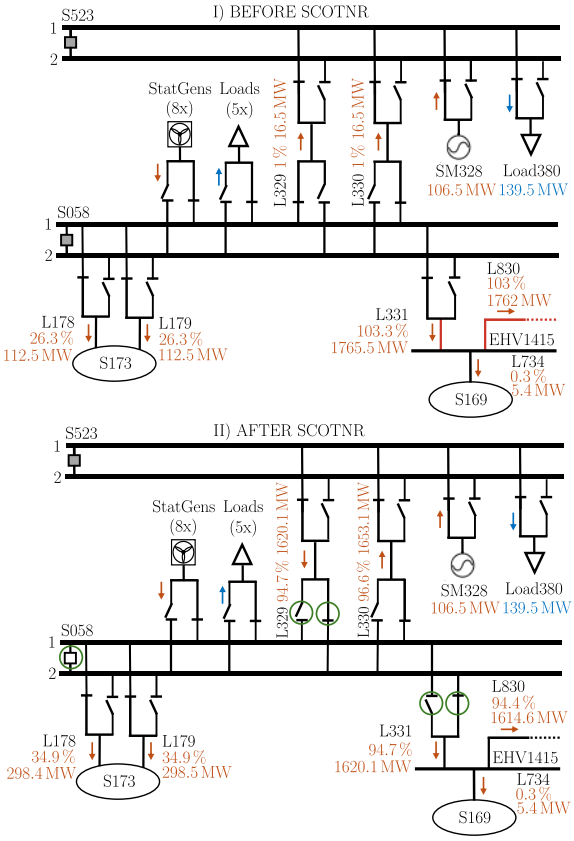

Figure 3.2: Power flow results before and after SCOTNR. Busbar splitting actions (green circles) are applied in S058 to solve congestions on lines #331 and #830.

worst N_c contingencies with $\bar{L}_c \leq 150\%$, performing the optimization by increasing N_c from 50 up to 200. The most secure topology is obtained for $N_c = 150, 200$. The optimal switching operations to be performed varying N_c are listed in Table 3.6.

As shown in Fig. 3.2b, the substation #58 should be split: the congested line #331 and another line (#329) change connection busbar and the congestions are cleared. In the optimal topology, with separate busbars, by connecting lines #329 and #331 on busbar 2 in station #58, the excess wind power travels a longer path, flowing to station #523 via line #330, then returning to station #58 by crossing #329 in the opposite direction. This results in a congestion mitigation on the lines concerned, with a significant increase in the loading on the parallel lines towards station #523.

Furthermore, it would be easy to verify that by shutting down the thermal generator, lines #331 and #830 would still be charged at 99.2% and 98.9% respectively, although the parallel lines towards substation #523 would be weakly charged at around 4%. Therefore, it can be assumed that the switching operations had a greater

Table 3.6: Optimal switching operations varying N_c

N_c	**Switching operations**
50	Substation S058 splits Line #331 connected to busbar 2 in S058 Line #830 connected to busbar 2 in S058
100	Substation S058 splits Line #179 connected to busbar 2 in S058 Line #329 connected to busbar 2 in S058 6/8 Wind generators connected to busbar 2 in S058
150	Substation S058 splits Line #329 connected to busbar 2 in S058 Line #331 connected to busbar 2 in S058
200	Substation S058 splits Line #329 connected to busbar 2 in S058 Line #331 connected to busbar 2 in S058

decongestant effect.

Concerning line switching, it is not selected as a definitive switching operation because, although it may be chosen in some Benders iterations, it fails the N-1 security check performed in the SP. At most, such maneuvers can be tolerated temporarily and used as corrective actions.

All numerical simulations were performed in a Python environment on a computer with 32 GB RAM, 12th Gen Intel® Core™ i9-12900F CPU @ 2.40 GHz, 16 physical cores and 24 logical processors, using up to 24 threads. Graph analyses are carried out by means of *NetworkX*, while the MILP optimization framework is built within *Pyomo* library using Gurobi 12.0 [61], which uses Branch&Bound and Primal-Dual Simplex algorithms to solve the MP and the SP, respectively.

In all cases, the SCOTNR problem cannot be solved in reasonable time preserving its whole pseudo-parallel structure. The full SCOTNR MILP program was however tested considering the pre-processing through Algorithm 1 and Algorithm 2, and imposing a time limit of 1 hour. A suboptimal solution was obtained only for $N_c = 50$, whereas the problem becomes intractable as the number of contingency cases considered increases. In theory, no convergence or infeasibility problems are reported, but it would not make sense to wait for a solution for a time that is incompatible with SCADA/EMS requirements, also because in the meantime, the network evolves over time towards other operating conditions. Table 3.7 shows the CPU time required to solve the SCOTNR problem.

The adopted Benders decomposition proved successful in solving the SCOTNR problem on a large transmission system. Solution times were calculated by adding up

Table 3.7: Preventive SCOTNR CPU times [s]

	Full SCOTNR MILP	**Benders Decomposition**
50	3206.00	165.53
100	> 3600.00	149.44
150	> 3600.00	526.58
200	> 3600.00	425.78

the contributions of all MPs and SPs, disregarding the time taken to communicate information from MP to SP, which was considered negligible. The minimum, average and maximum times required to solve MP and SP as N_c varies are shown in Fig. 3.3.

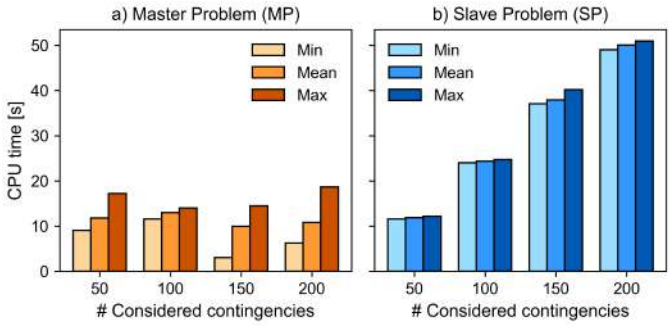

Figure 3.3: MP and SP CPU times varying N_c.

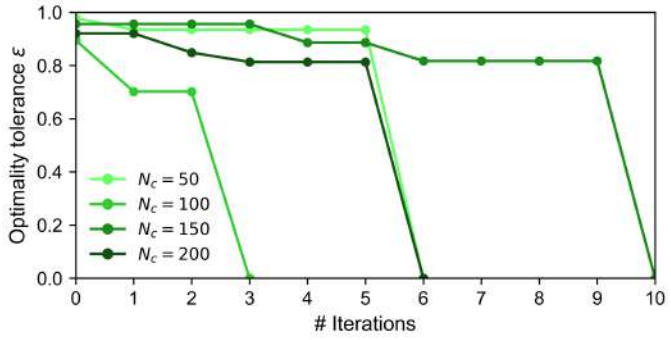

Figure 3.4: Benders Decomposition algorithm convergence.

The MP does not seem to be affected by the number of contingency cases, but rather by the number of added cutting constraints. However, although no significant variations were observed thanks to the reduction in the solution search space, in general, solving the MP tends to take longer in the last iterations. On the other hand, N_c greatly influences the solution times of the SP, showing an almost linear trend as N_c increases. Even if the SP is implemented as a unique big LP program, the solver do not automatically distribute all the subproblems on multiple processors. A parallel

computing architecture for solving SP can certainly further reduce computation times.

The convergence in terms of the optimality tolerance ϵ is shown in Fig. 3.4, from which it can be seen that the number of iterations required to reach the optimality condition does not depend on N_c, but rather on the quality of the Benders cuts added in each iteration of the MP.

3.5 Remarks & future developments

This chapter addressed the challenge of solving a deterministic preventive N-1 SCOTNR problem on three different size benchmark systems and on a large-scale test system using different solution approaches. The adoption of a MILP formulation proved useful for identifying switching operations for N-1 security constrained congestion management purposes.

The C&CG iterative solution algorithm was essential for the problem tractability on 118 Double-Bus System. Test results showed that topological changes combined with redispatch allow to ensure system security with lower operation costs. In certain cases, topological operations were proved to be essential to avoid load shedding and reduce system costs as well. The proposed approach allowed to reach an optimal solution even considering a very large set of contingencies (166) on 118 Double-Bus System.

The Benders decomposition approach was also essential for the problem tractability and for obtaining optimal solutions within a reasonable time frame, although the search for purely cost-free actions makes solving the problem even more burdensome and presents limitations.

Comparing the two solution methods, the C&CG algorithm exhibited superior characteristics for practical engineering applications. Although Benders decomposition algorithm maintains a smaller master problem by including only cut constraints, it generally requires a higher number of iterations to converge (the N-1 security constraints are not explicitly formulated). More critically, it relies on the derivation of dual variables (lagrangian multipliers) from the subproblems. In contrast, C&CG generates primal cuts, which simplifies the implementation significantly. This feature allows the N-1 security check subproblems to be solved using efficient, off-the-shelf contingency analysis tools in a co-simulation architecture, treating the security check

as a *black box* without the need to extract complex dual information. Consequently, C&CG offers a more robust and flexible framework for integrating real-world grid models.

Regarding real-world applicability, the high observability of transmission networks—guaranteed by state estimation systems in control rooms—makes the proposed methodology highly relevant. It can serve as an advanced Decision Support System (DSS) for TSOs, identifying non-intuitive switching actions that human operators might overlook, thereby unlocking the *hidden flexibility* of the existing infrastructure.

However, the current DC formulation has inherent limitations. Future developments must address the AC SCOTNR problem to verify the feasibility of solutions in terms of voltage stability and reactive power constraints. A good proposal would be to integrate SCOTNR into ORPF routines, although, given the SCADA/EMS time requirements of the latter, implementing a full AC preventive model with N-1 security constraints would require powerful and expensive computing tools in the control room. To solve the AC problem efficiently without compromising computational speed, future research should explore innovative relaxation techniques to handle MINLP optimization problems. This would allow for the co-optimization of switching decisions with other continuous voltage control variables, providing a fully comprehensive tool for secure grid operation.

Chapter 4

Optimal Transmission Network Reconfiguration Algorithms for the Secure Operation of the National Electric Transmission System

The research activity described in this chapter, carried out in collaboration with the Italian transmission system operator (TSO) Terna SpA, involves the analysis of network models and actual operating conditions of the National Electric Transmission System, with the application of the methodologies developed for the practical implementation of the Optimal Transmission Network Reconfiguration (OTNR) algorithms described in the previous chapters.

This results in the development of a Python/DIgSILENT PowerFactory co-simulation framework aimed to enable automated simulation procedures for static network analyses (load flow, sensitivity calculations, and N-1 contingency analysis). The software tool allows the integration of PowerFactory's simulation capabilities within external optimization routines and the management of highly detailed network models consistent with the TSO's naming conventions.

Tests conducted on the Sicilian transmission grid highlighted both the potential and the computational challenges related to the scalability of topological optimization models.

4.1 Sicilian Transmission Grid

The Sicilian transmission system is interconnected with the mainland grid via the 380 kV Rizziconi-Bolano-Paradiso-Sorgente, Scilla-Villafranca 1, and Scilla-Villafranca 2 connections. The first distinctive feature of the three transmission lines concerns the configuration of the Sorgente and Rizziconi substations, whose 380 kV sections are split to connect to different sections, equipping the protection systems with the necessary redundancies to minimize the possibility of separation of the island from the rest of Italy. Each of the two Scilla-Villafranca cable connections is equipped with two shunt reactors. Bolano and Paradiso are overhead-cable transition substations, isolated in SF6 and equipped with cable-side switches only (Bolano-Paradiso).

4.1.1 Sicily-Mainland power exchange limits

The substations in Rizziconi (Calabria) and Sorgente (Sicily) are each built with two separate sections in order to minimize the probability of simultaneous loss of the entire Sicily-Mainland interconnection, an event considered highly improbable. The considerations regarding operating modes and power exchange limits are summarized in this paragraph and are based on the assumption that total and simultaneous loss of the interconnection is not possible when the grid is intact.

The grid is defined as intact when a single contingency affecting these connections does not result in the separation of the Sicilian system from the mainland system. In addition to the case where all connections are in-service, the network is still defined as intact if only one of the connections is unavailable due to maintenance/failure or switched-off for operation:

- Sorgente-Villafranca 1;
- Sorgente-Villafranca 2;
- Scilla-Villafranca 1;
- Scilla-Villafranca 2;
- Scilla-Rizziconi 2.

In the above cases, in fact, a single contingency never leads to separation.

A non-intact grid is also defined as the out-of-service condition of a line (or combination of lines) for which a single contingency can lead to network separation and the consequent formation of a frequency island.

The maximum import and export power flow values for the Sicilian network (Sicily-Calabria interconnection non-intact) and import/export flows along the separation section (in the case of a non-intact Calabrian ring) are determined downstream a static and dynamic security analysis carried out on a provisional basis by the designated TSO unit and confirmed in real-time using the control room tools. Where the aforementioned tools are unavailable or not functioning, power exchange limits will be based on the market outcomes or on specific assessments of the transits allowed in security conditions from north to south and from south to north.

When the grid is intact and operates in normal state, depending on whether the logic of the EDA defense system (automatic disconnection processor) [110] is implemented or not, the reference power exchange limits are defined in [111] (subject to recalculation in day-ahead and intraday processes) and actually set to:

- Mainland → Sicily: 1550 MW (with EDA defense system), 1100 MW (without EDA defense logic);
- Sicily → Mainland: 1200 MW (with EDA defense system), 1000 MW (without EDA defense logic);

These limits are valid if the upward and downward balancing resources in Sicily are sufficient to cover the risks described in the TSO's documentation on the operating rules for the operation of the connections between Sicily and Calabria and the Calabrian ring.

In non-intact grid conditions, power exchange limits will be determined by the need to contain the over/under frequency transient in the event of a trip leading to the separation of the Sicilian network from the mainland network, with the aim of minimizing the EAC (automatic load balancing system) [110] probability of intervention by the EAC relays installed in Sicily, resulting in the disconnection of a widespread user base.

4.1.2 Case Study: DIgSILENT PowerFactory model

In order to test the applicability of the OTNR algorithms, numerical simulations are carried out on an equivalent reduced grid model obtained through network reduction

[112] from the whole Italian transmission network model. Boundaries were defined at the Scilla and Bolano substations. Equivalent impedances represent the two Bolano-Rizziconi and Scilla-Rizziconi connections, as well as taking into account the impedances of the upstream network. In particular, the Scilla substation is considered as a slack node in all analyses.

The complete grid model includes the high-voltage network (380 kV and 220 kV sections), as well as the sub-transmission network (150 kV) up to the primary substations and generation plants, representing a more detailed model compared to the one described in [113].

Topologically, the network is partitioned into sites interconnected solely by transmission lines. Each site may contain one or more substations, each characterized by its own busbar configuration. These are connected to each other via lines or transformers.

The number of modeled electrical components is listed in Table 4.1, respectively for the complete network model and the equivalent for Sicily.

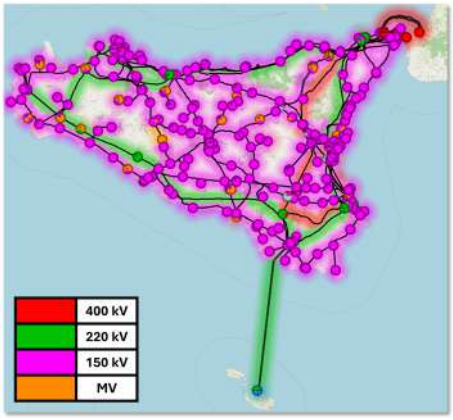

Figure 4.1: Voltage levels of Sicilian Transmission Grid

Table 4.1: Number of electrical components modeled in DIgSILENT PowerFactory

# Components	Whole Italian Transmission System	Equivalent Sicilian Transmission System
Sites	5852	375
Substations	10063	641
Busbars	12656	767
Lines	8139	529
2-Windings Transformers	3621	227
3-Windings Transformers	381	14
Synchronous Generators	2047	65
Static Generators	995	117
Loads	7200	412
Shunt Devices	236	24
Switch Devices	96894	5673

4.2 DC Preventive Security-Constrained Optimal Transmission Line Switching (SCOTLS)

In this paragraph, a preventive Security-Constrained Optimal Transmission Line Switching (SCOTLS) problem is formulated and used as a congestion management tool. The aim is to find secure network configurations under N and N-1 conditions by integrating transmission line switching actions. The optimization problem is formulated as Mixed-Integer Linear Programming (MILP) under DC Load Flow (DCLF) assumptions.

The objective function generally minimizes the control actions to be performed. Therefore, when executed in *cost-free mode*, with fixed generation and load active power injections, the SCOTLS problem seeks to find an optimal topology that complies with security constraints exclusively by switching-off the transmission lines. However, considering only binary control variables makes the problem purely combinatorial, which easily becomes unbounded when applied to large-scale systems, and no criteria have been identified to narrow the solution search space. For this reason, a more general formulation is proposed, also allowing for the redispatch of generation units in operation. In particular, since the main scope is to solve a technical optimization problem by leveraging the in-service network assets as much as possible, particularly expensive remunerative services (e.g., generation start-ups and shut-downs, load shedding) are intentionally neglected. However, redispatching the in-service generation units when necessary becomes essential for reasons related to system balancing, especially in the event of contingencies. Furthermore, the introduction of continuous control variables greatly simplifies the problem solution facilitating convergence and compliance with the time requirements of SCADA/EMS systems.

4.2.1 Mathematical Formulation

Let us model the transmission system as a substations-branches graph $G(\mathcal{N}, \mathcal{B})$, where the set of substations $\mathcal{N}$ includes busbars, terminals and other electrical components (e.g., generators $\mathcal{G}$, loads $\mathcal{D}$, etc.). Assuming that in the initial operating condition the grid is intact (all branches are in service and the busbar couplers in substations are closed), each substation represents an effective node in the system.

The set of transmission branches $\mathcal{B}$ involves transmission lines ($\mathcal{L}$), 2-windings ($\mathcal{T}_2$) and 3-windings tranformers ($\mathcal{T}_3$).

For the sake of simplicity, only transmission line contingencies are considered. Let us $c \in \mathbb{N}$ each line contingency case, where $c = 0$ denotes the pre-contingency state conditions (N security) and $c = 1, ..., N_c$ the system post-contingency conditions (N-1).

Based on the general formulation provided in Chapter 3 and reported also below, the preventive N-1 SCOTLS problem can be formulated as follows. Therefore, in compact form:

$$\begin{aligned} \min_{\boldsymbol{x}_0,...,\boldsymbol{x}_c,\boldsymbol{u}_0} \quad & f_0(\boldsymbol{x}_0, \boldsymbol{u}_0) \\ \text{soggetta a:} \quad & \boldsymbol{g}_c(\boldsymbol{x}_c, \boldsymbol{u}_0) = \boldsymbol{0}, \quad \forall c \geq 0 \\ & \boldsymbol{h}_c(\boldsymbol{x}_c, \boldsymbol{u}_0) \leq \boldsymbol{0}, \quad \forall c \geq 0 \end{aligned} \tag{4.1}$$

where $f_0(\boldsymbol{x}_0, \boldsymbol{u}_0)$ is the objective function, $\boldsymbol{g}_c$ (resp. $\boldsymbol{h}_c$) are the equality (resp. inequality) constraints for the c-th contingency state (with $c = 0$ corresponds to the base case), $\boldsymbol{x}$ and $\boldsymbol{u}$ represent the dependent variables and control variables, respectively. The first ($\boldsymbol{x}_c$) are referred to each contingency condition, whereas $\boldsymbol{u}_0$ must be the same $\forall c \geq 0$, such that the grid is secure under both N and N-1 conditions and no corrective actions will be needed in the post-contingency states.

In the case of the SCOTLS problem, the decision variables $\boldsymbol{u}_0$ can be either continuous (e.g., generation rescheduling) or integer (line switching). In particular, in this formulation, the variable $\sigma_l \in \{0, 1\}$ represents the line l connection state, taking the value 1 when the line l is in-service (0 otherwise).

The explicit MILP formulation of the preventive SCOTLS problem is proposed below, where in general, the objective function minimizes the generation power production (P_g) and/or the number of transmission lines to be switched-off:

$$\min f_0(P_g, \sigma_l) = \alpha_1 \cdot \sum_{g \in \mathcal{G}} c_g P_g + \alpha_2 \cdot \sum_{l \in \mathcal{L}} w_l (1 - \sigma_l) \tag{4.2}$$

where c_g are theoretically generation costs (or merit-order weight coefficients), and w_l a small constant used to weight cost-free line switching actions. The binary parameters $\alpha_1 \in \{0, 1\}$ and $\alpha_2 \in \{0, 1\}$ are introduced to activate (when equal to 1) or deactivate (when equal to 0) the objectives in (4.2).

The constraints include:

- *DC Load Flow power balance equations*:

$$\theta_i^c = \hat{\theta}_{ref}, \quad i = \text{slack substation} \tag{4.3}$$

$$\sum_{g\in\mathcal{G}_i} P_g - \sum_{d\in\mathcal{D}_i} P_d - \sum_{b\in\mathcal{B}_i^F} P_{bij}^c + \sum_{b\in\mathcal{B}_i^T} P_{bji}^c = 0, \quad \forall i \in \mathcal{N},\ \forall c = 0,\dots,N_c \tag{4.4}$$

  where P_g and P_d are the generation and load active power injections in substation i, respectively; θ_i^c the nodal voltage angles and P_b^c the branch active power flows in the contingency state c.

- *Generation units' technical limits*:

$$\underline{P}_g \cdot a_g \le P_g \le \overline{P}_g \cdot a_g, \quad \forall g \in \mathcal{G} \quad (\text{if} \quad \alpha_1 = 1) \tag{4.5}$$

  where $\underline{P}_g$ and $\overline{P}_g$ are the minimum/maximum active power technical limits, respectively, and $a_g \in \{0,1\}$ the generator's availability.

- *Line switching constraints*:

$$-M_l(2-\sigma_l-\gamma_l^c) \le b_l(\theta_{l,i}^c - \theta_{l,j}^c) - P_{lij}^c, \quad \forall l \in \mathcal{L},\ \forall c = 0,\dots,N_c \tag{4.6}$$

$$b_l(\theta_{l,i}^c - \theta_{l,j}^c) - P_{lij}^c \le M_l(2-\sigma_l-\gamma_l^c), \quad \forall l \in \mathcal{L},\ \forall c = 0,\dots,N_c \tag{4.7}$$

$$-\bar{P}_l\gamma_l^c\sigma_l \le P_{lij}^c \le \bar{P}_l\gamma_l^c\sigma_l, \quad \forall l \in \mathcal{L},\ \forall c = 0,\dots,N_c \tag{4.8}$$

  with similar expressions for P_{lji}^c. Denoting the line's rating as $\bar{P}_l$, these are on/off constraints formulated according to the Big-M (M_l) formulation detailed in Chapter 3, where γ_l^c is binary parameter defined for each line l and contingency case c, equal to 0 if l is open in the contingency state $c > 0$, 1 otherwise.

- *2-windings transformers constraints*:

$$P_{tij}^c = b_{ij}(\theta_i^c - \theta_j^c - \Delta\theta_t), \quad \forall t \in \mathcal{T}_2,\ \forall c = 0,\dots,N_c \tag{4.9}$$

$$-\bar{P}_t \le P_{tij}^c \le \bar{P}_t, \quad \forall t \in \mathcal{T}_2,\ \forall c = 0,\dots,N_c \tag{4.10}$$

  formulated according to DCLF assumptions, specifying the dependence on the phase shift $\Delta\theta_t$ introduced by the transformer's vector group. (For instance,

$\Delta\theta_t = -\pi/6$ in the case of a group 11 transformer and $\Delta\theta_t = 0$ in the case of group 0).

- *3-windings transformers constraints*:
  To integrate 3-winding transformers into the SCOTLS problem formulation, the modeling technique based on representing each winding by an equivalent star (Y) model 2-winding transformer was adopted. This configuration connects the three physical windings (w)—High Voltage (i), Medium Voltage (j), and Low Voltage (k)—to a common fictitious star point, characterized by a virtual phase angle $\theta_t^{*,c}$. The total equivalent susceptance of the transformer b_t is defined as the sum of the individual winding susceptances ($b_t = b_t^i + b_t^j + b_t^k$). Then, $\theta_t^{*,c}$ is calculated for each contingency case as the weighted average of the voltage angles, accounting for the phase shifts $\Delta\theta_t^w$ introduced by the vector groups:

$$\theta_t^{*,c} = \frac{1}{b_t}\left[b_t^i\left(\theta_i^c + \Delta\theta_t^i\right) + b_t^j\left(\theta_j^c + \Delta\theta_t^j\right) + b_t^k\left(\theta_k^c + \Delta\theta_t^k\right)\right], \quad \forall t \in \mathcal{T}_3 \tag{4.11}$$

  For each winding $w \in \{i, j, k\}$, the active power flow $P_{t,w}^c$ entering the star point under a specific contingency state c is determined as follows:

$$P_{t,w}^c = \begin{cases} b_t^i\left(\theta_i^c - \theta_t^{*,c} + \Delta\theta_t^i\right), & \text{if } w = i \\ b_t^j\left(\theta_j^c - \theta_t^{*,c} + \Delta\theta_t^j\right), & \text{if } w = j \\ b_t^k\left(\theta_k^c - \theta_t^{*,c} + \Delta\theta_t^k\right), & \text{if } w = k \end{cases}, \quad \forall t \in \mathcal{T}_3,\ \forall c = 0, \ldots, N_c \tag{4.12}$$

  Finally, the operational security is ensured by enforcing thermal capacity limits on each winding w. The power flow must remain within the maximum rating $\bar{P}_t$ for all transformers $t \in \mathcal{T}_3$ across all considered scenarios c:

$$-\bar{P}_t \leq P_{t,w}^c \leq \bar{P}_t, \quad \forall t \in \mathcal{T}_3,\ \forall w \in \{i, j, k\},\ \forall c = 0, \ldots, N_c \tag{4.13}$$

Other cardinality constraints may be added for practical reasons, such as an upper bound limit $\overline{N}$ on the number of switching operations allowed:

$$\sum_{l \in \mathcal{L}} (1 - \sigma_l) \leq \overline{N} \tag{4.14}$$

4.2.2 Solution Algorithm

Since the optimization problem (4.2)-(4.14) is characterized by a pseudo-parallel structure due to the presence of several N-1 security constraints defined $\forall c > 0$, an iterative Column-and-Constraint Generation (C&CG) algorithm is proposed to efficiently solve the SCOTLS problem under all the considered N_c line contingency cases. Given the significant computational burden of a classic OTLS problem, in addition to the extension and topological complexity of real transmission systems, this kind of approach is essential as it avoids explicitly formulating all N-1 security constraints in the optimization routine, while still allowing (in the case of convergence) a valid and secure solution to be obtained for the N_c contingency states considered.

The overall MILP problem (4.2)-(4.14) can be decomposed into a smaller MILP master problem (MP) and a set of N_c independent LP slave problems (SPs). The sequence MP-SPs is solved iteratively until a convergence stop criterion is met. The MP determines an optimal solution in a pre-contingency state ($c = 0$), whereas each SP can be formulated as a feasibility problem that checks the N-1 security ($\forall c > 0$). Note that the SPs can be solved sequentially or parallelized across multiple CPUs, in fact, for fixed decision variables set by the MP, each contingency state is independent. For this reason, the parallel resolution of all SPs can be replaced by a static security assessment stage (i.e., an N-1 contingency analysis calculation).

The proposed C&CG algorithm is based on a co-simulation procedure that alternately involves solving a reduced MILP optimization routine and performing an N-1 contingency analysis. It begins with the MP solution (for $c = 0$), which does not include contingency security constraints in the first iteration and provides a solution lower bound (LB). The MP output is a combination of control variables $\hat{\boldsymbol{u}}_0$ to be submitted to the feasibility test carried out by the N-1 contingency analysis. Downstream the latter, a rapid contingency ranking is performed by monitoring the maximum branch loading violation in each contingency state. The maximum violation observed corresponds to the worst contingency detected by the security check performed on the solution provided by the MP. This quantity is added to the value of the objective function calculated by the MP, obtaining a solution upper bound (UB). At this step, LB and UB are compared, and if the stop criterion is still not met, the worst contingency identified is considered as an additional contingency state in the MP at the next iteration.

The overall solution procedure is stated in Algorithm 7, where ν is the iteration

counter and $\Omega_C^{(\nu)}$ the set of binding contingencies to be iteratively added to MP. Based on the conjecture of [108], $\Omega_C^{(\nu)}$ will be updated in the iterative process only with the most binding contingencies, leading to a solution that is very close to the SCOTLS solution obtained by keeping them all.

Algorithm 7 N-1 Preventive SCOTLS C&CG Iterative Solution Algorithm

Set $\nu \leftarrow 0$, $\varepsilon \leftarrow 10^{-2}$, $\Omega_C^{(\nu)} \leftarrow \varnothing$
$LB^{(\nu)} \leftarrow -\infty$, $UB^{(\nu)} \leftarrow +\infty$
while $\nu \leq \nu^{max} \wedge (UB^{(\nu)} - LB^{(\nu)})/UB^{(\nu)} \geq \varepsilon$ **do**
    $\hat{\boldsymbol{u}}_0^{(\nu)} \leftarrow$ solve $MP^{(\nu)}$
    $LB^{(\nu)} = f_0(\hat{\boldsymbol{u}}_0^{(\nu)})$
    Fix $\boldsymbol{u}_c^{(\nu)} = \hat{\boldsymbol{u}}_0^{(\nu)}$
    Perform N-1 Contingency Analysis
    N-1 branch loading violations calculation: $\Phi_c^{(\nu)} = \max(0, L_{b,c}^{\%} - L_{b,c}^{max})$
    $UB^{(\nu)} = f_0(\boldsymbol{u}_0)^{(\nu)} + \max\{\Phi_c^{(\nu)}\}$
    Compute $(UB^{(\nu)} - LB^{(\nu)})/UB^{(\nu)}$
    Update $\Omega_C^{(\nu)} \leftarrow \Omega_C^{(\nu-1)} \cup \arg\max_c(\Phi_c^{(\nu)})$
    $\nu = \nu + 1$
end while

Please, note that if the MP is infeasible when $\nu > 0$, this implies that the last contingency added does not pass the security check and cannot be handled, so it must be removed from the set $\Omega_C^{(\nu)}$.

4.2.3 Software Implementation

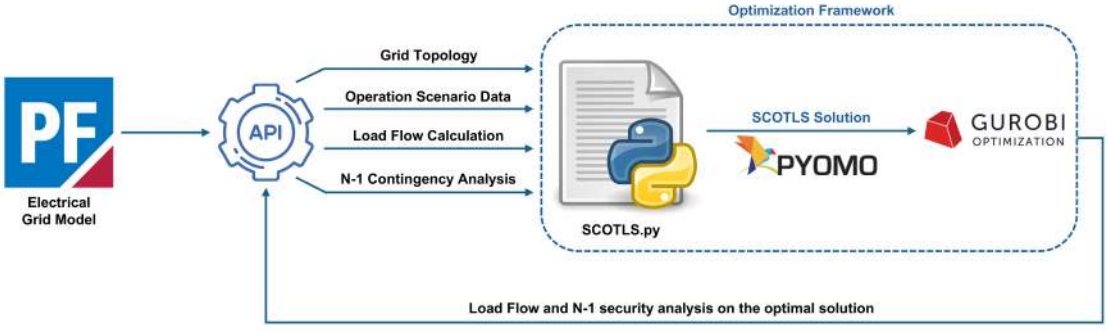

Figure 4.2: SCOTLS Python/PowerFactory co-simulation framework.

All numerical simulations were performed in a Python environment on a computer with 32 GB RAM, 12th Gen Intel® Core™ i9-12900F CPU @ 2.40 GHz, 16 physical cores and 24 logical processors, using up to 24 threads. DIgSILENT PowerFactory

is used to represent the grid and to perform DCLF and N-1 contingency analysis calculations. The MILP optimization framework is built within *Pyomo* library using Gurobi 12.0 for the problem solution.

Algorithm 7 is implemented within a Python/PowerFactory co-simulation procedure (Fig. 4.2). This is integrated within an external Python script, interfaced with DIgSILENT PowerFactory software via Application Programming Interface (API), exploiting the programming skills detailed in [114].

Fig. 4.2 illustrates an automated co-simulation loop where Python environment acts as the master orchestrator and DIgSILENT PowerFactory serves as the specialized sub-calculator for power system analysis. In the context of the proposed C&CG algorithm, the implementation is structured as follows: the *Optimization Framework* box represents the MP (that handles the integer decision variables, i.e., the status of transmission lines to be switched-off). Within the *SCOTLS.py* external script, the mathematical model is built using *Pyomo* library and solved using Gurobi optimizer. Once a SCOTLS solution is found, it is passed back to the PowerFactory simulation environment. This latter, interfaced through the API, acts as the SPs in the C&CG iterative process. From the optimal grid topology found by the MP at a certain iteration, switching commands are sent to PowerFactory, which executes the DCLF, the N-1 contingency analysis and identifies violations. Once the worst contingency case is detected, the corresponding security constraints are added back into the *Pyomo* model. The MP is then re-solved with this expanded set of constraints. This iterative process continues until the N-1 security check confirms that the optimal solution provided is secure under all the N_c considered contingencies.

By using this co-simulation architecture, the algorithm avoids modeling thousands of power flow equations and contingency constraints directly inside the optimizer (which would be computationally prohibitive). Instead, it uses PowerFactory to dynamically detect only the critical constraints that are actually needed to define a secure solution, significantly improving the computational efficiency.

4.2.4 Case Study & Test Results

The preventive SCOTLS problem has been solved for the Sicilian transmission grid model on two different operating conditions:

- Case 1 - base case scenario with N-1 security constraints violations;
- Case 2 - congested scenario characterized by high export to the mainland.

In both cases, SCOTLS is solved either in *cost-free mode* ($\alpha_1 = 0, \alpha_2 \neq 0$, fixed generation and load demand), or by allowing redispatching actions by using the available in-service units ($\alpha_1 \neq 0, \alpha_2 \neq 0$). Only transmission line contingencies that do not cause islanding, blackout, or uncontrollable overloads will be considered within the N-1 security constraints. This is because these contingencies are identified as non-ordinary events according to the EU Regulation 2017/1485 and to the methodology approved by ACER in the document *Methodology for coordinating operational security analysis* (CSAM, art. 75) [115]. Therefore, among 529 modeled transmission lines, following a topological analysis of the graph $G(\mathcal{N}, \mathcal{B})$ connectivity, 388 contingency cases were considered in the optimization routine. All transmission branch loadings must be within 100% and 120% under N and N-1 conditions, respectively.

4.2.4.1 Case 1: Base Case Scenario

In a first study case, the grid operates in a secure state under N conditions: the load demand is 1.78 GW and the local generation is 1.61 GW (mostly renewable), then Sicily imports roughly 170 MW from the mainland grid. No congestion or overloads were detected from the initial load flow analysis. Downstream the N-1 contingency analysis (performed considering 388 ordinary line contingencies) the maximum branch loading violations of Table 4.2 can be observed for each contingency case.

Since no overloads are detected, the solution of the simple OTLS problem (without N-1 security constraints) in *cost-free mode* coincides with the power flow results of the initial operating condition. Therefore, the optimization problem converges to the initial operating point and no line switching action is identified as necessary. Consequently, if an optimal topology is to be found in advance, a set of N-1 security constraints must necessarily be taken into account.

With the *cost-free mode*, SCOTLS has been solved by allowing a maximum of 2 switching operations. Two 150 kV lines should be opened: ARKP_IMASP_I150

Table 4.2: Ranking of the 10 worst line contingencies in terms of maximum branch loading detected (Initial operating condition - Case 1)

Contingency case	**Max Loading %**	**On branch**
CSGPDIFVLP_I150	129.29	RO2PDIROFPZI150
MSBPTIBELPDI150	126.22	SVKPTIARKP_I150
GRDPDIGRKP_I150	125.24	SVKPTIARKP_I150
CSGPDIGRKP_I150	123.24	RO2PDIROFPZI150
SRGPTICSTPDI150	118.60	RO2PDIROFPZI150
CSTPDIFVLP_I150	112.55	RO2PDIROFPZI150
ISBPZIISBPZI380	104.28	RO2PDIROFPZI150
ISBPZIPRIPTI380	104.28	RO2PDIROFPZI150
GRDPDISVKPTI150	101.63	SVKPTIARKP_I150
PTRPTIMSBPTI150	97.83	RO2PDIROFPZI150

Table 4.3: Ranking of the 10 worst line contingencies in terms of maximum branch loading detected (Optimal solution - Case 1 *cost-free*)

Contingency case	**Max Loading %**	**On branch**
CSGPDIFVLP_I150	113.00	RO2PDIROFPZI150
CSGPDIGRKP_I150	106.90	RO2PDIROFPZI150
SRGPTICSTPDI150	102.23	RO2PDIROFPZI150
MSBPTIBELPDI150	99.80	ACRP_IACKPDI1501
CSTPDIFVLP_I150	96.13	RO2PDIROFPZI150
EGNP_IPRIPTI380	93.62	PRSPTIEGNP_I150
GRDPDIGRKP_I150	90.36	ACRP_IACKPDI1501
SREP_ISRNPDI150	89.55	AUSP_IMEFPZI150
VFTPTIBGTP_I150	88.80	VFTPTIT1500201
CSZPTIBGTP_I150	88.80	VFTPTIT1500201

and COFPZIRO2PDI150. The imposed N-1 security constraints are all satisfied, as can be observed from the contingency ranking performed on the optimal solution in Table 4.3.

However, switching-off ARKP_IMASP_I150 and COFPZIRO2PDI150 implies that the loads in Mascali and Contesse RT substations are radially connected. The total load radially connected was 85.8 MW, increased to 89.4 MW after SCOTLS solution. If an additional constraint were imposed whereby the amount of radially connected load must be lower than the initial condition, the SCOTLS problem would be infeasible. However, since this amount does not increase significantly, the optimal solution obtained can be considered acceptable.

The solutions obtained in the iterative process of Algorithm 7 are summarized in Table 4.4, where SCOTLS is successfully solved in 3 iterations. The transmission lines listed in the last column represent the binding contingencies added to the set $\Omega_C^{(\nu)}$.

Table 4.4: C&CG Algorithm Iterative Process Monitoring (Case 1 *cost-free*)

# It.	# Switched-off lines	# N-1 worst loading violations	Worst violation [p.u.]	On branch
0	0	4	0.0929	CSGPDIFVLP_I150
1	1	2	0.0867	MSBPTIBELPDI150
2	2	0	0	None

When generation redispatch is enabled, instead, the C&CG algorithm still converges within 3 iterations (Table 4.5) and the same two lines should be switched-off again.

Table 4.5: C&CG Algorithm Iterative Process Monitoring (Case 1 with redispatch)

# It.	# Switched-off lines	# N-1 worst loading violations	Worst violation [p.u.]	On branch
0	1	5	0.3856	CSGPDIFVLP_I150
1	1	2	0.0725	MSBPTIBELPDI150
2	2	0	0	None

4.2.4.2 Case 2: High Export Scenario

This scenario was obtained using a preventive DC SCOPF routine based on Case 1 scenario. Considering the initial grid topology, energy resources were dispatched fostering the integration of renewables and forcing Sicily to operate in export mode (a constraint on Sicily-Calabria power exchange has been specifically imposed, limiting it to between 1000 MW and 1100 MW).

The load demand is 1.68 GW and the local generation is 2.68 GW (mainly wind and solar), then Sicily exports 1 GW to the Mainland grid. Six 2-winding transformers and the following 150 kV transmission lines are congested: CEFPZISSFPZI150, CRCPTICMFP_I150, and ZAFPZISSFPZI150 (Fig. 4.3).

Figure 4.3: Congested transmission lines in Case 2.

Table 4.6: Ranking of the 10 worst line contingencies in terms of maximum branch loading detected (Optimal solution - Case 2)

Contingency case	**Max Loading %**	**On branch**
CFLPDIFIUPDI150	120.00	CEFPZISSFPZI150
ANPPPIMLLPTI2202	120.00	ANPPPIMLLPTI2201
ANPPPIMLLPTI2201	120.00	ANPPPIMLLPTI2202
CFLPDISSCPDI150	109.71	CEFPZISSFPZI150
CTLP_IPN2P_I220	109.09	ANPPPIT2200151
CTTPTIMNPP_I150	109.09	ANPPPIT2200151
MNBP_IMRBP_I150	109.09	ANPPPIT2200151
ISBPZIPRIPTI380	109.09	ANPPPIT2200151
ISBPZIISBPZI380	109.09	ANPPPIT2200151
FRFPTIARFP_I150	109.09	ANPPPIT2200151

In this case, the SCOTLS problem in *cost-free mode* is infeasible, making it necessary to simultaneously enable the redispatch of the available in-service units. Thanks to the redispatch, the power exchanged in export is reduced to 185 MW. In fact, the total downward redispatch is 815.6 MW, with roughly 572 MW absorbed by the pumped-hydro power plants in the Anapo substation. The total upward redispatch is only 0.6 MW and no conventional power plant needs to be started-up or shut-down. Wind and solar power generation is fully exploited.

Lines ZAFPZISSFPZI150 and CAMP_ICASPDI150 should be switched-off and the amount of radially connected load does not vary from the initial condition. The line contingency ranking related to the optimal solution in this case is reported in Table 4.6. These switching operations are necessary to ensure the required level of N-1 security, in fact through N-1 contingency analysis, by closing these two lines with the same amount of redispatched power, overloads greater than 120% occurred in 4 contingency cases.

4.2.5 Computational performances

From a computational point of view, solving the preventive SCOTLS problem is particularly costly.

With regard to Case 1, considerations can be made by observing Fig. 4.4 and Fig. 4.5.

Although converging with the same number of iterations, the total time required to solve the SCOTLS problem varies depending on whether redispatch is enabled as a control action. When disabled (Fig. 4.4), the solution is obtained in just over 200 seconds, even though the severity of the violations in the first two iterations is

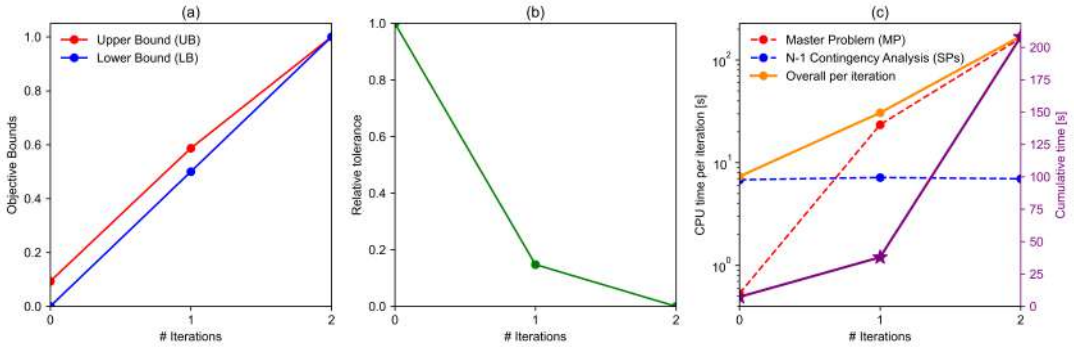

Figure 4.4: Case 1 (*cost-free*) CPU times.

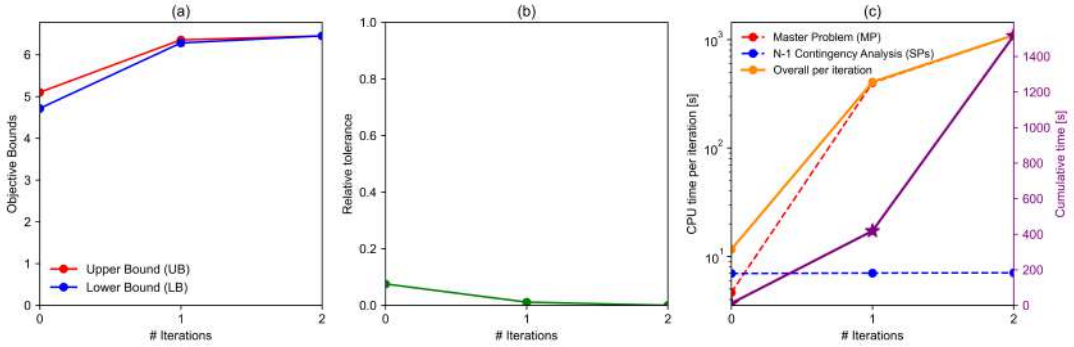

Figure 4.5: Case 1 (redispatch) CPU times.

greater than when redispatch is enabled. Conversely, when redispatch is enabled (Fig. 4.5), the total CPU time increases to more than 20 minutes due to the wider solution search space, but the violations of the security constraints are significantly smaller from the first iteration onwards. From the comparison of Fig. 4.4*a* and 4.5*a*, it can be seen that the value of the objective function must increase in the iterations as contingency states are added. From figures 4.4*c* and 4.5*c*, it is clear that the overall CPU time is strongly influenced by the MP solving time. In fact, since the N-1 security check function performed by the SPs is entrusted to the contingency analysis tool, the time required for its execution remains almost constant (within 5 seconds on a personal computer without parallelizing the calculation between multiple processors). On the contrary, as the number of contingency states in the MP increases, its resolution time grows superlinearly.

The CPU times related to the Case 2 are reported in Fig. 4.6. In this case, solving the SCOTLS problem took just over 1 minute, allowing for the possibility of switching-off a maximum of $\overline{N} = 2$ transmission lines. By increasing the number of switching operations allowed ($\overline{N} = 3$), the optimization problem "explodes", requiring almost 2 hours to obtain a valid solution (Fig. 4.7*c*). This last test was carried out

for demonstration purposes only.

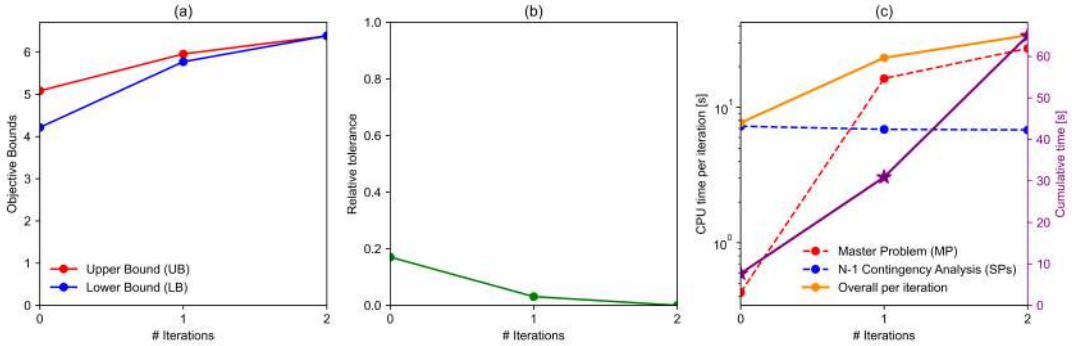

Figure 4.6: Case 2 CPU times (redispatch with $\overline{N} = 2$).

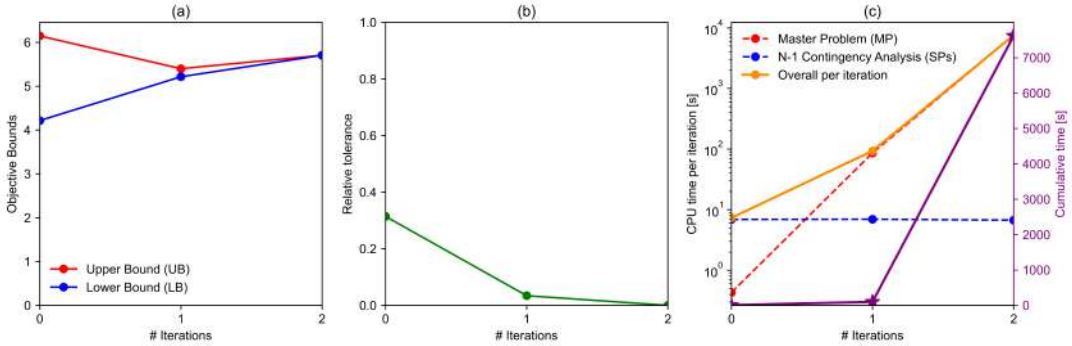

Figure 4.7: Case 2 CPU times (redispatch with $\overline{N} = 3$).

4.3 AC Optimal Transmission Network Reconfiguration as a corrective post-contingency congestion management tool

In this paragraph, an AC Optimal Transmission Network Reconfiguration (OTNR) problem is proposed as a decision support tool for system operators, enabling power flow redistribution by means of topological changes (including line switching and substation splitting). The optimization problem aims to minimize potential branch loading violations in the event of line contingencies. The solution is tackled using a customized Genetic Algorithm (GA), capable of handling the non-linearity of power flow equations and the topological complexity of real transmission networks. The methodology is tested on a detailed model of the Sicilian section of the Italian transmission grid, incorporating a realistic representation of substations. The algorithm

is developed within a Python-DIgSILENT PowerFactory co-simulation framework, improving the scripting automation of the simulation architecture used in this thesis.

4.3.1 Mathematical Formulation

Let us consider the single-phase equivalent circuit of a balanced three-phase transmission system, characterized by the following sets of electrical components: $\mathcal{N}$ is the set of busbars, $\mathcal{B}$ the set of transmission branches (lines and transformers), $\mathcal{G}$ and $\mathcal{D}$ the sets of generators and loads, respectively. Assuming that generation and load are known in a given operating condition, the deterministic corrective AC OTNR problem aims to comply with network constraints during operation exclusively through topological variations (i.e., by performing cost-free switching actions). This leads to a non-convex MINLP optimization problem whose control variables $\boldsymbol{u}$ belong to the domain $\mathbb{N}$ of natural integers. In particular, in the case where the controllable assets are switching devices (circuit breakers, busbar couplers $k \in \mathcal{K}$ and disconnectors $h \in \mathcal{H}$), the decision variables are binary (or Boolean), since their value $\{0, 1\}$ indicates the open/closed connection status of these components. For the sake of completeness and formality, the dependent variables and known parameters of the optimization problem will be denoted by $\boldsymbol{x}$ and $\boldsymbol{p}$, respectively.

In this work, the applicability of the problem is tested for post-contingency congestion management purposes. It follows that the underlying formulation is valid when determining cost-free corrective actions in case of security constraints violation due to a contingency event.

Therefore, the objective function adopted is a quadratic penalty function that allows the limits of the branches to be treated as *soft* constraints:

$$\min_{\boldsymbol{u}} f(L_b) = \sum_{b \in \mathcal{B}} \left(\frac{L_b - \bar{L}}{100} \right)^2, \text{ where: } \bar{L} = \begin{cases} 100 & \text{if } L_b > 100\% \\ L_b & \text{if } L_b \leq 100\% \end{cases} \tag{4.15}$$

subject to:

$$P_i(\boldsymbol{x}, \boldsymbol{u}, \boldsymbol{p}) = 0, \quad \forall i \in \mathcal{N} \tag{4.16}$$

$$Q_i(\boldsymbol{x}, \boldsymbol{u}, \boldsymbol{p}) = 0, \quad \forall i \in \mathcal{N} \tag{4.17}$$

$$\underline{v}_i \leq v_i \leq \overline{v}_i, \quad \forall i \in \mathcal{N} \tag{4.18}$$

$$\underline{Q}_g \cdot a_g \leq Q_g \leq \overline{Q}_g \cdot a_g, \quad \forall g \in \mathcal{G}^{pv} \tag{4.19}$$

It can be observed that (4.15) converges to zero when the branch loading L_b (%) on all monitored network branches is below a maximum tolerable threshold $\overline{L}$ (equal to 100% under N security conditions, 120% under N-1). Note that all solutions corresponding to non-zero values of (4.15) can theoretically be considered acceptable, provided that the set of the optimal control variables satisfies all the remaining constraints (4.16)-(4.19) and ensures that the grid is connected. Infinitesimal values of (4.15) can therefore identify equally valid solutions.

The constraints (4.16) and (4.17) represent the ACLF nodal balance equations for active and reactive power at node i, where P_i and Q_i are the net power injections at each bus i, which in turn depend on the network admittance matrix, generation, load, and, of course, the connection status of the network elements. The network constraints consist of compliance with the operating limits on the bus voltage magnitude (4.18) and the reactive power limits of the *pv*-controlled synchronous generators according to their availability a_g (4.19), since downstream of switching operations, and with constant active power and voltage setpoints, the generating units can adjust the production (or absorption) of reactive power to balance the grid.

Finally, since the transmission network is operated with a meshed topology, only connected solutions will be considered valid.

4.3.2 Solution Algorithm

The approach adopted for the GA solution algorithm is based on the author's study carried out in [1] (Chapter 2). In this OTNR problem, the control variables can be organized in a vector $\boldsymbol{u}$ as in Fig. 4.8 (chromosome), where:

- $\sigma_l \in \{0, 1\}$ is the transmission lines l connection state;
- $\sigma_k \in \{0, 1\}$ is the busbar coupler k connection state;
- $\sigma_h^b \in \{0, 1\}$ is the disconnector h connection state at one end of the branch b (line l or transformer t);
- $\sigma_h^g \in \{0, 1\}$ is the disconnector h connection state of the generator g;
- $\sigma_h^d \in \{0, 1\}$ is the disconnector h connection state of the load d;
- $\sigma_h^s \in \{0, 1\}$ is the disconnector h connection state of the shunt device s.

Figure 4.8: Representation of a generic individual (chromosome) of the population.

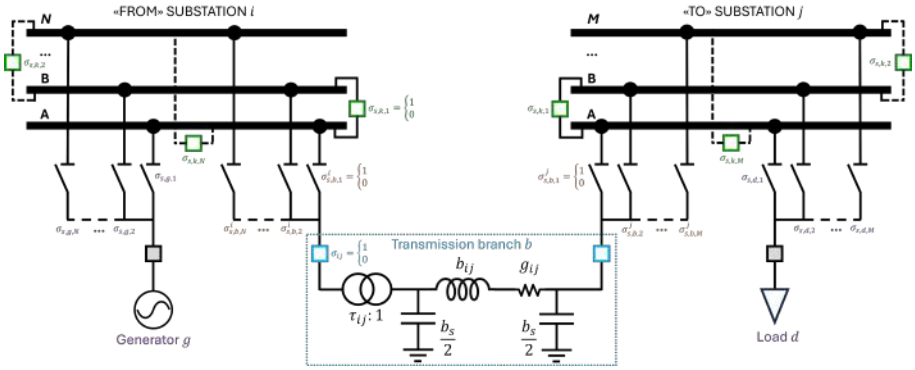

Figure 4.9: Generalized model of the network elements connection in substations.

With reference to Fig. 4.9, which shows how network elements can be connected in substations in the case of configurations that are more complex than the double-busbar system, it is clear that it would not make sense to keep more than one disconnector closed per element. Therefore, given the high number of binary control variables, it would be inconvenient to consider a chromosome vector that is too large, also because ineffective or redundant combinations could easily be generated during the GA's iterations.

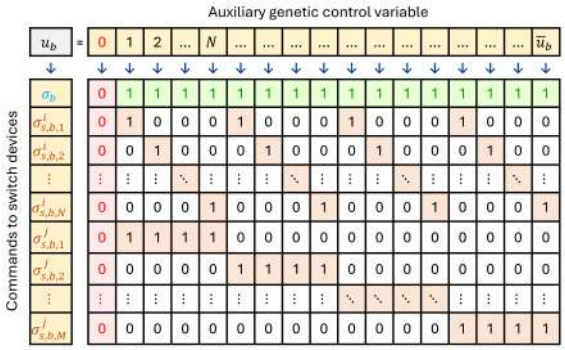

Figure 4.10: Correspondence between u_b and the connection mode of a transmission branch

For this reason, at the root of the proposed AC OTNR problem lies a reformulation of the chromosome $\boldsymbol{u}$. An intuitive graphical representation of the reformulation of chromosome $\boldsymbol{u}$ is shown in Fig. 4.10. Considering the more complex case of a transmission branch b, a genetic variable $u_b \in \mathbb{N}$ can be defined for each controllable element. The value of this variable varies in the integer numbers domain from 0 to a maximum value $\overline{u}_b$, depending on the number of possible combinations according to which the element can connect to the substations. The value 0 corresponds to

the out-of-service of the element in question; therefore, it is only permitted for switchable elements (for security reasons, generally shunts and lines). In the case of a branch b, connected between a substation with N busbars and another with M busbars, all possible useful switching combinations can be easily generated by concatenating identity matrices as shown. Therefore, each integer value of the variable u_b corresponds to a column vector of 0s and 1s representing the relationship between the states of the disconnectors and the circuit breakers associated with each end of the branch. Finally, it is easy to verify that for 1-terminal elements (generators, loads, and shunts), it is sufficient to define a single identity matrix with dimensions equal to the number of disconnectors with which the element in question is equipped.

The AC OTNR routine begins with an initial population sampling of N_{pop} individuals, where each individual is a vector containing the genetic control variables and represents a possible solution of the problem. Then, an ACLF calculation is performed for each individual so that the objective function (4.15) can be computed and compliance with constraints verified. In subsequent stages, the population is updated according to the genetic operators' of selection, crossover, and mutation generating new offsprings of individuals in which the best replaces the worst until a stop criterion is met. Please refer to Chapter 2 for a detailed discussion of genetic operators. A Binary Tournament Selection criterion is adopted, followed by a two-point crossover and a bitflip mutation. The overall GA procedure is represented is the diagram of Fig. 4.11.

In order to ensure the uniqueness of the individuals, each generated individual is checked against the others to ensure that it has not been created before. If a duplicate is detected, a sampling algorithm keeps generating new individuals until it finds a unique one. This guarantees that every individual in the initial population is distinct, improving genetic diversity and reducing redundancy in the search process.

4.3.3 Case Study & Test Results

The AC OTNR problem is built within *Pymoo* [86], an open-source Python library that offers state-of-the-art global optimization algorithms. This is used in the Python/DIgSILENT PowerFactory co-simulation framework, where the latter is used for ACLF calculations in the GA iterations.

For practical reasons, in the solution search space, the connection status of lines

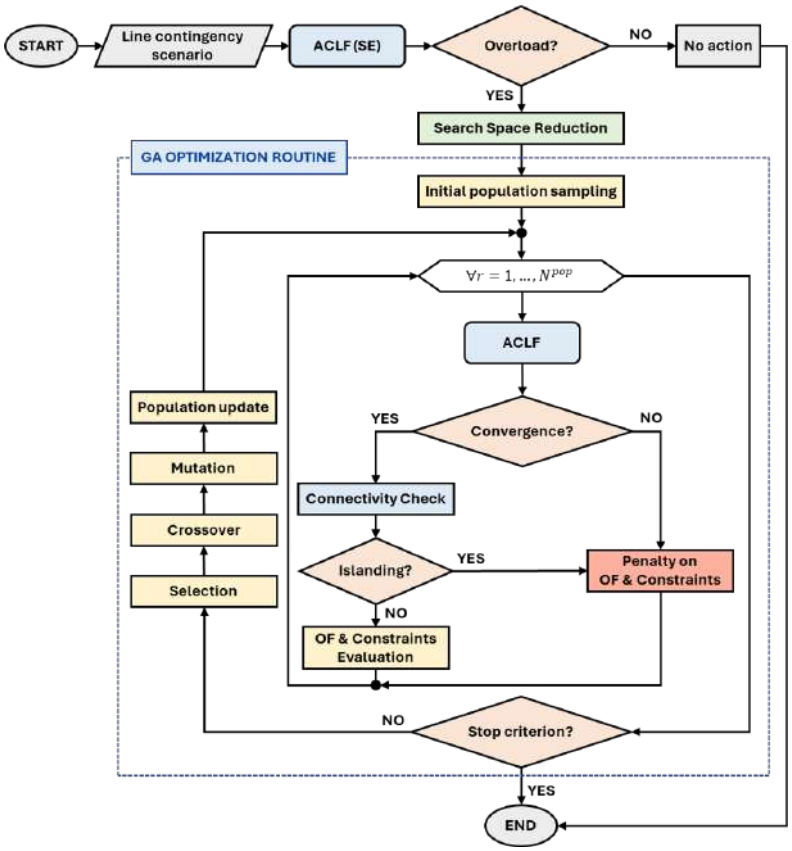

Figure 4.11: AC OTNR Genetic Algorithm.

and busbar switches that are owned by the TSO and installed on the 150 kV and 220 kV portions of the grid are considered as control variables. The HV 380 kV and MV lines are not controlled, as well as those whose disconnectors at the ends are open, those discharged still in-service and those identified as critical contingencies. Among the various grid assets, compliance with network constraints is verified only for those owned by the TSO, excluding grid components installed on the MV sections (handled by the local distribution system operators).

4.3.3.1 Optimizing the grid conditions in the pre-contingency state

In the analyzed operating conditions, the load demand is 1.78 GW and the local generation is 1.96 GW. Two 150 kV lines (ZAFPZISSFPZI150 and CEFPZISSFPZI150) are overloaded due to high power generation (540 MW) at Termini substation.

An N-1 contingency analysis was performed to derive critical line contingencies (Table 4.7):

Unlike tests with the preventive DC SCOTLS, the starting operating condition

Table 4.7: Ranking of the 5 worst line contingencies in terms of maximum branch loading detected

Overloaded line	**Loading % (pre-contingency)**	**Loading % (post-contingency)**	**Contingency case**
ZAFPZISSFPZI150	118.44	149.72	CORPTICRCPTI220
CEFPZISSFPZI150	101.38	134.62	CFLPDIFIUPDI150
CRCPTICMFP_I150	99.61	135.20	CFLPDIFIUPDI150
CEFPZITNKP_I150	98.01	132.92	CFLPDIFIUPDI150
TNKP_ICMFP_I150	98.01	132.92	CFLPDIFIUPDI150

for the AC OTNR is characterized by a realistic topological configuration in which there are outages due to maintenance. The control variables considered are 357/391, where 278/529 refer to transmission lines and 79/402 refer to busbar couplers.

As shown in Fig. 4.12, GA converged in 25 generations taking about 134 seconds. The objective function is successfully minimized to 0 from a value of 0.0342 corresponding to the initial operating condition. This implies that all overloads have been resolved.

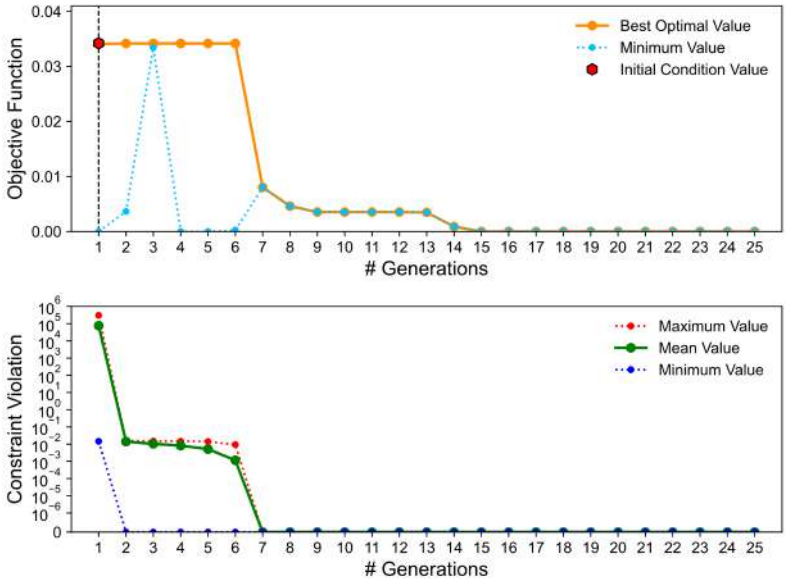

Figure 4.12: AC OTNR convergence.

From a topological point of view, 6 line switching operations and 3 busbar coupler reclosures are suggested in the Augusta, Sorgente, and Cattolica Eraclea substations. However, among the identified maneuvers, some may be unnecessary or have no effect on the network. The strictly necessary actions were selected through successive ACLF analyses.

Another ACLF analysis was conducted on the final operating condition in order to check the correctness of the solution found: Sicily is still exporting power to the

Mainland grid, there are no voltage violations on the HV busbars, and the overloads are solved. In the optimal condition, ZAFPZISSFPZI150 and CEFPZISSFPZI150 are loaded at 7.04% and 84.54%, respectively.

4.3.3.2 Optimizing the grid conditions in a post-contingency state

Extensive tests (not shown for the sake of brevity) were carried out optimizing the grid in post-contingency states, attempting to eliminate violations of network constraints (voltage and current) following a single contingency event. Local optimal solutions can be found with computational times that vary depending on the severity of the contingency event, ranging from 2 minutes to over an hour, depending on how far the initial operating condition is from an optimal local condition.

4.4 Remarks & Future directions

In this chapter two different methodologies have been applied to solve DC SCOTLS and AC OTNR on a realistic-sized transmission system, respectively. A first approach consisted of formulating a deterministic N-1 preventive SCOTLS problem under DCLF assumptions. This modeling technique revealed sufficient for congestion management purposes, allowing to find N-1 secure topologies without the need for post-contingency corrective actions. The proposed analytic approach is theoretically applicable within SCADA/EMS systems, provided that adequate computational resources are available (e.g., fast contingency analysis tools, parallel computing architectures).

Current developments concern the integration of substation splitting actions, which require a generalization of the topological constraints representing the connection relationships between busbar couplers and substation element disconnectors. Compared to the preventive SCOTNR model presented in Chapter 3 (valid for double-bus substations), it is therefore necessary to generalize the topological constraints in order to represent more complex configurations.

Regarding the approach for the AC OTNR, the proposed methodology is effectively able to mitigate overload phenomena by resorting to cost-free control actions. The approach proves useful in deciding corrective control actions in pre-contingency state or in the event of a single line contingency. In case of constraint violations under N conditions, the optimal topology derived may not necessarily meet the N-1 security

criteria. In fact, it would be appropriate to adapt the reconfiguration algorithm so that preventive control actions can be performed for N-1 security purposes. In this regard, an N-1 contingency analysis calculation should be performed downstream the ACLF for each individual, making the problem even more computationally challenging. However, since each portion of the network is managed by a dedicated control and operation center defined by geographic area, the computational burden used to solve the OTNR problem over an area is theoretically compatible with SCADA/EMS time requirements. Specific precautions are necessary in the practical implementation of real-world applications. The CPU time to solve the OTNR problem can be for sure reduced by parallelizing the evaluation phase in the GA and adopting more sophisticated techniques to reduce the solution search space. Nevertheless, this may prove insufficient in online corrective applications if more effective criteria for exploring the solution space are not considered.

Chapter 5

Optimal Network Reconfiguration Algorithms for Optimizing the Reliability and Quality of Supply in Primary Distribution Networks

Building upon the methodologies and optimization strategies developed in the previous chapters for transmission systems, this chapter extends the concept of Optimal Network Reconfiguration (ONR) to the distribution network level, addressing a complementary yet equally crucial aspect of modern power system operation.

While transmission-level reconfiguration primarily aims at congestion management, voltage profile improvement, and N-1 security enhancement, the distribution-level ONR faces different and increasingly complex challenges as well. This chapter, therefore, represents a conceptual and methodological shift from the optimization of large-scale transmission systems—where controllability and redundancy dominate—to the optimization of distribution networks, where limited observability, radial topology, and specific automation requirements drive the design of the reconfiguration algorithms. Moreover, the growing penetration of distributed energy resources (DERs), their variability and the need for automated fault management, require adaptive topological reconfiguration strategies capable of ensuring both operational efficiency and quality of supply.

Following these considerations, the motivation for this chapter stems from the ongoing transformation of traditional distribution grids into active and intelligent

networks. By extending reconfiguration optimization from the transmission to the distribution domain, the proposed research aims to develop methodologies that can be effectively integrated within Supervisory Control and Data Acquisition (SCADA) and Distribution Management Systems (DMS) environments, thus bridging the gap between academic optimization models and operational decision-making tools used by Distribution System Operators (DSOs).

The adoption of ONR tools is crucial in enhancing the operational efficiency, security, and reliability of smart distribution grids. ONR allows network operators to maintain grid integrity and ensure high quality of supply to end-users by optimally managing the network's topological configuration. To make ONR fully applicable within a real-time SCADA/DMS framework, it is essential to integrate practical Fault Detection, Isolation, and Recovery (FDIR) strategies commonly employed in real distribution networks.

In this context, the research conducted in this chapter addresses the ONR problem through deterministic optimization models based on both Mixed-Integer Linear Programming (MILP) [4, 5, 15] and Mixed-Integer Second Order Cone Programming (MISOCP) [3, 6, 7]. These formulations simultaneously consider connectivity and radiality constraints, as well as additional constraints related to selectivity and coordination of protection devices.

The proposed approaches have been tested on various case studies, ranging from the standard IEEE 33-Bus test system to realistically sized primary distribution networks with over a thousand nodes and distributed generation. The results demonstrate that ONR can lead to significant reductions in active power losses and improvements in quality-of-supply indices.

To complement the methodological contributions, an open-source software tool was developed in Python, interfacing with platforms such as OpenDSS, which allows solving realistic ONR problems while capturing the automation logics implemented by DSOs for FDIR. This open-source framework provides a replicable and extensible environment for testing and further development of ONR solutions, facilitating their practical adoption in real-world distribution systems.

5.1 Literature Review & Motivation

Optimal Network Reconfiguration (ONR) is a SCADA/DMS function that permits to find the switching operations necessary to optimize distribution network conditions. In general, ONR permits to minimize losses, balance load and generation, control voltages [116]. Even though its role in smart distribution grid operation was already recognized in the early sketches of advanced DMS [116], its adoption in real-time operation can be limited due to the necessity of ensuring reliable distribution automation (DA) schemes for fault protection.

Nowadays, fault detection, isolation, and recovery (FDIR) is accomplished through DA, employing smart protections, Intelligent Electronic Devices (IEDs), fault passage indicators and detectors [117]. Although each Distribution System Operator (DSO) adopts different approaches, according to power quality targets or DA deployment plans, most FDIR schemes are based on selectivity logics and on the knowledge of upstream/downstream relationships between the DA components.

Since, changes in the distribution network topology can affect the functionality of such protection schemes, this chapter proposes a methodology to include FDIR logics within the formulation of ONR. The formulation permits also to adopt ONR for the fulfillment of reliability targets, such as average frequency or duration of faults. Starting from the first Mixed-Integer Linear Programming (MILP) formulation [4], an organic and detailed model that permits to achieve an analytical solution of the combinatorial ONR problem, including an explicit formulation of AC Load Flow (ACLF) equations, is proposed. Specific advancements with respect to the state-of-art are detailed in the followings.

Generally, the ONR is a Mixed-Integer Non Linear Programming (MINLP) optimization problem, widely addressed in the literature, and solved using multiple approaches such as analytical [4, 118–130] and metaheuristic [122, 131–134], focusing primarily on the challenges related to the non-linearity and combinatorial nature of this problem.

A literature taxonomy of deterministic distribution ONR models cited in this work is given in Table 5.1. The use of deterministic models simplifies the verification and validation of results, considering that a global optimal solution is theoretically guaranteed when the problem is well-posed. Furthermore, decisions are based on explicit rules, allowing the choices made by the model to be easily justified to grid

operators or energy regulators.

Table 5.1: Literature Taxonomy of Deterministic Distribution ONR Models Cited In This Work

	Formulation			Solution Method		Objective Function		Constraints					DN Model		
#	MILP	MIQCP/MISOCP	MINLP	AA	G/MA	SOF	MOF	ACLF	RAD	CONN	REL	PD&DA	BTS	RTS	$\|\Omega_n\| \geq 500$
[118, 119]	✓			✓		✓		✓	✓	✓			✓		
[120]		✓		✓			✓	✓	✓	✓			✓		
[131]			✓		✓	✓		✓	✓	✓			✓		
[121]	✓			✓			✓	✓	✓	✓			✓		
[132, 133]			✓		✓		✓	✓	✓		✓		✓		✓
[134]			✓		✓	✓		✓	✓	✓	✓		✓		
[122]			✓		✓		✓	✓	✓	✓		✓	✓		
[123]	✓		✓	✓	✓	✓		✓		✓			✓		
[124, 125]		✓		✓			✓	✓	✓	✓	✓		✓		
[126]	✓	✓		✓		✓		✓	✓	✓			✓		
[127]		✓		✓	✓	✓		✓	✓	✓			✓		✓
[128]	✓	✓		✓		✓		✓	✓	✓			✓		✓
[129]		✓		✓			✓	✓	✓	✓	✓	✓	✓	✓	
[4, 130]	✓			✓		✓	✓		✓	✓	✓	✓		✓	✓
Present	✓	✓	✓	✓	✓	✓	✓	✓	✓	✓	✓	✓	✓	✓	✓

*AA: Analytic Approach, G/MA: Genetic/Metaheuristic Algorithms, SOF: Single Objective Function, MOF: Multiobjective Function, RAD: Radiality, CONN: Connectivity, REL: Reliability, PD&DA: Protection Devices & Distribution Automation, BTS: Benchmark Test Systems, RTS: Real Test Systems.

Some formulations allow to find more reliable topologies preventing or limiting the risk of disruption for end-users [4, 125, 129]. Anyway, such models require knowledge of additional parameters (customers to be supplied, failure rates, unavailabilities, etc.), equally providing methods and standards for exploiting them in deterministic ONR problems.

Several approaches exist, on the other hand, to integrate the non-linear ACLF equations as constraints by obtaining feasible topologies that meet security requirements during operation. Genetic algorithms (GAs) and metaheuristics are capable of handling MINLP models, often leveraging rapid LF or non-linear optimization routines on a set of fixed topologies generated according to appropriate criteria, iteratively penalizing any non-convergent or infeasible solutions [133, 134]. To efficiently solve a non-convex MINLP problem, some analytical formulations linearize network equations through MILP techniques [118, 119, 123, 126], while others use tighter relaxation methods based on Mixed-Integer Quadratic Convex Programming (MIQCP) [120, 127, 128] or Mixed-Integer Second Order Cone Programming (MISOCP) [124, 125]. The latter, prove to be lighter and mostly exact when applied on radial networks [135], leading to general and sound formulations even in the presence of integer variables and on-off constraints [**?**]. Other works derive effective MISOCP formulations from the *DistFlow* equations [136] or by exploiting the industrial voltage drop formula [129]. Thanks to their relaxation capabilities, MISOCP formulations allow also to represent hybrid systems which integrate Soft Open Points (SOPs).

For instance, the studies in [137, 138] successfully adopted MISOCP approaches in the solution of planning studies related to SOP allocation and optimization in multi-energy systems. In this context, the control of SOPs can be regarded as an alternative approach to reconfiguration, where energy flows are no longer constrained by discrete switching decision variables.

On the basis of the literature research and the taxonomy in Table 5.1, it can be observed that only few works deal with integrating the logic of protection devices within optimization while considering network constraints [122, 129]. As previously remarked, this is a relevant aspect to consider while assessing the actual feasibility of the reconfiguration, as it may affect FDIR logics. In addition, among the works that test ONR scalability on grid models with more than 500 buses [127, 128] or own realistic-sized DN models [132, 133], protection devices selectivity logics are never considered. This clearly represents an hindrance to the actual application of ONR, especially in the framework of real-time SCADA/DMS and power system operation.

Based on these rationales, this work proposes a full deterministic AC ONR formulation, based on MISOCP relaxation, which allows to develop an ONR problem which includes constraints on connectivity and radiality, and reliability functions based on FDIR logics. Scalability tests on realistic-sized distribution networks, comparisons with other solution methods, and validation using Monte Carlo simulation demonstrate the soundness of the methodology and its applicability in SCADA/DMS environments.

5.2 Fault Detection Isolation & Recovery Practices

This paragraph describes the most common FDIR techniques actually adopted by the Italian DSOs. The schemes are mostly based on the use of fault-passage indicators (in the Italian practice known with the acronyms RGDAT and RGDM [139]) which detect passage of fault currents and absence of voltage. The schemes are listed with growing degree of automation:

1. *Fault Detection Function (FRG)*: widely used DA technique to identify both single-phase to ground (SPG) and multi-phase faults [140], based on the detection of fault currents and absence of voltage. FDIR is based on the operation of circuit breakers (CBs) in primary substation and the automatic switching of disconnectors in secondary substations.

2. *Compensated Neutral Function (FNC)*: technique used only in distribution systems with compensated neutral [141]. The technique is also based on the detection of fault currents. In the case of SPG faults, switch disconnectors (SDs) are coordinated to achieve chronometric selectivity.

3. *Smart Fault Selection (SFS)*: more advanced FDIR technique based on logical selectivity achieved by coordinating CBs distributed along the feeders [142]. Horizontal communication between CBs is obtained through the use of IEC 61850.

5.2.1 Fault Detection Function (FRG)

The FRG technique is the simplest logic used for FDIR. It can be implemented on both cable and overhead lines, it is suitable for networks with either isolated or compensated neutral, and can be applied even without a communication system. Clearly, intervention times may vary from case to case according to the DSO operation rules and standards. This technique assumes that automatic CBs are installed only in the primary substations. Fault isolation is performed by SDs, or even simple disconnectors, which open during the auto-reclosing sequence of CBs, when no-voltage (and no-current) conditions are detected.

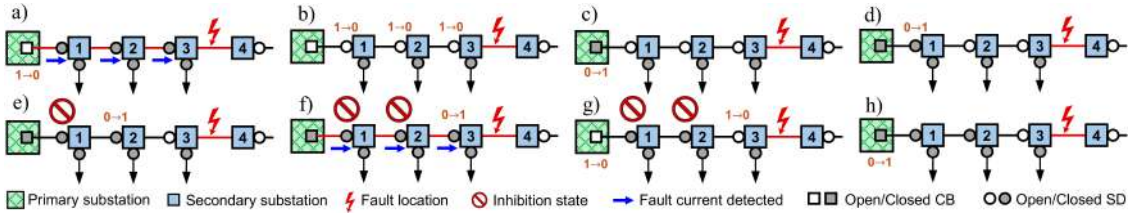

Figure 5.1: FRG technique: *a)* Fault occurence and CB trip, *b)* SDs automatic opening, *c)* First CB reclosure, *d)* First SD reclosure, *e)* Second SD reclosure with first SD in inhibition state, *f)* Third SD reclosure with first and second SDs in inhibition state, *g)* CB re-opening and third SD re-opening, *h)* Final configuration and fault isolation [3].

The CB in the primary substation trips when a fault current is detected (Fig. 5.1a). In the case of a permanent fault, after the second trip, the DA equipment in secondary substations commands the opening of all the SDs through which the fault current has flowed (Fig. 5.1b). These switching operations allows the CB to reclose, since the fault has been isolated (Fig. 5.1c). All SDs which have been previously switched off, having detected the restoration of voltage on the upstream side will try to reclose. This operation is done automatically, following a chronological order from

upstream to downstream (Figs. 5.1d, 5.1e, 5.1f). Whenever a SD recloses without leading to a fault, it enters an inhibition state for any following interruption (e.g., for secondary substations #1 and #2 in Fig. 5.1f). Differently, the SD whose reclosing causes a re-energization of the fault, will remain open (Fig. 5.1g). At the end of the auto-reclosing sequence (Fig. 5.1h), only the SD #3 will be left open, whereas power will be restored on all upstream branches. The entire DA function is usually designed to operate within the 3 minutes time limit of short interruptions, according to the EN 50160.

5.2.2 Compensated Neutral Function (FNC)

The FNC technique can be applied to DNs operated with compensated neutral, and is based on chronometric selectivity during SPG faults. Since SPG currents are characterized by low intensity, due to the presence of a ground fault neutralizer (e.g., Petersen coil), SDs can therefore be deployed and properly coordinated to achieve selectivity. The intervention logic is schematically shown in Fig. 5.2.

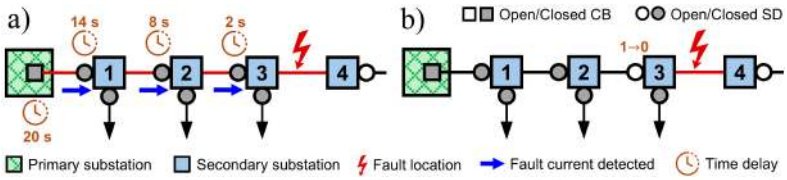

Figure 5.2: FNC technique: *a)* Fault detection with chronometric selectivity, *b)* Final configuration and fault isolation [3].

In the case of SPG fault, the SDs which see the passage of a fault current will open automatically with a predefined delay. This delay grows moving upstream, so that the SD closest to the fault will open first (Fig. 5.2b). The CB in the primary substation, unless the fault occurred in the first section, remains closed for the entire duration of the FDIR procedure, minimizing the number of clients which will experience an interruption. In the case of non-SPG faults, SDs cannot interrupt the short circuit current and the DA system reverts back to FRG.

5.2.3 Smart Fault Selection (SFS)

This DA technique requires the adoption of CBs along the distribution feeders. Logical selectivity is achieved by exploiting horizontal communication functions between the IEDs assigned to the protection functions. This technique has been introduced to

achieve very short fault detection and minimize the number of interrupted customers. The protection logic exploits the structure of the IEC 61850 protocol which allows, thanks to its bi-directional client-server organization, to send interrupt messages (e.g. GOOSE message) at horizontal level, thus achieving logical selectivity.

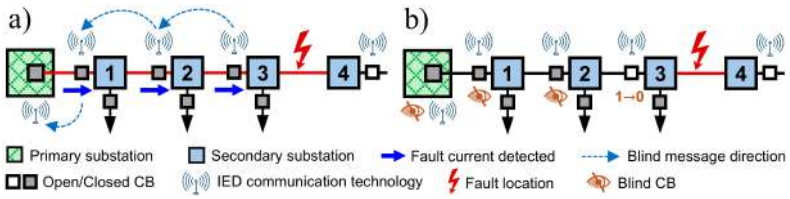

Figure 5.3: SFS technique: *a)* Fault detection through IEDs, *b)* Final configuration and fault isolation. [3].

As shown in Fig. 5.3, each CB detecting the passage of a short-circuit current sends a blind message to the upstream CBs. The CB closest to the fault, will not receive any blinding message and will trip first, preventing upstream or lateral paths to be interrupted.

This technique is the most advanced of the three, however is the one that requires more investments in DA. First of all CBs must be employed along the feeder (SDs cannot interrupt high currents). In addition, in order to implement the SFS, the following conditions must be met by the communication system:

- communication between primary and secondary substations must be established;
- GOOSE messages must be transported efficiently over extended distances;
- low latency between devices must be ensured (< 100 ms);
- secure delivery of information, and in particular GOOSE messages, must be also ensured;
- a large number of devices must handled, approximately around one hundred per each primary substation.

In addition, the presence of IEDs is required in secondary cabins (in the Italian practice this role is covered by the so-called RGDM devices). SFS technique can also perform automatic restoration of downstream substations. However in several cases, for safety reasons, restoration is performed manually by the control center operators.

5.3 Nomenclature

The nomenclature in Table 5.2 refers to the formulation of the ONR problems described in this chapter.

Table 5.2: Nomenclature of the Distribution ONR Model.

Indices	
i, j	Indices for generic bus
ij, ji	Indices for generic branch
z, a, b, k, m	Indices for generic zone
h	Index for feeder ancestor zone
s	Index for generic switch
Sets	
Ω_b, Ω_n, Ω_z	Branches, Buses, Zones
$\Omega_{sw} \subset \Omega_b$	Switches
$\Omega_h \subset \Omega_z$	Feeders
$\Omega_{ss} \subset \Omega_z$	Substations
Parameters	
b_{ij}, g_{ij}	Branch ij susceptance / conductance
b_i^s, g_i^s	Branch ij half charging shunt susceptance / conductance at bus i
$\varphi_{k,m}^G, \varphi_{k,m}^D$	Artificial generation (G) or demand (D) at zone k with respect to zone m
p_i^G, p_i^D	Active power generation (G) and load demand (D) at bus i
q_i^G, q_i^D	Reactive power generation (G) and load demand (D) at bus i
$\overline{S}_{ij}$	Max. apparent power flow of branch ij
$\underline{v}_i$, $\overline{v}_i$	Voltage magnitude technical limits at bus i
N	Number of customers
λ	Failure rate [faults/year]
ρ	Average downtime per failure [h]
$\bar{\rho}$	Time to complete automatic re-closing [h]
Continuous real variables	
v_i, θ_i	Voltage magnitude and angle at bus i
p_{ij}, p_{ji}	Active power flow on branch ij or ji
q_{ij}, q_{ji}	Reactive power flow on branch ij or ji
c_{ii}, c_{ij}, s_{ij}, c_{ii}^j	Auxiliary variables of MISOCP relaxation
$\varphi_{s,m}$	Artificial flow through switch s with respect to zone m
f_z	Frequency of failures in zone z
U_z	Total hours of downtime in zone z
EENS	Expected Energy Not Served [kWh/year]
SAIDI	System Average Interruption Duration Index [h/year]
SAIFI	System Average Interruption Frequency Index [faults/year]
Binary integer variables	
x_s	*Switch status*: equal to 1 if switch s (from bus i / zone a to bus j / zone b) is closed, 0 otherwise.
$\alpha_{k,m}$	*Upstream condition*: 1 if zone k is upstream to zone m, 0 otherwise.
$\beta_{k,m}$	*Kinship condition*: 1 if zones k and m belong to the same feeder, 0 otherwise.
$\gamma_{h,k,m}$	*Common ancestor condition*: 1 if both zones k and m are descendants of the same feeder ancestor zone h, 0 otherwise.

5.4 ONR MILP Formulation

In this paragraph, a deterministic ONR problem, aimed to improve quality of supply indices, taking into account the automatic FDIR techniques, is formulated for balanced primary distribution grids and solved using MILP solvers. The developed formulation allows connectivity, radiality, and FDIR fault selectivity logics to be rigorously enforced, making the ONR problem tractable for commercial solvers and implementable in industrial applications.

5.4.1 Distribution Network Zone Partitioning

Given the very large number of possible integer variables, the computational complexity of the problem can be drastically reduced considering that distribution networks are weakly meshed systems, and that most branch elements cannot be switched automatically. During faults, only few switches are called to ensure the functions of fault detection and isolation.

Then, a practical way to reduce the number of binary variables is to adopt a simple pre-optimization zone partitioning algorithm as in [143]. Further details on this will be provided in Paragraph 5.5. In a generic distribution grid, it is possible to define a zone z as a set of interconnected buses and branches which are only bounded by switches. There are no automatic switches inside a zone, and therefore, through the zone partitioning, an equivalent zone-switch graph of the network can be obtained. In this graph, each zone represents a vertex, whereas switches are the edges which interconnect the zones. Typically, there are no meshes inside a zone and, consequently, if the zone-switch graph is radial, then the whole distribution network is also radial. This partitioning permits, not only to reduce the number of integer variables, but also the number of connectivity constraints and kinship conditions between different portions of the grid.

As previously remarked, zones do not contain switches; any fault within a zone can be cleared and isolated only by a switch, outside of the zone, in the upstream path to the source. In fact, for a generic zone z, it is possible to evaluate failure rate λ_z and an average downtime per failure ρ_z. Under the assumption of high repairability (mean time to repair significantly lower than mean time to fail), λ_z is obtained by summing up the failure rates λ of each component within z (e.g., busbars, terminals, branch elements etc.). This is possible because all fault events

within the zone are series events. Instead, the average downtime time ρ_z is obtained dividing the sum of all series outage hours (i.e., the products $\lambda \cdot \rho$) by λ_z.

5.4.2 Objective function

The ONR MILP optimization problem considers the switches' connection state $x_s \in \{0, 1\}$ as the only control variable. Therefore, to optimize the system's quality of supply, the objective function (OF) to be minimized consists of the weighted sum of three typical power quality indices, Expected Energy Not Served (EENS), System Average Interruption Duration Index (SAIDI), and System Average Interruption Frequency Index (SAIFI):

$$\min(w_1 \cdot \text{EENS} + w_2 \cdot \text{SAIDI} + w_3 \cdot \text{SAIFI}) \tag{5.1}$$

where w_1, w_2, w_3 are weight coefficients.

The indices in (5.1) are evaluated at the zonal level, aggregating the results of each zone as follows [144]:

$$\text{EENS} = \sum_{z \in \Omega_z} p_z^D \cdot U_z \quad \text{[kWh/year]} \tag{5.2}$$

$$\text{SAIDI} = \frac{\sum_{z \in \Omega_z} U_z \cdot N_z}{\sum_{z \in \Omega_z} N_z} \quad \text{[h/year]} \tag{5.3}$$

$$\text{SAIFI} = \frac{\sum_{z \in \Omega_z} f_z \cdot N_z}{\sum_{z \in \Omega_z} N_z} \quad \text{[faults/year]} \tag{5.4}$$

The minimization of (5.1) is subject to equality and inequality constraints to ensure that the network remains radial and connected after ONR. In addition, different reliability functions for f_z and U_z can be considered depending on which FDIR technique is implemented by the DSO (FRG, FNC, or SFS), and resulting in three different MILP formulations.

5.4.3 Connectivity and radiality constraints

If the network is operated with a radial topology, then also its equivalent zonal graph must be radial. The necessary but not sufficient condition for radiality [126] is thus:

$$\sum_{s \in \Omega_{sw}} x_s = |\Omega_z| - |\Omega_{ss}| \tag{5.5}$$

Assuming that power is generated in any zone $z \in \Omega_{ss}$, where substations are located, and that a unit load demand is applied at a generic zone m, each switch s (connecting zone a to zone b) is affected by the circulation of an artificial power flow $\varphi_{s,m}$. Therefore, connectivity is ensured if, for each m-th zone, the following zonal balance equations are respected:

$$\sum_{\substack{s \in \Omega_{sw} \\ b=k}} \varphi_{s,m} - \sum_{\substack{s \in \Omega_{sw} \\ a=k}} \varphi_{s,m} + \varphi^G_{k,m} = \varphi^D_{k,m} \quad \forall k, m \in \Omega_z \tag{5.6}$$

where $\varphi^D_{k,m} = 1$ if $k = m$ (0 otherwise), and $\varphi^G_{k,m} = 1$ if $k \in \Omega_{ss}$ (0 otherwise).

The artificial flow $\varphi_{s,m}$ represents the power flowing on s when the unit load demand is applied in m. Therefore $\varphi_{s,m}$ is non-zero only if the switch s is in the radial path from the power source to the zone m. In this case, $\varphi_{s,m}$ assumes the value $+1$ or -1, depending on the orientation of the switch s.

The artificial flow $\varphi_{s,m}$ is related to the connection state of s through the following constraint:

$$|\varphi_{s,m}| \leq x_s \quad \forall s \in \Omega_{sw}, \forall m \in \Omega_z \tag{5.7}$$

5.4.4 Kin relationships

For a generic zone m, it is possible to determine if any other zone is upstream through the following constraints:

$$\alpha_{a,m} \geq |\varphi_{s,m}|, \quad \forall s \in \Omega_{sw}, \forall m \in \Omega_z \tag{5.8}$$

$$\alpha_{b,m} \geq |\varphi_{s,m}|, \quad \forall s \in \Omega_{sw}, \forall m \in \Omega_z \tag{5.9}$$

As long as the switch s is part of the radial path between two zones, then $\alpha_{a,m} = \alpha_{b,m} = |\varphi_{s,m}| = 1$.

Thanks to the upstream condition, it is possible to determine if two zones k and

m belong to the same feeder. This is done by introducing the binary variables $\gamma_{h,k,m}$ and $\beta_{k,m}$, and the following constraints:

$$\gamma_{h,k,m} \geq \alpha_{h,k} + \alpha_{h,m} - 1, \quad \forall k, m \in \{\Omega_z \backslash \Omega_{ss}\}, \forall h \in \Omega_h \tag{5.10}$$

$$\beta_{k,m} = \sum_{h \in \Omega_h} \gamma_{h,k,m}, \quad \forall k, m \in \{\Omega_z \backslash \Omega_{ss}\} \tag{5.11}$$

Please note that $\gamma_{h,k,m}$, and therefore $\beta_{k,m}$, will be different from zero only if k and m are descendants of the same ancestor zone h. Moreover, since (5.10) and (5.11) involve a large number of constraints, the problem size can be reduced by formulating them only for $m \leq k$, according to the symmetry relations observed for the variables $\beta_{k,m}$ and $\beta_{m,k}$ [130]. Thus, given the $k \times m$ matrix containing the elements $\beta_{k,m}$, it is sufficient to define only the elements which belong to the bottom triangular part including the main diagonal.

5.4.5 FDIR Reliability Functions

In general, the terms in (5.1) can be written as functions of the variables $\alpha_{k,m}$ and $\beta_{k,m}$:

$$f_z = \mathcal{F}_1(x_s, \alpha_{k,m}, \beta_{k,m}), \quad \forall z \in \Omega_z \tag{5.12}$$

$$U_z = \mathcal{F}_2(x_s, \alpha_{k,m}, \beta_{k,m}), \quad \forall z \in \Omega_z \tag{5.13}$$

These functions represent additional linear constraints that can be integrated together with (5.5)-(5.11), and depend on network parameters. As explained in the following, they are formulated according to the FDIR practices adopted by Italian DSOs.

5.4.5.1 FRG constraints

In general, when FRG is implemented, the failure frequency of a generic zone z is given by the sum of the failure rates of all other zones in the same feeder, and therefore:

$$f_z^{\mathrm{FRG}} = \sum_{k \in \Omega_z} \beta_{k,z} \cdot \lambda_k, \quad \forall z \in \Omega_z \tag{5.14}$$

The previous equation affirms that any fault happening in a feeder will cause an interruption of all other zones in the same feeder. However, thanks to the FDIR

function, the fault will be isolated within the end of the CB auto-reclosing. This means that only faults happening in the direct upstream path to the source will cause a long interruption. All other faults (in a downstream or lateral path) will be cleared within a time $\bar{\rho}$ that depends on the time necessary to isolate the fault. Thus, unavailability for each zone z can be formulated as:

$$U_z^{\mathrm{FRG}} = \sum_{k \in \Omega_z} [\alpha_{k,z} \cdot \lambda_k \cdot \rho_k + (\beta_{k,z} - \alpha_{k,z}) \cdot \lambda_k \cdot \bar{\rho}], \quad \forall z \in \Omega_z \tag{5.15}$$

In (5.15), U_z is the sum of two components. The first term takes into account the interruption due to a fault in the upstream path. The second term considers what happens if the fault is on a downstream or lateral path. This second term is null in the case of an upstream fault since both $\beta_{k,z}$ and $\alpha_{k,z}$ equal 1.

5.4.5.2 FNC constraints

In order to assess fault frequency and unavailability, it is necessary to introduce different failure rates for SPG ($\lambda_k^{'}$) and non-SPG faults ($\lambda_k^{''}$), equal to $\frac{1}{3}\lambda_k$ and $\frac{2}{3}\lambda_k$, respectively (5.16). In the case of SPG fault, FNC automation guarantees selectivity and, therefore, a zone is interrupted only when a fault happens in another zone that is in the direct upstream path to the source. Faults in a downstream or lateral path will not cause interruption. For non-SPG fault the same assumptions made for FRG stand, and therefore:

$$f_z^{\mathrm{FNC}} = \sum_{k \in \Omega_z} [\alpha_{k,z} \cdot \lambda_k^{'} + (\beta_{k,z} + \beta_{z,k}) \cdot \lambda_k^{''}], \quad \forall z \in \Omega_z \tag{5.16}$$

$$U_z^{\mathrm{FNC}} = \sum_{k \in \Omega_z} [\alpha_{k,z} \cdot (\lambda_k^{'} + \lambda_k^{''}) \cdot \rho_k + (\beta_{k,z} + \beta_{z,k} - \alpha_{k,z}) \cdot \lambda_k^{''} \cdot \bar{\rho}], \quad \forall z \in \Omega_z \tag{5.17}$$

5.4.5.3 SFS constraints

This kind of DA assumes that each CB crossed by a short circuit current sends a blinding message to the CBs in the upstream path, the CB closest to the fault will trip first and avoid interruption in the upstream or lateral paths. In this case, kinship constraints (5.10) and (5.11) are not needed and therefore:

$$f_z^{\mathrm{SFS}} = \sum_{k \in \Omega_z} \alpha_{k,z} \cdot \lambda_k, \quad U_z^{\mathrm{SFS}} = \sum_{k \in \Omega_z} \alpha_{k,z} \cdot \lambda_k \cdot \rho_k, \quad \forall z \in \Omega_z \tag{5.18}$$

5.5 ONR MILP - Case study & Test results

The proposed ONR MILP approach is applied to a realistic-sized distribution network, supplying electricity to a town in southern Italy [132]. The grid serves about 35,000 customers spread over an area of roughly 100 km^2, including urban and rural areas, and counting about 60,000 inhabitants [133, 145]. The distribution network is connected to the sub-transmission via a 150/20 kV primary substation. As in Fig. 5.4, the distribution is organized on 11 feeders. Four of them are below the transformer TR A, which supplies the urban area. The remaining seven circuits are feeding the rural and industrial areas, and are connected to TR B.

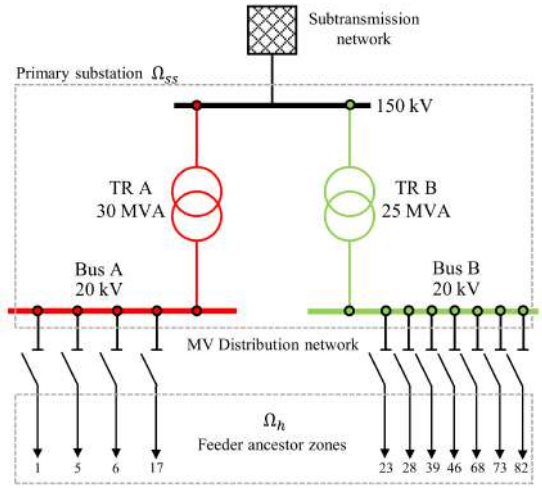

Figure 5.4: Simplified diagram of the distribution network interconnection with the subtransmission grid [4].

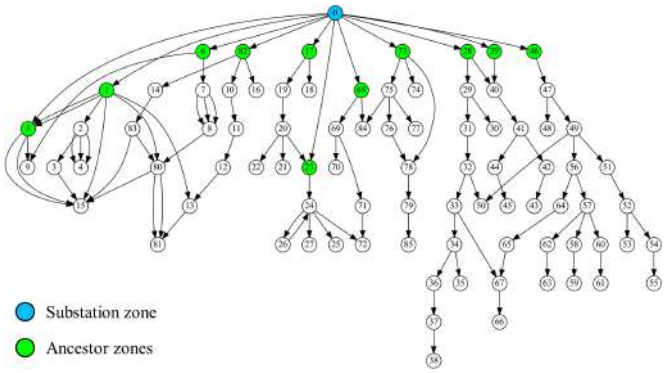

Figure 5.5: Distribution network's oriented zonal graph with all the switches closed [4].

The distribution network has a total of 902 nodes, 924 lines (cable and overhead), and 110 telecontrolled switches. As a result of the zonal partitioning, the DN is

divided into 86 zones. Of these, 11 zones are ancestors directly connected to the substation by means of an automatic CB. The full zonal graph of the network is shown in Fig. 5.5.

In this figure, all switches are closed and the feeder ancestor zones are colored in green. It can be noted that, in general, the urban feeders (under TR A) are more meshed than the rural/industrial ones. To ensure radiality, 25 switches must be opened, whereas the closed ones are 85.

Failure rates and restoration times for buses and branches were derived according to the surveys in [146]. It was assumed that the auto-reclosing scheme at the head-feeder CBs employs a maximum time $\bar{\rho}$ of 3 minutes. This time limit considers the practices currently employed by DSOs to avoid long duration interruptions (see the European voltage characteristics standard EN 50160).

All cases assume same input data, such as load demand p_z^D, number of customers N_z, unavailability and restoration time.

Software tools employed:
The ONR MILP problem was solved in Python programming environment. Network data were imported automatically from a distribution network model built in OpenDSS. The solving routine was developed using the Pyomo library [147], and subsequently tackled employing the commercial solver Gurobi 11.0.1 with default settings [148]. All numerical simulations were performed on a computer with 32 GB RAM, 12th Gen Intel® Core™ i9-12900F CPU @ 2.40 GHz, 16 physical cores and 24 logical processors, using up to 24 threads. All cases assume same input data, such as load demand p_z^D, number of customers N_z, unavailability and restoration time.

5.5.1 Base Case

An initial random network configuration (Initial Radial Topology or IRT) was assumed as base case (see Fig. 5.6). The initial values of EENS, SAIDI and SAIFI can be calculated solving the ONR problem, after having fixed the variables x_s for all switches and obtained the values of λ_z and U_z. The results obtained assuming the worst case (FRG) are used to normalize the terms in (5.1). In the tests, it was assumed that each normalized term in (5.1) weights the same. After normalization the objective function assumes the value of 1 in the IRT-FRG case. This permits to easily compare the impacts that ONR and the adoption of FDIR techniques bring in terms of system reliability.

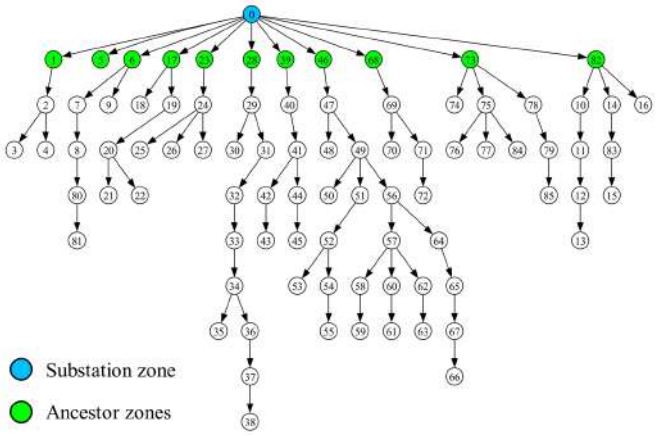

Figure 5.6: Distribution network initial radial topology [4].

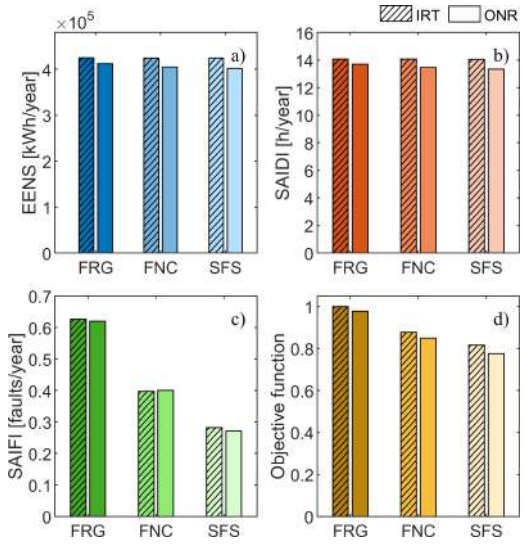

Figure 5.7: Monitored quality indices and objective function: *a)* EENS, *b)* SAIDI, *c)* SAIFI, *d)* objective function (5.1) [4].

5.5.2 ONR MILP results

As shown in Fig. 5.7 bottom-right, in the base case, the values obtained of the objective function (5.1) confirm that the best performances are reached with SFS. FNC performs better than FRG, but worse than SFS. In general, the main improvement can be only obtained in terms of SAIFI, since FNC and SFS are able to prevent the tripping of CBs in the substation. EENS and SAIDI, instead, cannot be much improved because the tripping of the CB leads, in most cases and for most zones, only to short interruptions. Improvements for all indices can be obtained only through a reconfiguration.

The optimal radial topologies obtained solving the ONR problem and assuming

different FDIR techniques are shown in Figs. 5.8a, 5.8b, and 5.8c, respectively for the FRG, FNC and SFS technique. The three topologies are radial and connected. The topological modifications with respect to IRT are also shown: red dashed arrows represent switches that have been opened, whereas blue arrows the switches that have been closed. Black arrows indicate switches whose status remained unchanged.

Fig. 5.7 shows also the results obtained in terms of EENS, SAIDI and SAIFI. Graphs in the bottom-right confirm the same results obtained before (SFS better than FNC, FNC better than FRG). However, in this case, it is possible to observe an improvement also in terms of outage duration and energy not served. This is due to the fact that ONR is able to associate the zones characterized by higher loads and number of customers to the feeders that have the lowest chance to experience a fault.

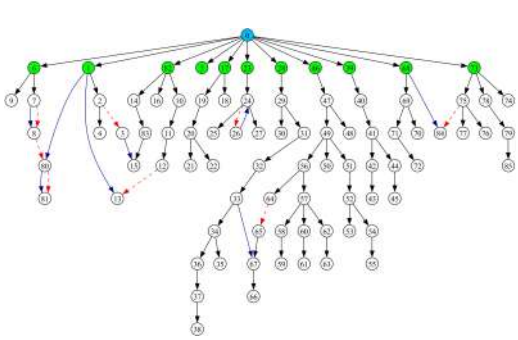

(a) FRG technique

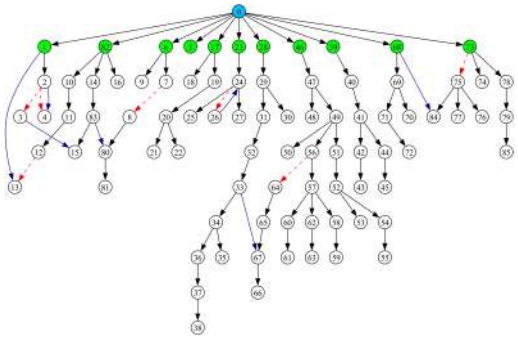

(b) FNC technique

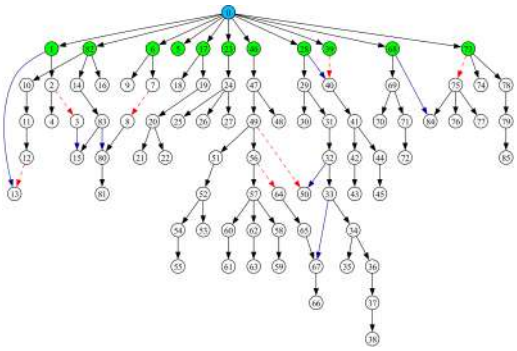

(c) SFS technique

Figure 5.8: Optimal configurations in different FDIR cases: a) FRG, b) FNC, c) SFS [4].

The percentage variations of all indices with respect to the IRT case are shown numerically in Table 5.3. Please note that the three terms minimized in (5.1) are competing and, therefore, the minimization of one index can impact on the other two. This explains why, for example, in the FNC case SAIFI after optimization is slightly

worse than before (Fig. 5.7 bottom-left). Numerical results confirm that quality of supply can be improved through distribution network reconfiguration and suggest that best improvements can be obtained when the most sophisticated distribution automation techniques are adopted.

Table 5.3: Percentage Variation from the Initial Radial Topology

FDIR	**ΔEENS**	**ΔSAIDI**	**ΔSAIFI**	**Δ*f***
FRG	-2,94%	-2,64%	-0.97%	-2.19%
FNC	-4,62%	-4,19%	0.91%	-3,13%
SFS	-5,30%	-5,08%	-3.69%	-4,92%

5.5.3 Computational performances

Computing times are very low and theoretically compatible with the time requirements of on-line SCADA/DMS functions (solution required 8.73 s for FRG, 1.05 s for FNC, and 0.30 s for SFS). The three reconfigured topologies are achieved with zero optimality gap (MIP gap) in FNC and SFS cases, 0.084% for FRG. The solution of the ONR-SFS problem is the fastest simply because the problem is much lighter. Given the formulation of λ_z and U_z, constraints (5.10) and (5.11) can be skipped, and the use of variables $\gamma_{h,k,m}$ and $\beta_{k,m}$ avoided. In the SFS case, the solver used a simplex-based method, whereas the solution of FRG and FNC cases required the use of the Gomory Cutting Planes technique to relax the binary variables to achieve convergence.

The number of switching maneuvers required to reach the new topology are more or less the same, and do not seem to have influence on the computational effort. FNC and SFS techniques required seven transitions from open to closed ($0 \rightarrow 1$) and from closed to open ($1 \rightarrow 0$), whereas FRG needed eight transitions.

5.6 Development of an Open-Source ONR Software Tool

This paragraph describes in detail the algorithms and routines necessary to develop an open-source software architecture capable of solving the ONR MILP problem formulated in Paragraph 5.4, addressing the challenges arising from mathematical complexity and computational effort.

The research activity described is part of the Project on "Evolution, planning, management and electricity networks operation" project, funded by Italian Ministry of the Environment and Energetic Safety (MASE), involving the Italian National Agency ENEA, Politecnico di Bari and other research institutes. The project aims to support the assessment of adequacy, operational security, resilience and reliability performances, and to enable advanced operation and planning of decarbonized energy systems, also through the implementation of a suite of open-source tools. Detailed features of the project are described in [149].

The software was developed relying on open-source tools and platforms only. OpenDSS was employed for network representation and data exchange, whereas the entire code is developed using Python language and open-source libraries. The ONR optimization problem was formulated through the Pyomo library [60, 147], which supports the use of external solvers, either being commercial or open-source products. An overall scheme of the ONR software is given in Fig. 5.9, where is possible to distinguish several subroutines, whose detail is given in the following sub-paragraphs.

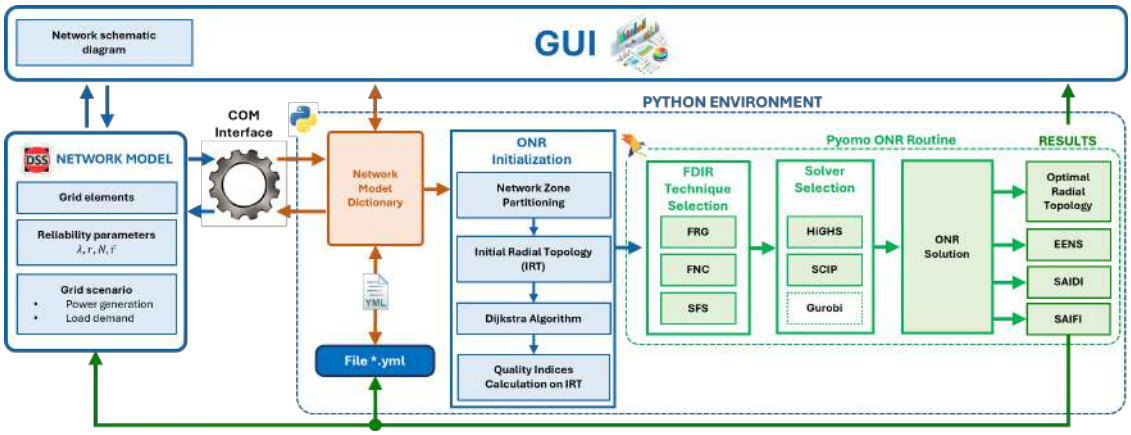

Figure 5.9: Schematic diagram of the open-source ONR tool [5].

5.6.1 Data Parsing

The very first part of the code ensures import/export of network data. In order to ensure a functional access to the characteristics and properties of Open-DSS electrical network models, a custom routine for the grid models management was developed in Python language. The aim of the routine is to manage the electrical grid elements properties, and to offer a systemic access to Open-DSS calculation features, within

a dedicated Graphical User Interface (GUI). Through an assisted procedure, it is possible to import custom *.dss* grid models, to recall predefined benchmark models, or to define a new grid, by inserting elements and relative parameters and topology. All elements parameters are accessible in the GUI, and can be modified on the basis of user needs, as well as exported for future purposes.

This routine was developed to support all the software tools in [149], including ONR. Well known limitations of Open-DSS, that is not able to identify specific elements categories such as batteries, wind or PV generators, or DC elements, are bypassed by an elements taxonomy functionality, through which the tool is able to properly categorize elements, thus assigning the relative features and properties. This feature allows to expand the set of properties associated to specific network elements. For example it is possible to assign reliability parameters to objects which do not support this property in Open-DSS.

All the elements properties (category, topological data, parameters, and study results) are stored in a dedicated dictionary in the Python environment, in order to assure a quick accessibility to all the features of the grid model. The dictionary can be exported as a YAML file (*.yml), and imported in future sessions to recall the former grid model and case study.

5.6.2 Distribution Network Zone Partitioning Algorithm

Before formulating and solving the ONR problem, it is necessary to run some initialization routines. At this step, network data have been extracted from the Open-DSS model and imported into a dictionary. The network topology is known through buses, branches and switches information. As described in the previous section, the ONR methodology is based on partitioning the distribution grid into zones. Each zone contains a set of nodes and branches, and is connected to other zones by means of switches.

The algorithm used for zone partitioning is described in Algorithm 8. Zones are created looping on branches and through simple *if* statements in the Part 1. The algorithm is based on the fact that each branch (and its sending and receiving buses) must be associated to a single zone. Therefore, switches are made to be the only elements that do not belong to a zone, but actually connect two zones. In the Part 2, potential isolated buses not assigned to a zone are found and a new one is defined. Finally, in the Part 3, possible empty zones are removed. Zone information is finally

saved as a property in the elements dictionary.

Algorithm 8 Zone Partitioning Routine

Set $b \leftarrow 1$, $n \leftarrow 1$, $z \leftarrow 1$, $\Omega_z \leftarrow \varnothing$
Part 1: Zones creation
while $b \leq$ number of branches **do**
    select branch b
    if branch b is not a switch **then**
        Set $i \leftarrow$ bus-sending, $j \leftarrow$ bus-receiving of branch b
        if i, j are already assigned respectively to zone z_i and z_j **then**
            if $z_i \neq z_j$ **then**
                move all buses in z_j into z_i
                empty z_j
            end if
        else if only i is assigned to a zone **then**
            assign j to the same zone as i
        else if only j is assigned to a zone **then**
            assign i to the same zone as j
        else if both i, j are not assigned to a zone **then**
            define a new zone z in Ω_z, assign i and j to z
        end if
    end if
    $b \leftarrow b + 1$
end while
Part 2: Control of nodes not assigned to zones
while $n \leq$ number of nodes **do**
    if node n is not assigned to any zone **then**
        define a new zone z in Ω_z and assign node n_{th} to z
    end if
    $n \leftarrow n + 1$
end while
Part 3: Control of zones left empty
while $z \leq$ number of zones **do**
    if zone z is empty **then**
        remove z from Ω_z
    end if
    $z \leftarrow z + 1$
end while
renumber all zones left in Ω_z

5.6.3 ONR Initialization

The topology of the network is known through the position (open/close) of each switch. Switches positions are imported from Open-DSS during the initial data parsing, however, in any case, the tool permits also to generate a random radial initial configuration (Initial Radial Topology, IRT).

The tool first checks if the imported network model is connected and radial, then checks if the equivalent zonal graph is also radial. Please note that, given the

type of assumed protection automation techniques, radiality of the zonal graph is a requirement, whereas meshes within a single zone do not affect reliability analysis.

Connectivity and radiality are checked using the Dijkstra's algorithm [150] in the library NetworkX [91]. At the end of this procedure also kinship relationships between zones are known, allowing to calculate the initial value of the reliability indices (5.2) - (5.4). The solution found is the starting point of the ONR problem, and permits also to normalize (5.1) through weights.

5.6.4 ONR Implementation

The ONR routine is built within Pyomo [147], an open-source Python library that enables the definition, solving, and analysis of optimization models. Thus, its main function is to translate the mathematical formulation of the optimization problem into the programming language used by commercial solvers. The main advantages lie in the simplicity of model implementation, as Pyomo is based on object-oriented programming (OOP) where the optimization problem is built as a class whose objects are the variables, the constraints and the objective functions [60]. This promotes code reuse, modularity, and maintainability allowing users to use different solvers for solving their models without the need to change the syntax used in writing the script. This interoperability proves essential when there is a need to test the same model using different solving techniques, thus being able to use the solver that is best suited for solving the model.

5.6.5 Solver Selection

The Pyomo library permits to implement the optimization problem using several solvers. However, typically, only few solvers can be actually used, since each one can tackle only specific formulations. The two open-source solvers which were found able to solve efficiently the proposed ONR problem are HiGHS [151] and SCIP [152], both able to solve MILP models, and available using *amplpy*. This is an interface that allows to access AMPL (A Mathematical Programming Language), a tool connected with most open-source and commercial solvers, from Python environment, and to model and solve optimization problems [153]. In this case, *amplpy* has been used just as an utility to access two of the open-source solvers of AMPL available as Python packages. It should be noted that, in order to compare their performances, the tool

was programmed to find solutions also with the commercial solver Gurobi [61, 148], which is not open-source, but free academic licences can be obtained.

5.6.6 Graphic User Interface (GUI)

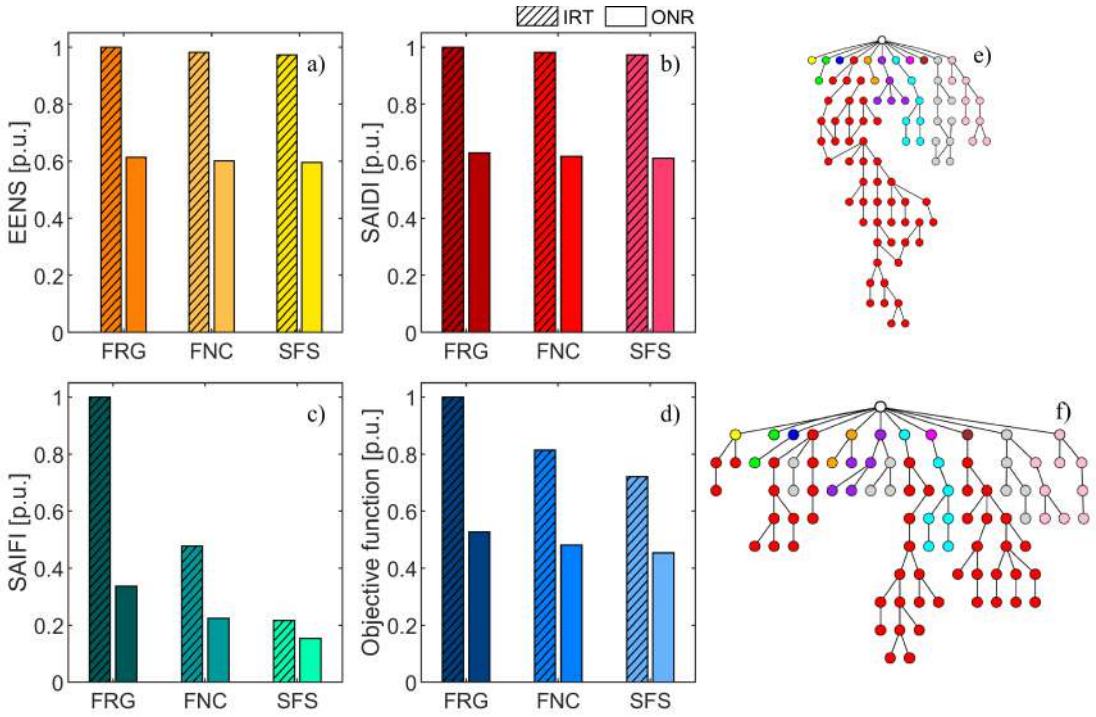

Figure 5.10: GUI example: monitored quality indices normalized with respect to the FRG case and objective function: *a)* EENS, *b)* SAIDI, *c)* SAIFI, *d)* objective function (5.1). DN's topologies: *e)* zonal graph based on IRT, *f)* zonal graph based on ONR [5].

Results of the optimization can be easily read and compared with the initial solution through a GUI (Fig. 5.10). The interface is based on the open-source libraries NetworkX and Graphviz [154] which allow to easily draw a connected graph.

The open-source software platform, named ARSTool, is available in [155]. ARSTool is a freeware tool for studying electrical power systems, capable of assessing their adequacy, reliability, security, and resilience. Using a dedicated GUI, users can create or import network models, entering typical parameters and topological information. The tool allows basic functions such as Load Flow and reliability calculations to be performed. It also offers advanced features such as predictive anomaly analysis, network adequacy analysis, and network reconfiguration to increase reliability.

5.6.7 Test results with ONR Open-Source Software Tool

The realistic-sized distribution network used in the tests described in Paragraph 5.5 has been updated and considered among the benchmark systems of the developed software platform. Overall, the updated versione of the grid model has 1014 nodes, 2 transformers, 924 lines (654 cable and 270 overhead), and 112 telecontrolled switches. As a result of the zone partitioning algorithm (Algorithm 7), the distribution network is divided into 88 zones. Of these, 11 zones are ancestor zones directly connected to the substation by means of an automatic CB. If all the switches are closed, the meshed topology consists of 25 cycles-basis, which means that a radial configuration, according also to (5.5), requires that 25 switches must be off.

An initial topology (IRT) was assumed also in these tests. The analyzed operating condition is now characterized by poor reliability indices since a large number of users are connected to the same feeder (Fig. 5.10c). Therefore, significant improvements in quality of supply indices can be expected. The best absolute results are obtained with SFS, while FNC performs better than FRG. In general, the main differences were found in terms of SAIFI. The adoption of FNC and SFS techniques can reduce fault frequency through selectivity functions, avoiding the tripping of the substation CBs. Improvements for all indices can be obtained only applying the ONR, especially in the case of EENS and SAIDI.

The three topologies obtained solving the ONR problem and assuming different FDIR techniques are all radial and connected. In Fig. 5.10, the results obtained in terms of EENS, SAIDI and SAIFI are shown, as well as the IRT and the reconfigured topology. Graphs in the bottom-right confirm that SFS is better than FNC, and FNC is better than FRG.

It is possible to observe an improvement also in terms of outage duration and energy not served. This is due to the fact that ONR is able to associate the zones characterized by higher loads and number of customers to the feeders that have the lowest chance to experience a fault. The percentage variations of all indices with respect to the IRT case are shown numerically in Table 5.4.

Table 5.4: Percentage Variation from the Initial Radial Topology

FDIR	**ΔEENS**	**ΔSAIDI**	**ΔSAIFI**	**Δf**
FRG	-38.59%	-36.98%	-66.39%	-47.32%
FNC	-38.76%	-37.20%	-53.11%	-40.93%
SFS	-38.73%	-37.25%	-29.12%	-37.11%

Please note that the three terms minimized in (5.1) are competing and, therefore, the minimization of one index can impact on the other two. In this specific case, the three weights used to normalize the objective function were chosen uniformly, equal to $\frac{1}{3}$ divided by the value of each index calculated on the IRT. Numerical results confirm that quality of supply can be improved through DN reconfiguration and suggest that best improvements can be obtained when the most sophisticated distribution automation techniques are adopted.

All numerical simulations were performed on a computer with 32 GB RAM, 12th Gen Intel® Core™ i9-12900F CPU @ 2.40 GHz, 16 physical cores and 24 logical processors, using up to 24 threads. Computing times are very low and theoretically compatible with the time requirements of on-line SCADA/DMS functions, as reported in Table 5.5.

Table 5.5: CPU Time [s]

	Licensed solver	**Open-Source solvers**	
FDIR	Gurobi	HiGHS	SCIP
FRG	19.77	544.82	943.37
FNC	1.24	1.79	8.5
SFS	0.69	0.71	1.24

The three reconfigured topologies were all achieved with zero optimality gap (MIP gap) regardless of chosen solver. The solution of the ONR-SFS problem is the fastest simply because the problem is much lighter; given the formulation of λ_z and U_z, constraints (5.10) and (5.11) can be skipped, and the use of variables $\gamma_{h,k,m}$ and $\beta_{k,m}$ avoided. In fact, the ONR problem included 63780 variables (10035 continuous, and 53745 binary) and 112908 constraints concerning FRG and FNC cases. Regarding SFS, ONR problem encompassed the same number of continuous variables but only 7809 binary ones, and 66972 constraints.

The solution of the FRG case required instead the largest timings, especially with open-source solvers. This is probably due to the fact that this is the most complex problem and that suboptimal solutions can be very close one to another, especially in terms of SAIFI improvements. The choice of a higher MIP gap could improve significantly the timings.

The number of switching maneuvers required to reach the new topology are more or less the same. However, although even open-source solvers have been able to obtain the same minimum of the objective function, slightly different topologies have

been found. This demonstrates that multiple optimal topologies can exist with the same quality indices.

5.7 ONR MISOCP Formulation

The ONR model described in this Paragraph significantly improves and extends the MILP ONR approach previously presented, which did not include network equations (with the risk of finding infeasible topologies or operation conditions with poor electrical characteristics).

The specific advancements are here summarized:

- formulation of ONR problem that includes FDIR logics and incorporates a sound mathematical formulation of the ACLF equations through MISOCP relaxation;
- inclusion of technical constraints on voltages or overloads;
- improved formulation of the objective function that can include targets on reliability and operating conditions;
- scalability test on a realistic-sized distribution network;
- comparison with other approaches (global optimization algorithms);
- validation of the approach through Monte Carlo simulation.

In particular, a full deterministic AC ONR problem, aimed to improve quality of supply indices, taking into account the automatic FDIR techniques, is formulated and solved employing ACLF MISOCP relaxation techniques. The developed formulation allows the physical constraints of distribution network, connectivity, radiality, and FDIR fault selectivity logics to be rigorously enforced, making the ONR problem tractable for commercial solvers and implementable in industrial applications.

5.7.1 General MINLP Formulation

The proposed AC ONR problem still considers the switches' connection state $x_s \in \{0, 1\}$ as control variable and preserves the zonal approach. Below is the MINLP formulation of the AC ONR problem, in which the objective function now also

includes the minimization of system's active power losses (P_{loss}), in addition to the power quality indices (EENS, SAIDI, SAIFI):

$$\min(w_1 \cdot P_{loss} + w_2 \cdot \text{EENS} + w_3 \cdot \text{SAIDI} + w_4 \cdot \text{SAIFI}) \tag{5.19}$$

According to ACLF equations, and assuming known generation and load at each bus i, active and reactive power balance must be complied on each node:

$$p_i^G - p_i^D = \sum_{j \in i, j \neq i} p_{ij} + \sum_{j \in i, j \neq i} p_{ji}, \quad \forall i \in \Omega_n \tag{5.20}$$

$$q_i^G - q_i^D = \sum_{j \in i, j \neq i} q_{ij} + \sum_{j \in i, j \neq i} q_{ji}, \quad \forall i \in \Omega_n \tag{5.21}$$

where p_{ij} and q_{ij} can be expressed in polar form depending on branch connection state x_{ij} as follows, $\forall ij \in \Omega_b$:

$$p_{ij} = [(g_{ij} + g_i^s)v_i^2 - v_i v_j (g_{ij} \cos\theta_{ij} + b_{ij} \sin\theta_{ij})]x_{ij} \tag{5.22}$$

$$q_{ij} = [-(b_{ij} + b_i^s)v_i^2 - v_i v_j (g_{ij} \sin\theta_{ij} - b_{ij} \cos\theta_{ij})]x_{ij} \tag{5.23}$$

with $\theta_{ij} = \theta_i - \theta_j$. Eqns. (5.22)-(5.23) allow to effectively zero the contribution of a generic branch when x_{ij} is zero.

The system active power losses can be expressed as:

$$P_{loss} = \sum_{ij \in \Omega_b} (p_{ij} + p_{ji}) \tag{5.24}$$

In order to assure a secure operation of the grid the following constraints are introduced:

$$\underline{v}_i \leq v_i \leq \overline{v}_i, \quad \forall i \in \Omega_n \tag{5.25}$$

$$p_{ij}^2 + q_{ij}^2 \leq \overline{S}_{ij}^2, \quad \forall ij \in \Omega_b \tag{5.26}$$

where (5.25) limits bus voltage magnitude within allowed boundaries, and (5.26) defines an upper bound $\overline{S}_{ij}$ for branch apparent power flow to avoid overloads.

Finally, the topological constraints (5.5)-(5.11) specific to the previous ONR MILP model can be integrated together with the reliability functions (5.14)-(5.18), chosen according to the FDIR practice adopted.

5.7.2 AC Load Flow MISOCP Relaxations

Since (5.22) and (5.23) are nonlinear expressions which include binary variables, (5.20), (5.21), (5.24) and (5.26) are also non linear, then minimizing (5.19) leads to a MINLP optimization problem that may be intractable with commercial solvers. In order to obtain equivalent linear expressions for (5.22) and (5.23), let us firstly consider the voltage phasor $\overline{V}_i$ on each node i:

$$\overline{V}_i = v_i \cdot e^{\mathrm{j}\theta_i} = v_i(\cos\theta_i + \mathrm{j}\sin\theta_i) = e_i + \mathrm{j}f_i, \quad \forall i \in \Omega_n \tag{5.27}$$

where:

$$v_i = \sqrt{e_i^2 + f_i^2} \quad , \quad \theta_i = \arctan\left(f_i/e_i\right) \tag{5.28}$$

Three auxiliary continuous variables can be defined according to SOCP OPF relaxations [135] in order to provide an exact formulation for balanced radial networks:

$$c_{ii} := v_i^2 = e_i^2 + f_i^2, \quad \forall i \in \Omega_n \tag{5.29}$$

$$c_{ij} := v_i v_j \cos\theta_{ij} = e_i e_j + f_i f_j, \quad \forall ij \in \Omega_b \tag{5.30}$$

$$s_{ij} := -v_i v_j \sin\theta_{ij} = e_i f_j - e_j f_i, \quad \forall ij \in \Omega_b \tag{5.31}$$

The new variables defined in (5.29)-(5.31) share the same symmetry properties as the goniometric functions cosine ($c_{ij} = c_{ji}$) and sine ($s_{ij} = -s_{ji}$), respectively. In addition, they meet the following conditions:

$$\underline{c}_{ii} \leq c_{ii} \leq \overline{c}_{ii}, \quad \forall i \in \Omega_n \tag{5.32}$$

$$\underline{c}_{ij} \leq c_{ij} \leq \overline{c}_{ij}, \quad \forall ij \in \Omega_b \tag{5.33}$$

$$\underline{s}_{ij} \leq s_{ij} \leq \overline{s}_{ij}, \quad \forall ij \in \Omega_b \tag{5.34}$$

$$c_{ij}^2 + s_{ij}^2 = c_{ii}c_{jj}, \quad \forall ij \in \Omega_b \tag{5.35}$$

where (5.32) corresponds to (5.25) with $\underline{c}_{ii} = \underline{v}_i^2$ and $\overline{c}_{ii} = \overline{v}_i^2$, $\underline{c}_{ij} = 0$ and $\overline{c}_{ij} = \overline{s}_{ij} = -\underline{s}_{ij} = \overline{v}_i\overline{v}_j$ according to [156], while (5.35) reflects the first fundamental relationship of trigonometry as demonstrated in [157]. Therefore, $\forall ij \in \Omega_b$, (5.22) and (5.23) can

be written as follows:

$$p_{ij} = [(g_{ij} + g_i^s)c_{ii} - g_{ij}c_{ij} + b_{ij}s_{ij}]x_{ij} \tag{5.36}$$

$$q_{ij} = [-(b_{ij} + b_i^s)c_{ii} + b_{ij}c_{ij} + g_{ij}s_{ij}]x_{ij} \tag{5.37}$$

with similar expressions for p_{ji} and q_{ji}.

Note that (5.36) and (5.37) are linear for in-service branches that are not switchable ($x_{ij} = 1$), but they are still non linear for switchable elements due to the products between the auxiliary continuous variables and the binary variable x_{ij}. Then, an additional auxiliary variable $c_{ii}^j := c_{ii}x_{ij}$ can be defined for each switchable branch so that on/off constraints can be formulated as in [**?**], $\forall ij \in \Omega_{sw}$:

$$p_{ij} = (g_{ij} + g_i^s)c_{ii}^j - g_{ij}c_{ij} + b_{ij}s_{ij} \tag{5.38}$$

$$q_{ij} = -(b_{ij} + b_i^s)c_{ii}^j + b_{ij}c_{ij} + g_{ij}s_{ij} \tag{5.39}$$

$$\underline{c}_{ij}x_{ij} \leq c_{ij} \leq \overline{c}_{ij}x_{ij} \tag{5.40}$$

$$\underline{s}_{ij}x_{ij} \leq s_{ij} \leq \overline{s}_{ij}x_{ij} \tag{5.41}$$

$$\underline{c}_{ii}x_{ij} \leq c_{ii}^j \leq \overline{c}_{ii}x_{ij} \tag{5.42}$$

$$c_{ii} - \overline{c}_{ii}(1 - x_{ij}) \leq c_{ii}^j \tag{5.43}$$

$$c_{ii}^j \leq c_{ii} - \underline{c}_{ii}(1 - x_{ij}) \tag{5.44}$$

$$4c_{ij}^2 + 4s_{ij}^2 + (c_{ii}^j - c_{jj}^i)^2 \leq (c_{ii}^j + c_{jj}^i)^2 \tag{5.45}$$

where (5.38) and (5.39) replace (5.22) and (5.23), (5.40) and (5.41) substitute (5.33) and (5.34), respectively. Constraints (5.42)-(5.44) make v_i and v_j meet the allowable limits even when a branch (i, j) is to be switched-off. Finally (5.45) is the relaxation of non-convex constraints (5.35) valid for switchable branches.

Furthermore, $\forall ij \in \Omega_b$, (5.46) represents the active power losses along a branch and (5.47) enforces source-destination flow paths, ensuring that each unit of load is matched by a unit of generation [158]:

$$p_{ij} + p_{ji} = (g_{ij} + g_i^s)c_{ii}^j + (g_{ij} + g_j^s)c_{jj}^i - 2g_{ij}c_{ij} \tag{5.46}$$

$$p_{ij} + p_{ji} \geq 0 \tag{5.47}$$

The result is a MISOCP problem that can be solved with commercial solvers.

5.8 Metaheuristics & Global Optimization Approaches

This paragraph describes the procedure followed for the implementation of a Genetic Algorithm (GA) to solve the whole MINLP AC ONR problem. This implementation is proposed for comparison purposes in terms of solution quality and computational performances. For this reason, a general discussion is provided, as the main objective of this work is not to tailor metaheuristic algorithms for the efficient resolution of the problem.

The primary advantage of using a metaheuristic approach, lies in the possibility of simplifying the mathematical structure of the problem. In the case of ONR, the solution space consists solely of sets of possible open/closed (0/1) combinations of the controllable switches. Each set (*individual*) selected as a potential solution by the algorithm can be uniquely associated with kinship and ancestor relationships, zonal upstream/downstream conditions, and reliability indices. By solving simple sub-problems, it is therefore possible to assign a specific value of the objective function to be minimized to each topological configuration. Specifically, the objective function and the constraints are calculated for each individual of every generation if and only if that individual corresponds to a radial and connected topology. Solutions characterized by meshed or disconnected configurations are penalized according to a factor proportional to the current generation number, effectively preventing their exploration in subsequent generations. As in all GAs, the ONR routine begins with an initial population sampling of N individuals, where each individual is a vector containing the control variables (e.g., the status of the controllable switches). For each individual, the objective function value is calculated, and compliance with connectivity and radiality constraints is verified. In the subsequent phases, the population is updated based on genetic operators—selection, crossover, and mutation—generating new individuals where those with better objective function values replace the worse ones until a stopping criterion is met. Usually, the initialization of a population of individuals is based on random sampling mechanisms; however, this can lead to solutions far from the desired optimum, requiring a high number of iterations to achieve convergence. For this reason, a simple method was used to quickly discard solutions that are worse than the initial operating condition during the GA execution. Starting from an initial connected and radial topology, the initial population is obtained by considering connected and radial topologies achievable

through a single opening and a single closing switching operation relative to the initial configuration, ensuring a population composed of unique individuals. In a classic GA, individuals are compared based on their fitness functions; however, in the transition from one generation to the next, individuals must be properly selected to participate in mating. To improve convergence, a "binary tournament" criterion [159] was employed: given a subset of individuals from the population, they are randomly compared in pairs based on their fitness values. For each pair, the better individual is selected as the tournament winner to then undergo the subsequent crossover phase as a "parent". Once the parents have been selected, the crossover phase begins. This operator combines the genetic information of two parents to create one or more individuals that may have better fitness than the parents. Among the existing techniques, the two-point crossover [160] was chosen: a standard crossover type based on fragmenting the gene at two random points on the chromosome. The method involves the random selection of two points in the chromosome (the vector of binary variables representing the switch statuses) of a pair of individuals (parents); the information between these two points is swapped and passed to the pair of individuals in the next generation (offspring). In this way, the new pair of individuals exhibits common characteristics with the pair from the previous generation. The mutation phase helps increase population diversity, avoiding the drawback of falling into local optima. It is performed after the new individuals are created through crossover. Specifically, Bit Flip Mutation (BFM) was adopted because it operates on binary variables [161]. BFM is one of the simplest and most commonly used mutation techniques in genetic algorithms. It operates on binary individuals where each element is represented by a single bit (0 or 1). During mutation, each bit has a small probability of being mutated—that is, changing its state from 0 to 1 or vice versa. The mutation probability of a bit is determined by the mutation rate, which is usually set to a low value to maintain a balance between exploration and exploitation of the individual. BFM introduces small, localized changes to the individual, allowing the genetic algorithm to explore nearby solutions in the search space. In the GA algorithm, new generations of individuals are obtained by alternating crossover and mutation according to probability distribution functions. Crossover promotes the exploitation of the best current solutions by combining them to obtain potentially superior ones, while mutation is useful for avoiding local optima by introducing random variations. The GA terminates after a predetermined maximum number of

generations or upon reaching a stop criterion. The chosen stop criterion is based on reaching a certain number of occurrences of an acceptable optimal solution, consistent with the tolerances imposed on the variability rate of individuals, the objective function between successive generations, and the violation of problem constraints [86]. The GA tested during this activity was implemented using the open-source platform *Pymoo* [162], operating within the Python programming environment. The basic structure of the algorithm is shown in Figure 5.11 in the form of a flowchart.

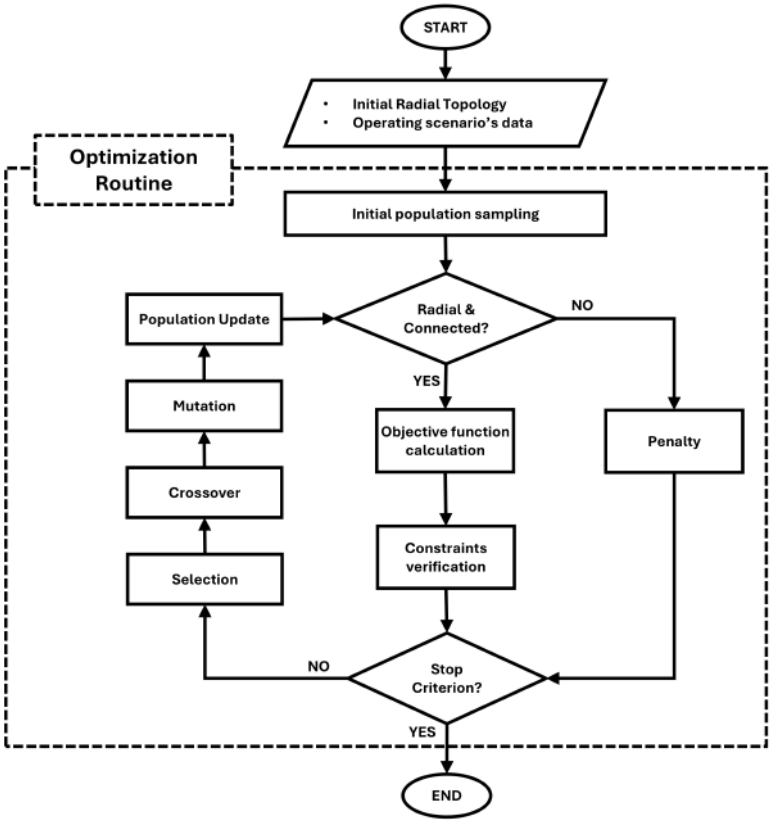

Figure 5.11: GA for the solution of the MINLP AC ONR problem.

5.9 ONR MISOCP - Case studies & Test results

First numerical experiments were carried out on a realistic model of primary distribution network [6], derived from the developments in the research project "ATLANTIDE", aimed to build a set of representative scenarios of Italian distribution networks [163]. Other simulations were performed on the IEEE 33-Bus test system [164] for replicability purposes, and on the 1014-Bus realistic-sized primary distribution network model in order to test the problem scalability.

5.9.1 Early implementations of the MISOCP model

The first test were carried out on a primary distribution network model which comprises 102 buses, 81 lines, 34 switches, 2 two-windings transformers in the primary substation, 137 loads, plus a consistent amount of RES distributed generation, consisting of 13 photovoltaics generators (PV) and 8 wind turbines (WT) all installed under the same feeder. Compared to the original grid model of [163], several switches were added to allow many possible topological configurations. The values of λ and ρ were derived from [146] for each bus and for each branch. After the partitioning, the network was split into 19 zones. The overall problem consisted of 1796 continuous variables, 1250 binary variables, and 1310 equality and 6377 inequality constraints.

The grid was modeled using OpenDSS [165], since this tool was also used to validate the quality of the ACLF solution. The ONR mathematical model is implemented in Python programming language within Pyomo library [147] and then solved using Gurobi 11.0 [61]. The method used by Gurobi is the dual simplex algorithm, which is usually chosen for the MIP root relaxation and combined with cutting planes whenever an integer variable assumes a fractional value in the optimal solution. The ONR routine was tested, starting from a same initial topology, under two operating conditions, both characterized by large RES generation: a day-time scenario with prevalent PV production (a), and a night-time scenario with relevant wind power production (b). In both tests, voltages were constrained within $\pm 5\%$ from the nominal value.

Voltage profiles before and after ONR are shown in Fig. 5.12 (blue line) for all buses. Both scenarios are characterized by high voltages due to RES production. In case (a), the voltage is higher averagely due to the extensive impact of PV generation. In case (b) local wind generation caused voltage to rise beyond the emergency threshold of 1.1 p.u. in few network nodes.

Fig. 5.12 shows the effect of reconfiguration (yellow line). In both cases, all violations were cleared by redistributing power flows among zones, even considering a $\pm 5\%$ narrow boundaries. The figure permits also to check the accuracy of the MISOCP relaxation, comparing the relaxed ACLF solution (yellow) with the exact AC solution (green). It can be observed that the two solutions are almost overlapped.

The effects of ONR can be also observed in terms of currents concerning case (b), in which 5 lines were overloaded in zone 14 before ONR. Figure 5.13 highlights how the DN topology varies after ONR through the representation of zonal graphs in the

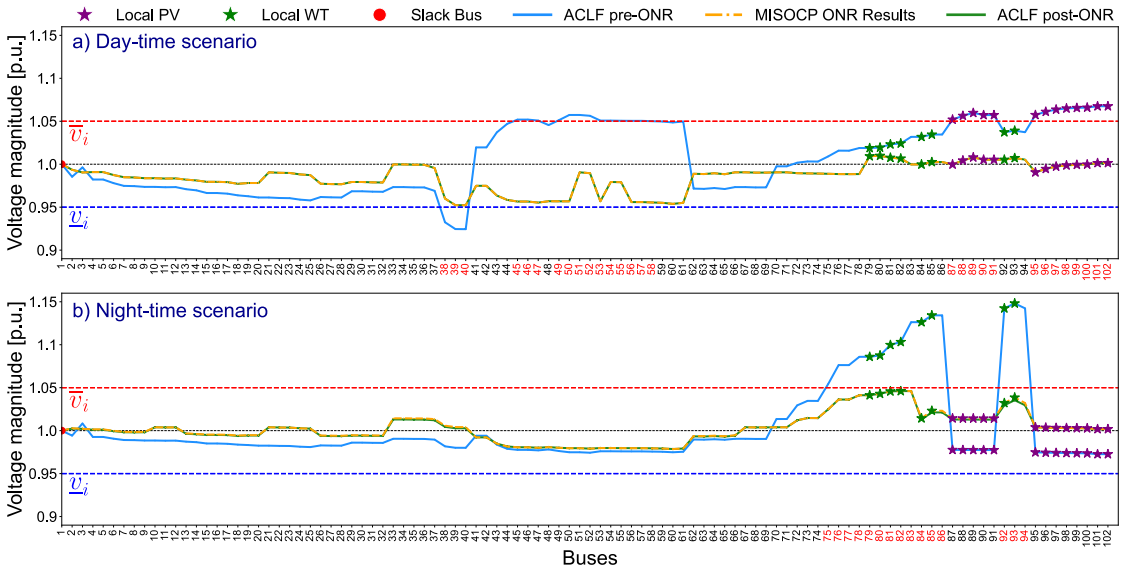

Figure 5.12: ONR voltage profiles in cases (a) and (b); buses where voltage constraints were initially violated are marked in red [6].

simulated scenarios. Reconfiguration allowed, not only to solve congestions in zone 14, but also to achieve a more uniform distribution of the currents flowing in the DN, and a consequent reduction of power losses.

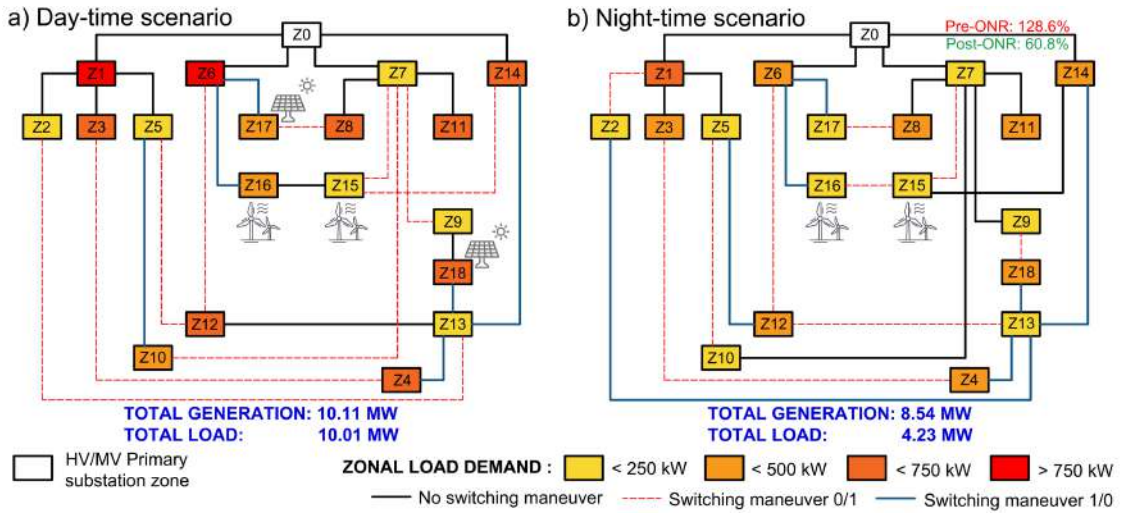

Figure 5.13: Zonal graphs of optimal DN topologies. The red and green numbers upstream of zone Z14 in (b) indicates the average loading detected before and after ONR, respectively [6].

Improvements obtained in terms of power losses, and quality of supply indices are shown Table 5.8.

All terms in the objective function were minimized. A suitable choice of weights

Table 5.6: Percentage Variation from the Initial Condition

	ΔP_{loss}	$\Delta EENS$	$\Delta SAIDI$	$\Delta SAIFI$	Δf
a)	−61.95%	−7.88%	−8.73%	−4.38%	−7.55%
b)	−68.33%	−12.83%	−13.38%	−4.40%	−10.78%

can be used to target specific indicators. Thresholds on SAIDI and SAIFI can also be set according to grid codes. In other tests, not shown here for the sake of brevity, further improvements of quality of supply indices were obtained by relaxing voltage limits (±10% around nominal voltage). However, the improvement in terms of reliability (only few %) did not justify the loss in terms of quality of voltage. The use of tighter constraints is in general advised since, in this formulation, there is no representation of LV circuits, where voltage can further deviate from nominal, depending on the localization of distributed generation or load.

In order to assess computational performances and validate the scalability of the proposed approach in real-sized networks, a third test case (c) is presented. This case solves an ONR applied to the model of a real primary DN with 1014 buses and 112 controllable switches [143, 166]. The implementation of the ONR on this DN lead to a MISOCP problem characterized by 19579 continuous variables, 53792 binary variables, and 16181 equality and 116300 inequality constraints.

Detailed results are not shown for brevity, however, Table 5.7, which summarizes the OF values and CPU times obtained by solving the ONR MISOCP problem in all proposed cases, shows how the proposed approach can still be solved within the time framework of typical SCADA/DMS operating functions.

Table 5.7: Computational Performances Comparison

DN Model	**ONR MISOCP**		**ONR GA**		**ONR PSO**	
	OF [p.u.]	**CPU [s]**	**OF [p.u.]**	**CPU [s]**	**OF [p.u.]**	**CPU [s]**
102 Bus (a)	0.9245	39.13	0.9872	379.55	0.9663	730.93
102 Bus (b)	0.8922	9.77	0.9241	308.11	0.9363	650.43
1014 Bus (c)	0.5893	319.62	0.7336	1652.94	0.8343	1924.85

All numerical simulations were performed on a computer with 16 GB RAM, 11th Gen Intel® Core™ i7-1195G7 CPU @ 2.90 GHz. ONR solutions are achieved with zero optimality gap (MIP gap) in all cases. Computing times recorded are compatible with SCADA/DMS time requirements: solution required 39.13 s for Case (a), 9.77 s for Case (b), and 319.62 s for Case (c). In order to quantify the tightness of the MISOCP formulation through a metric, the Distance to Cone Boundary

($DCB = \ln|c_{ij}^2 + s_{ij}^2 - c_{ii}c_{jj}|$) is evaluated as in [167] for each in-service branch, lying between -11 and -18, i.e., $|c_{ij}^2 + s_{ij}^2 - c_{ii}c_{jj}| \in \mathcal{O}(10^{-8}, 10^{-5})$, proving a good exactness in all cases.

Results are also compared to the ones obtained by solving the same problem using general purpose GA and PSO global optimization tools in Pymoo library [162]. In all cases, the ONR MISOCP performed better than the metaheuristic approaches in terms of both CPU time and optimality of the solution. The performances of metaheuristics could be improved by tailoring the GA/PSO to the ONR problem, however this is out of the scope of this work. In general, the proposed analytic approach is preferable to metaheuristic approaches because, being based on sound and rigorous mathematical foundations, it leads to formulations that are easier to understand and interpret, allows for detailed analysis of the results obtained, and guarantees greater reliability of the results.

5.9.2 Scalability test & Validation

Simulations were carried out on the IEEE 33-Bus test system [164] and on a realistic-sized primary distribution network model [4]. The first system was used for the sake of replicability, whereas the second permitted to validate the MISOCP formulation and test its scalability. Network models and ONR routines were implemented in Python language, using Pyomo library for the optimization problem construction, and solved with Gurobi 11.0.1 commercial solver.

Failure rates and restoration times for buses and branches were derived from the IEEE Std. 493 [146]. It was assumed that auto-reclosing schemes at head-feeder CBs employ a maximum time $\bar{\rho}$ of 3 minutes. This time limit permits to avoid long duration interruptions, according to the European Norm on voltage standard characteristics EN 50160.

For all proposed test cases, ONR results are analyzed considering the three FDIR techniques previously defined (FRG, FNC, SFS).

5.9.2.1 IEEE 33-Bus Test System

The IEEE 33-Bus test system is a 12.66 kV distribution grid consisting of 33 buses and 37 branches, as shown in Fig 5.14a.

In the base case [168], [169], the total active and reactive power demand is 3.71 MW

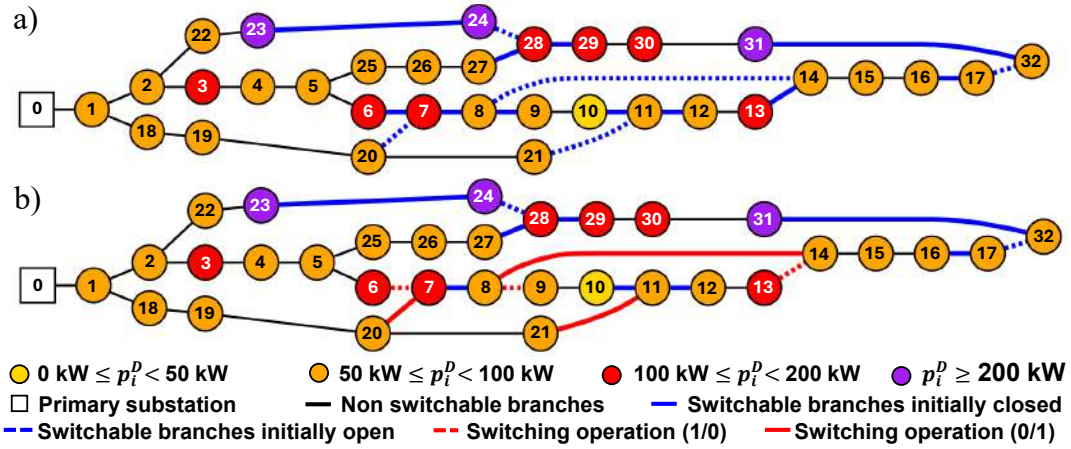

Figure 5.14: IEEE 33-Bus Test System graphs: *a)* before ONR, *b)* after ONR [3].

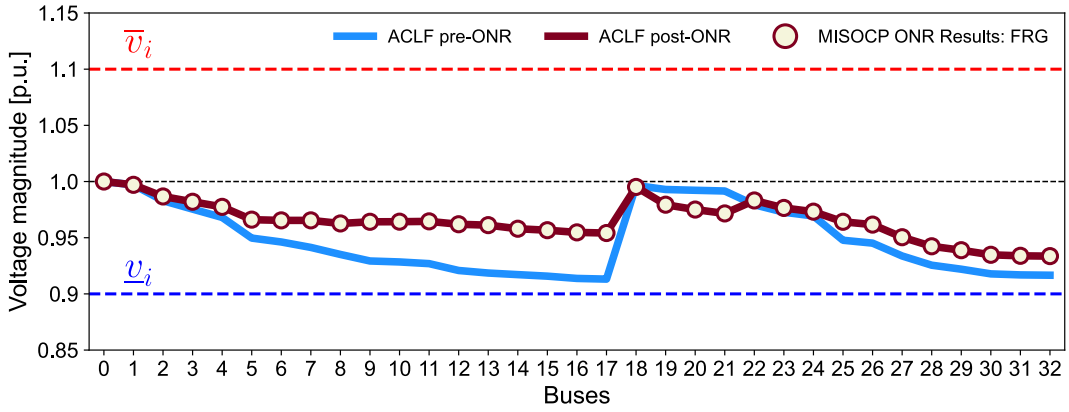

Figure 5.15: IEEE 33-Bus Test System voltage profiles before and after ONR [3].

and 2.30 MVAr, respectively, whereas the total active power losses are 202.38 kW. The minimum voltage magnitude is 0.9131 p.u., at bus #17. In this condition, no overloads are detected. The voltages obtained through ONR are generally closer to nominal values, as shown in Fig. 5.15. The minimum voltage is now 0.9336 p.u. (at bus #32). The voltages associated to the MISOCP relaxation (FRG case) are plotted using a circle mark, showing good accuracy in the approximation of the ACLF solution. The topology obtained running the ONR algorithm is shown in Fig. 5.14b. For instance, the same optimal topology was found for all FDIR schemes.

Table 5.8 shows, for all FDIR cases, how terms in the objective function were minimized. The weights in the objective function were set to normalize each term with respect to the initial values obtained for the worst case (i.e., FRG). Since all three formulations led to the same topology, results in terms of losses are similar.

In general a quality of supply improvement was observed in all three cases,

thanks to a more uniform distribution of buses on the laterals and to optimized kinship relationships. The greatest relative reduction was achieved in the FRG case (EENS -32.6%, SAIDI -36.8% and SAIFI -37.8%), whereas lowest absolute values are obtained with FNC and SFS. These two techniques perform best since they are based on selectivity principles and can better exploit the changes in kinship relationships between zones. Compared to FRG, FNC and SFS yield most significant improvements in terms of frequency, rather than unavailability since non-selective faults (see eqn. (5.15)) are anyway cleared within $\bar{\rho}$.

Table 5.8: ONR Results for IEEE 33-Bus Test Case

		P_{loss} [kWh]	EENS [MWh/year]	SAIDI [hours/year]	SAIFI [faults/year]
FRG	**Base**	202.38	2.5927	0.6547	0.1894
	ONR	141.96	1.7481	0.4137	0.1177
FNC	**Base**	202.38	2.5834	0.6520	0.1370
	ONR	141.96	1.7425	0.4121	0.0861
SFS	**Base**	202.38	2.5787	0.6507	0.1108
	ONR	141.96	1.7397	0.4113	0.0703

5.9.2.2 1014-Bus Real Distribution Network Model

The adopted model is based on real data from an actual primary distribution grid supplying electricity to a municipality in Italy [145]. The primary substation is composed of two 150/20 kV transformers and organized on 11 feeders. The model still comprises 1014 nodes, 270 cabled lines (urban areas), 654 overhead lines (rural and industrial areas) and 112 controlled switches. An overall renewable generation capacity of 10 MW has been considered installed.

The grid was reconfigured under two different operating conditions: a high load day-time scenario (Case 1) and a low load night-time scenario (Case 2). In these tests, voltages were constrained within ±5% around the nominal value.

In Case 1 (Fig. 6a), characterized by an overall demand of 27.09 MW, lower limit voltage violations affected the urban area. Overload events were also observed, with a maximum loading of 151% in the rural area. The optimal radial topologies are depicted in Figs. 6b, 6c, 6d for the FRG, FNC, and SFS cases, respectively. All overloads have been cleared, and voltages brought back above the 0.95 p.u. limit.

Since the reliability function formulation is similar, the optimized topologies in the FRG and FNC cases are very similar.

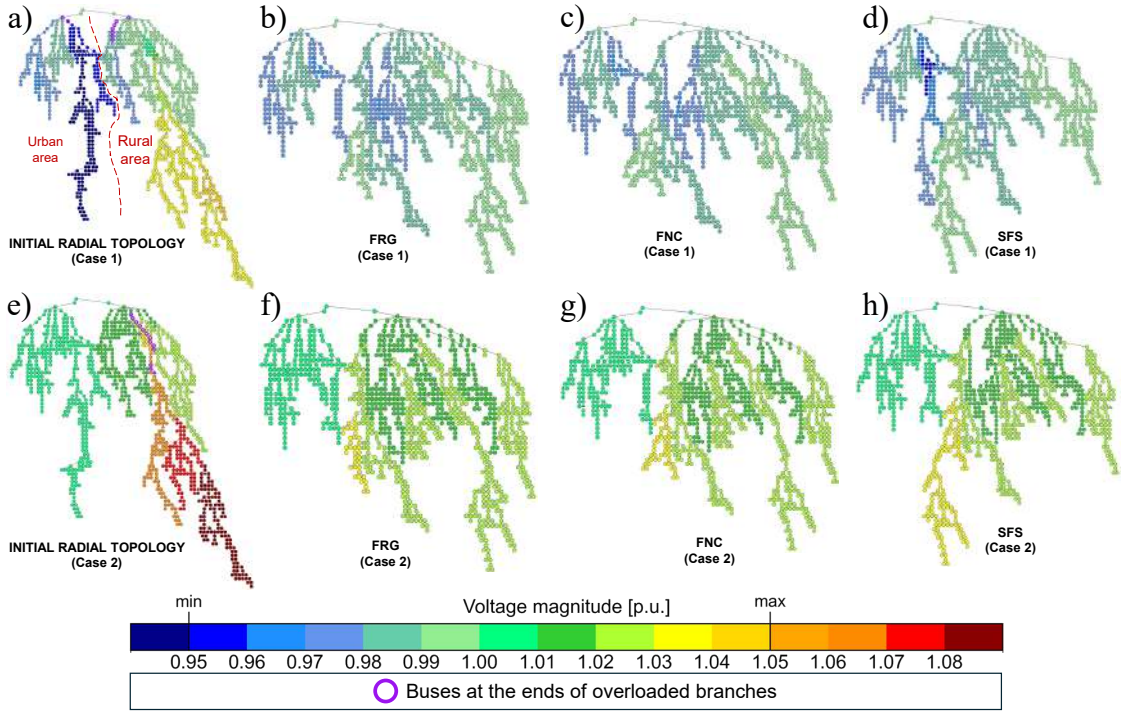

Figure 5.16: Initial and optimized grid topologies in Case 1 (a-d) and Case 2 (e-h) [3].

In Case 2 (Fig. 6e), the overall demand was 6.84 MW, and overvoltages were observed in the rural area due to renewable surplus generation. In addition, a maximum 109% loading occurred on one feeder in the rural area. In all cases, grid constraint violations are solved after ONR (Figs. 6f, 6g, 6h). As expected, switching operations were mostly located in the rural area where overvoltages were experienced. Again, FRG (Fig. 6f) and FNC (Fig. 6g) solutions are very similar.

The results in terms of active power losses and quality of supply indicators are shown in Table 5.9.

Please note that, compared to the previous simulations on IEEE 33-Bus, reliability indices are visibly higher. This is due to the increased extension of buses, and lines in both terms of number and length. Moreover the repairing times assumed on the basis of [146], led to zonal unavailabilities values (U_z) mostly in the 16-20 hours/year range. The adoption of more recent data-sets could probably lead to more favorable assumptions in terms of unavailability. In relative terms, ONR yielded the most significant improvements in terms of P_{loss} (Case 2), since the reconfiguration allowed to bring generators closer to loads and minimize reverse power flows. In terms of reliability, most relevant improvements were observed in terms of SAIFI. Nevertheless, EENS and SAIDI were also significantly improved in all cases.

Table 5.9: ONR Results for 1014-Bus Distribution Network Model

			P_{loss} [kWh]	EENS [MWh/year]	SAIDI [h/year]	SAIFI [faults/year]
Case 1	**FRG**	**Base**	717.13	273.2302	12.5684	1.8908
		ONR	419.96	247.2756	10.5107	1.2582
	FNC	**Base**	717.13	271.9638	12.5302	1.1273
		ONR	405.18	245.8881	10.4112	0.8417
	SFS	**Base**	717.13	271.3306	12.5111	0.7456
		ONR	447.86	243.7402	10.2906	0.6121
Case 2	**FRG**	**Base**	266.40	86.0368	12.5684	1.8908
		ONR	79.26	71.3946	10.4968	1.2375
	FNC	**Base**	266.40	85.7788	12.5302	1.1273
		ONR	67.94	70.1536	10.3098	0.8618
	SFS	**Base**	266.40	85.6498	12.5111	0.7456
		ONR	62.15	69.9146	10.2750	0.6113

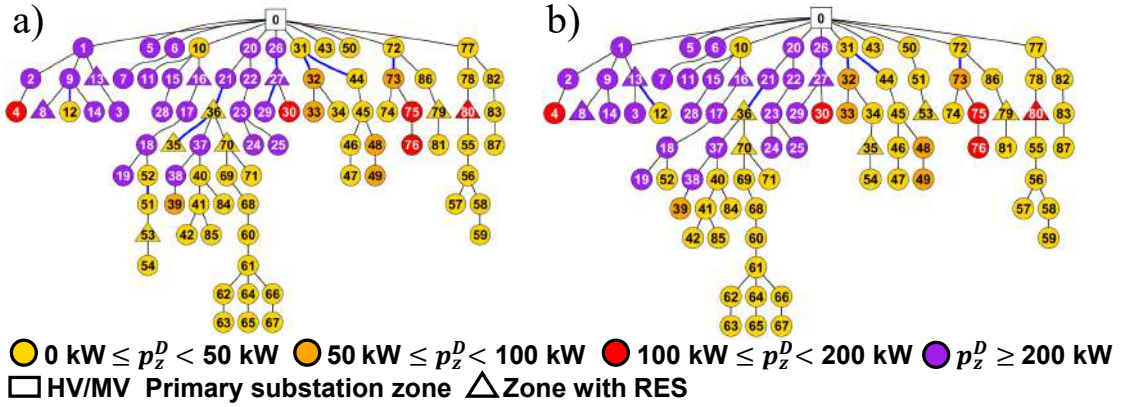

Figure 5.17: Zonal graphs related to the optimal radial topologies obtained through SFS ONR on 1014-Bus (Case 1): *a)* ONR MISOCP , *b)* ONR MILP [3].

The Case 1 (SFS technique) was used to compare the proposed MISOCP formulation with a simplified MILP formulation. The latter, previously presented in [4], does not allow to take into account network constraints, potentially leading to solutions, optimized in terms of reliability, but still infeasible due to violations of grid constraints. By comparing the two solutions, showed in Fig. 5.17, it can be observed how the topology obtained with the MISOCP approach can be characterized by lower performances in terms of reliability, since more zones are connected to a same feeder.

For instance, with the MISOCP approach, zones #35, #51, #53 and #54 are characterized by higher U_z and f_z values, compared to the MILP case. These zones have been moved at the end of some laterals and downstream paths, respect to ancestor zones #10 and #20.

This choice, which apparently lead to worst results in terms of reliability, is

made by the MISOCP algorithm in order to alleviate congestions and undervoltage problems. In particular, the renewable generation in zones #35 and #53 allows to alleviate demand of the feeders below ancestor zones #10 and #20. In the MILP case, zones #35, #51, #53 and #54, stayed below ancestor zones #31 and #50. In this case, the reliability indices are lower, but the solution still presents the violation of grid constraints under #10 and #20.

5.9.2.3 Metrics and Computational Performances

Finally, in order to validate the proposed approach, the tightness of the MISOCP solution has been quantified through some metrics in Table 5.10.

Table 5.10: MISOCP Relaxation Tightness Indicators

DN Model	**FDIR Logic**	**MAE (v_i) [p.u.]**	**ε^{loss} [p.u.]**	***DCB***
33 Bus	**FRG**	$2.48 \cdot 10^{-5}$	$5.66 \cdot 10^{-6}$	$[-18, -14]$
	FNC	$2.48 \cdot 10^{-5}$	$5.66 \cdot 10^{-6}$	$[-18, -14]$
	SFS	$2.49 \cdot 10^{-5}$	$1.51 \cdot 10^{-6}$	$[-20, -14]$
1014 Bus (Case 1)	**FRG**	$5.35 \cdot 10^{-4}$	$9.54 \cdot 10^{-6}$	$[-20, -9]$
	FNC	$6.71 \cdot 10^{-4}$	$6.27 \cdot 10^{-5}$	$[-21, -10]$
	SFS	$9.62 \cdot 10^{-4}$	$5.87 \cdot 10^{-5}$	$[-20, -9]$
1014 Bus (Case 2)	**FRG**	$5.27 \cdot 10^{-4}$	$1.29 \cdot 10^{-4}$	$[-22, -6]$
	FNC	$8.06 \cdot 10^{-4}$	$6.11 \cdot 10^{-6}$	$[-20, -7]$
	SFS	$6.61 \cdot 10^{-4}$	$5.32 \cdot 10^{-5}$	$[-20, -7]$

The Distance to Cone Boundary ($DCB = \ln|c_{ij}^2 + s_{ij}^2 - c_{ii}c_{jj}|$), calculated according to [135] for each in-service branch, proved satisfactory accuracy of the relaxed solution. This is confirmed also by the maximum absolute error (MAE) on bus voltage magnitudes and active power losses mismatch ε^{loss}, calculated with respect to the theoretical ACLF solution.

Computational performances were assessed comparing the proposed MISOCP approach with the MILP formualtion and with the solution of the generical MINLP problem obtained through a meta-heuristic approach (GA). GA was implemented using the global optimization tools in Pymoo library [162]. Numerical simulations were performed on a computer with 16 GB RAM, 11th Gen Intel® Core™ i7-1195G7 CPU @ 2.90 GHz. Comparative results are shown in Table 5.11 and Table 5.12 in terms of solution optimality and CPU time, respectively.

The tests on IEEE 33-Bus demonstrated similar performances for both the MISOCP and MILP formulations, with only very negligible differences in computational burden and solution quality. It took less than 1 s for the solver to reach convergence,

whereas the GA needed almost an entire minute. Substantial differences, however, were observed for the 1014-Bus network, especially with the FRG technique. Since in Case 2 the optimal solutions are coincident regardless of the use of MILP or MISOCP, using the first approach is computationally more advantageous. The MILP approach is without any doubt the fastest one, especially when the FRG technicque is used. However, it should be reminded that this approach does not take into account network equations, cannot include losses in the objective function and grid constraints. The comparison with the more complete MISOCP formulation in terms of computational performances is therefore unfair.

The MISOCP approach performed always better than GA, in terms of both CPU time and optimality of the solution. Even though the performances of the GA could be theoretically improved by tailoring its formulation to our problem, this is out of the scope of this work. In general, the proposed analytic approach is preferable because, being based on sound and rigorous mathematical foundations, it leads to formulation that is easier to interpret, allows for detailed analysis of the results obtained, and guarantees greater reliability of the results.

Table 5.11: ONR Objective Function Comparison [p.u.]

DN Model	FDIR Logic	ONR MILP	ONR MISOCP	ONR GA
33 Bus	**FRG**	0.6427	0.6426	0.6427
	FNC	0.5855	0.5855	0.5855
	SFS	0.5569	0.5569	0.5570
1014 Bus (Case 1)	**FRG**	0.7982	0.8020	0.8596
	FNC	0.7237	0.7243	0.7943
	SFS	0.6775	0.6781	0.7392
1014 Bus (Case 2)	**FRG**	0.7727	0.7727	0.7822
	FNC	0.6967	0.6967	0.6995
	SFS	0.6507	0.6507	0.6570

Table 5.12: ONR Solving Time Comparison [s]

DN Model	FDIR Logic	ONR MILP	ONR MISOCP	ONR GA
33 Bus	**FRG**	0.42	0.76	56.13
	FNC	0.39	0.62	52.95
	SFS	0.37	0.59	39.28
1014 Bus (Case 1)	**FRG**	68.43	585.79	2907.43
	FNC	9.47	460.86	2552.46
	SFS	3.58	298.91	2306.27
1014 Bus (Case 2)	**FRG**	75.43	395.77	2643.46
	FNC	11.61	32.37	2384.56
	SFS	3.97	20.18	2161.42

5.9.2.4 ONR Validation through Monte Carlo Analysis

This subsection aims to validate the proposed deterministic approach, which assesses reliability operation based on static load scenarios. To this purpose, a Monte Carlo (MC) simulation for fault events is combined with the copula approach for stochastic load modeling. This hybrid approach allows to capture topological uncertainties, related to time and position where failures occur, and operational uncertainties related to net load demand at the exact moment of failure. In particular, the spatial correlation of loads in the DN has been modeled, using a copula approach to construct the multivariate joint probability distribution of loads, based on historical data series. The result is a matrix $\mathbf{C}$ of size $N_{scenarios} \times N_{loads}$, where each row represents a load demand scenario, based on the correlations between the network's nodes.

A reliability analysis was conducted by simulating the 1014-Bus network over an extended time horizon (e.g., 10^5 years) to ensure statistical convergence of the indices. The validation process proceeds generating, for each component of the network, a time sequence of Time To Failure (TTF) and Time To Repair (TTR) by randomly sampling the statistical distributions. Regarding TTF, an exponential distribution based on the failure rate λ has been adopted, whereas a log-normal distribution with a standard deviation of ρ has been employed for TTR.

When a failure occurs at time t, through a topological analysis, the probabilistic model identifies the nodes that are no longer powered. The load stochasticity is taken into account considering one of the $N_{scenarios}$ generated by the copula approach.

The outages duration per customer, and the number of outages per customer, were calculated considering the frequency and duration of the failure event. The energy not served was calculated multiplying the duration of the failure event with the stochastic load demand of nodes not supplied. The outcomes of the probabilistic model was then compared to the deterministic MISOCP-ONR solution obtained considering the static scenario, with the average net-load profiles coming out of the historical data series.

The statistical probability distributions of each objective and the comparison with the analytical solution are shown in Fig. 5.18. All four expected values are very close to the ones obtained with the deterministic approach. Therefore, the tests confirmed that the results obtained by applying the proposed methodology to an average deterministic scenario are consistent with the expected values derived from a MC simulation. The results remain consistent even when accounting for system

losses, which are inherently non-linear. Clearly, variance around the expected values can be reduced if topologies are optimized using generation and load profiles based on shorter time intervals (e.g., seasonal data).

Since voltage and current values are calculated according to deterministic hypotheses, the approach cannot fully account for security violations arising from specific operating conditions, such as extreme events of overgeneration or overload. Nevertheless, the approach is general enough to be applied to multiple time series, which can theoretically take into account several scenarios, each characterized by a certain probability of occurrence. This, however, could lead to an unnecessarily oversized or computational burdensome problem, as it would need to include in calculations scenarios characterized by low probability of occurrence. Instead, we believe that the proposed approach, given its good convergence and computational performance, could be integrated within a SCADA/DMS framework, to identify current optimal topologies during operation, therefore according to updated information or forecasts on power system conditions. Ultimately, the applicability of reconfiguration in the (extended) real-time framework depends on the actual capability to develop fully adaptive distribution automation and protection functions, as also further discussed in the conclusion.

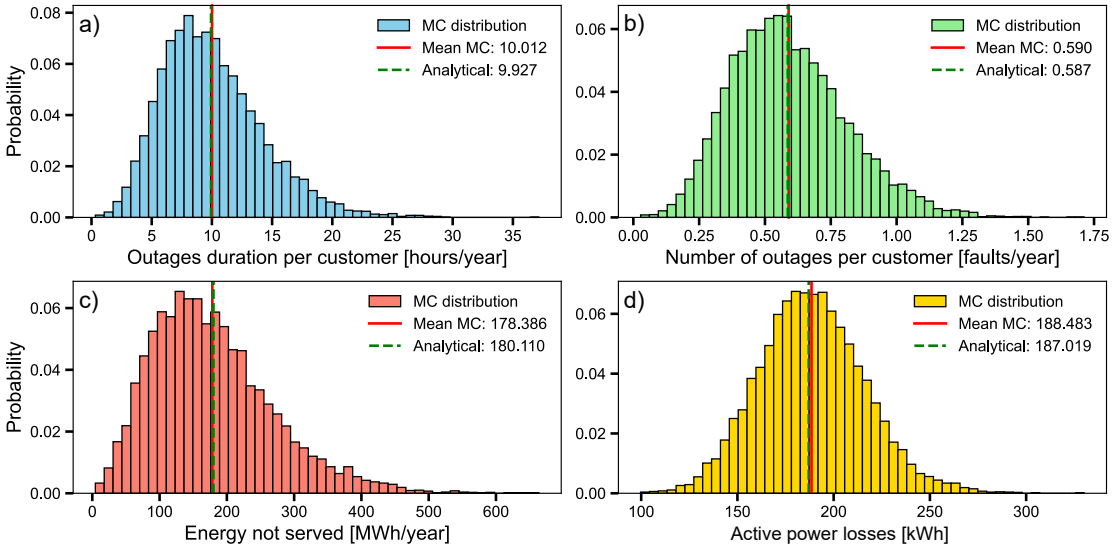

Figure 5.18: Statistical probability distributions for each term of the ONR objective function: *a)* Outage duration per customer, *b)* Number of outages per customer, *c)* Energy not served, *d)* Active power losses [3].

5.10 ONR for Mitigating the Impact of Adverse Weather Events

Adverse weather events can impact failure rates of grid components, leading to a degradation of power system conditions both in terms of reliability and security. This paragraph investigates how ONR techniques can be adopted to mitigate the effects of most common adverse weather events (AWEs), such as heat waves, floodings and high speed wind gusts. The proposed ONR formulation is based on the integration of full AC network equations and operating constraints through MISOCP techniques. The formulation is also based on the assessment of how failure and repair rates change over AWE conditions. A full description of possible approaches to update reliability parameters in relation to weather conditions is also given. Numerical tests are performed on a realistic-sized (1014-buses) distribution network model. The results have demonstrated the feasibility and scalability of the approach, making the ONR a suitable tool for enhancing grid reliability and security during AWEs. The adoption of the ONR during extreme events has led to feasible optimal configurations that improved system reliability and losses.

5.10.1 Literature review & Contributions

Driven by climate change, extreme Adverse Weather Events (AWEs) are becoming more frequent and intense, thereby elevating the risk of equipment failure, intensifying the probability of cascade events [170], multiple outages and blackouts[171, 172]. Due to the unpredictability of such events and to the lack of robust and suitable risk assessment models, it is difficult to quantify a precise correlation between AWEs and components damage [173]. However, suitable strategies of operational planning can be adopted to enhance power grid resilience, preserving service to customer [174].

For this purpose, many studies have developed fragility curves [175, 176], to correlate critical weather conditions, such as wind speed [177–179], flood depth [180, 181], with component failure or damage probabilities. In [182], the impact of heat waves on distribution systems is analyzed, estimating how the failure rates of underground cables can be modified on the basis of meteorological data and a historical failure database. In [183], a reliability model is validated through empirical dependencies of component failure and repair rates on wind speed and lightning

intensity.

The potentials of adopting ONR under AWEs were explored in [184], where the coordinated reconfiguration, jointly with distributed resources management helped mitigate the effects of hurricanes on end users and operation costs. In [185, 186], the combination of dynamic reconfiguration and demand-response allowed to improve power system resilience under weather-based outages. In [187], a bi-level reconfiguration model is presented. The first level of the proposed methodology aimed to minimize the cost of expected outages before storm or hurricane, while the second level minimized the cost of outages post AWE. The work presented in [188] introduced a coordinated approach of network reconfiguration and wind-turbine allocation aimed at minimizing load curtailment during extreme AWEs.

In this paragraph, an ONR architecture based on MISOCP is developed and used to investigate whether feasible optimal topologies that satisfy the network operational requirements can be found and adopted during adverse weather conditions to improve reliability. The influence of AWEs on the reliability of the power system is assessed by taking into account the specific vulnerabilities of different network components. Underground cables and urban substations may be exposed to elevated temperatures during Heat Waves (HWs) due to the formation of urban heat islands [189]. Underground equipment, together with secondary substations, may instead be affected by flooding during intense rainfall if located in high flood risk areas. Similarly, towers, pole-mounted transformers, and overhead lines can be damaged or experience faults under severe Wind Gusts (WGs), particularly when vegetation is present near them.

The impact of AWEs including HWs, floodings, and WGs is integrated into the ONR problem through updated failure rates and repair times for components susceptible to these events. The methodology is applied to a realistic-sized grid model that represents a distribution network that supplies a town in Southern Italy.

A preliminary study on this topic was conducted in [15] and for extension purposes, the contributions of this study are:

- sound and complete formulation of a deterministic ONR problem, based on a full ACLF model represented through MISOCP relaxation;
- integration of FDIR distribution automation logics;
- inclusion of security constraints on voltage magnitudes and branch ratings in

order to find only feasible optimal topologies;

- improved formulation of the objective function that now includes both targets on reliability and operating conditions;
- definition of a deterministic approach to model the evolution and duration of AWEs (e.g., heat waves, floodings, and wind gusts) within grid reliability studies;
- an update strategy for failure and repair rates of grid components, tailored to the specific physical impact of different AWE types.
- comparison of results obtained with the previous formulation in [15], based on a simpler MILP problem.

5.10.2 ONR solution algorithm under AWEs

A key requirement for assessing the impact of AWEs on distribution grid reliability is an ONR tool integrated into the SCADA/DMS sufficiently accurate and capable of providing a solution within a reasonable time frame. This should be complemented by historical weather event data and a methodology to estimate electrical equipments' failure and repair rates. Considering the MISOCP-ONR problem formulated in Paragraph 5.7, in this section, a two-stage solution procedure is proposed to derive alternative topologies under AWEs still fulfilling network constraints.

To assess the impact of weather events on a distribution network, a simple workflow procedure is proposed in Fig. 5.19 to illustrate the approach adopted to perform numerical simulations.

Stage 1 allows to evaluate the impact of AWEs on reliability, using the system topology which optimizes normal weather conditions. In Stage 2, the ONR problem is solved for each AWE, finding different optimized topologies.

5.10.2.1 Stage 1 - Normal Weather ONR

Stage 1 starts with the assignment of component standard failure rates (λ) and repair times (ρ), according to [146, 190], followed by a network zone partitioning execution. The ONR routine is launched to find a network topology that minimizes (5.19), the solution represents the optimal topology that, during normal weather conditions,

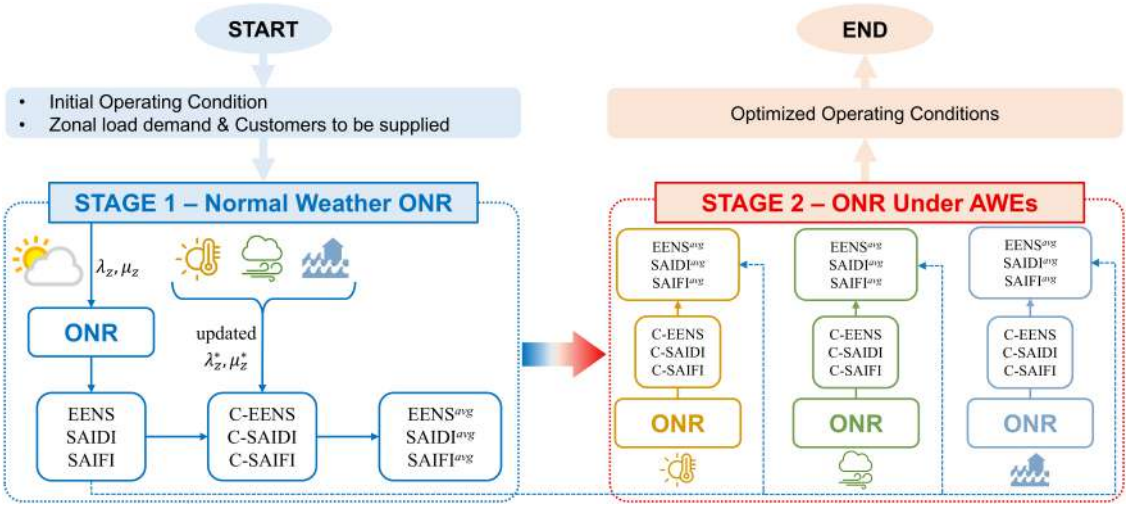

Figure 5.19: ONR workflow procedure considering AWEs [7].

minimizes the reliability indices EENS, SAIDI, SAIFI, and active power losses. This first optimal topology is then used as benchmark to analyze the ONR outcomes under AWEs.

As explained in [191], average reliability indices can be defined as follows:

$$\begin{aligned} \text{EENS}^{avg} &= \gamma_1 \cdot \text{EENS} + \gamma_2 \cdot \text{C-EENS} \\ \text{SAIDI}^{avg} &= \gamma_1 \cdot \text{SAIDI} + \gamma_2 \cdot \text{C-SAIDI} \\ \text{SAIFI}^{avg} &= \gamma_1 \cdot \text{SAIFI} + \gamma_2 \cdot \text{C-SAIFI} \end{aligned} \tag{5.48}$$

where EENS, SAIDI, and SAIFI, are the reliability indices evaluated with (5.2)-(5.4), during normal weather conditions, considering normal failure rates and repair times (λ, ρ). C-EENS, C-SAIDI, and C-SAIFI, are the conditional reliability indices evaluated with (5.2)-(5.4) and considering updated failure rates and repair times λ^* and ρ^*, used to take into account the influence of AWEs on components reliability. The weights γ_1 and γ_2 allow to estimate the duration of normal and AWE conditions, indicated with N (h) and A (h), respectively:

$$\gamma_1 = \frac{N}{N+A}, \quad \gamma_2 = \frac{A}{N+A} \tag{5.49}$$

The optimal topology found in this stage is used to evaluate (5.2), (5.3) and (5.4) during normal weather and AWE conditions, assuming in the second case, updated reliability parameters λ^* and ρ^* that leads to conditional reliability indices.

Please note that in this stage, the conditional reliability indices are not optimized,

but only calculated ex-post based on the optimal topology found under normal weather conditions, meaning that better solutions that minimize them could exist.

5.10.2.2 Stage 2 - ONR under AWEs

Stage 2 assumes that the network topology can be optimized whenever AWEs are expected. This means that different topologies will be used to assess the overall reliability indices. In this stage, the conditional reliability indices are optimized solving the ONR problem. The solution represents the optimal topology that minimizes the conditional reliability indices C-EENS, C-SAIDI, C-SAIFI, and power losses for each AWE condition.

The average reliability indices can still be calculated with (5.48), but, unlike Stage 1, the conditional reliability indices are evaluated based on a different topology, optimized for each AWE. In the absence of historical failure data, reliability parameters λ^* and ρ^* are modified by applying a suitable correction factor to the standard λ and ρ, trying to find a compromise between the common practices and values found in literature. These assumptions are working hypothesis used to investigate how ONR can help in mitigating the impact of AWEs, rather than building an actual probabilistic model [192].

5.10.3 Characterization and duration of the AWEs

The duration of the three types of AWEs considered in this study are calculated accessing to historical data of temperature (°C), precipitation intensity (mm) and wind speed (m/s), using the MEteorological Reanalysis Italian DAtaset [193].

5.10.3.1 Heat Waves

HW events could be evaluated by means of three indices [194]. The first one, the significant excess heat index (SEHI_i) is calculated as the difference between the arithmetic mean of the average temperatures measured on a period of three days and the 95^{th} percentile of the daily mean temperature based on the previous 30 years of data (1994-2023).

$$\text{SEHI}_i = \frac{T_i + T_{i+1} + T_{i+2}}{3} - T_{95} \tag{5.50}$$

The second one is the acclimatization excess heat index (AEHI_i), calculated as the difference between arithmetic mean of the average temperatures calculated over the

three days and the previous 30 days indicating the unusual temperature rise.

$$\mathrm{AEHI}_i = \frac{T_i + T_{i+1} + T_{i+2}}{3} - \frac{T_{i-1} + \ldots + T_{i-30}}{30} \tag{5.51}$$

The two indices are then used to calculate the excess heat factor for the day i (EHF_i). If this index is positive for at least 3 days consecutively, then the HW event has occurred.

$$\mathrm{EHF}_i = \max(1, \mathrm{AEHI}_i) \cdot \mathrm{SEHI}_i \tag{5.52}$$

Once the HW event has been evaluated, the following relations has been used to modify the underground lines and transformers component failure rates. An exponential growth Weather-Dependent Failure Rate model was adopted (5.53) to quantify the increase in the probability of failure of the underground cables as a function of thermal stress.

$$\lambda_{line}(T(t))^* = \lambda \cdot e^{\alpha(T(t) - T_{crit})} \tag{5.53}$$

The exponential form represents the statistical adaptation of Arrhenius chemical law for the degradation of insulators. A value of $\alpha = 0.07$ was derived from Montsinger rule [195]. An activation threshold $T_{crit} = 30°C$ was set.

In order to directly correlate environmental and operational variables with the rate of transformer degradation, the aging acceleration factor (5.54) with the steady-state thermal model has been adopted, in accordance with IEEE Std C57.91 [196].

$$\lambda_{tr}(T(t))^* = \lambda \cdot \exp\left(\frac{15000}{383} - \frac{15000}{T_H(t) + 273}\right) \tag{5.54}$$

In particular, the hot-spot temperature $T_H(t)$ is expressed as a function of time through the following equation:

$$T_H(t) = T_a(t) + \Delta\overline{T_o} \cdot \left(\frac{1 + R \cdot K^2}{1 + R}\right)^x + \Delta\overline{T_g} \cdot K^y \tag{5.55}$$

Specifically, the parameters adopted reflect a standard distribution transformer: $T_a(t)$ is the variable ambient temperature (during HW event), K is the Load factor. $\Delta\overline{T_o} = 55°C$ is the nominal oil over-temperature, $\Delta\overline{T_g} = 23°C$ is nominal winding hot-spot gradient, $R = 5$ is the Ratio between load losses and no-load losses at nominal load. Thermal exponents $x = 0.8$ and $y = 1.6$ have been used according

to the standard. In the absence of specific historical load profiles and to conduct a precautionary risk analysis, a constant load factor $K = 1$ was assumed.

5.10.3.2 Floodings

Floodings events are evaluated using a rainfall threshold, generally used for the estimation of possible occurrence of rainfall-induced landslides and flash flood triggering. The intensity-duration power law has the following form [197]:

$$\mathcal{I} = \eta \cdot \mathcal{D}^{-\sigma} \tag{5.56}$$

where $\mathcal{I}$ is the rainfall maximum intensity (mm/h), η is a scaling parameter, σ is the shape parameter and $\mathcal{D}$ the duration of the rainfall event (h). The parameters adopted in this study have been taken by [198], valid for a $\mathcal{D}$ values between 0.167 h and 24 h. If the maximum intensity of the rainfall event is above the threshold curve, then the flood is triggered. The flooding event is considered to affect components located within an high flood risk area of about 3 km^2 (according to the hydro-geological map of the DN area [199]).

In the absence of specific fragility curves for the components under examination, the study adopts a piecewise linear model (5.57), under the physical assumption that the mechanical stress acting on the components is directly proportional to the hydrostatic pressure exerted by the water column, which varies linearly with the depth of submersion (h). The modified failure rate is evaluated when a Flooding event is registered:

$$\lambda(h(t))^* = \lambda + \alpha \cdot (h_i(t) - h_{\text{crit}}), \quad \alpha = \frac{\lambda_{\max} - \lambda}{h_{\max} - h_{\text{crit}}} \tag{5.57}$$

The analysis adopts a conservative approach applied to dated critical infrastructure for underground secondary cabins, characterized by degraded resilience. For this reason the model assumes a zero trigger threshold ($h_{\text{crit}} = 0$ m). Risk saturation is set at $h_{\max} = 1.5$ m, above which infiltration becomes inevitable for standard components. A maximum failure rate of $\lambda_{\max} = 5$ faults/year has been chosen, reflecting the transition from random failure to accelerated stress failure, making failure highly probable within the typical duration of the flood event. For underground cables, the model adopts a lower sensitivity damage curve (reduced α), justified by the nature of modern conductors (e.g. XLPE insulated), which are inherently waterproof.

5.10.3.3 Wind gusts

WG events depending on wind speed, and their impact on power system's reliability is widely explored by the use of fragility curves [177–179]. In this study, the WG event is considered verified if the wind speed at 10 meter altitude is greater than 8 m/s, because of the increasing overhead lines' faults recorded, according to [183]. To estimates the failure rates during WG events, a quadratic relation (5.58) is used, according to [200]:

$$\lambda(\omega(t)) = \lambda \cdot (\omega(t)/\omega_{\text{crit}})^2 \tag{5.58}$$

where $\omega(t)$ is the wind speed registered, $\omega_{crit} = 8$ m/s is the threshold value.

5.10.4 Case Study & Test Results

Numerical simulations were carried out on the 1014-Bus realistic-sized distribution network model, solving the MISOCP-ONR model under AWEs adopting the SFS technique (computationally lighter) and comparing the results obtained with the previous MILP formulation, detailed in [201].

5.10.4.1 ONR results - Normal weather

After the assignment of component standard reliability parameters (λ, ρ) in the initial topology, the zone partitioning algorithm and ONR are executed. The zonal reliability parameters (λ_z, ρ_z), zonal number of customers N_z and zonal active power demand P_z^D, evaluated during normal weather are shown in Fig. 5.20; only λ_z, ρ_z will be modified when assessing different AWEs.

Taking into account the initial topology (Fig. 5.21a), the grid is characterized by a total active power demand of 37.45 MW, a total RES generation of 11.49 MW, whereas the total active power losses are 1.13 MW. A total of 394 voltage violations and 2 overloading violations are detected in the initial grid topology. Overvoltages are concentrated in the rural area, while undervoltages and overloading violations are located in the urban area.

After MILP-ONR, only 55 undervoltage violations and 1 overload persist, as can be seen in Fig. 5.21b, while MISOCP-ONR was able to solve all violations (Fig. 5.21c).

The MILP and MISOCP optimized topologies obtained in normal weather are also shown with zonal graphs in Fig. 5.22. Each feeder starts from an ancestor

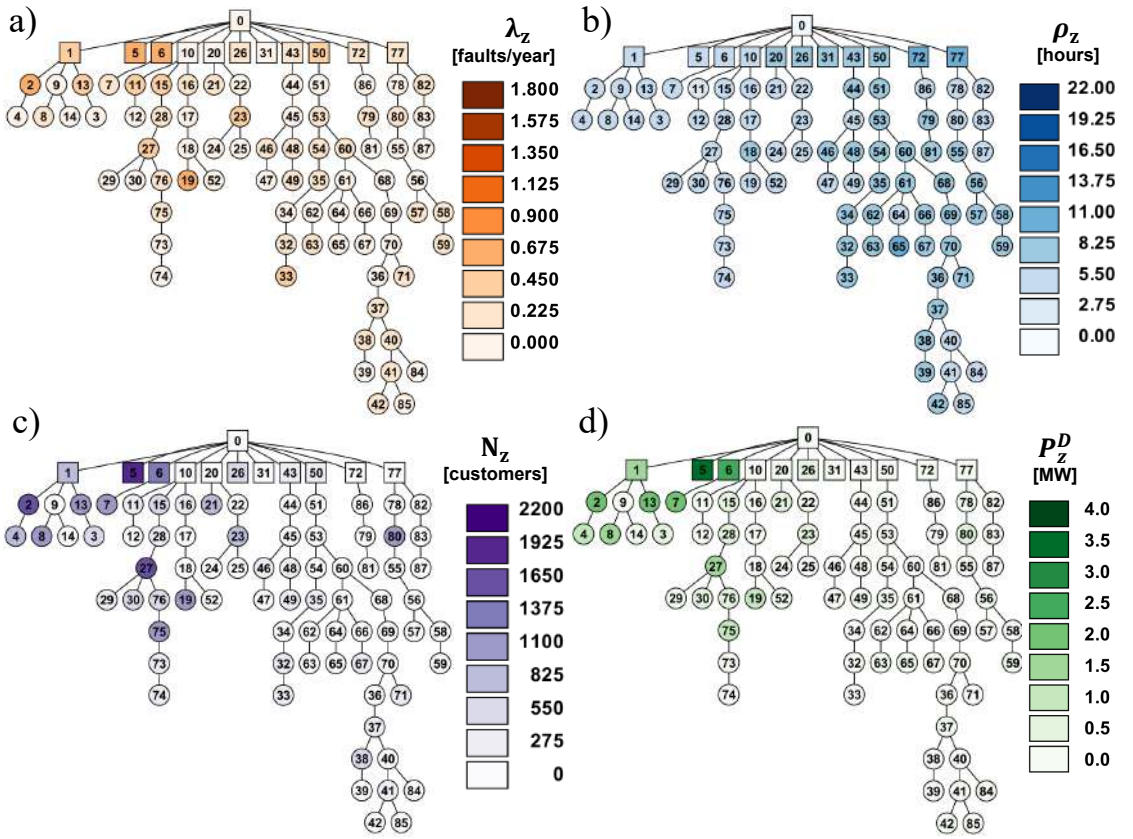

Figure 5.20: Initial zonal topology in normal weather: a) Zonal failure rate. b) Zonal average downtime per failure. c) Zonal number of customers. d) Zonal active power demand [7].

zone (colored square box) and is connected to the primary substation zone (white square box). The switch transitions from open to closed after the ONR are indicated with a red continued line. The colors adopted for the two topologies will be used as a reference in the following zonal graphs to emphasize the topological differences between the results obtained in normal and AWEs for the two formulations. Some differences can be noticed between the two topologies obtained. In the MILP result, the zones #12 and #19 are connected under the ancestor zone #1, improving the reliability and minimizing the number of upstream zones, but causing the violations of undervoltage and overloading to persist in the first feeder. In the MISOCP result, the zones #8, #9, and #14, are connected under the zone #12 on the fourth feeder, clearing all violations. The same topological rearrangements can be appreciated for the zones located on the sixth, seventh, and tenth feeder, for both ONR results.

Reliability indices evaluated on the initial and optimized topologies, during normal weather, are shown in Tab. 5.13.

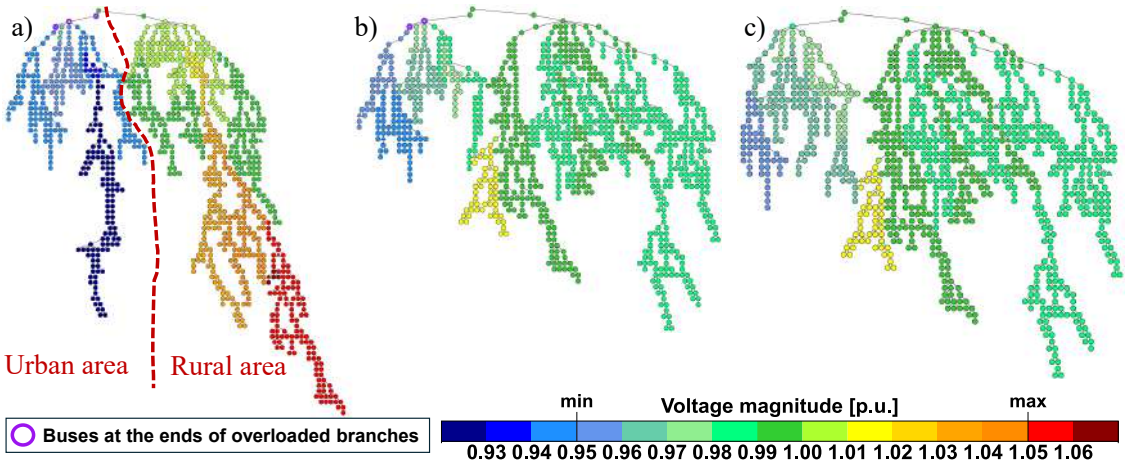

Figure 5.21: Initial and optimized grid topologies in Normal weather: a) Initial condition. b) MILP results. c) MISOCP results [7].

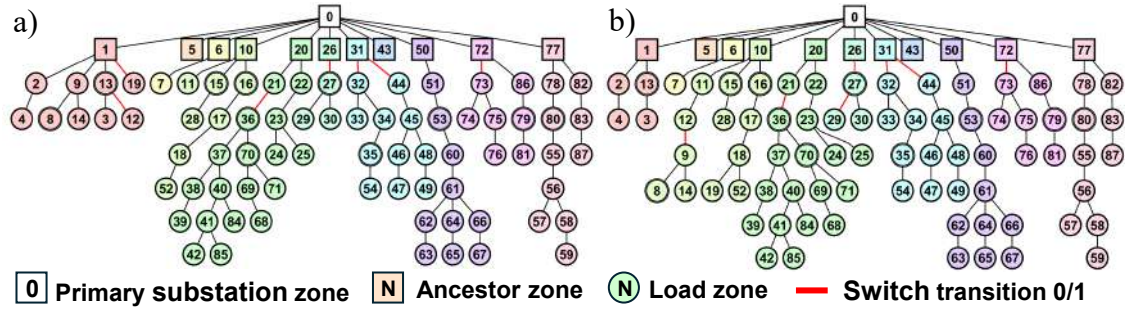

Figure 5.22: Optimized zonal topologies in normal weather: a) MILP result. b) MISOCP result [7].

The MILP result led to a major improvement in terms of reliability indices (18.09%, 22.11%, 22.49%, respectively), compared to the MISOCP result (17.15%, 21.43%, 21.82%). Despite this, the MISOCP approach led to a feasible topology, which also minimized total active power losses. The highest improvement is reached by the MISOCP results, in terms of P_{loss}, with a reduction of 42.19%, while the value of P_{loss} obtained with MILP-ONR is only assessed by an ACLF after ONR, so it is not minimized. As mentioned above, the two optimal topologies obtained during normal weather will also be used to evaluate the conditional reliability indices in the presence of each AWE, at the end of Stage 1.

5.10.4.2 ONR results - Heat waves

HWs are assumed to affect underground cables and MV/LV transformers, located mostly in urban areas and vulnerable to the temperature increase also due to the phenomenon of urban heat islands. The estimated total duration of these events is

Table 5.13: Reliability indices and system losses during normal weather

Method	**EENS [MWh/year]**	**SAIDI [hours/year]**	**SAIFI [faults/year]**	P_{loss} **[kWh]**
Initial Topology	284.052	8.7029	1.2055	1125.37
MILP	232.671	6.7786	0.9344	735.07
MISOCP	235.337	6.8383	0.9424	650.56

about 408 h/year. The failure rates of 208 underground cables and 236 distribution transformers have been updated with the mean value obtained from (5.53), (5.54), evaluated in the presence of HWs. The zonal reliability values during this AWE are shown in Fig. 5.23. Compared to the standard reliability parameters evaluated

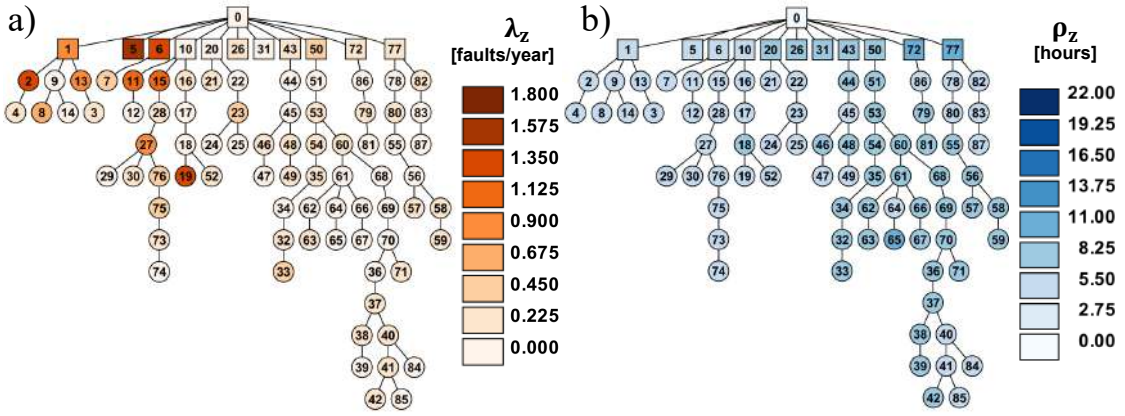

Figure 5.23: Initial zonal topology with modified reliability parameters: a) Zonal failure rate. b) Zonal average downtime per failure [7].

during normal weather, a general increase of λ_z, for the zones located in the urban area, can be observed.

The zonal topologies obtained are shown in Fig. 5.24, where the red-written zones include components influenced by HWs.

It can be observed that, after MILP-ONR (Fig. 5.24a), the zone #19, connected to the first feeder during normal weather, is now located below the zone #18, in the fourth feeder, to minimize its f_z. In fact, during HWs, the ancestor zone #1 is characterized by higher values of λ_z. The zone #52 has also been relocated under the ninth feeder, in which no components are influenced by HW, reducing the number of upstream zones on its path and then its f_z and its U_z; only 1 overload persists in this configuration.

In the MISOCP result (Fig. 5.24b), the zone #9 is no longer connected below the fourth feeder, due to the presence of the zone #11, now with higher λ_z, and remains located under the ancestor zone #1. This slightly increases the first feeder

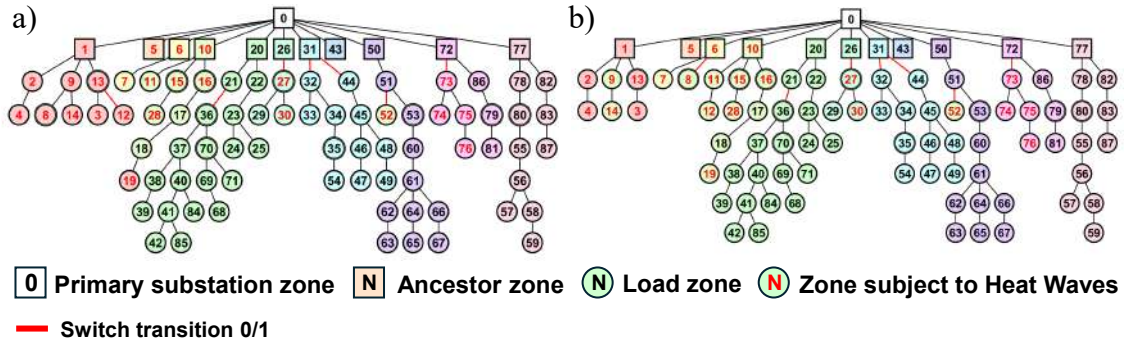

Figure 5.24: Optimal topology during heat waves: a) MILP results. b) MISOCP results [7].

demand, compared to the solution obtained during normal weather (Fig. 5.22b), but still respects the security limits. To clear overloads in the first feeder, the zone #8 has been moved under the ancestor zone #6. The zone 52 has been relocated under the eighth feeder, as in the MILP results.

Conditional reliability indices evaluated on the optimized topologies, during HWs are shown in Tab. 5.14.

Table 5.14: Conditional reliability indices and system losses during Heat Waves

Method	**Optimized AWE topology**	**C-EENS [MWh/year]**	**C-SAIDI [hours/year]**	**C-SAIFI [faults/year]**	P_{loss} **[kWh]**
MILP	Normal	373.446	9.6319	1.4340	735.07
	Heat Waves	371.879	9.5486	1.4156	673.57
MISOCP	Normal	375.432	9.6698	1.4383	650.56
	Heat Waves	374.779	9.6596	1.4347	639.14

Improvements can be observed for both MILP and MISOCP results, compared to the optimal topologies found during normal weather. The reliability indices minimized after MISOCP-ONR are higher compared to the MILP result, as the MISOCP approach aims to mitigate the overload still present in the MILP optimized topology. The greatest improvement in reliability indices is observed for C-SAIDI and C-SAIFI, with a reduction of 0.86% and 1.28%, respectively, in the MILP result, and 0.69% and 0.95% in the MISOCP result. The C-EENS index is subject to a lower reduction of 0.42% and 0.27%, respectively. The reduction obtained in terms of P_{loss} is the highest between the different AWEs, with an improvement of 1.75% after MISOCP-ONR.

Table 5.15 compares the average indices obtained considering the actual duration of HWs. It can be seen that the values of the average reliability indices evaluated in Stage 1 and 2 are very close for both approaches, with similar optimal topologies obtained to those found during normal weather. The increased values of λ^* on the

already high-failure-rate components led both problems to move in the same direction, seeking to minimize reliability indices by reorganizing the same most critical zones.

Table 5.15: Average reliability indices considering Heat Waves

Method	Stage	EENS [kWh/year]	SAIDI [h/year]	SAIFI [faults/year]
MILP	**1**	239.228	6.9115	0.9577
	2	239.155	6.9076	0.9568
MISOCP	**1**	241.862	6.9701	0.9655
	2	241.815	6.9670	0.9649

The almost same results, obtained with MISOCP approach during the two Stages, prove that the topology found in normal weather is close to being suitable for the AWE, with few different switching transitions needed to find the optimal one.

5.10.4.3 ONR results - Floodings

In case of floodings, the failure rates and repair times of 14 underground lines and 8 secondary underground substations, located in areas with high risk of flooding, were updated, by the mean value obtained with (5.57), calculated whenever a flooding event occurs. The repair time has been modified by adding the average duration of flooding events to the standard repair time of components. Unlike the HWs events, the repair time has also been modified accounting for the impossibility of conducting maintenance in completely flooded areas. The estimated total duration of these events is about 180 h/year.

The zonal reliability values, evaluated during floodings, are shown in Fig. 5.25, despite the limited number of components influenced by this AWE, a considerable increase can be observed in terms of λ_z and ρ_z.

The optimized topologies are shown with zonal graphs in Fig. 5.26, where red-written zones are influenced by floodings. The zones affected by flooding events are only four: zones #5, #11, #12, and #13. After MILP-ONR (Fig. 5.26a), zone #3, connected under zone #13 during normal weather, have been connected under zone #2, outside the floodings risk-area and having a lower ρ_z. Zone #12 is now connected below zone #13, decreasing the possibility that a failure can occur on the fourth feeder. The zone #11 remains connected to the fourth feeder (green), having no other possible configurations, as for HWs. Concerning the zone #5, since it is subject to possible flooding and is characterized by the highest λ_z, yet no other zone can be connected to it without worsening the reliability performances. In this

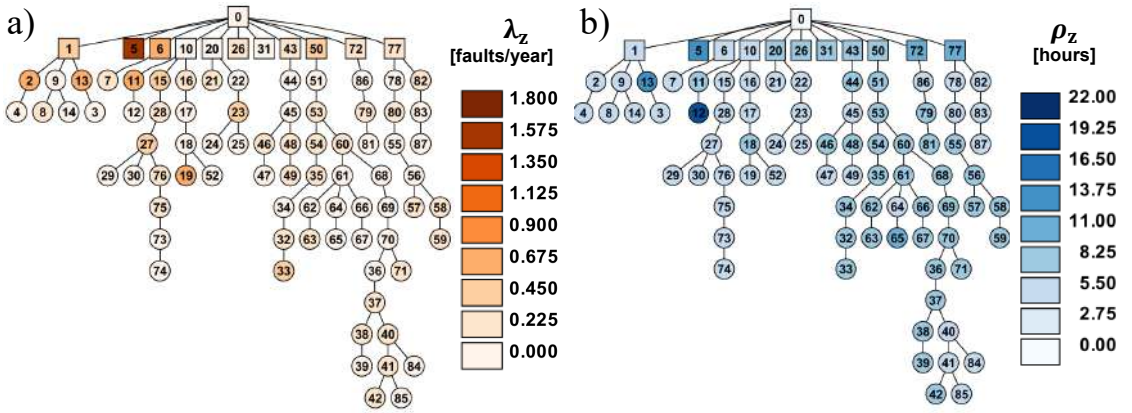

Figure 5.25: Initial zonal topology with modified reliability parameters: a) Zonal failure rate. b) Zonal average downtime per failure [7].

optimized topology, 61 undervoltage violations and 2 overloading persist on the grid.

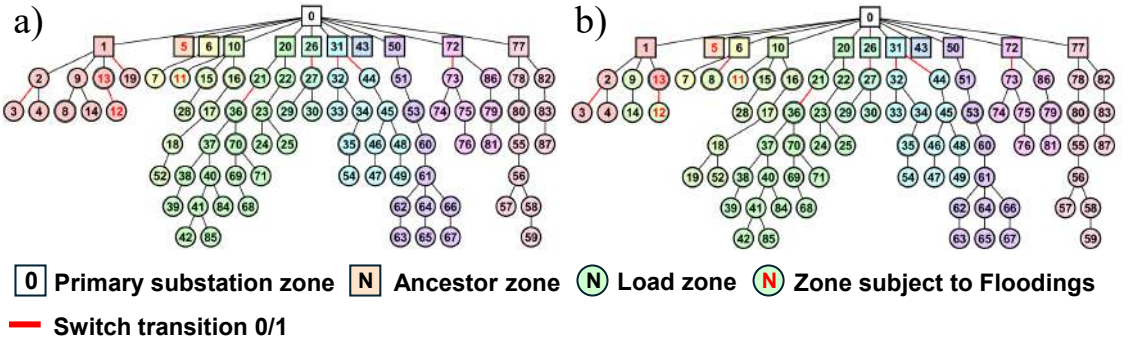

Figure 5.26: optimized zonal topologies during floodings: a) MILP results. b) MISOCP results [7].

Also in the MISOCP result (Fig. 5.26b), the zones #3 and #12 have been connected under the first feeder. In order to avoid undervoltage violations registered in the MILP configuration, the zone #8 connected below zone #12 during normal weather has been moved under the ancestor zones #6, improving f_z and U_z.

The conditional reliability indices calculated on the optimal topologies during floodings are shown in Tab. 5.16.

Table 5.16: Conditional reliability indices and system losses during Floodings

Method	**Optimized AWE topology**	**C-EENS [MWh/year]**	**C-SAIDI [hours/year]**	**C-SAIFI [faults/year]**	P_{loss} **[kWh]**
MILP	Normal	346.561	8.5720	1.0022	735.07
	Floodings	341.324	8.4610	0.9995	752.45
MISOCP	Normal	367.522	9.0190	1.0246	650.56
	Floodings	343.520	8.5094	1.0046	639.49

The optimized AWE topologies allowed for a great improvement in both the MILP and MISOCP results. The highest improvement for reliability indices is observed for C-EENS and C-SAIDI (reduced by 1.51% and 1.29% after MILP-ONR, 6.53% and 5.65% after MISOCP-ONR). The C-SAIFI is subject to the lowest reduction (0.27% and 1.95%). Total active power losses are subject to a reduction 1.70%, minimized in MISOCP-ONR.

The average reliability indices in Tab.5.17 differ more in the both MILP and MISOCP approaches, compared to HWs, with flooding being a more localized event and heavily affecting a limited number of components. This unpredictable increase

Table 5.17: Average reliability indices considering Floodings

Method	Stage	EENS [kWh/year]	SAIDI [h/year]	SAIFI [faults/year]
MILP	**1**	235.011	6.8154	0.9358
	2	234.904	6.8132	0.9357
MISOCP	**1**	238.053	6.8831	0.9441
	2	234.949	6.8142	0.9358

in the reliability parameters highlights that the topology obtained during normal weather is not the optimal one to adopt for this type of AWE. Compared with HW results, in this case, only a few components reach high failure rate and repair time values, leading to the ONR to rearrange specific zones for system reliability improvements.

5.10.4.4 ONR Results - Wind Gusts

Considering WGs, the reliability parameters were updated for 548 overhead lines and 606 towers and pole mount transformers, located mostly in rural areas and more easily subject to faults due to the proximity of trees. The repair time has been modified by adding the average duration of the WG events to the standard repair times of components. The failure rates has been modified considering the mean value derived by (5.58). The estimated overall duration of these events is about 401 h/year. The zonal reliability values, evaluated during WGs are shown in Fig. 5.27.

Although a large number of zones are influenced by WGs, a lower λ_z increase is registered compared to previous AWEs. The highest ρ_z are now registered on the right side of the grid, in the rural area.

The new topologies found are shown with zonal graphs in Fig. 5.28 (where red-written zones are influenced by WGs).

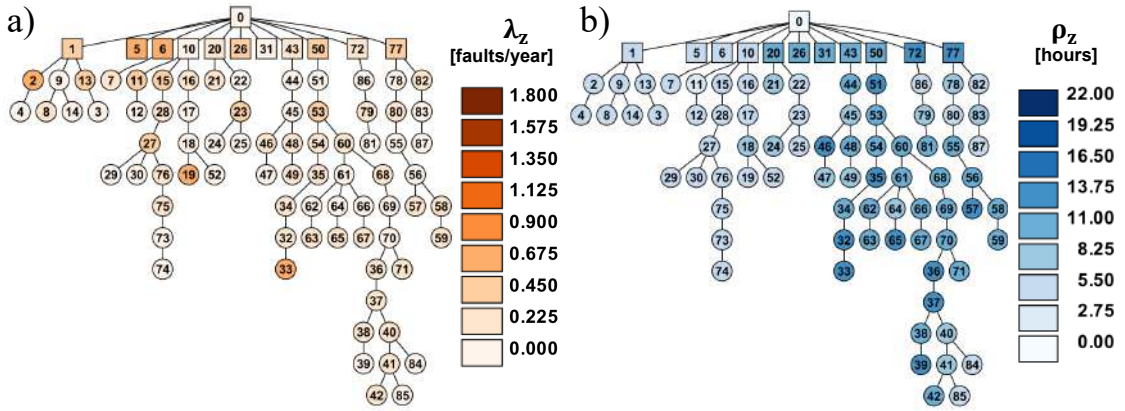

Figure 5.27: Initial zonal topology with modified reliability parameters: a) Zonal failure rate. b) Zonal average downtime per failure [7].

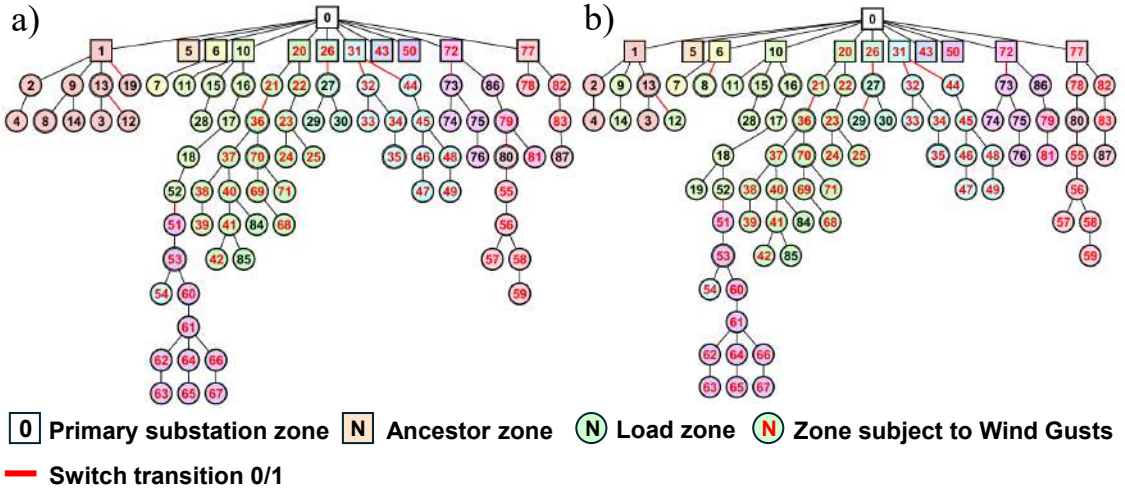

Figure 5.28: optimized zonal topologies during Wind Gusts: a) MILP result. b) MISOCP result [7].

The MILP result in Fig. 5.28a shows how some of the zones afferent to the right half-bar and previously connected under ancestor zone #50 (zones #51, #53, #60-#67) now influenced by the WG are now connected to the zones related to the left half-bar (under ancestor zone #10), reducing their U_z, despite the increase in the number of upstream zones. Moreover, some of the zones previously connected to the eleventh feeder are now moved to the tenth feeder, below the zone #79, in order to improve reliability on the last feeder. 37 undervoltage violations and 1 overload persist.

In the MISOCP result (Fig. 5.28b), in addition to the same reorganization of zone #51, #53, #60-#67 that occurred with MILP-ONR, zone #9, #14 and #12 presents the same configuration obtained for floodings, with zone #8 moved under

the third feeder, to avoid violations. Furthermore, the zones #79 and #81, remain connected under ancestor zone #72, to reduce active power losses but worsen the reliability.

Conditional reliability indices, calculated on the optimized topology during WGs, are shown in Tab.5.18.

Table 5.18: Conditional reliability indices and system losses during Wind Gusts

Method	**Optimized AWE topology**	**C-EENS [MWh/year]**	**C-SAIDI [hours/year]**	**C-SAIFI [faults/year]**	P_{loss} **[kWh]**
MILP	Normal	290.176	9.0233	1.0173	735.07
	Wind Gusts	286.563	8.8572	1.0218	811.85
MISOCP	Normal	292.867	9.0829	1.0253	650.56
	Wind Gusts	289.106	8.9210	1.0251	645.82

Different improvement in terms of reliability has been found with respect to the other AWEs. The greatest reduction was found in terms of C-SAIDI (1.84% and 1.78% with the MILP and MISOCP result, respectively) and C-EENS (1.24% and 1.28%). C-SAIFI increased by 0.43% with MILP-ONR while it was reduced by 0.02% after MISOCP-ONR. The total active power losses have been reduced by 0.72%, minimized in the MISOCP-ONR. Few reconfiguration maneuvers can be made due to the low number of switches located in the rural area. This means that for many buses it is not possible to improve reliability by connecting to other feeders.

The average reliability indices in Tab. 5.19 show that, despite the limitation previously described, the most improved average index in the case of WGs is SAIDI, subject to the higher reduction and directly dependent on the updated reliability parameter λ^* and ρ^*.

Table 5.19: Average reliability indices considering Wind gusts

Method	**Stage**	**EENS [kWh/year]**	**SAIDI [h/year]**	**SAIFI [faults/year]**
MILP	**1**	235.303	6.8813	0.9382
	2	235.138	6.8737	0.9384
MISOCP	**1**	237.971	6.9410	0.9462
	2	237.799	6.9336	0.9462

Compared to flooding events, the values obtained with MISOCP-ONR in Stages 1 and 2 are closer, due to the fact that the components influenced by WG are characterized by low standard failure rates. This, in addition to a moderate severity of the recorded WG events, limits the improvements in terms of the average reliability indices obtained with the new optimal configuration found.

5.11 Primary Distribution Network Re-energization through Multiple Black Start Units

The increasing integration of distributed generation into distribution networks poses challenges to grid security and reliability, primarily due to the inherent intermittency and non-dispatchability of renewable energy sources (RES). Energy storage systems can mitigate these issues by enhancing RES controllability, thereby transforming them from a source of uncertainty into a flexible asset that contributes to system reliability. This study proposes a re-energization algorithm designed to exploit the microgrids (MGs) capabilities in ensuring energy supply during extreme events (e.g., blackouts). Specifically, the algorithm enables secure partitioning into network islands ensuring power balance.

The methodology is based on the concepts previously outlined for the formulation of the ONR problem. It is therefore presented at the end of this chapter with the aim of highlighting how reconfiguration problems can be appropriately modified to implement different control actions and also provide other grid services (i.e., re-energization and restoration process).

5.11.1 A Brief Literature Review

The growth of energy produced from renewable energy sources (RES) involves a reduction in the energy generated from fossil fuels, as required by the environmental policies of the various countries. However, the diffusion of RES implies a decrease in reliability due to their intermittent nature and consequent difficulties in operation planning. These characteristics can affect the system dispatch and commitment processes and also increase the risk of blackouts [202].

Power system restoration procedures are required following the blackout [202, 203], also provided by Terna's Grid Code in the plan for re-powering and re-energizing the transmission network [19]. At first, the black start units (BSUs) start up themself through their auxiliary generator. Specifically, the latter is employed to energize the main generator and establish a power island with the local load. Subsequently the BSUs energize the transmission grid restoring the power supply to the other non-BSUs. Finally, all the generation units in operation restore the demand across the system. The power plants (e.g., hydropower plants and gas turbines) that provide

black start service must satisfy certain criteria presented in [204], together with the possible application of RES and energy storage systems (ESSs) in providing this service. Some architectures and controls for islanding operation are presented in [205].

In [206] an integrated wind-photovoltaic-battery energy storage system (W-PV-BESS) characterized by a reduced number of electronic converters with an energy management system (EMS) is presented. The EMS allows to enable both the grid-connected and off-grid modes, also allowing black start service. In [207], a feasibility study is carried out considering a wind farm equipped with a storage system as a possible BSU used to power a thermal power plant. The storage system is employed to provide black start service and powering the wind farm, while the wind turbines are used to feed the nearby thermal power plant. In [208] a power management strategy is proposed to coordinate the resources in a microgrid (MG) composed by photovoltaic generation and a hybrid ESS, consisting of a supercapacitor and Lithium-Ion battery power converter systems. In particular, a power management strategy is described in order to keep the power balance and the healty MG state. The MG presents four operation modes in which one operates in black start state. In [209] an inverter controller for islanding operation is presented to provide also primary and secondary regulation services. In [210] the authors carry out black start tests under different starting modes of a ground source heat pump integrated with a hybrid ESS composed of a battery-supercapacitor system. An other study proposed a configuration method for ESS based on analytic hierarchy process [211], in which the ESS is designed to supply a wind turbine. Once the first turbine is started up, the wind energy produced is used to re-power the remaining ones allowing the wind farm to provide black start service. In [212] the authors present a stratified optimization strategy for manage the batteries' state of charge to avoid over-charging and over-discharging during black start operation of PV-BESS system.

In [213] the concept of multi-microgrid (MMG) as a structure composed by several MGs, distributed generation units, and controllable medium voltage loads is introduced. The authors study the structure of this MMG, its control strategy and finally propose a black start strategy. This one is based on a serial restoration strategy in which one of the MG is identified as the main source. In [214] a MG's controller is designed to allow the shift from grid-connected to islanding mode, and conversely, without requiring a control structure reconfiguration.

According to [215], during an under-frequency transient, it is possible to define isolated portions of the grid in order to face a generalized blackout, fostering the reconstruction of the electricity system during the recovery phase. In this regard, this paragraph addresses the possibility of exploiting MGs as BSUs, creating islanded sub-networks able to self-balancing. Specifically, a re-energization optimization problem is formulated and implemented to associate the unsupplied load in the distribution network with the MGs previously identified as BSUs by the transmission system operator. This results in a MILP optimization problem that maximizes the load demand to be supplied following a blackout event and preserving the power balance in the islanded sub-networks.

5.11.2 Re-energization Optimization Problem

In this section, a MILP optimization problem aimed to maximize the number of end-users supplied by BSUs after a blackout event, is formulated. If it exists, the optimal solution consists in creating islanded sub-networks, i.e., black start areas (BSAs), that are capable of self-balancing.

5.11.2.1 Zone subdivision

Following a blackout event, the re-energization of load nodes via BSUs depends on the presence of controllable switchable devices, and considering that the number of devices is limited compared to the number of connecting branches of a generic primary distribution network, the mathematical formulation of the proposed MILP problem is based on a zonal subdivision of the network. A zone z is defined as a set of network elements (nodes, branches, loads, and generation resources) connected exclusively by switches. As in the case of ONR problems [4, 5, 15], this modelling approach allows to simplify the grid topology into optimization frameworks and to reduce the number of variables and constraints in pursuit the computational effort. For this study's purpose, let Ω_Z be the set of zones into which the distribution network is partitioned. Three subsets of zones can be distinguished, depending on their role in the re-energization procedure:

- *Source-zones*: in a source-zone $r \in \Omega_R$, where $\Omega_R \subset \Omega_Z$, at least one BSU is installed, still operating or able to start up by itself after the blackout event and supplying local loads.

- *Load-zones*: in a load-zone $l \in \Omega_L$, where $\Omega_L \subset \Omega_Z$, all the interconnected load and generation nodes are de-energized following the blackout event. All the components within a zone l can be re-energized only if l results connected with any source-zone r.

- *Resynchronization-zones*: in a resynchronization-zone $p \in \Omega_P$, where $\Omega_P \subset \Omega_Z$, a synchronization device is installed in order to perform the resynchronization operation of the isolated portion of the network during the black start procedure. The interconnected load and generation nodes in this zone are de-energized following the blackout event. All the components within a zone p can be re-energized only if p results connected with a source-zone r. Load zones l and source zone r, need to be connected to a resynchronization-zone p during black start procedures.

An illustrative representation of zone subsets, for the re-energization problem, is shown in Fig. 5.29. The BSA comprises the set of load zones connected to a source zone. Each BSA is electrically isolated from the others and includes at most one resynchronization zone, which identifies the boundary and the only way for the BSA to be reconnected with the rest of the main grid through the primary substation (PS zone).

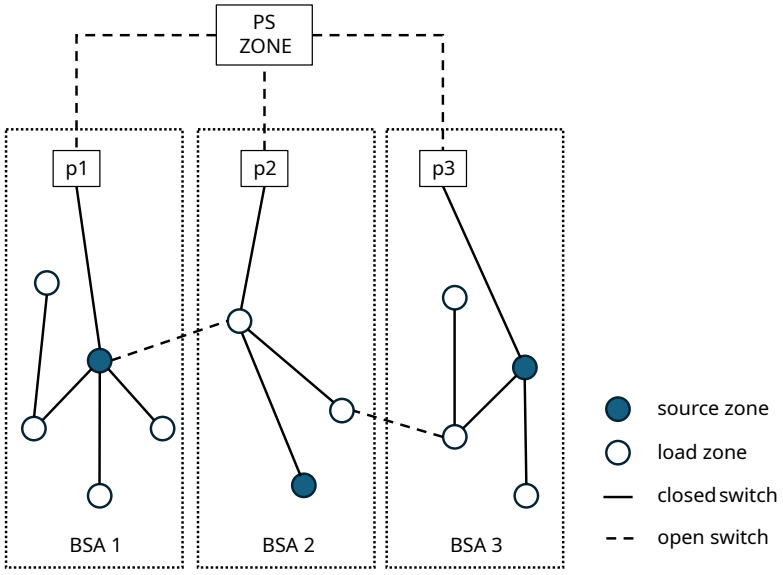

Figure 5.29: Illustrative example of zone subsets employed in the re-energization optimization problem [8].

5.11.2.2 Objective function

The objective function is to maximize the load demand to be supplied in all load-zones following a blackout event:

$$\max_{x_{ij}} \sum_{l \in \Omega_L} (P_L^l \cdot \sum_{r \in \Omega_R} W_{l,r}) \tag{5.59}$$

where P_L^l is the pre-blackout active power load demand required in a load-zone l, $W_{l,r}$ is a binary variable representing the power supply condition of a load-zone l from a source-zone r. If the zone l is re-energized from the BSU located in zone r, $W_{l,r}$ is equal to 1 (0 otherwise). The decision variables x_{ij} are binary and represent the connection states of the controllable switch protection devices (Ω_{sw}) in the distribution network. In fact, following the blackout event, these can be controlled to reconnect the de-energized zones and aggregate them within islanded BSAs, capable of self-balancing their loads by means of BSUs.

5.11.2.3 Fictitious power flows & zonal balancing constraints

Assuming that a fictitious unitary power demand is required in a load-zone l, and that the power is generated and delivered from a source-zone r, a real continuous variable $f_{i,j,r}$ can be defined. This represents the fictitious power flow transiting from a generic zone i to an other zone j connected through a switch (i, j) and supplied by a source-zone r. The fictitious power flow $f_{i,j,r}$ is related to the switch connection state through the following constraints:

$$-|\Omega_L| \cdot x_{ij} \leq f_{i,j,r} \leq |\Omega_L| \cdot x_{ij}, \quad \forall (i,j) \in \Omega_{sw}, \forall r \in \Omega_R \tag{5.60}$$

Thus, $f_{i,j,r}$ consequently identifies the number of load-zones $|\Omega_L|$ connected and fed by a source-zone r, through the switch (i, j). An extreme case could topologically corresponds to a configuration in which all zones l are fed from a single zone r, with the remaining source zone completely isolated from the rest of the network. Negative values for $f_{i,j,r}$ can be considered, depending on the orientation of the switches, making the formulation general and suitable for different network models. The zonal balancing constraints can now be defined, exploiting the variable $f_{i,j,r}$. These constraints are defined separately for load zones and source zones, considering for the first set of constraints, a positive convention for the fictitious power flow

entering the zone, negative if outgoing the zone, the opposite is made for the second set.

$$\sum_{\substack{j\in\Omega_Z \\ i=l, j\neq i}} f_{j,i,r} - \sum_{\substack{j\in\Omega_Z \\ i=l, j\neq i}} f_{i,j,r} = W_{l,r}, \quad \forall l \in \Omega_L, \forall r \in \Omega_R \tag{5.61}$$

$$\sum_{\substack{j\in\Omega_Z \\ i=r, j\neq r}} f_{i,j,r} - \sum_{\substack{j\in\Omega_Z \\ i=r, j\neq r}} f_{j,i,r} = \sum_{l\in\Omega_L} W_{l,r}, \quad \forall r \in \Omega_R \tag{5.62}$$

Eq. (5.61) defines, for each load-zone l, the balance between the sum of the fictitious power flows into and out of the zone l, for a given zone r. The variables $f_{j,i,r}$, $f_{i,j,r}$ and $W_{l,r}$, differ from zero only if the zone l is supplied by the BSU in r. Therefore, considering the orientation of the switch, if the receiving zone of the switch coincides with the zone l, the fictitious power flow is taken positive, otherwise it is taken negative. Eq. (5.62) represents, for each zone r, the balance between the sum of the fictitious power flow that is supplied by and to the zone r. If the sending zone of the switch coincides with zone r, the fictitious power flow is taken positive, otherwise it is taken negative. The balance must be equal to the number of load zones l connected to each zone r.

5.11.2.4 Source independence constraints

In order to obtain multiple islanded BSAs, fed independently by their own BSUs, the following constraints are also introduced:

$$\sum_{r\in\Omega_R} W_{l,r} \leq 1 \quad \forall l \in \Omega_L \tag{5.63}$$

It follows that the power supply of zone l cannot occur simultaneously from multiple BSUs. This means that if the load-zone l is fed by source-zone r, the variable $W_{l,r}$ is equal to 1, thus, the value of the variable related to the same zone l and referred to the remaining source zones of the network must necessarily be equal to 0. If load-zone l is not supplied by any source-zone, the value of $W_{l,r}$ will be 0 for each source-zone r.

5.11.2.5 Resynchronization zones independence constraints

In order to perform the subsequent resynchronization of the isolated portions of the network with the main grid, each island must necessarily be connected to a zone p

in which there is a synchroniZation device. This zone must represent the borders of the BSA. Therefore, the following constraint must be considered:

$$\sum_{(i,j)\in\Omega_{sw}} x_{ij} \leq 1 \quad \forall p \in \Omega_P, i = p \vee j = p \tag{5.64}$$

The Eq. (5.64) is applied only to switches connected directly to a resynchronization zone, allowing each p to be connected at most to one closed switch. In order to guarantee the presence of only one zone p for each island, the following relationship is taken into account:

$$\sum_{p\in\Omega_P} W_{p,r} = 1 \quad \forall r \in \Omega_R \tag{5.65}$$

with Eq. (5.65), no more than one zone p connected to a source zone r is allowed.

5.11.2.6 Islanded BSAs radiality constraints

In order to obtain islanded BSAs, the variable $W_{l,r}$ is related to the connection state of switches as follows:

$$\sum_{\substack{l\in\Omega_L \\ r\in\Omega_R}} W_{l,r} = \sum_{s\in\Omega_{sw}} x_{ij} \tag{5.66}$$

These constraints allow to accept configurations in which not all load-zones l are supplied, taking into account the hypothetical condition in which the BSUs may not have sufficient capacity to meet the required active power load demand. These relations make possible to obtain a network topology with multiple radial BSAs, since the number of closed switches must be equals to the number of load-zones l connected and powered by source-zones.

5.11.2.7 BSAs adequacy constraints

Finally, the BSUs capacity must be sufficient to cope the active power demand of supplied load zones, by the following constraint:

$$\sum_{l\in\Omega_L} W_{l,r} \cdot P_L^l \leq P_G^r, \quad \forall r \in \Omega_R \tag{5.67}$$

In Eq. (5.67), the active power capacity of source in r must satisfy the active power demand of a load zone l only if the variable $W_{l,r}$ is equal to 1.

5.11.3 Case study & Test results

Simulations were carried out on a 69-Bus Test system [164], the test system is a 12.66 kV distribution network consisting of 69 buses and 73 branches. An illustrative base topology, as found in literature, is shown in Fig. 5.30a. In this configuration, the total active power load demand is about 3.801, 89 kW, this data are used as the pre-blackout total load demand to be supply from the BSUs.

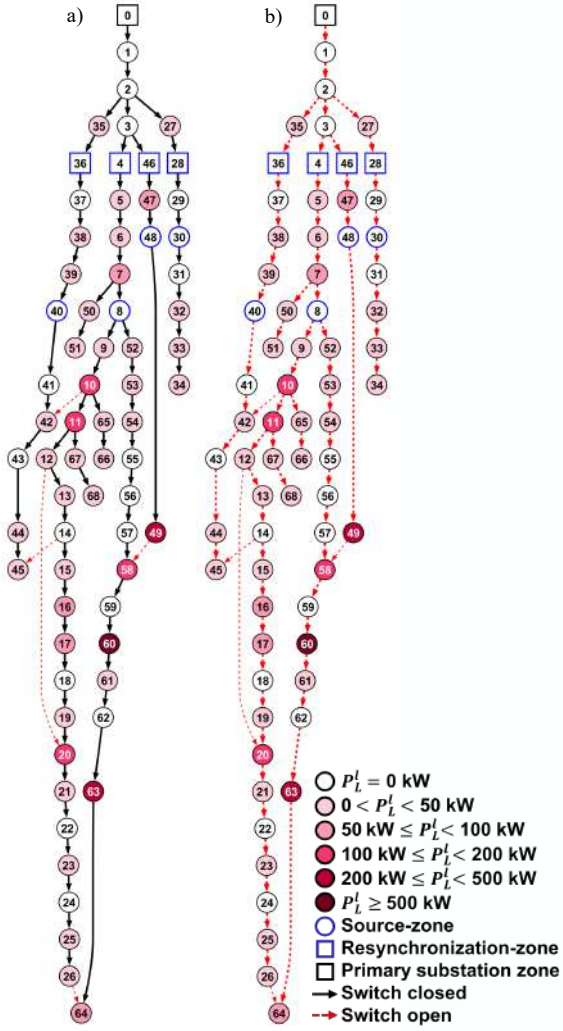

Figure 5.30: 69 Bus Test System graph: *a) pre-blackout condition. b) post-blackout condition* [8].

In this test system, branches are assumed to be all switchable, therefore, the execution of the zone subdivision algorithm leads to a subdivision of the network into 69 zones, where every zone consists of a single bus and the set of loads and generation connected to it. The combination of closed (black line) and open switches

(red dashed line) ensures a radial configuration, considering the primary substation as the only source (black contour square), with arrow directions indicating the switch's orientation. In addition to the Distribution Network's base model, the presence of 4 BSUs was assumed located in zone 8, 30, 40, 48, with a nominal active power of about 1600, 600, 1350, and 1200 kW, respectively. Moreover, 4 resynchronization zones are considered (zone 4, 28, 36, 46) and shown in blue contour square. The heat map shows the active power load demand for each load zone, from a minimum of 1 kW (zone 19), to a maximum of 1244 kW (zone 60). The re-energization algorithm was tested and validated assuming different operating scenario. However, only the most base case scenario is presented, with the aim of analyzing the effects of different BSUs capacity considering the benchmark loads data of the 69-Bus Test system.

Simulation tests were performed modeling the Distribution Network using OpenDSS software [165], while the mathematical problem is implemented in Python language, using the Pyomo library [60, 147] for the optimization problem construction, and the commercial solver Gurobi 11.0.1 with default settings [148] for the solution. For this study's purpose, the initial Distribution Network configuration is assumed to be in a post-blackout condition, completely de-energized (Fig. 5.30b), with the BSUs that only supplies the active power load demand requested within the source zones. All switches in the network are considered to be open, with no load zone supplied, the set of variables $W_{l,r}$ is obviously equal to 0 for any source zone r.

Fig. 5.31 shows the topologies found as a result of the re-energization algorithm, considering the 50% and 100% of the BSUs' capacity. The solutions obtained involve the formation of 4 BSAs, each one supplied by a single BSU. Switches connecting zones belonging to the same BSA are identified by four different colours (purple, magenta, orange, and blue), with each BSA respecting the proper radiality constraint. As can be seen, each BSA is connected to a single resynchronization zone, supplying their local active power load demand.

Considering the first topology obtained (Fig. 5.31a) with 50% of the BSUs' capacity, it is evident that some load zones results not connected, (16, 21, 23, 25, 26, 44, 50, 60, 61, 63-66 and 68), remaining unpowered. This is due to the fact that zone 8, 40, and 48 does not have enough active power generated to satisfy the load demand, while zone 30 supplies all the possible load zones in its downstream path. In addition, other zones with no active power demand (22, 24, 59, 62), also results not supplied. The arrows in the graph indicate the orientation of switches in the network model,

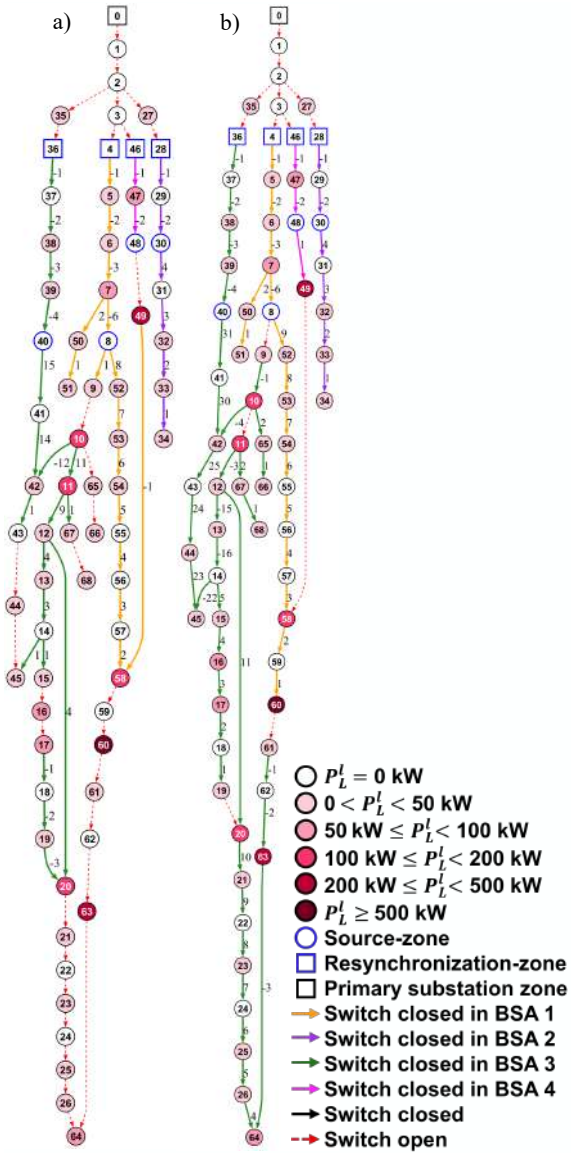

Figure 5.31: 69 Bus Test System graph after re-energization algorithm: a) 50% of BSUs capacity. b) 100% of BSUs capacity [8].

with the respective values of the fictitious active power flows transiting through them. The positive or negative values depends on how the switches are oriented with respect to the fictitious flow leaving the source zones. For example, zone 8, is connected to 15 load zones, the fictitious active power flow flowing through the switches directly connected to it is about +8, +1 and -6, indicating a total of 15 zones connected to it. The negative value of the variable $f_{i,j,r}$ considers the switch to be in the opposite direction with respect to the fictitious power flow outgoing the source zone. Looking at the zones 27 and 35, they remain not supplied by any source zone, because of their topological disposition. In fact, they cannot be supplied to

respect the resynchronization independent zone's constraint (Eq. 5.64).

In the second topology (Fig. 5.31b),the totality of load zones has been supplied exploiting the 100 % of the BSUs' capacity. In this zone 60 is supplied by the source zone 8, while zone 49, previously connected to zone 8, is now connected to the source zone 48, due to increased capacity. BSU zone 30, can connect at most load zones 32, 33, and 34, with no other switches available for re-energization of further load zones. In this topology achieved, zones without active power load demand are connected to BSUs zones in order to guarantee the supplying of downstream load zones (22, 24, 59, 62).

Table 5.20: BSAs results with 50% of BSUs capacity

BSA n.	**r**	**p**	P_G^r**[kW]**	**BSA**P_L **[kW]**	**max** P_L^l**[kW]**	**Nswitch**	**Usage [%]**
1	8	4	800,00	759,55	384,70	15	94.94
2	30	36	300,00	65,50	26,00	6	21.83
3	40	28	675,00	674,92	145,00	19	99.98
4	48	46	600,00	463,70	384,70	2	77.28
Total	/	/	2.375.00	1.963,67	/	42	82.68

Table 5.20, shows results information about BSAs obtained with 50% of the BSUs' capacity. The higher total active power load demand is supplied by source zone 8, related to its high capacity (800 kW), the BSA number 3 turns out to be the most extended one, with 19 switch closed and 19 load zones supplied. Globally, 31 switches remains open, located in the upstream path of the resynchronization zones, and in the downstream portion of the network. With the 50% of the BSUs' capacity considered, 22 zones results not supplied by any source zone. The percentage usage of the BSUs located in zone 8 and 40 is more than 90%, a lower percentage of usage is observed for the BSUs in zones 30 and 48. Regarding the BSA number 2, no other switches are present to supply additional load zones by zone 30, while the connection of zone 49 ($384,70$ kW) to zone 48 would exceed the capacity limit of the BSU.

Table 5.21: BSAs results with 100% of BSUs capacity

BSA n.	**r**	**p**	P_G^r**[kW]**	**BSA**P_L **[kW]**	**max** P_L^l**[kW]**	**Nswitch**	**Usage [%]**
1	8	4	1.600,00	1590,85	1244,00	15	99.42
2	30	36	600,00	65,50	26,00	6	10.92
3	40	28	1.350,00	1245,14	227,00	35	92.23
4	48	46	1.200,00	848,40	384,70	3	70.70
Total	/	/	4.750,00	3.749,89	/	59	78.94

Table 5.21, shows the results information about the BSAs obtained with the total capacity of the BSUs. The higher active power load demand is supplied by source

zone 8, related to its high capacity (1650 kW), the BSA number 3 still results the most extended, with 35 closed switches and 35 load zones supplied. With the total capacity of the BSUs considered, only 14 switches remain open and 6 zones results not supplied, located upstream of the resynchronization zones, thus they cannot be fed. The percentage of BSU's usage is over 90% only for zones 8 and 40. In particular, zone 48 could supply zone 58 (100 kW), but the following connection of zone 60 would exceed the capacity limit of 1200 kW, leaving the load zone not fed. Zone 30 has the lowest percentage of usage due to the network topology, resulting in the same number of closed switches and load zones supplied as in the previous case. The overall BSUs' percentage usage is $78,94\%$, resulting in a total active power demand supplied of $3.749,89$ kW, with only 52 kW not fed and related to the active power load demand located upstream the resynchronization zones. The mathematical problem has been solved in less than 10 s using the commercial solver Gurobi.

5.11.4 Remarks & Future research objectives

This concluding paragraph presented a MILP re-energization optimization problem to ensure energy supply for the end-users following a blackout event. The possibility of exploiting MGs to operate in islanding mode and their ability to self-start providing black start service is addressed. The aim of the proposed method was identifying several islanded sub-networks inside the distribution network using the BSUs to ensure power balancing and the synchro-check presence in every BSA. The necessity to include synchronization organs in each BSA is motivated by the need to assure proper system operation and effective reconnection of the identified BSAs with the main grid. The test results demonstrated that increasing BSUs' capacity lead to an higher amount of active power load demand fed and highlights how the position of MGs in the network can affect the quantity of load demand supplied. However, the resulting BSAs must be such that local network constraints are met. Future developments will include the full grid model representation and the BSUs dispatch criteria. Furthermore, an optimal MGs location algorithm for grid expansion planning purposes could be integrated to assess which MGs would provide the greatest benefit according to their position and capability.

5.12 Final considerations

The research presented in this chapter addressed the Optimal Network Reconfiguration (ONR) problem, focusing on enhancing the operational security, reliability and quality of supply of MV distribution systems. The primary objective was to define an optimization framework capable of identifying optimal topological configurations that minimizes power quality indices under varying operating conditions. This lead to the development of a comprehensive ONR formulation which could embed AC network equations and the actual protections logics, used by DSO for FDIR functions, within a combinatorial reconfiguration problem. Three different formulations were proposed according to the most common FDIR techniques currently adopted by Italian DSOs.

The ONR problem was initially formulated as a Mixed-Integer Linear Programming (MILP) model and subsequently refined into a Mixed-Integer Second-Order Cone Programming (MISOCP) formulation. This progression allowed for a more accurate representation of the physical constraints of the network while maintaining computational tractability. The proposed MISOCP approach was validated through the implementation of the ONR problem on benchmark systems and a realistic-sized primary distribution network. Test results proved the feasibility of the approach, helping also to understand how different FDIR practices affect quality of supply.

The MISOCP model is validated by solving the full MINLP AC ONR problem by leveraging general purpose global optimization algorithms (i.e., GA and metaheuristics). The results demonstrated that, while MISOCP provides global optimality under specific conditions, metaheuristic algorithms provides local optimality with longer calculation times. However, the implementation of a global optimization algorithm has proven to be an effective strategy for navigating the complex, discrete search space typical of ONR.

With respect to other formulations, the proposed one permitted to improve reliability, while clearing at the same time violations of network constraints. This approach allowed to include network-related components in the formulation of the objective function (for example in this case for the minimization of system losses). The proposed approach can be easily adapted to different objectives and constraints, improving the range of its applicability to planning and operation functions. In fact, the adoption of ONR as a suitable tool for DSO capable to enhance system's resilience against adverse weather events is also provided. Simulations indicated that

anticipating the onset of conditions such as heat waves, flooding, and wind gusts through the modification of reliability parameters allows for network reconfiguration that improves expected quality of supply indices.

Computational timings proved scalability and compatibility with real-time operation requirements. This is a relevant result, because the main rationale behind this study is that taking into account FDIR logics in the ONR formulation can facilitate the actual application of these functions at SCADA/DMS level. In this context, it must be emphasized that, in order to preserve FDIR functionalities after reconfiguration, adaptive protection schemes must be deployed. Most FDIR schemes are based on the use of smart fault-passage indicators and IEDs, which already possess robust capability for remote control and retuning of protection settings. Regarding the most modern Italian scheme (i.e., SFS), adaptive protection could theoretically be achieved by re-routing the GOOSE messages exchanged by IEDs, according to the updated upstream/downstream relationships established after reconfiguration. While preliminary tests conducted by the author have successfully proven the feasibility of this approach, detailed implementation and validation will be reserved for future research.

This work lays the foundation for future developments of more advanced tools, which will focus on use of real-time and historical data to track dynamically the grid topology evolution, and allow to further enhance the integration of reconfiguration tools in real-time DSO operations.

Conclusions

The research presented in this doctoral thesis addressed the fundamental challenges of modern power systems, by proposing a series of approaches where operational security and economic efficiency are pursued through the optimal coordination of markets and physical grid assets. By analyzing the transition toward renewable-dominated grids, this work has confirmed the hypothesis that network flexibility must be treated as a cross-voltage-level system property that cannot be separated from the necessary security requirements for the operation continuity. Both are accessible through advanced optimization tools capable of bridging the gap between planning and real-time operation.

The scientific validity and the industrial relevance of the proposed methodologies are supported by extensive numerical simulations performed on both standard benchmark systems and, crucially, on realistic network models. The key findings and contributions that support this thesis can be categorized as follows:

Integrated Market-Security Coordination: the development of a Network-Constrained Unit Commitment and Economic Redispatch (NCUCER) framework highlighted the need for managing the aleatory nature of load and renewable energy sources (RES) considering the sequential interaction between Day-Ahead and Ancillary Service Markets. Load and RES forecast errors can be efficiently compensated while rescheduling generation programs, procuring reserve services and fulfilling network constraints even employing a deterministic approach. Results on the NREL-118 bus system show that a co-optimized approach allows transmission system operators (TSOs) to validate the technical feasibility of market schedules effectively, ensuring system adequacy and security. The thesis proved that integrating unit commitment constraints into redispatch procedures significantly reduces the risk of insufficient reserve procurement, providing a transparent tool to evaluate the *true* economic cost of security requirements.

Unlocking "Cost-Free" Flexibility in Transmission Systems through Network Topology Reconfiguration: a major result of this work is the quantification of the benefits derived from topology control in transmission systems. Network reconfiguration strategies serve as additional cost-free flexibility resources to be integrated within dispatch activities. This led to the exploration of both analytical and metaheuristic optimization techniques to treat complex combinatorial mixed-integer optimization problems, aimed to include discrete control resources in the decision-making activities of system operators.

Effects of topology control on voltage: by integrating line switching operations into Optimal Reactive Power Flow (ORPF) tools, the thesis proved that, under specific grid conditions (e.g., low load scenarios, high RES production, etc.), reducing network mesh may effectively contribute to improve the system voltage profile, in combination with conventional voltage control devices. However, the proposed approach acts as a corrective control to restore the voltage within the security limits. In fact, in the event of voltage violations, the ORPF is able to appropriately vary the position of the transformer tap changers, connect/disconnect shunt compensation devices, and modify the network topology through line switching operations. If they exist, although the optimal solutions found are AC feasible (the ORPF is solved preserving its MINLP formulation), the operating conditions identified can only be maintained temporarily, representing corrective measures that do not necessarily comply with N-1 security requirements. For this reason, innovative strategies to consider N-1 security constraints within the ORPF will need to be further considered without compromising actual real-world applicability in terms of computational resources.

Preventive N-1 Security: By formulating and solving a preventive N-1 Security-Constrained Optimal Transmission Network Reconfiguration (SCOTNR) problem, the thesis demonstrates that topological operations are not merely corrective or temporary emergency measures. When strategically predetermined, they may serve as additional cost-free control resources. In this regard, N-1 security becomes essential, particularly in highly loaded scenarios where providing congestion management services is mandatory to ensure system security. Even in these cases, network reconfiguration can effectively complement (or replace) costly generation dispatch, or reduce the need for load shedding (avoiding penalties for the TSO). The adoption of optimization decomposition techniques, allowed to efficiently manage the computational growth of this kind of problem, whose size increases based on how

many N-1 security constraints (contingency states) are considered. Numerical tests on realistic network models revealed computational difficulties in terms of problem scalability (even in its reduced SCOTLS form), which required the integration of practical screening and contingency filtering algorithms to obtain solutions in times compatible with the requirements of SCADA/EMS systems.

Quality of supply optimization in primary distribution networks: extending the topology optimization to the distribution level, the thesis introduced a novel formulation of Optimal Network Reconfiguration (ONR) that explicitly models the automated logic of Fault Detection, Isolation, and Recovery (FDIR) practices commonly employed in primary distribution systems. Modeling them using linear constraint relationships made it possible to quantify the benefits of topological changes in terms of reliability by calculating and optimizing typical quality of supply indicators monitored by DSOs (i.e., EENS, SAIDI, and SAIFI). Unlike standard academic models which often neglect protection coordination, the proposed formulations (MILP and MISOCP) were tested and validated on a realistic-sized distribution network model considering FDIR logics, proving capable of reconfiguring the network, operating it radially and connected without violating physical constraints.

General characteristics of the ONR model and adverse weather event characterization: the proposed ONR model proved also effective in mitigating the impact of adverse weather events (e.g., heat waves, floodings, wind gusts). A methodology to model them, characterize their duration and effects, and integrate them into a deterministic ONR framework for operation planning purposes was successfully proposed, proving that the grid topology can be proactively adapted to minimize failure risks during such events, thereby validating the method as a crucial tool for climate resilience.

Methodological Soundness and Practical development of optimization software tools: finally, the soundness of the research is enriched and supported by the development of versatile co-simulation frameworks (External Python scripts interfaced with specialized software such as Pandapower, DIgSILENT PowerFactory and OpenDSS). The methodologies used for implementing optimization algorithms, visualizing and interpreting results proved to be general and applicable in all studies conducted. The result is the definition of a structured analysis and simulation procedure that can be easily replicated by both academic users and energy companies. Regardless of the use case and applications, for the correct implementation of all the optimization

routines presented, it is essential to have a consistent network model and to develop specific scripting automation functions for data handling and manipulations, network calculation execution, and result verification. The same methodological flow has also proven effective in managing realistic datasets, characterized by naming, modeling, and calculation conventions typically used by real system operators.

Future developments

The methodologies developed in this thesis lay a solid foundation for the next generation of grid control tools. However, the path toward fully autonomous and self-healing grids presents several opportunities for further research. For this reason, the studies presented in this thesis have laid the groundwork for further developments. The potential directions for future research are listed as follows:

- *AC-Feasibility in Preventive Optimization*: while the DC approximations used in the preventive N-1 SCOTNR model were necessary for computational tractability, as well as simplifying the topological relationships between the various connected network elements, future work must focus on integrating full AC feasibility constraints directly into the preventive N-1 analysis. As grids become more loaded and dominated by inverter-based resources, voltage stability and reactive power flows become binding constraints.

- *Computational Scalability for Real-Time Applications*: although decomposition techniques (C&CG, Benders) have significantly improved solving times, the application of these tools in a real-time SCADA/EMS environment to a national-scale grid still remains a challenge and requires further acceleration. Future research should explore parallel computing architectures and advanced heuristics to handle the combinatorial complexity of national-scale networks within minutes. High-performance computing techniques may consist in a massive parallelization of the N-1 contingency analysis.

- *TSO-DSO Coordination Mechanisms*: this thesis addressed transmission and distribution largely as separate optimization domains. However, with the rise of distributed generation and flexibility markets, TSO and DSO actions are increasingly coupled. A logical development is the creation of a coordinated

TSO-DSO reconfiguration framework. For instance, optimizing the distribution topology (ONR) to provide reactive power support or load relief to the transmission node, or coordinating black-start operations where Black Start Units (BSUs) actively support transmission restoration.

- *Transition to Online Distribution Management & Adaptive Control*: the methodologies presented are primarily suitable for operational planning (offline or day-ahead). To fully realize the "Smart Grid" paradigm, these algorithms must evolve into Online Closed-Loop Control applications. This involves processing real-time telemetry data (PMUs, Smart Meters) to trigger reconfiguration dynamically. Future work could investigate Robust Optimization or Stochastic Programming approaches that explicitly account for real-time uncertainty in RES generation, ensuring that the computed topology remains valid even if generation fluctuates rapidly within the hour.

References

[1] R. Cometa, A. Velini, M. R. Nasab, S. Bruno, and M. La Scala, "Optimal Transmission Grid Assets Maneuvering for Improving Voltage Profile in RES Scenarios," in *2024 IEEE International Humanitarian Technologies Conference (IHTC)*, 2024, pp. 1–7.

[2] R. Cometa, F. Lorusso, M. Menga, A. Velini, R. Musca, S. Bruno, and M. La Scala, "Preventive N-1 Security-Constrained Optimal Transmission Network Reconfiguration," in *2026 IEEE Power & Energy Society General Meeting (PESGM)*, 2026 (to be appeared).

[3] R. Cometa, A. Velini, M. R. Nasab, F. Lorusso, M. La Scala, and S. Bruno, "A MISOCP Formulation for Distribution Optimal Network Reconfiguration Considering Fault Detection Isolation & Recovery Practices," *IEEE Transactions on Industry Applications*, 2026 (under review).

[4] R. Cometa, M. R. Nasab, F. Lorusso, A. Velini, M. La Scala, and S. Bruno, "Integration of FDIR Practices in Distribution Optimal Network Reconfiguration Routines," in *2024 IEEE International Conference on Environment and Electrical Engineering and 2024 IEEE Industrial and Commercial Power Systems Europe (EEEIC / I&CPS Europe)*, 2024, pp. 1–6.

[5] R. Cometa, A. Velini, F. Lorusso, A. Ricca, R. Sbrizzai, and S. Bruno, "An Open-Source Optimal Network Reconfiguration Tool for Improving Distribution Grid Reliability," in *2024 AEIT International Annual Conference (AEIT)*, 2024, pp. 1–6.

[6] R. Cometa, A. Velini, M. La Scala, R. Musca, M. Minetti, A. Bonfiglio, and S. Bruno, "Employing MISOCP Relaxations to Solve Distribution Optimal Network Reconfiguration," in *2025 IEEE Power & Energy Society General Meeting (PESGM)*, 2025, pp. 1–5.

[7] A. Velini, R. Cometa, F. Lorusso, M. La Scala, and S. Bruno, "Mitigating the Impact of Adverse Weather Events Via MISOCP-Optimal Network Reconfiguration," *IEEE Transactions on Industry Applications*, 2026 (under review).

[8] F. Lorusso, A. Velini, R. Cometa, M. Marco, S. Bruno, and M. La Scala, "Primary distribution network re-energization through multiple black start units," in *2025 IEEE International Conference on Environment and Electrical Engineering and 2025 IEEE Industrial and Commercial Power Systems Europe (EEEIC / I&CPS Europe)*, 2025, pp. 1–6.

[9] M. R. Nasab, R. Cometa, S. Bruno, G. Giannoccaro, and M. La Scala, "Power Systems Simulation and Analysis: A Review on Current Applications and Future Trends in DRTS of Grid-Connected Technologies," *IEEE Access*, vol. 12, pp. 121 320–121 345, 2024.

[10] R. Cometa, G. Tricarico, M. Dicorato, and G. Forte, "A Two-Stage Energy and Service Market Framework Involving Unit Commitment and Network-based Redispatch," *Energies*, 2026 (under review).

[11] M. R. Nasab, P. Ghalebani, S. Bruno, R. Cometa, and M. La Scala, "Adaptive PI Control of PMSM for Electric Vehicle Application Based on Sliding-mode Extremum Seeking Algorithm," in *2023 Asia Meeting on Environment and Electrical Engineering (EEE-AM)*, 2023, pp. 1–6.

[12] S. Bruno, R. Cometa, M. G. Ippolito, M. La Scala, G. C. Miglionico, R. Musca, and E. R. Sanseverino, "Power Oscillations Damping Control using BESS with Real-Time PHIL Co-Simulation Validation," in *2024 IEEE Power & Energy Society General Meeting (PESGM)*, 2024, pp. 1–5.

[13] M. R. Nasab, R. Cometa, S. Bruno, and M. La Scala, "Adaptive Scheme for Stability Margin Estimation of Grid-Connected DFIG Based Wind Turbines," in *2024 IEEE International Conference on Environment and Electrical Engineering and 2024 IEEE Industrial and Commercial Power Systems Europe (EEEIC / I&CPS Europe)*, 2024, pp. 1–6.

[14] M. R. Nasab, R. Cometa, P. Ghalebani, S. Bruno, and M. La Scala, "Distributed Adaptive Droop Control Method for Flexibility Enhancement of Islanded DC Microgrids Including Electric Springs," in *2024 Energy Conversion Congress & Expo Europe (ECCE Europe)*, 2024, pp. 1–6.

[15] A. Velini, R. Cometa, F. Lorusso, M. La Scala, and S. Bruno, "Optimal Network Reconfiguration for Mitigating the Impact of Adverse Weather Events on Distribution Networks," in *2024 IEEE International Humanitarian Technologies Conference (IHTC)*, 2024, pp. 1–7.

[16] M. R. Nasab, R. Cometa, C. Iurlaro, M. M. Islam, S. Bruno, and M. La Scala, "Stand-alone DC Microgrids for Rural Areas: A Decentralized Energy Management and Voltage Regulation Approach," in *2024 IEEE International Humanitarian Technologies Conference (IHTC)*, 2024, pp. 1–7.

[17] M. Menga, R. Cometa, G. Cassettino, C. Iurlaro, S. Bruno, and M. La Scala, "Impact of reactive power dispatch in a recursive two-stage optimal control algorithm for isolated electrical networks," in *2025 IEEE International Conference on Environment and Electrical Engineering and 2025 IEEE Industrial and Commercial Power Systems Europe (EEEIC / I&CPS Europe)*, 2025, pp. 1–6.

[18] A. Bonfiglio, S. Bruno, R. Cometa, M. Minetti, R. Musca, and A. Vasile, "Adaptive feedforward grid-forming controls to preserve inertial capabilities in power systems," in *2025 IEEE PES Innovative Smart Grid Technologies Conference Europe (ISGT Europe)*, 2025, pp. 1–5.

[19] Terna SpA, Grid Code annex A10, "Piano di Rialimentazione e Riaccensione del sistema elettrico nazionale," https://www.terna.it/it/sistema-elettrico/codici-rete/codice-rete-italiano, 2020, (Italian Only).

[20] Terna S.p.A., *Italian Grid Code: Code for Transmission, Dispatching, Development and Security of the Grid*, Terna S.p.A., approved by the Authority with resolutions no. 79/05 and 49/06. Latest version available at https://www.terna.it/en/electric-system/grid-codes/italian-grid-code.

[21] ARERA - Autorità di Regolazione per Energia Reti e Ambiente, "Delibera 345/2023/r/eel: Approvazione del testo integrato del dispacciamento elettrico (tide)," https://www.arera.it/it/, 2026.

[22] T. Wolgast, S. Ferenz, and A. Nieße, "Reactive power markets: A review," *IEEE Access*, vol. 10, pp. 28 397–28 410, 2022.

[23] A. Vicenzutti, F. Marzolla, M. Chiandone, S. Tessitore, C. Pisani, G. M. Giannuzzi, and G. Sulligoi, "Mimo control architectures for secondary voltage regulation in electrically coupled transmission grids: Design and dynamic performance," *IEEE Access*, vol. 13, pp. 18 005–18 023, 2025.

[24] K. Poplavskaya, M. Joos, V. Krakowski, K. Knorr, and L. De Vries, "Redispatch and balancing: Same but different. links, conflicts and solutions," in *2020 17th Int. Conf. on the European Energy Market (EEM)*. IEEE, 2020, pp. 1–6.

[25] ENTSO-E. Cross border electricity balancing pilot projects. [Online]. Available: https://docstore.entsoe.eu/major-projects/network-code-implementation/cross-border-electricity-balancing-pilot-projects/Pages/default.aspx

[26] All NEMO Committee. Single Day-ahead Coupling (SDAC). [Online]. Available: https://www.nemo-committee.eu/sdac

[27] ——. Single Intraday Coupling (SIDC). [Online]. Available: https://www.nemo-committee.eu/sidc

[28] ENTSO-E. Electricity balancing. [Online]. Available: https://www.entsoe.eu/network_codes/eb/

[29] R. Domínguez, G. Oggioni, and Y. Smeers, "Reserve procurement and flexibility services in power systems with high renewable capacity: Effects of integration on different market designs," *International Journal of Electrical Power & Energy Systems*, vol. 113, pp. 1014–1034, 2019.

[30] Gestore Mercati Energetici, GME. Spot market mpe. [Online]. Available: https://www.mercatoelettrico.org/en-us/Home/Markets/ElectricityMarket/Spot-Market-MPE#MGP

[31] F. Lisi, L. Grossi, and F. Quaglia, "Evaluation of cost-at-risk related to the procurement of resources in the ancillary services market. the case of the italian electricity market," *Energy economics*, vol. 121, p. 106625, 2023.

[32] N. Yang, Z. Dong, L. Wu, L. Zhang, X. Shen, D. Chen, B. Zhu, and Y. Liu, "A comprehensive review of security-constrained unit commitment," *Journal of Modern Power Systems and Clean Energy*, vol. 10, no. 3, pp. 562–576, 2022.

[33] S. Tsegaye, F. Shewarega, and G. Bekele, "A review on security constrained economic dispatch of integrated renewable energy systems," *EAI Endorsed Transactions on Energy Web*, vol. 8, no. 32, p. e13, Sep. 2020.

[34] Z. Yu, H. Zhong, G. Ruan, and X. Yan, "Network-constrained unit commitment with flexible temporal resolution," *IEEE Transactions on Power Systems*, vol. 40, no. 1, pp. 73–84, 2025.

[35] D. Mende, D. S. Stock, T. Hennig, L. Löwer, and L. Hofmann, "Multiobjective optimization in congestion management considering technical and economic aspects," in *2016 IEEE PES Asia-Pacific Power and Energy Engineering Conference (APPEEC)*. IEEE, 2016, pp. 1061–1066.

[36] A. Pitto, D. Cirio, and E. Ciapessoni, "Probabilistic security-constrained preventive redispatching in presence of correlated uncertainties," in *2020 AEIT International Annual Conference (AEIT)*. IEEE, 2020, pp. 1–6.

[37] M. Fan and L. Huang, "Generator redispatch control strategy with big data for power systems with renewable energy," in *2019 IEEE Power & Energy Society General Meeting (PESGM)*. IEEE, 2019, pp. 1–5.

[38] C. Klabunde and M. Wolter, "Mixed integer linear programming time-series based redispatch optimization," in *2020 IEEE PES ISGT-Europe Conf.* IEEE, 2020, pp. 504–508.

[39] J. M. Morales, A. J. Conejo, and J. Pérez-Ruiz, "Economic valuation of reserves in power systems with high penetration of wind power," *IEEE Transactions on Power Systems*, vol. 24, no. 2, pp. 900–910, 2009.

[40] M. S. Silva Pinto and O. R. Saavedra, "Power reserve dispatch to mitigate variability of generation output due to wind ramps," in *2020 IEEE PES Transmission & Distribution Conference and Exhibition-Latin America (T&D LA)*. IEEE, 2020, pp. 1–6.

[41] M. Abdelmalak and M. Benidris, "Proactive generation redispatch to enhance power system resilience during hurricanes considering unavailability of renewable energy sources," *IEEE Transactions on Industry Applications*, vol. 58, no. 3, pp. 3044–3053, 2022.

[42] U. Münz and A. Mesanovic, "Optimal redispatch and primary reserve allocation for power systems with uncertain load and generation," in *2016 European Control Conf. (ECC)*. IEEE, 2016, pp. 1806–1811.

[43] J. García-González, A. M. San Roque, F. A. Campos, and J. Villar, "Connecting the intraday energy and reserve markets by an optimal redispatch," *IEEE Transactions on Power Systems*, vol. 22, no. 4, pp. 2220–2231, 2007.

[44] E. De Tuglie, M. Dicorato, M. La Scala, and P. Scarpellini, "Dynamic security preventive control in a deregulated electricity market," in *Proc. of PSCC 1999 Trondheim*, 1999, pp. 125–131.

[45] H. Goudarzi, M. Rayati, A. Sheikhi, and A. M. Ranjbar, "A clearing mechanism for joint energy and ancillary services in non-convex markets considering high penetration of renewable energy sources," *International Journal of Electrical Power & Energy Systems*, vol. 129, p. 106817, 2021.

[46] J. Aguilar, C. Bordons, and A. Arce, "Chance constraints and machine learning integration for uncertainty management in virtual power plants operating in simultaneous energy markets," *International Journal of Electrical Power & Energy Systems*, vol. 133, p. 107304, 2021.

[47] S. S. Reddy, P. Bijwe, and A. Abhyankar, "Optimum day-ahead clearing of energy and reserve markets with wind power generation using anticipated real-time adjustment costs," *International Journal of Electrical Power & Energy Systems*, vol. 71, pp. 242–253, 2015.

[48] X. Liu and A. J. Conejo, "Day-ahead reserve determination in power systems with high renewable penetration," *International Journal of Electrical Power & Energy Systems*, vol. 156, p. 109703, 2024.

[49] F. Charbonnier, T. Morstyn, and M. D. McCulloch, "Coordination of resources at the edge of the electricity grid: Systematic review and taxonomy," *Applied Energy*, vol. 318, p. 119188, 2022.

[50] D. Shah and S. Chatterjee, "A comprehensive review on day-ahead electricity market and important features of world's major electric power exchanges," *International Transactions on Electrical Energy Systems*, vol. 30, no. 7, p. e12360, 2020.

[51] G. Tricarico, R. Wagle, M. Dicorato, G. Forte, F. Gonzalez-Longatt, and J. L. Rueda, "Zonal day-ahead energy market: A modified version of the ieee 39-bus test system," in *2022 IEEE PES ISGT Asia*. IEEE, 2022, pp. 86–90.

[52] Gestore Mercati Energetici (GME). Spot electricity markets. [Online]. Available: https://www.mercatoelettrico.org/en/Mercati/MercatoElettrico/MPE.aspx

[53] B. Stott, "Review of load-flow calculation methods," *Proceedings of the IEEE*, vol. 62, no. 7, pp. 916–929, 1974.

[54] H. Ronellenfitsch, M. Timme, and D. Witthaut, "A dual method for computing power transfer distribution factors," *IEEE Transactions on Power Systems*, vol. 32, no. 2, pp. 1007–1015, 2017.

[55] A. Gómez Expósito, J. L. M. Ramos, and J. R. Santos, "Slack bus selection to minimize the system power imbalance in load-flow studies," *IEEE Transactions on Power Systems*, vol. 19, no. 2, pp. 987–995, 2004.

[56] I. Peña, C. Brancucci Martínez-Anido, and B.-M. Hodge, "An extended ieee 118-bus test system with high renewable penetration," *IEEE Transactions on Power Systems*, vol. 33, no. 1, pp. 281–289, 2017.

[57] An Extended IEEE 118-Bus Test System With High Renewable Penetration. [Online]. Available: https://item.bettergrids.org/handle/1001/120

[58] M. Dicorato, G. Tricarico, G. Forte, and F. Marasciuolo, "Technical indicators for the comparison of power network development in scenario evaluations," *Energies*, vol. 14, no. 14, p. 4179, 2021.

[59] D. Comanescu, G. Grigoras, G. Cartina, and F. Rotaru, "Determination of typical load profiles in hydro-power plant by clustering techniques," in *2010 12th International Conference on Optimization of Electrical and Electronic Equipment*, 2010, pp. 1294–1297.

[60] W. E. Hart, C. D. Laird, J.-P. Watson, D. L. Woodruff, G. A. Hackebeil, B. L. Nicholson, J. D. Siirola *et al.*, *Pyomo-optimization modeling in python*. Springer, 2017, vol. 67.

[61] Gurobi Optimization. (2025) Gurobi optimization. Accessed: June 2025. [Online]. Available: https://www.gurobi.com

[62] G. Tricarico, M. Dicorato, G. Forte, and F. Gonzalez-Longatt, "Contributions to tertiary reserve requirements under operating conditions and uncertainties," in *2022 18th International Conference on the European Energy Market (EEM)*. IEEE, 2022, pp. 1–6.

[63] A. Ellis, R. Nelson, E. Von Engeln, R. Walling, J. MacDowell, L. Casey, E. Seymour, W. Peter, C. Barker, B. Kirby, and J. R. Williams, "Reactive power performance requirements for wind and solar plants," in *2012 IEEE Power and Energy Society General Meeting*, 2012, pp. 1–8.

[64] Terna SpA, Grid Code annex A10, "Partecipazione alla regolazione di tensione," https://www.terna.it/it/sistema-elettrico/codici-rete/codice-rete-italiano, 2000, (Italian Only) (accessed on August, 2023).

[65] Terna SpA, Grid Code annex A17, "Centrali eoliche: Condizioni generali di connessione alle reti at, sistemi di protezione regolazione e controllo," https://www.terna.it/it/sistema-elettrico/codici-rete/codice-rete-italiano, 2023, (Italian Only) (accessed on August, 2023).

[66] Terna SpA, Grid Code annex A68, "Centrali fotovoltaiche: Condizioni generali di connessione alle reti at, sistemi di protezione regolazione e controllo," https://www.terna.it/it/sistema-elettrico/codici-rete/codice-rete-italiano, 2023, (Italian Only) (accessed on August, 2023).

[67] G. Tricarico, R. Wagle, J. C. Martinez, F. Gonzalez-Longatt, M. Dicorato, G. Forte, and J. L. Rueda, "A co-simulation procedure for optimal reactive power control in active distribution networks," in *2023 IEEE International Conference on Environment and Electrical Engineering and 2023 IEEE Industrial and Commercial Power Systems Europe (EEEIC / ICPS Europe)*, 2023, pp. 1–6.

[68] Terna SpA, Grid Code annex A9, "Piano di difesa del sistema elettrico," https://www.terna.it/it/sistema-elettrico/codici-rete/codice-rete-italiano, 2023, (Italian Only) (accessed on August, 2023).

[69] C. Bingane, M. F. Anjos, and S. Le Digabel, "Tight-and-cheap conic relaxation for the optimal reactive power dispatch problem," *IEEE Transactions on Power Systems*, vol. 34, no. 6, pp. 4684–4693, 2019.

[70] Z. Yang, A. Bose, H. Zhong, N. Zhang, Q. Xia, and C. Kang, "Optimal reactive power dispatch with accurately modeled discrete control devices: A successive linear approximation approach," *IEEE Transactions on Power Systems*, vol. 32, no. 3, pp. 2435–2444, 2017.

[71] X. Geng, L. Xie, and D. Obadina, "Chance constrained optimal reactive power dispatch," in *2018 IEEE Power Energy Society General Meeting (PESGM)*, 2018, pp. 1–5.

[72] S. E. Kayacık and B. Kocuk, "An misocp-based solution approach to the reactive optimal power flow problem," *IEEE Transactions on Power Systems*, vol. 36, no. 1, pp. 529–532, 2021.

[73] M. M. Sánchez-Mora, D. L. Bernal-Romero, O. D. Montoya, W. M. Villa-Acevedo, and J. M. López-Lezama, "Solving the optimal reactive power dispatch problem through a python-digsilent interface," *Computation*, vol. 10, no. 8, p. 128, 2022.

[74] C. H. Liang, C. Y. Chung, K. P. Wong, and X. Z. Duan, "Parallel optimal reactive power flow based on cooperative co-evolutionary differential evolution and power system decomposition," *IEEE Transactions on Power Systems*, vol. 22, no. 1, pp. 249–257, 2007.

[75] Z. Sahli, A. Hamouda, A. Bekrar, and D. Trentesaux, "Reactive power dispatch optimization with voltage profile improvement using an efficient hybrid algorithm," *Energies*, vol. 11, no. 8, p. 2134, 2018.

[76] M. S. Saddique, A. R. Bhatti, S. S. Haroon, M. K. Sattar, S. Amin, I. A. Sajjad, S. S. ul Haq, A. B. Awan, and N. Rasheed, "Solution to optimal reactive power dispatch in transmission system using meta-heuristic techniques—status and technological review," *Electric power systems research*, vol. 178, p. 106031, 2020.

[77] S. Bruno, M. Di Lullo, G. Felici, F. Lacalandra, and M. La Scala, "Tight unit commitment models with optimal transmission switching: Connecting the dots with perturbed objective function," in *2014 Complexity in Engineering (COMPENG)*, 2014, pp. 1–8.

[78] Ministero dell'Ambiente e della Sicurezza Energetica, "Piano nazionale integrato per l'energia e il clima," https://www.mase.gov.it/comunicati/clima-energia-litalia-ha-inviato-il-pniec-bruxelles, July, 2024.

[79] Terna SpA, Grid Code chapter 4, "Regole per il dispacciamento," https://www.terna.it/it/sistema-elettrico/codici-rete/codice-rete-italiano, 2004, (Italian Only) (accessed on August, 2023).

[80] M. Mahdavi, H. H. Alhelou, P. Gopi, and N. Hosseinzadeh, "Importance of radiality constraints formulation in reconfiguration problems," *IEEE Systems Journal*, vol. 17, no. 4, pp. 6710–6723, 2023.

[81] S. Hayat, S. Khan, A. Khan, and M. Imran, "A computer-based method to determine predictive potential of distance-spectral descriptors for measuring the -electronic energy of benzenoid hydrocarbons with applications," *IEEE Access*, vol. 9, pp. 19 238–19 253, 2021.

[82] R. Li, Z. Liu, Y. Zeng, and J. Ma, "Representing the topology of complex networks based on graph embedding," in *2022 International Conference on Networking and Network Applications (NaNA)*, 2022, pp. 1–7.

[83] S. Sharif and J. Taylor, "Real-time implementation of optimal reactive power flow," in *Proceedings of the 1999 American Control Conference (Cat. No. 99CH36251)*, vol. 6, 1999, pp. 4203–4207 vol.6.

[84] Z. Michalewicz, *"Genetic algorithms + Data Structures = Evolution Programs"*. Springer Science & Business Media, 2013.

[85] K. Deb, K. Sindhya, and T. Okabe, "Self-adaptive simulated binary crossover for real-parameter optimization," in *Proceedings of the 9th Annual Conference on Genetic and Evolutionary Computation*, ser. GECCO '07. New York, NY, USA: Association for Computing Machinery, 2007, p. 1187–1194. [Online]. Available: https://doi.org/10.1145/1276958.1277190

[86] J. Blank and K. Deb, "Pymoo: Multi-objective optimization in python," *IEEE Access*, vol. 8, pp. 89 497–89 509, 2020.

[87] R. Christie, University of Washington, "IEEE 118-Bus System Case," 1993.

[88] C. Lyu, "A modified IEEE 118-Bus System with time series data," 2023. [Online]. Available: https://dx.doi.org/10.21227/dafq-e974

[89] A. A. Anderson, S. Kincic, B. A. Jefferson, B. J. Mcgary, C. K. Fallon, D. K. Ciesielski, J. E. Wenskovitch, and Y. Chen, "A Real-Time Operations Manual for the IEEE 118 Bus Transmission Model," Pacific Northwest National Lab.(PNNL), Richland, WA (United States), Tech. Rep., 2022.

[90] L. Thurner, A. Scheidler, F. Schäfer, J.-H. Menke, J. Dollichon, F. Meier, S. Meinecke, and M. Braun, "pandapower—an open-source python tool for convenient modeling, analysis, and optimization of electric power systems," *IEEE Transactions on Power Systems*, vol. 33, no. 6, pp. 6510–6521, 2018.

[91] "NetworkX Documentation," accessed: 2024-07-15. [Online]. Available: https://networkx.org/documentation/stable/index.html

[92] E. B. Fisher, R. P. O'Neill, and M. C. Ferris, "Optimal transmission switching," *IEEE Transactions on Power Systems*, vol. 23, no. 3, pp. 1346–1355, 2008.

[93] M. Flores, L. H. Macedo, and R. Romero, "Alternative mathematical models for the optimal transmission switching problem," *IEEE Systems Journal*, vol. 15, no. 1, pp. 1245–1255, 2021.

[94] A. Hinneck and D. Pozo, "Optimal transmission switching: Improving solver performance using heuristics," *IEEE Transactions on Power Systems*, vol. 38, no. 4, pp. 3317–3330, 2023.

[95] M. Aguilar-Moreno, S. Pineda, and J. M. Morales, "A graph-based iterative strategy for solving the all-line transmission switching problem," *arXiv preprint arXiv:2502.10333*, 2025.

[96] M. Heidarifar and H. Ghasemi, "A network topology optimization model based on substation and node-breaker modeling," *IEEE Transactions on Power Systems*, vol. 31, no. 1, pp. 247–255, 2016.

[97] B. Morsy, A. Hinneck, D. Pozo, and J. Bialek, "Security constrained OPF utilizing substation reconfiguration and busbar splitting," *Electric Power Systems Research*, vol. 212, p. 108507, 2022.

[98] M. Heidarifar, M. Doostizadeh, and H. Ghasemi, "Optimal transmission reconfiguration through line switching and bus splitting," in *2014 IEEE PES General Meeting | Conference Exposition*, 2014, pp. 1–5.

[99] A. Khodaei and M. Shahidehpour, "Transmission switching in security-constrained unit commitment," *IEEE Transactions on Power Systems*, vol. 25, no. 4, pp. 1937–1945, 2010.

[100] T. Han, D. J. Hill, and Y. Song, "Formulating connectedness in security-constrained optimal transmission switching problems," *IEEE Transactions on Power Systems*, vol. 37, no. 5, pp. 4137–4140, 2022.

[101] B. Kocuk, S. S. Dey, and X. A. Sun, "New Formulation and Strong MISOCP Relaxations for AC Optimal Transmission Switching Problem," *IEEE Transactions on Power Systems*, vol. 32, no. 6, pp. 4161–4170, 2017.

[102] A. Tiwari, A. Mohapatra, and S. R. Sahoo, "Robust topology control of ac power networks with injection uncertainties," *IEEE Transactions on Power Systems*, pp. 1–14, 2025.

[103] R. A. Jabr, "Outer approximation method for discrete ac optimal power flow," *IEEE Transactions on Power Systems*, vol. 40, no. 2, pp. 1943–1954, 2025.

[104] M. Heidarifar, P. Andrianesis, P. Ruiz, M. C. Caramanis, and I. C. Paschalidis, "An optimal transmission line switching and bus splitting heuristic incorporating ac and n-1 contingency constraints," *International Journal of Electrical Power & Energy Systems*, vol. 133, p. 107278, 2021.

[105] Y. Sun, Z. Tian, W. Wu, Y. Du, B. Wang, and Y. Xi, "Iterative relaxation solution for ac optimal transmission network reconfiguration considering bus splitting," *IET Generation, Transmission & Distribution*, vol. 15, no. 22, pp. 3204–3214, 2021.

[106] S. Meinecke, D. Sarajlić, S. R. Drauz, A. Klettke, L.-P. Lauven, C. Rehtanz, A. Moser, and M. Braun, "SimBench—A Benchmark Dataset of Electric Power Systems to Compare Innovative Solutions Based on Power Flow Analysis," *Energies*, vol. 13, no. 12, 2020. [Online]. Available: https://www.mdpi.com/1996-1073/13/12/3290

[107] S. Fattahi, J. Lavaei, and A. Atamtürk, "A bound strengthening method for optimal transmission switching in power systems," *IEEE Transactions on Power Systems*, vol. 34, no. 1, pp. 280–291, 2019.

[108] F. Capitanescu, M. Glavic, D. Ernst, and L. Wehenkel, "Contingency filtering techniques for preventive security-constrained optimal power flow," *IEEE Trans. on Power Systems*, vol. 22, no. 4, pp. 1690–1697, 2007.

[109] S. Pineda, J. M. Morales, A. Porras, and C. Dominguez, "Tight big-ms for optimal transmission switching," *Electric Power Systems Research*, vol. 234, p. 110620, 2024.

[110] Terna S.p.A., "Glossario – media / glossario dei termini," https://www.terna.it/it/media/glossario, 2026, accessed: 2026-02-04; Glossario di termini dell'energia elettrica e della trasmissione.

[111] Gestore dei Mercati Energetici S.p.A. (GME), "Mgp – informazioni preliminari – limiti di transito," https://gme.mercatoelettrico.org/it-it/Home/Esiti/Elettricita/MGP/InformazioniPreliminari/LimitiDiTransito, 2026, accessed: 2026-02-04.

[112] F. K. Ariyo *et al.*, "Electrical network reduction for load flow and short-circuit calculations using powerfactory software," *American Journal of Electrical Power and Energy Systems*, vol. 2, no. 1, pp. 1–6, 2013.

[113] R. Benato, G. Gardan, L. Rusalen, G. M. Giannuzzi, C. Pisani, and R. Zaottini, "An admittance matrix algorithm solving the power flow solution of the italian transmission network," in *2021 AEIT International Annual Conference (AEIT)*, 2021, pp. 1–6.

[114] F. Gonzalez-Longatt and J. L. R. Torres, *Advanced smart grid functionalities based on powerfactory*. Springer, 2018.

[115] ENTSO-E, "Methodology for coordinating operational security analysis," European Network of Transmission System Operators for Electricity (ENTSO-E), All TSOs' proposal for a methodology for coordinating operational security analysis 4.a.180710, July 10 2018. [Online]. Available: https://eepublicdownloads.entsoe.eu/clean-documents/Network%20codes%20documents/Implementation/sys/4.a.180710_Methodology_for_coordinating_operational_security_analysis.pdf

[116] J. Fan and S. Borlase, "The evolution of distribution," *IEEE Power and Energy Magazine*, vol. 7, no. 2, pp. 63–68, 2009.

[117] M. S. Thomas and J. D. McDonald, *Power system SCADA and smart grids*, 2017.

[118] S. Lei, C. Chen, Y. Song, and Y. Hou, "Radiality constraints for resilient reconfiguration of distribution systems: Formulation and application to microgrid formation," *IEEE Transactions on Smart Grid*, vol. 11, no. 5, pp. 3944–3956, 2020.

[119] A. Ajaja and F. D. Galiana, "Optimal reconfiguration of distribution networks using milp and supporting hyperplanes (hyper)," in *2013 IEEE Power & Energy Society General Meeting*. IEEE, 2013, pp. 1–5.

[120] N. C. Koutsoukis, D. O. Siagkas, P. S. Georgilakis, and N. D. Hatziargyriou, "Online reconfiguration of active distribution networks for maximum integration of distributed generation," *IEEE Trans. Autom. Sci. Eng.*, vol. 14, no. 2, pp. 437–448, 2016.

[121] L. A. Gallego, J. M. López-Lezama, and O. G. Carmona, "A mixed-integer linear programming model for simultaneous optimal reconfiguration and optimal placement of capacitor banks in distribution networks," *IEEE Access*, vol. 10, pp. 52 655–52 673, 2022.

[122] B. Khorshid-Ghazani, H. Seyedi, B. Mohammadi-ivatloo, K. Zare, and S. Shargh, "Reconfiguration of distribution networks considering coordination of the protective devices," *IET Generation, Transmission & Distribution*, vol. 11, no. 1, pp. 82–92, 2017.

[123] E. Ramos, A. Exposito, J. Santos, and F. Iborra, "Path-based distribution network modeling: application to reconfiguration for loss reduction," *IEEE Transactions on Power Systems*, vol. 20, no. 2, pp. 556–564, 2005.

[124] P. A. Karafotis, I. K. Bazionis, and P. S. Georgilakis, "Optimal distribution network reconfiguration for reliability improvement in presence of DG," in *MEDPOWER 2020*, vol. 2020, 2020, pp. 354–360.

[125] P. A. Karafotis, V. A. Evangelopoulos, and P. S. Georgilakis, "Reliability-oriented reconfiguration of power distribution systems considering load and res production scenarios," *IEEE Transactions on Power Delivery*, vol. 37, no. 6, pp. 4668–4678, 2022.

[126] M. Mahdavi, H. H. Alhelou, P. Gopi, and N. Hosseinzadeh, "Importance of radiality constraints formulation in reconfiguration problems," *IEEE Systems Journal*, 2023.

[127] H. Hijazi and S. Thiébaux, "Optimal distribution systems reconfiguration for radial and meshed grids," *International Journal of Electrical Power & Energy Systems*, vol. 72, pp. 136–143, 2015.

[128] R. A. Jabr, R. Singh, and B. C. Pal, "Minimum loss network reconfiguration using mixed-integer convex programming," *IEEE Trans. on Power systems*, vol. 27, no. 2, pp. 1106–1115, 2012.

[129] J. C. López, M. Lavorato, and M. J. Rider, "Optimal reconfiguration of electrical distribution systems considering reliability indices improvement," *International Journal of Electrical Power & Energy Systems*, vol. 78, pp. 837–845, 2016.

[130] R. Cometa, A. Velini, F. Lorusso, A. Ricca, R. Sbrizzai, and S. Bruno, "An open-source optimal network reconfiguration tool for improving distribution grid reliability," in *2024 AEIT International Annual Conference (AEIT)*, 2024, pp. 1–6.

[131] A. M. Helmi, R. Carli, M. Dotoli, and H. S. Ramadan, "Efficient and sustainable reconfiguration of distribution networks via metaheuristic optimization," *IEEE Trans. Autom. Sci. Eng.*, vol. 19, no. 1, pp. 82–98, 2021.

[132] S. Bruno, S. Lamonaca, M. La Scala, and U. Stecchi, "Integration of optimal reconfiguration tools in advanced distribution management system," in *2012 3rd IEEE PES Innovative Smart Grid Technologies Europe (ISGT Europe)*, 2012, pp. 1–8.

[133] S. Bruno and M. La Scala, "A MINLP Approach for Network Reconfiguration and Dispatch in Distribution Systems," *Computational Intelligence Applications In Smart Grids: Enabling Methodologies For Proactive And Self-organizing Power Systems*, p. 51, 2014.

[134] N. N. Mansor and V. Levi, "Operational planning of distribution networks based on utility planning concepts," *IEEE Transactions on Power Systems*, vol. 34, no. 3, pp. 2114–2127, 2019.

[135] A. Tiwari, A. Mohapatra, and S. R. Sahoo, "Tightening SOCP relaxation of AC Optimal Power Flow with Linearized Arc-tangent Constraints," in *2023 IEEE PESGM*, 2023, pp. 1–5.

[136] J. A. Taylor and F. S. Hover, "Convex models of distribution system reconfiguration," *IEEE Transactions on Power Systems*, vol. 27, no. 3, pp. 1407–1413, 2012.

[137] S. Wang, F. Luo, C. Wang, Y. Lyu, R. Mu, J. Fo, and L. Ge, "Collaborative configuration optimization of soft open points and hydrogen-based distributed multi-energy stations considering spatiotemporal coordination and complementarity," *Journal of Modern Power Systems and Clean Energy*, 2025.

[138] S. Wang, F. Luo, J. Fo, Y. Lv, and C. Wang, "Two-stage spatiotemporal decoupling configuration of sop and multi-level electric-hydrogen hybrid energy storage based on feature

extraction for distribution networks with ultra-high dg penetration," *Applied Energy*, vol. 398, p. 126438, 2025.

[139] A. Cerretti, G. Scrosati, and L. Consiglio, "Upgrade of ENEL MV network automation to improve performances in presence of faults and to deal DG," in *CIRED 2011*, 2011, pp. 6–9.

[140] H. Bentarzi, A. Ouadi, and A. Abdelmoumene, "A new framework of smart auto-recloser," in *2018 IEEE 12th International Conference on Compatibility, Power Electronics and Power Engineering (CPE-POWERENG 2018)*, 2018, pp. 1–5.

[141] M. A. F. Boaski, C. dos Santos, M. Sperandio, D. P. Bernardon, M. J. Ramos, and D. S. Porto, "Coordination and selectivity of protection devices with reliability assessment in distribution systems," *System Reliability*, 2017.

[142] C. D'adamo, G. Valtorta, L. Consiglio, A. Cerretti, L. D'orazio, A. Malerba, and F. Marmeggi, "Smart fault selection: new operational criteria and challenges for the large-scale deployment in e-distribuzione's network," *CIRED-Open Access Proceedings Journal*, vol. 2017, no. 1, pp. 1475–1478, 2017.

[143] R. Cometa, A. Velini, F. Lorusso, A. Ricca, R. Sbrizzai, and S. Bruno, "An open-source optimal network reconfiguration tool for improving distribution grid reliability," in *2024 AEIT International Annual Conference (AEIT)*, 2024, pp. 1–6.

[144] "IEEE Guide for Electric Power Distribution Reliability Indices," *IEEE Std 1366-2012 (Revision of IEEE Std 1366-2003)*, pp. 1–43, 2012.

[145] S. Bruno, M. La Scala, and U. Stecchi, "Monitoring and control of a smart distribution network in extended real-time dms framework," in *CIGRE 2011 Bologna Symposium*, 2011.

[146] "IEEE Recommended Practice for the Design of Reliable Industrial and Commercial Power Systems," *IEEE Std 493-2007*, pp. 1–383, 2007.

[147] Pyomo Development Team. (2022) Pyomo documentation 6.4.2. Accessed: September 2023. [Online]. Available: https://pyomo.readthedocs.io/en/stable/

[148] Gurobi Optimization. (2024) Gurobi optimizer reference manual. Accessed: April 2024. [Online]. Available: https://www.gurobi.com/documentation/current/refman/index.html

[149] A. Ricca, G. Adinolfi, R. Ciavarella, G. Graditi, and M. Valenti, "Innovative software for reliability, resilience, security and adequacy assessment of ac and dc grids and microgrids," in *2023 AEIT International Annual Conference (AEIT)*. IEEE, 2023, pp. 1–6.

[150] J. Y. Yen, "Finding the k shortest loopless paths in a network," *management Science*, vol. 17, no. 11, pp. 712–716, 1971.

[151] "HiGHS solver," accessed: 2024-07-15. [Online]. Available: https://dev.ampl.com/solvers/highs/index.html

[152] "SCIP solver," accessed: 2024-07-15. [Online]. Available: https://dev.ampl.com/solvers/scip/index.html

[153] "AMPL open-source solvers," https://ampl.com/products/solvers/open-source-solvers/, accessed: 2024-07-15.

[154] "Graphviz," accessed: 2024-07-15. [Online]. Available: https://graphviz.org/

[155] ENEA, *ARSTool*, 2023, the research was funded by the Italian Ministry of Environment and Energy Security (MASE) under the framework program on "Ricerca di Sistema Elettrico Nazionale". [Online]. Available: https://www.ricercasistemaelettrico.enea.it/siti-e-sw-prodotti/arstool.html

[156] B. Kocuk, S. S. Dey, and X. A. Sun, "Strong SOCP relaxations for the optimal power flow problem," *Operations Research*, vol. 64, no. 6, pp. 1177–1196, 2016.

[157] A. F. Soofi, S. D. Manshadi, G. Liu, and R. Dai, "A socp relaxation for cycle constraints in the optimal power flow problem," *IEEE Transactions on Smart Grid*, vol. 12, no. 2, pp. 1663–1673, 2021.

[158] D. Bienstock and G. Muñoz, "Approximate method for ac transmission switching based on a simple relaxation for acopf problems," in *2015 IEEE Power Energy Society General Meeting*, 2015, pp. 1–5.

[159] Z. Michalewicz, *Genetic Algorithms + Data Structures = Evolution Programs*, 3rd ed. Berlin, Heidelberg: Springer Science & Business Media, 2013.

[160] A. J. Umbarkar and P. D. Sheth, "Crossover operators in genetic algorithms: A review," *ICTACT Journal on Soft Computing*, vol. 6, no. 1, pp. 1083–1092, October 2015.

[161] F. Chicano, A. M. Sutton, L. D. Whitley, and E. Alba, "Fitness probability distribution of bit-flip mutation," *Evolutionary Computation*, vol. 23, no. 2, pp. 217–248, September 2013.

[162] J. Blank and K. Deb, "Pymoo: Multi-Objective Optimization in Python," *IEEE Access*, vol. 8, pp. 89 497–89 509, 2020.

[163] F. Pilo, G. Pisano, S. Scalari, D. Dal Canto, A. Testa, R. Langella, R. Caldon, and R. Turri, "Atlantide — digital archive of the italian electric distribution reference networks," in *CIRED 2012 Workshop: Integration of Renewables into the Distribution Grid*, 2012, pp. 1–4.

[164] S. Mishra, D. Das, and S. Paul, "A comprehensive review on power distribution network reconfiguration," *Energy Systems*, vol. 8, pp. 227–284, 2017.

[165] EPRI, *OpenDSS Documentation*, 2023, accessed: 2024-09-19. [Online]. Available: https://opendss.epri.com/opendss_documentation.html

[166] R. Cometa, M. R. Nasab, F. Lorusso, A. Velini, M. La Scala, and S. Bruno, "Integration of FDIR Practices in Distribution Optimal Network Reconfiguration Routines," in *24th EEEIC International Conference on Environment and Electrical Engineering*, 2024.

[167] A. Tiwari, A. Mohapatra, and S. R. Sahoo, "Tightening SOCP relaxation of AC Optimal Power Flow with Linearized Arc-tangent Constraints," in *2023 IEEE PESGM*, 2023, pp. 1–5.

[168] B. Amanulla, S. Chakrabarti, and S. Singh, "Reconfiguration of power distribution systems considering reliability and power loss," *IEEE transactions on power delivery*, vol. 27, no. 2, pp. 918–926, 2012.

[169] S. Deb, K. Tammi, K. Kalita, and P. Mahanta, "Impact of electric vehicle charging station load on distribution network," *Energies*, vol. 11, no. 1, 2018. [Online]. Available: https://www.mdpi.com/1996-1073/11/1/178

[170] P. Liu, P. Liu, Y. Yang, J. Wu, G. Tian, Z. Zhang, and L. Chai, "Risk analysis and mitigation strategy of power system cascading failure under the background of weather disaster," *Processes*, vol. 13, no. 1, p. 45, 2024.

[171] A. E. Schweikert, L. Nield, E. Otto, and M. R. Deinert, "Resilience and critical power system infrastructure: Lessons learned from natural disasters and future research needs," *World Bank Policy Research Working Paper*, no. 8900, 2019.

[172] Y. Wang, C. Chen, J. Wang, and R. Baldick, "Research on resilience of power systems under natural disasters—a review," *IEEE Trans. Power Syst.*, vol. 31, no. 2, pp. 1604–1613, 2015.

[173] "Piano di lavoro per l'incremento della resilienza del sistema elettrico di e-distribuzione 2022-2024," E-distribuzione, Tech. Rep., 2024.

[174] M. Zadehbagheri, M. Dehghan, M. Kiani, and S. Pirouzi, "Resiliency-constrained placement and sizing of virtual power plants in the distribution network considering extreme weather events," *Electrical Engineering*, vol. 107, no. 2, pp. 2089–2105, 2025.

[175] F. Mujjuni, T. R. Betts, and R. E. Blanchard, "Evaluation of power systems resilience to extreme weather events: A review of methods and assumptions," *IEEE Access*, vol. 11, pp. 87 279–87 296, 2023.

[176] A. Serrano-Fontova, H. Li, Z. Liao, M. R. Jamieson, R. Serrano, A. Parisio, and M. Panteli, "A comprehensive review and comparison of the fragility curves used for resilience assessments in power systems," *IEEE Access*, 2023.

[177] M. Panteli, C. Pickering, S. Wilkinson, R. Dawson, and P. Mancarella, "Power system resilience to extreme weather: Fragility modeling, probabilistic impact assessment, and adaptation measures," *IEEE Trans. Power Syst.*, vol. 32, no. 5, pp. 3747–3757, 2016.

[178] S. Dunn, S. Wilkinson, D. Alderson, H. Fowler, and C. Galasso, "Fragility curves for assessing the resilience of electricity networks constructed from an extensive fault database," *Natural Hazards Review*, vol. 19, no. 1, p. 04017019, 2018.

[179] S. Najafi Ravadanegh, M. Karimi, and N. Mahdavi Tabatabaei, "Modeling and analysis of resilience for distribution networks," *Power Systems Resilience: Modeling, Analysis and Practice*, pp. 3–43, 2019.

[180] M. Movahednia, A. Kargarian, C. E. Ozdemir, and S. C. Hagen, "Power grid resilience enhancement via protecting electrical substations against flood hazards: A stochastic framework," *IEEE Trans Ind. Informat.*, vol. 18, no. 3, pp. 2132–2143, 2021.

[181] M. FEMA, "Multi-hazard loss estimation methodology, flood model: Hazus-mh mr4 technical manual," 2009.

[182] A. Mazza, Y. Zhang, C. Carrozzo, E. Bompard, G. Chicco, E. Roggero, and G. Galofaro, "Evaluation of the impact of heat-wave on distribution system resilience," in *2021 International Conference on Smart Energy Systems and Technologies (SEST)*. IEEE, 2021, pp. 1–6.

[183] K. Alvehag and L. Soder, "A reliability model for distribution systems incorporating seasonal variations in severe weather," *IEEE Trans.Power Del.*, vol. 26, no. 2, pp. 910–919, 2010.

[184] Q. Shi, F. Li, M. Olama, J. Dong, Y. Xue, M. Starke, C. Winstead, and T. Kuruganti, "Network reconfiguration and distributed energy resource scheduling for improved distribution system resilience," *International Journal of Electrical Power & Energy Systems*, vol. 124, p. 106355, 2021.

[185] H. Khazraj, B. Yousefi Khanghah, P. Ghimire, F. Martin, M. Ghomi, F. Faria da Silva, and C. Leth Bak, "Optimal operational scheduling and reconfiguration coordination in smart grids for extreme weather condition," *IET Generation, Transmission & Distribution*, vol. 13, no. 15, pp. 3455–3463, 2019.

[186] Y. Li, K. Xie, L. Wang, and Y. Xiang, "Exploiting network topology optimization and demand side management to improve bulk power system resilience under windstorms," *Electric Power Systems Research*, vol. 171, pp. 127–140, 2019.

[187] M. S. Khomami, K. Jalilpoor, M. T. Kenari, and M. S. Sepasian, "Bi-level network reconfiguration model to improve the resilience of distribution systems against extreme weather events," *IET Generation, Transmission & Distribution*, vol. 13, no. 15, pp. 3302–3310, 2019.

[188] S. Nikkhah, K. Jalilpoor, E. Kianmehr, and G. B. Gharehpetian, "Optimal wind turbine allocation and network reconfiguration for enhancing resiliency of system after major faults caused by natural disaster considering uncertainty," *IET Renewable Power Generation*, vol. 12, no. 12, pp. 1413–1423, 2018.

[189] A. Martinelli, D.-D. Kolokotsa, and F. Fiorito, "Urban heat island in mediterranean coastal cities: The case of bari (italy)," *Climate*, vol. 8, no. 6, p. 79, 2020.

[190] R. E. Brown, *Electric power distribution reliability*. CRC press, 2017.

[191] R. N. Allan *et al.*, *Reliability evaluation of power systems*. Springer Science & Business Media, 2013.

[192] R. Billinton and C. Wu, "Predictive reliability assessment of distribution systems including extreme adverse weather," in *Canadian Conference on Electrical and Computer Engineering 2001. Conference Proceedings (Cat. No. 01TH8555)*, vol. 2. IEEE, 2001, pp. 719–724.

[193] R. Bonanno, M. Lacavalla, and S. Sperati, "Merida - meteorological reanalysis italian dataset," May 2019. [Online]. Available: https://doi.org/10.5281/zenodo.2677593

[194] J. R. Nairn and R. J. Fawcett, "The excess heat factor: a metric for heatwave intensity and its use in classifying heatwave severity," *International journal of environmental research and public health*, vol. 12, no. 1, pp. 227–253, 2015.

[195] V. M. Montsinger, "Loading transformers by temperature," *Transactions of the American Institute of Electrical Engineers*, vol. 49, no. 2, pp. 776–790, 1930.

[196] "Ieee guide for loading mineral-oil-immersed transformers and step-voltage regulators," *IEEE Std C57.91-2011 (Revision of IEEE Std C57.91-1995)*, pp. 1–123, 2012.

[197] M. T. Brunetti, S. Peruccacci, M. Rossi, S. Luciani, D. Valigi, and F. Guzzetti, "Rainfall thresholds for the possible occurrence of landslides in italy," *Natural Hazards and Earth System Sciences*, vol. 10, no. 3, pp. 447–458, 2010.

[198] M. Diakakis, "Rainfall thresholds for flood triggering. the case of marathonas in greece," *Natural Hazards*, vol. 60, pp. 789–800, 2012.

[199] "Ministero dell'ambiente e della sicurezza energetica-geoportale nazionale." [Online]. Available: https://www.mase.gov.it/pagina/geoportale-nazionale

[200] R. Brown, S. Gupta, R. Christie, S. Venkata, and R. Fletcher, "Distribution system reliability assessment: momentary interruptions and storms," *IEEE Trans. Power Del.*, vol. 12, no. 4, pp. 1569–1575, 1997.

[201] A. Velini, R. Cometa, F. Lorusso, M. La Scala, and S. Bruno, "Optimal network reconfiguration for mitigating the impact of adverse weather events on distribution networks," in *2024 IEEE International Humanitarian Technologies Conference (IHTC)*. IEEE, 2024, pp. 1–7.

[202] Y. Zhao, T. Zhang, L. Sun, X. Zhao, L. Tong, L. Wang, J. Ding, and Y. Ding, "Energy storage for black start services: A review," *International Journal of Minerals, Metallurgy and Materials*, vol. 29, no. 4, pp. 691–704, 2022.

[203] L. H. Fink, K.-L. Liou, and C.-C. Liu, "From generic restoration actions to specific restoration strategies," *IEEE Transactions on power systems*, vol. 10, no. 2, pp. 745–752, 1995.

[204] J. G. O'Brien, M. Cassiadoro, T. Becejac, G. B. Sheble, J. D. Follum, U. Agrawal, E. S. Andersen, M. Touhiduzzaman, and J. E. Dagle, "Electric grid blackstart: Trends, challenges, and opportunities," 2022.

[205] M. Minetti and M. Fresia, "A review of primary and secondary control for islanded no-inertia microgrids," in *2021 IEEE International Conference on Environment and Electrical Engineering and 2021 IEEE Industrial and Commercial Power Systems Europe (EEEIC/I&CPS Europe)*. IEEE, 2021, pp. 1–7.

[206] H. Ghoddami, M. B. Delghavi, and A. Yazdani, "An integrated wind-photovoltaic-battery system with reduced power-electronic interface and fast control for grid-tied and off-grid applications," *Renewable Energy*, vol. 45, pp. 128–137, 2012.

[207] L. Liu, J. Wu, Z. Mi, and C. Sun, "A feasibility study of applying storage-based wind farm as black-start power source in local power grid," in *2016 International Conference on Smart Grid and Clean Energy Technologies (ICSGCE)*. IEEE, 2016, pp. 257–261.

[208] Y. Zhu, F. Zhuo, and H. Shi, "Power management strategy research for a photovoltaic-hybrid energy storage system," in *2013 IEEE ECCE Asia Downunder*. IEEE, 2013, pp. 842–848.

[209] M. Minetti, M. Fresia, and D. Mestriner, "An mpc approach for a pv-bess islanded system primary regulation," in *2021 IEEE International Conference on Environment and Electrical Engineering and 2021 IEEE Industrial and Commercial Power Systems Europe (EEEIC/I&CPS Europe)*. IEEE, 2021, pp. 1–6.

[210] Z. Q. Gao, Z. J. Xie, H. Fan, and L. Meng, "Hybrid energy storage system for gshp black start," *Advanced Materials Research*, vol. 953, pp. 748–751, 2014.

[211] C. Li, S. Zhang, J. Zhang, J. Qi, J. Li, Q. Guo, and H. You, "Method for the energy storage configuration of wind power plants with energy storage systems used for black-start," *Energies*, vol. 11, no. 12, p. 3394, 2018.

[212] J. Li, H. You, J. Qi, M. Kong, S. Zhang, and H. Zhang, "Stratified optimization strategy used for restoration with photovoltaic-battery energy storage systems as black-start resources," *IEEE Access*, vol. 7, pp. 127 339–127 352, 2019.

[213] L. Yu, J. Lei, X. Guo, P. Yang, Z. Zeng, Z. Xu, and Q. Zheng, "Study on black start strategy of multi-microgrids with pv and energy storage systems considering general situations," in *2015 6th International Conference on Power Electronics Systems and Applications (PESA)*. IEEE, 2015, pp. 1–6.

[214] S. M. Ashabani and Y. A.-R. I. Mohamed, "A flexible control strategy for grid-connected and islanded microgrids with enhanced stability using nonlinear microgrid stabilizer," *IEEE Transactions on Smart Grid*, vol. 3, no. 3, pp. 1291–1301, 2012.

[215] Terna SpA, Grid Code annex A9, "Piano di difesa del sistema elettrico," https://www.terna.it/it/sistema-elettrico/codici-rete/codice-rete-italiano, 2023, (Italian Only) (accessed on April, 2025).